Plant-wide modelling and control of nitrous oxide emissions from wastewater treatment plants

Boiocchi, Riccardo

Publication date:
2016

Document Version
Peer reviewed version

Plant-wide modelling and control of nitrous oxide emissions from wastewater treatment plants

Riccardo Boiocchi

PhD Thesis

September 2016

DTU Chemical Engineering
Department of Chemical and Biochemical Engineering

Technical University of Denmark

Deparment of Chemical and Biochemical Engineering

CAPEC-PROCESS Research Center

Plant-wide modelling and control of nitrous oxide emissions from wastewater treatment plants

Ph.D. thesis

Riccardo Boiocchi

Main supervisor:

Gürkan Sin

Co-supervisor:

Krist V. Gernaey

The present thesis is to be kept in confidential with the following people:

Associate Professor Jens Abildskov

Professor Mark Van Loosdrecht

Dr. Stefan Weijers

Table of content

Acknowledgments

It is kind of difficult to express fully the thanks I want to give by words. So what I am going to write down is just a very reductive version of what the real acknowledgements should be.

To start up, I want to thank Gürkan Sin and Krist Gernaey for the support given to me during these three long years, for having dealt with my stubbornness and my very long Italian-like sentences.

My family from Italy, my mother Nica and my father Marco, my brother Fabio and the novel sister-in-law Federica are thanked for all the skype talks and for the moral support given constantly to me. Also, special thanks to my grandparents Duilio and Luisa, who have been giving me always hope and optimism for the future keeping themselves fresh despite the very advanced age.

In addition I would like to mention the great company of Carina for the long talks in our office, always boasting each other's motivation, hopefully. Andreas is also thanked for all the idea exchanges. At the same time, all the other members in the research group CAPEC-Process, the PhD students, the professors, the researchers and the secretaries Eva and Gitte for creating the very nice environment indeed needed to accomplish the PhD work.

Then an unusual but special thanks goes to the High Performance Computing (HPC) service in DTU, which provided me with a very proficient platform which enabled me simulate my endless multiple simulations within short time. Without the existence of this service, I would not have been able to achieve most of the results presented in the thesis.

Finally, I should not, and I will not, be ashamed to thank - above all - the only one God, the Creator of all. Without His will I would not have been able to accomplish this work and get all the help, support and comfort mentioned above.

ABSTRACT

Nitrous oxide (N_2O) is a greenhouses gas with a global warming potential three hundred times stronger than carbon dioxide (CO_2). The IPCC report released in 2014 shows that the CO_2 equivalents emitted from the wastewater systems are increasing in the last decades. It was also estimated that 14% of those CO_2 equivalents comes from N_2O emissions. It becomes therefore relevant, within the context of reducing the carbon footprint of wastewater treatment (WWT) systems, to develop control strategies aimed at the minimization of the emissions of this gas. Till now, few operation strategies have been developed to reduce the amount of N_2O emitted from WWT plants. However, these strategies have been employed for mainly sequencing-batch systems, where mere regulations of the cycle frequency and/or of the length of aeration and anoxic phases are enough to drastically reduce the amount of N_2O emissions. However, in full-scale continuously-aerated wastewater treatment systems such control strategies cannot be implemented. Furthermore, the available control strategies developed for N_2O emissions are not online, namely they do not change the operating conditions automatically as a function of on-line measurements. All of this makes the technologies proposed till now too case-specific and quite a number of adaptations would be needed if the system is changed. During the present work, a generic control strategy for N_2O emission minimization is developed. More specifically, the control strategy is designed in order to prevent the typical biological mechanisms triggering N_2O production. Furthermore, for thorough and comprehensive evaluation of such a control strategy prior to its application in real full-scale WWT systems, the developed control strategy is implemented and simulated in different model environments and a multi-criteria evaluation, taking into account not only the N_2O emissions but also the effluent quality and the operational costs, is carried out. This is because the reduction of the carbon footprint of WWT plants cannot be achieved at the expense of worse effluent quality and unreasonably-high operational costs. To build simulation environments where N_2O controller could be benchmarked against a reference scenario, three different benchmark simulation models are developed by including N_2O-producing processes in the Benchmark Simulation Model N°2. As an outcome, three different benchmark simulation models - the BSM2Na, the BSM2Nb and the BSM2Nc – are available. A scenario analysis showed discrepancies among the N_2O predictions by the three models. Since there is at the moment no consensus model considered to describe reliably N_2O emissions from WWT plants, all the three models are used for testing the N_2O control strategy. In a second step, a comprehensive sensitivity analysis on the BSM2Na was carried out at the aim of extrapolating the main biological mechanisms responsible for N_2O emissions. It was found that the ratio between NOB and AOB activity could indicate the accumulation of those nitrification intermediates, like nitrite and hydroxylamine, which trigger the N_2O production via AOB denitrification. Given the interactive nature and multiple objectives typically required in biological systems, fuzzy-logic approach was chosen as a control technique for the implementation of the strategy. To avoid poor performance behaviour due to intuitive design, a systematic procedure for the design of fuzzy-logic controllers is developed using a partial nitritation/Anammox system as application case. The same systematic methodology is then adopted to tune the fuzzy-logic controller for low N_2O emissions. The ratio between measured nitrate produced and ammonium consumed in the aerobic zone (R_{NatAmm}) is used as controlled variable and oxygen supply is regulated accordingly. The results coming from the benchmarking of the control strategy in the three simulation models showed that, by controlling the ratio R_{NatAmm}, N_2O emissions were able to be drastically reduced within reasonable aeration energy

consumptions. To cope with the increased COD demand by heterotrophic denitrifiers, additional control actions regulating the flow rate for carbon addition in the anoxic compartment were implemented.

The results of the controller evaluated under comprehensive simulation tests indicate a promising potential for full-scale applications in order to reduce N_2O emission from WWTPs. In addition, implementation of the control concept requires minimum investment (only relevant sensors required and adaptation of aeration control algorithm of the plants) is expected to encourage its take up by WWT plant operators for managing CO_2 footprints of WWTPs.

CHAPTER 1
Introduction

Nitrous oxide (N_2O) is a greenhouse gas with a global warming potential that is three hundred times stronger than the one of carbon dioxide. The report by the IPCC 2014 [1] has shown that the carbon footprint of wastewater treatment plants (WWTPs) is constantly increasing. It is estimated that 14% of the carbon dioxide equivalent (CO_2eq) emitted from WWTPs originates from N_2O, while the remainder is from methane (CH_4). While CH_4 is used in WWTPs to produce energy, control strategies minimizing N_2O emissions have to be developed to reduce the carbon footprint of WWTPs. N_2O is undesirably produced during the typical biological processes removing nitrogen from wastewater. Once produced in the liquid phase, N_2O is released to the atmosphere by stripping. There are many environmental parameters which can trigger the production and consequent emission of N_2O, and understanding the importance of these parameters is the key to minimization of N_2O emissions. On-line control strategies based on the mechanisms found to be triggering N_2O emissions have to be developed. The performance of such developed control strategies then needs to be evaluated prior to their application in full-scale WWTPs. In this way frequent and time-consuming adaptations associated with experimental trial-and-error based approach for controller development can be avoided. Once a good performance for N_2O minimization is ascertained, the control strategies can then be able to be implemented in full-scale WWTPs for further refinement and improvement.

In this thesis, benchmark simulation models incorporating N_2O dynamics are first developed. They are used as the simulation environment where the control strategies aiming at mitigating N_2O emissions are tested and compared against one another as well as against a reference open-loop scenario. Secondly, sensitivity analyses are performed with the aim of extrapolating the main environmental conditions enhancing the emissions of N_2O. On the basis of the understandings and the mechanisms identified responsible for triggering N_2O production, a minimization strategy idea will be formulated and the control strategy development will follow. Given the high non-linearity of biological wastewater treatment processes, the multiple control objectives and the uncertainties associated to them, fuzzy-logic control is considered as the ideal control technique to work with. However, prior to applying fuzzy-logic control, a new and systematic methodology is developed for the design of such control strategies for biological applications exemplified for a partial nitritation/Anammox system. The methodology is generalized and exploited for the design of novel control strategies minimizing N_2O emissions. Different fuzzy-logic control strategies are developed and benchmarked in the previously developed simulation models with the aim of evaluating their performance. The evaluation will not only consider the capability of the controller of reducing the N_2O emissions, but also the impact on the effluent quality and on the operating costs. The asset of the novel control strategies will be evaluated by comparison against a default control strategy typically adopted in WWTPs to comply with the effluent ammonium concentration law limits. Finally, the robustness of the control strategies against sensor and actuator noises and delays will be checked in order to evaluate the suitability of their application to real WWTPs. The present study has therefore provided the much needed basic control technology development and feasibility assessment prior to moving for full-scale applications in real WWTPs in order to reduce the N_2O emissions.

This chapter will first present the typical nitrogen removal processes in WWTPs (Section 1.1), with the aim of afterwards describing the mechanisms found in the literature for enhancing N_2O production in WWTPs (Section 1.2). A brief overview of the state of the art of previously-developed benchmark simulation models for wastewater processes will be provided as well in order to introduce the background on which the simulation work will be built upon (Section 1.3). Current and proposed strategies mitigating N_2O reported in literature will be described in Section 1.4, before concluding with the gaps for further development in the field (Section 1.5).

1.1 Nitrogen removal biological processes in wastewater treatment plants

1.1.1 Autotrophic nitrification

Autotrophic nitrification is a biological process during which ammonia and ammonium nitrogen (NH_3 and NH_4^+, respectively) are oxidized to nitrate with oxygen as electron acceptor. This process is mediated by two different classes of autotrophic bacteria: ammonia-oxidizing and nitrite-oxidizing bacteria (AOB and NOB, respectively). The first mediate the aerobic oxidation of ammonium to nitrite (nitritation) while the second are responsible for the aerobic oxidation of nitrite to nitrate (nitratation). The half reaction describing nitritation is expressed by Eqn. (1.1) while Eqn. (1.2) is the half reaction describing nitratation.

$$NH_4^+ + 2H_2O \rightarrow NO_2^- + 8H^+ + 6e^- \quad (1.1)$$

$$NO_2^- + H_2O \rightarrow NO_3^- + 2H^+ + 2e^- \quad (1.2)$$

By balancing both reactions 1.1 and 1.2 with the oxygen reduction reaction, the complete reactions describing respectively nitritation and nitratation are respectively:

$$NH_4^+ + \frac{3}{2}O_2 \rightarrow NO_2^- + 2H^+ + H_2O \quad (1.3)$$

$$NO_2^- + \frac{1}{2}O_2 \rightarrow NO_3^- \quad (1.4)$$

The overall reaction which describes nitrification is then given by:

$$NH_4^+ + 2O_2 \rightarrow NO_3^- + 2H^+ + H_2O \quad (1.5)$$

By including the biomass growth during these processes and using $C_5H_7NO_2$ as the standard chemical formula for the biomass, reactions (1.3-1.4) become, respectively, as follows:

$$1.34NH_4^+ + 1.86O_2 + 2.66HCO_3^- \rightarrow 0.024C_5H_7NO_2 + 1.32NO_2^- + 1.06H_2O + 2.54H_2CO_3 \quad (1.6)$$

$$NO_2^- + 0.0025NH_4^+ + 0.4875O_2 + 0.0025HCO_3^- + 0.01H_2CO_3 \rightarrow 0.0025C_5H_7NO_2 + NO_3^- + 0.0075H_2O \quad (1.7)$$

The AOB-mediated oxidation of ammonium to nitrite has been found to occur through hydroxylamine (NH_2OH). In turn, the oxidation of NH_2OH to NO_2^- has been shown to occur via the intermediates nitroxyl radical (NOH^o) [2–5] and nitric oxide (NO) [6–8].

In conclusion, the oxidation of ammonium to nitrate can be schematized according to the intermediates that were mentioned before, as shown in Figure 1.1.

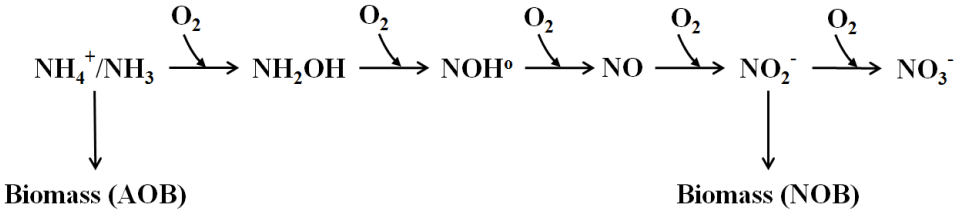

Figure 1.1: Schematic representation of the nitrification steps.

1.1.2 Heterotrophic denitrification

Heterotrophic denitrification is a biological process during which organic biodegradable carbon is oxidized with nitrate (NO_3^-) as terminal electron acceptor by facultative heterotrophs. These heterotrophs are called facultative since they can oxidize the organic matter by using either oxygen or oxidized nitrogen compounds as electron acceptors. If oxygen is present, HB will use oxygen instead of nitrogen oxides since this is more energy-efficient [9]. If oxygen is not present, facultative heterotrophs will use nitrogen oxides like nitrate and nitrite and reduce them into dinitrogen gas (N_2). When the concentration of N_2 exceeds its saturation concentration in the liquid phase, N_2 starts to be stripped off to the atmosphere. The reduction of nitrates occurs through intermediates such as nitrite, nitric oxide and nitrous oxide [10,11]. Figure 1.2 depicts the HB denitrification steps using methanol (CH_3OH) as representative substrate.

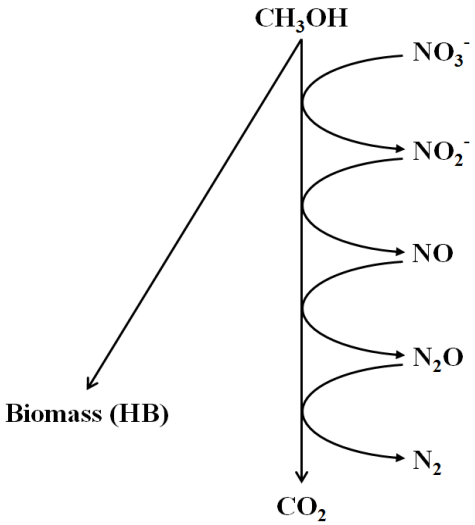

Figure 1.2: Schematic representation of the denitrification steps.

Each of the reduction steps shown in Figure 1.2 can be chemically described as follows:

I) Reduction of nitrate to nitrite:

$$NO_3^- + 2H^+ + 2e^- \rightarrow NO_2^- + H_2O \quad (1.8)$$

II) Reduction of nitrite to nitric oxide:

$$NO_2^- + 2H^+ + e^- \rightarrow NO + H_2O \quad (1.9)$$

III) Reduction of nitric oxide to nitrous oxide:

$$2NO + 2H^+ + 2e^- \rightarrow N_2O + H_2O \quad (1.10)$$

IV) Reduction of nitrous oxide to dinitrogen:

$$N_2O + 2H^+ + 2e^- \rightarrow N_2 + H_2O \quad (1.11)$$

Including the growth of heterotrophs according to Mutlu *et al.* [12], the complete chemical reaction describing denitrification on nitrate is:

$$NO_3^- + 1.08CH_3OH + 0.24H_2CO_3 \rightarrow 0.056C_5H_7NO_2 + 0.47N_2 + 1.68H_2O + HCO_3^- \quad (1.12)$$

1.1.3 Anaerobic ammonium oxidation

In addition to the conventional nitrification and denitrification processes, there is a novel process that is increasingly used for the treatment of domestic wastewaters due to its economical convenience: the anaerobic ammonium oxidation (Anammox). This process is mediated by anaerobic ammonia-oxidizing bacteria (AnAOB), which oxidize ammonium using nitrite as electron acceptor, according to the following reaction:

$$NH_4^+ + NO_2^- \rightarrow N_2 + 2H_2O \quad (1.13)$$

By including the growth of AnAOB according to Strous *et al.* [13] and using $CH_2O_{0.5}N_{0.15}$ as the chemical formula for AnAOB, reaction (1.13) becomes as follows:

$$NH_4^+ + 1.32NO_2^- + 0.066HCO_3^- + 0.13H^+ \rightarrow 0.26NO_3^- + 1.02N_2 + 0.066CH_2O_{0.5}N_{0.15} + 2H_2O \quad (1.14)$$

As can be noted, most of NH_4^+ is converted into dinitrogen using nitrite instead of oxygen as electron acceptor. Only approximately 11.3% of the total nitrogen reacted becomes nitrate. This last is produced as a consequence of nitrite oxidation carried out in order to supply electrons for carbon fixation [12]. Thus, for the same amount of total nitrogen removed, expenses due to air supply are considerably reduced by adopting this technology. Figure 1.3 schematizes the Anammox process.

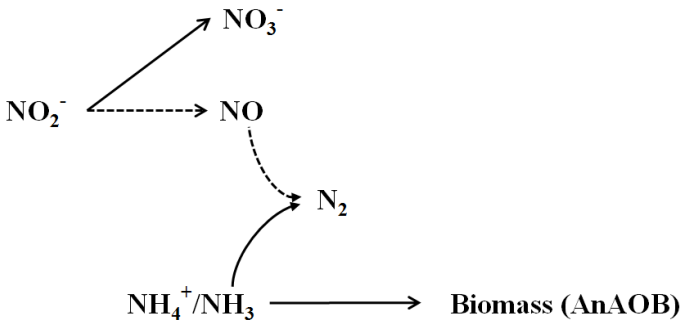

Figure 1.3: Schematic representation of the Anammox process.

Nowadays, the Anammox process is adopted for both main stream and side stream configurations. As main stream Anammox, the Anammox process is included in addition to the conventional nitrogen removal treatment processes. As side stream configuration, the Anammox process is used to treat the ammonium-loaded reject water from the dewatering unit prior to being recycled to the main treatment line.

1.2 Production pathways of nitrous oxide

Nitrous oxide is found to be produced as a result of the typical biochemical processes involved in the nitrogen removal. These processes are:

- denitrification by heterotrophic bacteria (HB denitrification),
- denitrification by ammonia-oxidising bacteria (AOB denitrification), and
- incomplete oxidation of hydroxylamine.

AnAOB and NOB are not expected to produce any N_2O [9,12].

As already presented, during HB denitrification, N_2O is produced as an intermediate compound. According to the AOB denitrification pathway, N_2O is produced as an end product of NO_2^- reduction via NO by AOB during the oxidation of NH_2OH. During the aerobic oxidation of NH_2OH, if the amount of NH_2OH produced exceeds the amount of the same chemical consumed, biochemical and chemical reactions producing N_2O using NOH^o or NO can be triggered [10,14].

There are many environmental parameters which can enhance the production of N_2O according to these three processes. For instance, it is well-known that a too high concentration of dissolved oxygen in an anoxic biological zone can inhibit the reduction of N_2O into N_2 by HB, thus promoting N_2O accumulation in the liquid phase and its subsequent emission [10,15]. Additionally, low availability of organic biodegradable carbon can lead to a similar result [16]. At the same time, a low concentration of oxygen in an aerobic reactor along with NO_2^- availability can trigger the production of N_2O by HB [17]. In some circumstances, HB can consume part of the N_2O produced according to the other production pathways. With regard to AOB denitrification, a lack of oxygen during nitrification is found to induce AOB to use nitrogen compounds as electron acceptors for NH_2OH oxidation [18,19]. Furthermore, an accumulation of NO_2^- is documented to promote AOB denitrification [10,18]. Eventual accumulation of

NH_2OH can trigger this pathway as well. With regard to the production of N_2O during incomplete NH_2OH oxidation, a number of reported results have shown that, at a high nitrogen oxidation rates [18–20], an accumulation of intermediates of NH_2OH oxidation occurs under conditions of high NH_4^+ and low NO_2^- concentrations. The high concentration of these intermediates then triggers chemical and biochemical reactions producing N_2O [2].

1.3 State of the art of Benchmark Simulation Models for wastewater treatment

Benchmark simulation models for wastewater treatment, such as the Benchmark Simulation Model nº1 (BSM1) by Alex *et al.* [21] and the Benchmark Simulation Model nº2 (BSM2) by Jeppsson *et al.* [22], are tools developed with the aim of providing a reference environment where control strategies and operation scenarios could be tested and compared with one another in an unbiased way. This in turn enables a thorough evaluation of the asset of control strategies to a wastewater treatment plant, prior to their implementation in the real system. These benchmark models provide a realistic layout of typical full-scale domestic WWTPs, combined with a comprehensive influent characterization, test procedures and performance evaluation criteria. The difference between the BSM1 and the BSM2 is substantially when comparing the plant layouts: while the BSM1 includes only the activated sludge biological reactors with a secondary settler, the BSM2 extends this platform by including a primary clarifier and a side stream for the treatment of the wastage sludge coming from primary and secondary clarifiers. This allows a more comprehensive evaluation of the plant performance, taking into account the plant-wide dynamics where the main stream affects the side stream and vice versa. For instance, the sludge quality disposed after the dewatering treatment depends on the amount of biomass built up in the mainstream activated sludge unit. On the other hand, the characterization of the reject stream from the dewatering unit recycled to the mainstream, rich in ammonium, can impact the performance of the mainstream and eventually the effluent quality. For these reasons, in this work the BSM2 platform is used as a basis.

1.4 Control strategies for N_2O emissions

Accomplishing those environmental conditions discouraging the three N_2O-production processes and/or promoting its consumption is the route to mitigate the emissions of N_2O.

In this context, plant-wide on-line control is to be considered as an effective tool widely adopted to manipulate the plant environmental conditions with specific objectives in function of different influent loads. Till now, several control strategies have been designed for different wastewater treatment related objectives such as oxygen and effluent ammonium concentration but none has the minimization of emitted N_2O as specific control objective. The study by Desloover *et al.* [15] presents a comprehensive overview of the possible N_2O mitigation strategies, as shown in Figure 1.4.

Overview of N_2O mitigation strategies

Objective	Approach	Outcome
Minimize aerobic N_2O production	Ensure stable substrate levels by gradual feeding regime, sufficient mixing and buffer volume capacity	Few NH_4^+ fluctuations
	Ensure sufficiently high DO (N/DN) or adapted aeration regime (1-stage PN/A)	Prevent NH_2OH and NO_2^- accumulation
	Ensure low free ammonia and low free nitrous acid	Prevent NO_2^- accumulation by NOB stimulation (N/DN)
	In case of high NO_2^-, ensure sufficiently high DO	Prevent NO_2^- accumulation
	Ensure constant DO (no repeated changes from anoxic to oxic), low NH_4^+, sufficiently high SRT, neutral pH, bio-augment with AOB (+NOB)	Prevent high sludge-specific activity and changes from low to high specific activity
	Bio-augment with AOB	Lower nitritation functionality dynamics
Minimize aerobic N_2O emissions	In case of active aeration: Lower aeration rate	Lower mass transfer coefficient (k_La)
	In case of passive aeration: Limit turbulence	Lower mass transfer coefficient (k_La)
	In case of bubble-less aeration: preferable in terms of N_2O emissions, for example, membrane aerated bioreactor (MABR)	Lower mass transfer coefficient (k_La)
Maximize anoxic N_2O consumption	Lower aerobic COD breakdown and COD-removing pre-settling (sewage), or provide external COD	Sufficiently high COD/N
	In case of external COD dosage: choose carbon source carefully (e.g. N_2O emissions ethanol > methanol)	Prevent incomplete denitrification
	Ensure efficient aeration in preceding stage (no overaeration) and provide sufficient anoxic HRT	No DO, stimulate complete denitrification
	Bio-augment with N_2O-consuming HDN *Pseudomonas stutzeri*	Increase N_2O reduction potential
	Ensure sufficient copper availability	Ensure N_2O reductase synthesis
End-of-pipe treatment	In case of capped BNR plants: biofilter, … (to be developed)	Lower N_2O release to environment

COD: chemical oxygen demand; DO: dissolved oxygen; HRT: hydraulic retention time; N/DN: nitrification/denitrification; PN/A: partial nitritation/anammox; SRT: sludge retention time; AOB: ammonia-oxidizing bacteria; NOB: nitrite-oxidizing bacteria; HDN: heterotrophic denitrifying bacteria.

Figure 1.4: Overview of N_2O mitigation strategies by Desloover *et al.* [15].

Among the strategies suggested, ensuring a good level of oxygenation in the aerobic zone with the aim of triggering NOB activity emerges. As a matter of fact, this would avoid the accumulation of nitrite, which is the substrate used by NOB, and thus discourage the use of the same compound by AOB. Furthermore, sufficient oxygenation can directly inhibit the nitrite uptake by AOB. Other strategies proposed are the reduction of the influent NH_4^+ fluctuations in order to avoid accumulation of NH_2OH and imbalance between AOB and NOB activity. This would limit the production of N_2O through both AOB denitrification and incomplete NH_2OH oxidation pathways. Enhancing the residence time of N_2O in the liquid phase by lowering the N_2O stripping capability can increase the possibility of its consumption by HB. However, since the stripping capability is directly proportional to the oxygen supply, there should be a trade-off oxygenation on the one side guaranteeing a balanced activity between NOB and AOB and, on the other side, increasing the residence time of N_2O in the liquid phase. With the aim of enhancing the enzymatic reduction of N_2O in the liquid phase by heterotrophic bacteria in the anoxic zone, avoiding oxygen inhibition and ensuring an optimal organic biodegradable carbon availability to have complete oxidation of nitrogen oxides into dinitrogen can be considered. Furthermore, increase of copper availability has been documented to trigger the production of the nitrous-oxide reductase enzyme by heterotrophs, which promotes the reduction of N_2O into N_2 [16]. Finally, for pre-denitrification systems, a decrease of the flow rate of the nitrogen oxide rich recycle stream would increase the anoxic hydraulic retention time and thus promote a complete HB denitrification.

Contextually to the minimization of the N_2O emissions, plant effluent limits and operational costs have to be considered. For example, the increase of the oxygenation level required to avoid nitrite accumulation by enhancement of NOB activity can be done at the expense of higher operational costs. Similarly, guaranteeing complete HB denitrification by addition of organic biodegradable carbon would increase plant operational costs as well, due to the cost of the carbon source added and the extra sludge production. Other strategies, like the reduction of influent ammonium fluctuations and of the internal nitrogen oxides recycle, can be considered as not leading to a significant increase of the operational costs. With regard to the effluent quality, the strategy which increases the oxygenation level is expected to decrease the concentration of ammonium in the effluent because high oxygen levels naturally trigger the aerobic AOB activity. However, the higher production of nitrates by NOB leads to higher requirements of organic biodegradable carbon for their complete reduction into N_2. Hence, a higher TN effluent concentration is expected to occur when increasing the aeration if the amount of organic carbon fed is not increased accordingly. Reducing influent ammonium fluctuations is expected to reduce the concentration of ammonium in the effluent. Enhancing the N_2O-to-N_2 reduction by HB through an increase of organic carbon availability leads to an improvement of the total nitrogen oxides removal efficiency, thus improving the effluent quality.

Until now, few strategies for mitigation of N_2O emissions have been attempted. In particular, Park *et al.* [23] have managed to reduce almost totally the N_2O emitted from a suspended activated sludge system by adding methanol, which triggered the last HB denitrification step. Similarly, in the experiments conducted by Zhu *et al.* [24], N_2O emissions were reduced by triggering its consumption by HB. In this case, not methanol but copper was added. However, Hu *et al.* [25] have found that step-feeding would help create an environment in the aerobic zone with high concentration of dissolved oxygen and low concentration of ammonium, which allows to have complete nitrification. This in turn showed to drastically reduce N_2O production. Sun *et al.* [26] addressed the accumulation of nitrite in the aerobic zone as the main cause for N_2O emissions. In their experiments with different aeration regimes, it was found that increasing aeration rate until a threshold can help achieving complete nitrification. In addition, it was found that N_2O emissions can be triggered by excessive depletion of biodegradable COD, needed to have complete HB denitrification. Identifying an optimal oxygen level in the aerated zone, such that nitrification is complete and HB denitrification is not inhibited, was deemed to be the key factor for achieving low N_2O emissions.

Behera *et al.* [27] developed a model-based predictive control for energy-efficient minimization of N_2O in a sequencing batch reactor (SBR) biological nitrogen removal system. The controller was not directly designed to have low N2O emissions but to set the ammonium concentration in the reactor at 1 mg $N.L^{-1}$ whereas the N_2O liquid concentrations were constrained between 10^{-6} g $N.m^{-3}$ and 10^{-3} g $N.m^{-3}$. Although the controller managed to limit the liquid concentrations of N_2O within the fixed range according to the model used, the results cannot be considered reliable due to the great mismatch between model predictions of N_2O (liquid and gas phase) and the experimental data. The constraint imposed could also be considered too subjective and case specific for the reactor used. Furthermore, it is not the liquid concentration but the emissions that need to be minimized.

Finally, in an investigation led by Rodriguez-Caballero *et al.* [28], shorter aerated phases in a full scale sequencing-batch reactor (SBR) were found to reduce N_2O emissions along with leading to lower nitrite accumulations.

1.5. Conclusion: problem statement for the PhD thesis

In conclusion, no on-line control strategies for N_2O emission minimization in full-scale continuously-aerated WWTPs are available at the moment. The only ones published are implemented for sequencing-batch operating reactors, where N_2O is more easily minimized through regulation of the duration of aerated and anoxic phase and/or frequency of cycles, and are not based on on-line measurements of influent and/or effluent concentrations. Furthermore, the strategies for N_2O emissions developed till now have not been developed on the basis of deep understanding of the microbiological dynamics according to which N_2O is produced. Rather, the strategies applied were developed ad hoc and hence resulted quite context-specific.

For this reason, the ultimate objective of the present PhD work is to systematically develop and test in different simulation environments a control strategy for N_2O emission minimization applied to full-scale WWTPs on the basis of understanding of the typical N_2O emission mechanisms. This way the performance of the controller will not be dependent on the particular plant configuration and only a minimal number of adaptations will be needed.

In addition, this work aims at comprehensively benchmarking the control strategies developed against a reference scenario taking into account not only the N_2O emissions, but also the effluent quality and the operating costs, namely a multi-criteria evaluation is performed. This is much needed because N_2O emissions have to be minimized within a plant-wide context where effluent limitations have to be respected and operating costs have to be reasonable. Given the complexity typical of biological processes and the uncertainty associated to the multiple control objectives, fuzzy-logic approach is adopted for the development of such a control strategy.

For these reasons, prior to developing control strategies aimed at N_2O emission mitigation, the following three sub-tasks need to be performed: (I) development of simulation environments to test the N_2O control strategies, (II) deduction the mechanisms enhancing N_2O emissions, and (III) development of a systematic methodology to design fuzzy-logic controllers applied to biological systems. More specifically, as a first step, novel N_2O-producing processes will be integrated into the default Benchmark Simulation Model n°2 by Jeppsson *et al.* [22]. Sensitivity analyses will be performed to deduce the main mechanisms responsible for N_2O emissions. Based on these identified mechanisms, the control idea will be able to be formulated. Since a systematic procedure to design membership functions for fuzzy-logic control is needed to avoid unexpected behaviours, a novel methodology for tuning fuzzy-logic control in connection with predefined control objectives is developed using a one-stage partial nitritation/Anammox system as case study. Once these subtasks are performed, the control strategy for N_2O emission minimization will be able to be developed and tested.

CHAPTER 2
Materials and Methods

In this chapter, the materials and methods exploited to develop the models and control strategies will be presented. In particular, the default BSM2 platform, the simulations performed and the criteria used to evaluate the different scenarios will be described in Section 2.1. In Section 2.2 the sensitivity analysis methodologies employed later in Chapter 4 are described.

2.1. The default Benchmark Simulation Model Nº2

2.1.1. Influent characterization

The BSM2 is ideally designed in order to treat a domestic wastewater that is relatively highly loaded with nitrogen. The influent load corresponds to about 100,000 people equivalent, of which 80,000 originates from households and 20,000 from industrial activities. The flow-rate-weighted average influent can be found in Table 2.1.

Table 2.1: flow-rate-weighted average influent composition of the BSM2.

State variable	Unit	Value
S_I	g COD.m^{-3}	27.23
S_S	g COD.m^{-3}	58.18
X_I	g COD.m^{-3}	92.5
X_S	g COD.m^{-3}	363.94
X_{HB}	g COD.m^{-3}	50.68
X_{AB}	g COD.m^{-3}	0
X_P	g COD.m^{-3}	0
S_{O2}	g (– COD).m^{-3}	0
S_{NO}	g N.m^{-3}	0
S_{NH}	g N.m^{-3}	23.86
S_{ND}	g N.m^{-3}	5.65
X_{ND}	g N.m^{-3}	16.13
S_{ALK}	mole.m^{-3}	7
TSS	g TSS.m^{-3}	380.34
Q	m^3.d^{-1}	20648.36
Temperature	ºC	14.86

With regard to the dynamic influent, Figure 2.1 shows the influent 609-day long dynamics of each state variable.

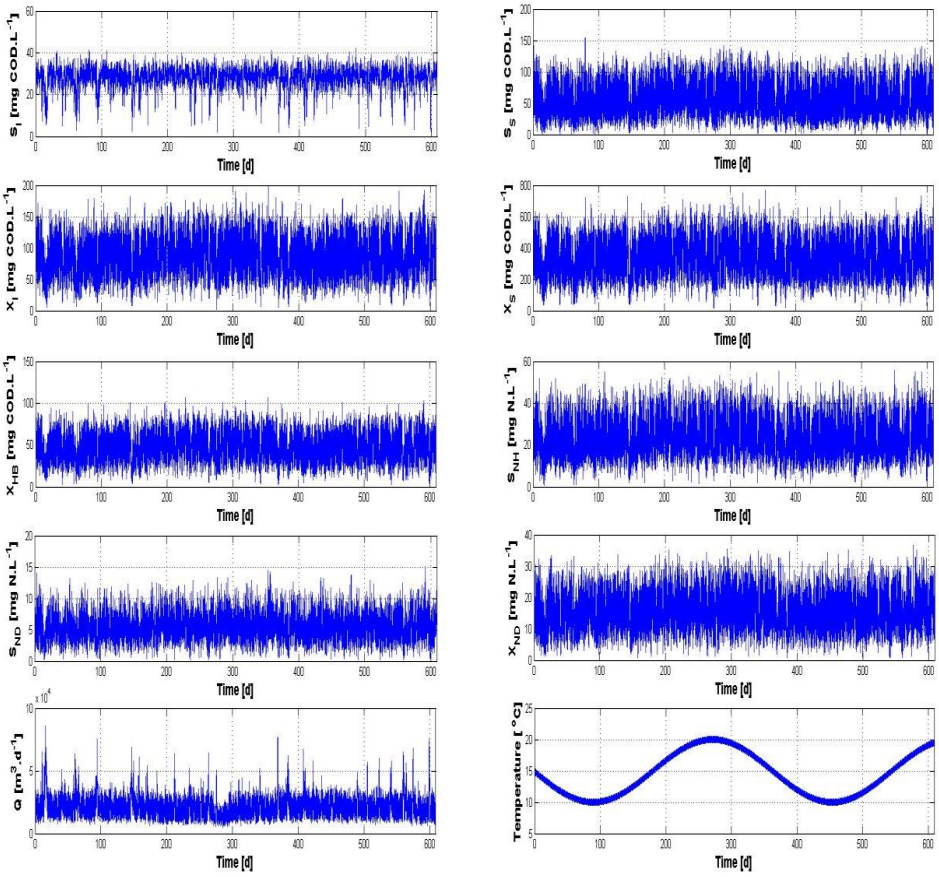

Figure 2.1: Dynamic profiles of the influent variables used in the BSM2 [22].

2.1.2 Plant configuration

The BSM2 layout is presented in Figure 2.2. As can be seen, it can be split into a main stream and side stream. From left to right, the mainstream consists of: a primary clarifier (PRIM), followed by a predenitrification zone consisting of two anoxic tanks (ANOX1 and ANOX2), which are then followed by three aerobic tanks (AER1, AER2 and AER3), and a secondary clarifier (SEC2). The activated sludge unit includes two recycles: (a) an internal recycle, where the mixed liquor from the last aerobic tank is transported to the anoxic zone to allow the HB-mediated reduction of the nitrogen oxides produced by autotrophic biomass, and (b) an external recycle, where part of the sludge settled in the secondary clarifier is pumped to the anoxic zone to keep a constant and high concentration of biomass in the biological system.

The side stream includes a thickener (THK), an anaerobic digester (AD), a dewatering treatment unit (DW) and a storage tank (ST). The THK receives wastage sludge from the secondary clarifier (SEC2) and separates the water from the sludge. The separated water is recycled on top of the primary clarifier

whereas the thickened sludge is diverted to the anaerobic digester together with the wastage sludge from PRIM. The biomass is then anaerobically decomposed in a well-mixed digester. Methane is thus produced. The digested sludge is then dewatered in DW while the nitrogen rich reject water resulting from this process is then recycled back to the main stream, either to the primary clarifier or to the activated sludge unit. The storage tank can be used to smooth the peaks of ammonium recycled from the side steam to the main stream.

The volumes of each treatment unit are presented in Table 2.1.

Given the volumes, a Sludge Retention Time (SRT) of approximately 15 days is maintained, whereas the HRT is 22 hours.

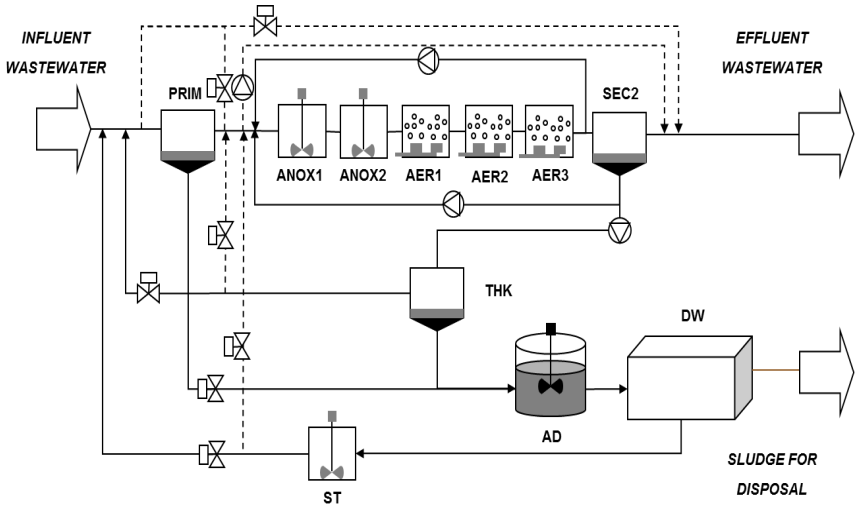

Figure 2.2: Layout of the Benchmark Simulation Model nº2 [22].

Table 2.2: Volumes of the each treatment unit of the BSM2

Unit	Volume [m^3]
PRIM	900
ANOX1	1500
ANOX2	1500
AER1	3000
AER2	3000
AER3	3000
SEC2	6000
AD	3400
ST	160

2.1.3 Default mathematical models used in the BSM2

Each treatment unit used in the BSM2 uses a mathematical model to describe the physical and biological processes occurring. Table 2.2 summarizes the default mathematical models used for each treatment unit.

Table 2.3: Mathematical models used in each treatment unit of the BSM2.

Unit	Model
PRIM	Extended model by Otterpohl and Freund [29]
ANOX1	ASM1 [30]
ANOX2	ASM1 [30]
AER1	ASM1 [30]
AER2	ASM1 [30]
AER3	ASM1 [30]
SEC2	Model by Takács *et al.* [31]
AD	ADM1 [32]

2.1.4 Performance assessment

Steady-state analysis

For the steady-state analysis, the total nitrogen concentration in each stream predicted by the BSM is considered and compared with the influent nitrogen load. This quantity is calculated according to Eqn. (2.1).

$$TN = S_{NH} + S_{NH2OH}{}^{*} + S_{NO3} + S_{NO2} + S_{NO} + S_{N2O} + S_{N2} + S_{ND} + X_{ND} + \\ +0.086 \cdot (X_{HB} + X_{AOB} + X_{NOB} + X_{AnAOB}) + 0.06 \cdot (X_I + X_P) + S_{NH2OH}\ * \quad (2.1)$$

*only when it is included in the model

Furthermore, the TN removal efficiency is calculated by neglecting those N species which are commonly unmeasured, such as S_{NH2OH}, S_{N2}, and N that is part of X_I and X_P.

Two nitrous oxide emission factors are calculated: one given by the sum of the N_2O emitted from the five biological main stream tanks per unit of influent Total Kjeldahl Nitrogen (TKN), and the other given by the sum of the N_2O emitted from the five biological main stream tanks per unit of TKN removed.

To track the contribution of the different pathways in the models used in this thesis, the N_2O produced according to the N_2O producing processes is generically calculated according to Eqn. (2.2).

$$N_2O_{prod,pathwayX} = V \cdot Coeff_{stoic} \cdot rate_{proc} \quad (2.2)$$

where:

- $N_2O_{prod,pathwayX}$ is the N_2O produced according to a particular pathway [g N_2O-N.d^{-1}],
- V is the reactor volume,

- $Coeff_{stoic}$ is the stoichiometric coefficient for N_2O in the stoichiometric matrix related to the specific N_2O producing process considered,
- $rate_{proc}$ is the rate of the N_2O producing process considered.

Similarly, to analyse the economical convenience of introducing the PN/A reactor in a full-scale WWTP, the oxygen consumptions are calculated according to Eqn. (2.3).

$$O_2 = V \cdot Coeff_{stoic} \cdot rate_{proc} \tag{2.3}$$

Dynamic analysis

The dynamic analysis will consider the dynamic results of the last year, i.e. from the 244th to 609th day in the simulation output, for the following specific outputs:

- *Effluent quality*

With regards to performance assessment, flow-weighted average values for the effluent concentration of the last 264 days of simulation are used and compared against the standard effluent limits of Table 2.4.

Table 2.4: Effluent limits used to evaluate BSM1 performance [21].

Pollutant	Effluent Law Limit
TN	18 g N.m^{-3}
COD	100 g COD.m^{-3}
BOD_5	10 g BOD.m^{-3}
TSS	30 g SS.m^{-3}
NH_X-N	4 g N.m^{-3}

The violations are measured as percentage of the total evaluation time when the concentration of each pollutant exceeds the corresponding effluent limit. Hence, the higher the value of this parameter is, the worse the effluent is considered to be. In addition to this evaluation of the effluent, the so-called Effluent Quality Index (EQI) is also calculated as a flow weighted sum of the average loads of the main pollutants, as expressed in Eqn. (2.4).

$$EQI = \frac{1}{t_{obs} \cdot 1000} \int_{t_{start}}^{t_{end}} (\beta_{TSS} \cdot TSS_e(t) + \beta_{COD} \cdot COD_e(t) + \beta_{TKN} \cdot S_{TKN,e}(t) + \\ + \beta_{NO} \cdot S_{NO,e}(t) + \beta_{BOD5} \cdot BOD_e(t)) \cdot dt \tag{2.4}$$

In Eqn. (2.4), t_{obs} is the evaluation period considered, given by the difference between t_{end} and t_{start}. β_{TSS}, β_{COD}, β_{TKN}, β_{NO} and β_{BOD5} are weighting factors, whose values are reported in Table 2.5. As can be noted, nitrogen species have much stronger impact on EQI than organic carbon related species. TSS_e, COD_e, $S_{TKN,e}$, $S_{NO,e}$ and $BOD_{5,e}$ are average loads of effluent TSS, COD, TKN, nitrogen oxides and BOD_5 respectively. EQI is conventionally measured in kilograms of pollutant units per day (kg poll. units. d^{-1}). The larger EQI is, the worse the effluent quality is.

Table 2.5: Weighting factors used in the expression for EQI [22].

β_{TSS}	β_{COD}	β_{TKN}	β_{NO}	β_{BOD5}
g poll.units.g^{-1} SS	g poll.units.g^{-1} COD	g poll.units.g^{-1} N	g poll.units.g^{-1} N	g poll.units.g^{-1} BOD_5
72	1	20	20	2

- *Aeration energy consumptions*

Aeration energy consumption should take into account the type of supplier, the bubble size, and the depth of submersion. Similarly to the BSM1, the BSM2 proposes a calculation method valid for Degrémont DP230 porous disks immerged under four meters of water [21]. This leads to assuming that one kilowatt-hour of energy is consumed per 1.8 kilos of oxygen transferred into the liquid system. Expressing mathematically the amount of oxygen transferred to a reactor is then done as follows:

$$O_{2,transferred} = V \cdot k_L a \cdot \left(S_{O2,sat} - S_{O2}\right) \tag{2.5}$$

, the amount of aeration energy consumed throughout a period of time is calculated as:

$$AEC = \frac{\int_{t_{start}}^{t_{end}} \sum_{i=1}^{5} V_i \cdot k_L a_i(t) \cdot \left(S_{O2,sat} - S_{O2,i}(t)\right) \cdot dt}{1.8 \cdot 1000 \cdot (t_{end} - t_{start})} \tag{2.6}$$

where:
- AEC is the aeration energy consumed [kWh.d^{-1}],
- V_i is the liquid volume of the reactor i [m^3],
- $k_L a_i$ is the oxygen mass transfer coefficient of the reactor i [d^{-1}],
- $S_{O2,sat}$ is the oxygen saturation concentration [g (-COD).m^{-3}],
- $S_{O2,i}$ is the oxygen concentration in reactor i [g (-COD).m^{-3}],
- t_{start} is the time corresponding to the beginning of the evaluation period [d],
- t_{end} is the time corresponding to the end of the evaluation period [d].

- *External carbon consumption*

The BSM2 includes inlets for the addition of a solution at 25% of ethanol, having thus a constant concentration of 400,000 mg COD.L^{-1} of soluble biodegradable COD (identified in the model as S_S). The costs due to external carbon addition are calculated on the basis of the volumetric flow rate of the added ethanol solution, as follows:

$$CC = \frac{COD_{ES} \cdot \int_{t_{start}}^{t_{end}} \sum_{i=1}^{5} q_{ES,i}(t) \cdot dt}{1000 \cdot (t_{end} - t_{start})} \tag{2.7}$$

where:
- *CC* is the external carbon consumption [kg COD.d^{-1}],

- COD_{ES} is the concentration of COD in the ethanol solution [mg COD.L^{-1}],
- q_{ES} is the flow rate of the ethanol solution added [$m^3.d^{-1}$].

- *Nitrous oxide emissions*

To analyse the controller performances in reducing N_2O emissions efficiently, the two N_2O emission factors, one per unit of influent TKN (N_2O_{ef1}) and the other per unit of TKN removed (N_2O_{ef2}), are calculated according to Eqns. (2.8) and (2.9), respectively. As can be seen, N_2O_{ef1} is calculated as the ratio between the sum of the N_2O emitted from the five biological tanks and the sum of the influent TKN to the plant, while N_2O_{ef2} divides the total N_2O emitted from the biological tanks by the summed difference between influent TKN and effluent TKN.

$$N_2O_{ef1} = \frac{\sum_{i(t_{start})}^{i(t_{end})}(N_2O_{ANOX1}(i) + N_2O_{ANOX2}(i) + N_2O_{AER1}(i) + N_2O_{AER2}(i) + N_2O_{AER3}(i))}{\sum_{i(t_{start})}^{i(t_{end})}((S_{NH,in}(i) + S_{ND,in}(i) + X_{ND,in}(i)) \cdot Q_{in}(i))} \tag{2.8}$$

$$N_2O_{ef2} = \frac{\sum_{i(t_{start})}^{i(t_{end})}(N_2O_{ANOX1}(i) + N_2O_{ANOX2}(i) + N_2O_{AER1}(i) + N_2O_{AER2}(i) + N_2O_{AER3}(i))}{\sum_{i(t_{start})}^{i(t_{end})}((S_{NH,in}(i) + S_{ND,in}(i) + X_{ND,in}(i)) \cdot Q_{in}(i)) - \sum_{i(t_{start})}^{i(t_{end})}((S_{NH,out}(i) + S_{ND,out}(i) + X_{ND,out}(i)) \cdot Q_{out}(i))} \tag{2.9}$$

- *Capability of the controllers to track the set point*

The capability of the controllers in tracking the given set points of a controlled variable (CV) will be evaluated on the basis of two indexes: the Integral Absolute Error (IAE) and the Integral Square Error (ISE), calculated according to Eqns. (2.10) and (2.11), respectively. As can be noted, the ISE penalises large deviations of the CV from the set points while IAE does not. Lower IAE and ISE values indicate better set point tracking capability.

$$IAE = \sum_{i(t_{start})}^{i(t_{end})} |CV(i) - CV_{SP}(i)| \tag{2.10}$$

$$ISE \sum_{i(t_{start})}^{i(t_{end})} (CV(i) - CV_{SP}(i))^2 \tag{2.11}$$

- *Aggressiveness of the controllers*

Since frequent changes of the manipulated variables (MVs) can require a higher frequency of instrumentation maintenance, the Total Variation (TV) of the manipulated variables is calculated according to Eqn. (2.12). More frequent maintenance corresponds to high TV values.

$$TV_{MV} = \sum_{i(t_{start})}^{i(t_{end})} |MV(i) - MV(i-1)| \tag{2.12}$$

2.2. Sensitivity analysis methods

2.2.1. Monte Carlo procedure

In order to present in mathematical terms the Monte Carlo approach, the notational conventions outlines below are used.

First of all, the mathematical model is represented by the following equations:

$$\frac{d\underline{x}}{dt} = f(t, \underline{x}, \underline{u}, \underline{P}) \tag{2.13}$$

$$\underline{x}(t_0) = \underline{x_0} \tag{2.14}$$

$$\underline{y} = g\left(\underline{x}(t)\right) \tag{2.15}$$

In Eqns. (2.13-2.15) t is the time, $\underline{x}$ is the vector of state variables, $\underline{x_0}$ is the vector of initial states, $\underline{u}$ is the vector of input variables, $\underline{P}$ is the vector of input parameters and $\underline{y}$ is the vector of output variables.

The sensitivity analysis according to the Monte Carlo procedure is performed according to the steps represented in Figure 2.3. As can be seen, the first step is to assign the uncertainty to the model inputs ($\underline{u}$ and/or $\underline{P}$) and eventual correlations between them. Afterwards, different input samples are produced using the Latin Hypercube Sampling (LHS) technique according to Iman and Conover [33]. The sampling matrix $\underline{\theta}$, having a number of rows equal to the number of samples and a number of columns equal to the number of uncertain inputs, is obtained. For each sample, a different model simulation is performed and different values of model outputs ($\underline{y}$) are thereby obtained. Mean values (μ) and standard deviations (σ) of these outputs are then calculated according to Eqns. (2.16-2.17) and the ratio between them (σ/μ) is used to evaluate the uncertainty of the model predictions. The higher the ratio is, the higher the uncertainty of the output prediction is considered. Values of σ-to-μ ratio equal or higher than unity are considered to indicate clearly high uncertainty of the predicted output, i.e. high propagation of input uncertainties to output predictions. Afterwards, a linear regression between each of the model simulation results and the set of uncertain inputs (Eqn. (2.18)) is performed. The regression is considered reliable if the coefficient of determination (R^2) between output values obtained from simulation and the corresponding linearized ones is equal to or higher than 0.7. The regression coefficients found for each uncertain input are then standardized according to Eqn. (2.19) in order to identify an unbiased measure for the impact of each uncertain input on the output with regard to the uncertainty of the inputs and of predicted outputs.

The sensitivity of all those outputs which could not be regressed with respect to the uncertain inputs was analysed through the Morris screening procedure, presented in the next subsection.

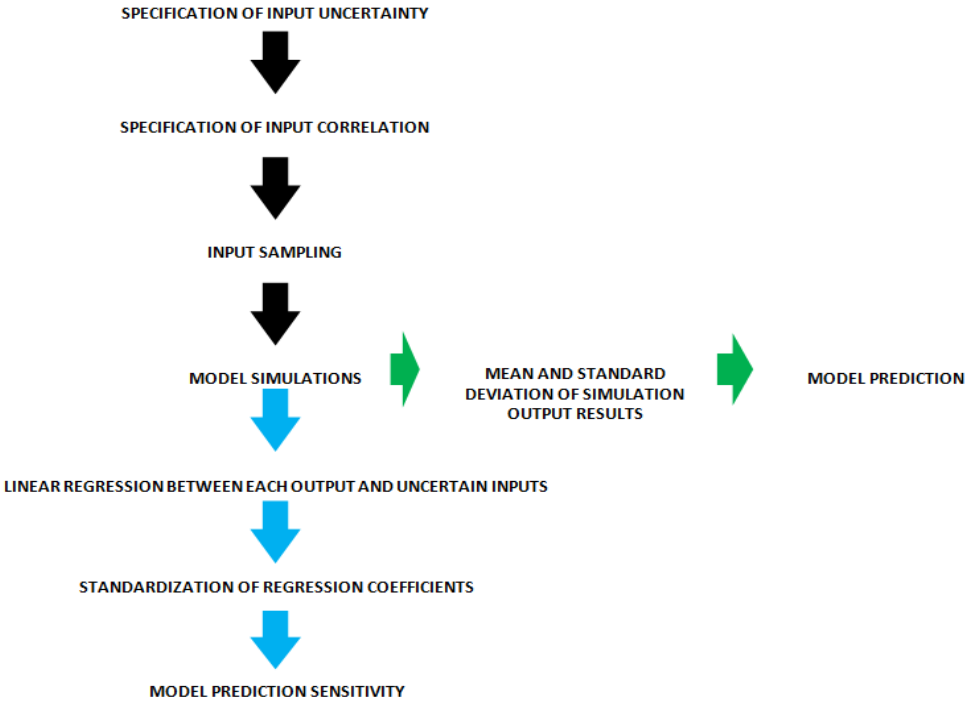

Figure 2.3: Step-wise procedure used for the uncertainty and sensitivity analysis according to the Monte Carlo procedure (green and blue, respectively) [34].

$$\mu(y) = \frac{\sum_{j=1}^{N} y^j}{N} \tag{2.16}$$

$$\sigma(y) = \sqrt{\frac{1}{N} \cdot \sum_{j=1}^{N} (y^j - \mu(y))^2} \tag{2.17}$$

$$y_{lin,reg} = a + \sum_{i} (b_i \cdot \theta_i) \tag{2.18}$$

$$\beta_i = \frac{\sigma(\theta_i)}{\sigma(y)} \cdot b_i \tag{2.19}$$

2.2.2. Morris screening procedure

As mentioned before, for those outputs which cannot be accurately regressed linearly, the Morris screening procedure, whose steps are depicted in Figure 2.4, is here used instead of the MC procedure. As can be seen, the procedure consists first in assigning the input uncertainty. Afterwards, the number of levels into which the input space (p) needs to be divided is decided, and thus the optimal perturbation factor (Δ) can be identified according to Eqn. (2.20). On the basis of a predefined number of repetitions for the calculation of the elementary effects and of Δ, the sampling according to the procedure by Morris [35] is performed. The sampling matrix $\underline{\theta}$ is thus obtained. For each input sample a different model simulation is performed. The simulation outputs are then used to calculate the elementary effects (EEs) at specific input points according to Eqn. (2.21). The EEs are then standardized by using the standard deviations of the uncertain input (σ_{θ_i}) and the standard deviation of the output (σ_y) resulting from the Monte Carlo simulations according to Sin and Gernaey [36] (see Eqn. (2.22)). Mean and standard deviation of the standardized elementary effects (SEE) are then calculated. The ranking of the impact of the parameters on each output is performed by comparing the mean of the SEE of those parameters having a standard deviation lower than the standard error of the mean (SEM_i), which is calculated by dividing the standard deviation of the standardised elementary effect of a particular parameter by the squared root of the total number of points according to which the input space is split up (Eqn. (2.23)).

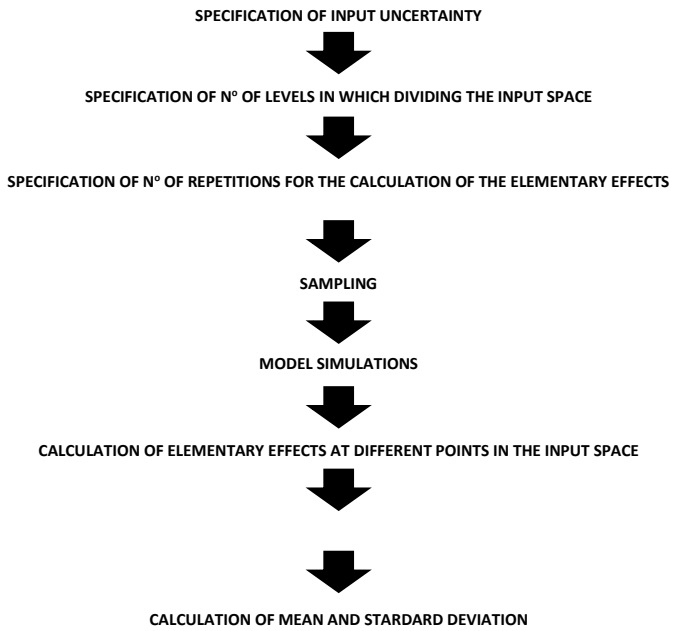

Figure 2.4: Stepwise procedure used for the sensitivity analysis according to the Morris screening procedure [35].

$$\Delta = \frac{p}{2 \cdot (p-1)} \tag{2.20}$$

$$EE_i^j = \frac{y\left(\theta_1^j, \theta_2^j, \dots\dots, \theta_i^j + \Delta_{OPT}, \dots\dots, \theta_{m-1}^j, \theta_m^j\right) - y(\underline{\theta}^j)}{\Delta} \tag{2.21}$$

$$SEE_i^j = EE_i^j \cdot \frac{\sigma_{\theta_i}}{\sigma_y} \tag{2.22}$$

$$SEM_i = \pm \frac{\sigma\left(SEE_i^j\right)}{\sqrt{r}} \tag{2.23}$$

CHAPTER 3
Model development

In this section, simulation models are developed with the purpose of providing a reference simulation environment where control strategies for the minimization of nitrous oxide emissions can be benchmarked. These benchmark simulation models (BSMs) will be developed on the basis of a previously established model, the Benchmark Simulation Model nº2 (BSM2) by Jeppsson *et al.* [22]. In particular, in order to include the N_2O production and emission dynamics, the BSM2 will be extended using three different mathematical models: the Activated Sludge Model for Greenhouse gases nº1 (ASMG1) by Guo and Vanrolleghem [37], the two-pathway model by Pocquet *et al.* [38] (2PM1) and the two-pathway model by Domingo-Felez *et al.* [39] (2PM2). The ASMG1 includes the N_2O production during HB and AOB denitrification processes, which have been suggested as the main N_2O production pathways in several full-scale measurement campaigns [17,40–42]. The other two models include the N_2O production by AOB both during denitrification and as a result of incomplete hydroxylamine oxidation. However, these two differ with respect to the modelling assumptions of the two pathways, which in turn can affect the overall dynamics of N_2O predicted. Resulting from their implementation, three new BSMs will be obtained respectively: the Benchmark Simulation Model nº2 for Nitrous oxide a (BSM2Na) with the ASMG1, the BSM2Nb with the 2PM1, and the BSM2Nc with the 2PM2. On each of these models, novel control strategies for N_2O emission minimization can be thoroughly tested and benchmarked against other control strategies. Having different BSMs incorporating different assumptions for the N_2O dynamics is a means to prove the robustness of a control strategy for N_2O emissions prior to its application in real plants. As a matter of fact, N_2O modelling has been shown to be affected by quite a large number of challenges and a consensus model has not been established yet. Some modelling approaches can be more representative of certain types of WWTPs whereas other approaches may show to be more suitable for other plants. Having a control strategy performing well for different N_2O modelling approaches can guarantee to a larger extent its successful performance when applied in reality.
In a second instance, with the aim of creating a benchmark simulation model where control strategies for novel treatment processes like the partial nitritation/Anammox (PN/A) could be tested and compared, the BSM2Na was extended by including a one-stage PN/A reactor treating the ammonium-rich water rejected from the dewatering unit. The Complete Autotrophic Nitrogen Removal model (CANRM) by Vangsgaard *et al.* [43] is used to the describe the biological and physical processes of this new unit. The PN/A treatment is increasingly in use [44] but development and testing control strategies aiming at its optimal operation have not frequently been developed and tested thoroughly.

This chapter is structured as follows:

- modification of the BSM2 default implementation prior to the extensions ,
- extension of the BSM2 with the ASMG1 by Guo and Vanrolleghem [37] (the BSM2Na),
- extension of the BSM2 with the 2PM1 by Pocquet *et al.* [38] (the BSM2Nb),
- extension of the BSM2 with the 2PM2 by Domingo-Felez *et al.* [39] (the BSM2Nc),
- extension of the BSM2Na with the CANRM by Vangsgaard *et al.* [43] (the BSM2NaPlusCANR),
- results and discussion of each extension.

Part of the results regarding the BSM2Na have been used and presented in Boiocchi *et al.* [45–47].

3.1 Modifications of the Benchmark Simulation Model nº2

3.1.1 Balancing the nitrogen cycle

Prior to being used, the Benchmark Simulation Model nº2 has been subjected to a review process to check the reliability of its default implementation. It emerged that the overall nitrogen balance was not closed. In particular, a fraction of the influent nitrogen was disappearing from the plant. The cause for this was the use of two different values for the nitrogen content in the biomass ($i_{N,XB}$) in the Activated Sludge Model nº1 (ASM1) and in the Anaerobic Digestion Model nº1 (ADM1). In particular in the ASM1 the value used was 0.086 g $N.g^{-1}$ COD whereas in the ADM1 it was 0.08 g $N.g^{-1}$ COD. Although the difference between the two parameters is not large, the high amount of biomass in the anaerobic digestion has made the discrepancy between N in the inlet and N in the outlet of plant noteworthy. $i_{N,XB}$ in the ADM1 was set to have the same value of the same parameter in the ASM1. Thus the nitrogen mass balance was able to be closed.

3.1.2 Modifications of the ASM1-to-ADM interface

As described previously, the BSM2 uses the interfacing method to map the state variables of the ASM1 into the ones of the ADM1 and vice versa. In the ASM1-to-ADM1 interface, the influent biomass was assumed to react first with available oxygen and secondly with nitrogen oxides (nitrate and nitrite nitrogen) to become carbon dioxide (CO_2). During its decay, all of its nitrogen content was assumed to become the soluble inorganic nitrogen (S_{NH}) of the ADM1. Such an assumption was taken in virtue of the fast rates of hydrolysis of particulate components and ammonification. The fact that the entire nitrogen contained in the biomass becomes ammonium was found not to be in line with the ASM1. As a matter of fact, there is a fraction of biomass which is not organic (i_{XP}) whose nitrogen ($i_{N,XP}$) cannot be easily converted into ammonium. Similarly, the original interface erroneously assumed that the entire COD content of the biomass could be oxidized into CO_2. These assumptions have been thoroughly corrected in the BSM2. Figure 3.1 shows the mapping of the biomass in the original BSM2 and in the corrected form. The corrections were performed in order to reproduce as closely as possible what happens during the transit of the wastage sludge from the secondary settler to the anaerobic digester, while at the same time conserving COD and nitrogen. There are two classes of biomass coming from the mainstream: autotrophic bacteria (X_{AB}) and heterotrophic bacteria (X_{HB}). In the interface, X_{AB} are assumed to decay instantaneously since the water has a very low content of their typical substrates, such as NH_4^+ and NO_2^-. Furthermore, the kinetics of these autotrophic microorganisms is quite slow. On the other hand, heterotrophic kinetics is much faster and their substrate, the biodegradable COD, can be more easily found in both the primary and the secondary sludge. Hence, in this case it was assumed that HB will grow on the available substrate by consuming first oxygen and secondly the available nitrogen oxides as electron acceptors, on the basis of the fact that consuming oxygen is more energy-efficient than consuming nitrogen oxides. If the soluble COD is not present, it is modelled that HB will use the slowly biodegradable organic matter (X_S) as substrate, assuming a fast hydrolysis of this type of material. Once the electron acceptors are depleted, also HB are modelled to decay. The first products of biomass decomposition are: (1) particulate organic nitrogen (X_{ND}), (2) particulate inert material (X_P), and (3) particulate organic material (X_S). X_S and X_{ND} are then mapped to form the particulate

components of the ADM1 like proteins (X_{pr}) first of all and, secondarily, carbohydrates (X_{ch}) and lipids (X_{li}). X_P is modelled, together with X_I, to become the X_I of the ADM1.

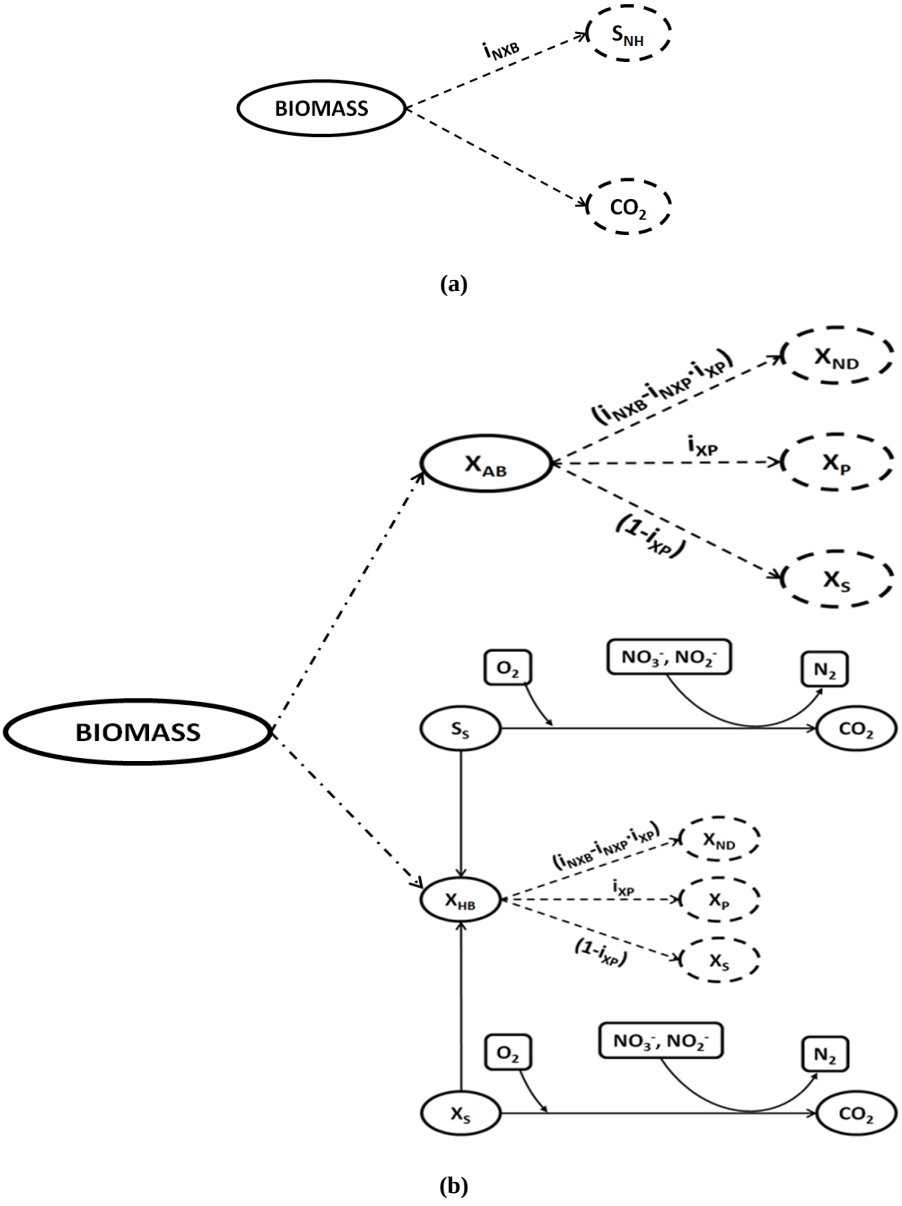

Figure 3.1: (a) biomass interfacing according to old BSM2**,** and **(b)** new interfacing of the biomass.

3.2 Inclusion of the Activated Sludge Model for Greenhouse gases no1 (ASMG1) – the BSM2Na

In this section, the inclusion of the Activated Sludge Model for Greenhouse gases nº1 (ASMG1) by Guo and Vanrolleghem [37] for the description of the biological processes in the activated sludge unit is presented.

3.2.1 The model

The model is an extension of the Activated Sludge Model nº1 (ASM1) by Henze *et al.* [30] with processes for the N_2O production by HB and AOB denitrification. A graphical representation of the main processes included is given in Figure 3.2 (CH_2O is the simplified chemical formula for the organic biodegradable substrate), whereas Tables (3.1-3.3) show their stoichiometry and kinetics. As can be seen, the ASM1 HB denitrification, modelled as one-step process, is replaced with the four-step HB denitrification by the Activated Sludge Model for Nitrogen (ASMN) developed by Hiatt and Grady [11]. More specifically, in the ASMN, the ASM1 reduction of nitrate and nitrite nitrogen to dinitrogen is split up into four sequential processes: (I) nitrate reduction to nitrite, (II) nitrite reduction to nitric oxide, (III) nitric oxide reduction to nitrous oxide, and (IV) nitrous oxide to dinitrogen. With regard to AOB denitrification, the model uses a modified version of the processes by Mampaey *et al.* [48]. In particular, AOB denitrification is modelled as a two-step process where nitrous oxide is produced as a result of enzymatic reduction of nitrite via nitric oxide during the oxidation of ammonium. A limited amount of oxygen is used as well because hydroxylamine (NH_2OH), obligatorily produced by AOB with oxygen, is the true substrate used during AOB denitrification. The function used to include the effect of the oxygen concentration on the rate is a Haldane-type kinetics (see Figure 3.3), where oxygen is enhancing AOB denitrification only for low concentrations (between 0 and 0.65 mg (-COD).L^{-1}) where the concentration of the substrate NH_2OH increases. At higher concentrations (above 0.65 mg (-COD).L^{-1}) AOB are modelled to be increasingly inhibited to use nitrite for the oxidation of NH_2OH; hence, oxygen has an inhibiting effect. AOB are assumed to grow during both their aerobic and their anoxic activity.

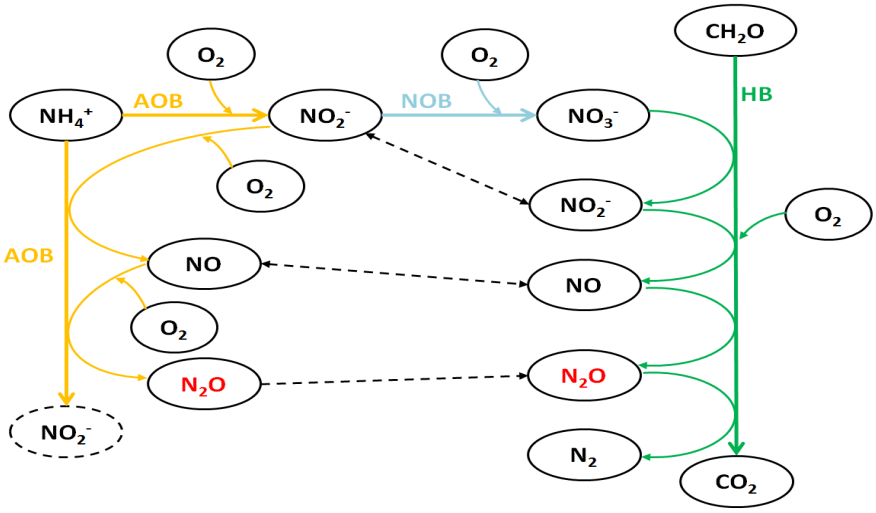

Figure 3.2: Main biological processes modelled in the ASMG1 by Guo and Vanrolleghem [37].

Table 3.1: **(a)** Stoichiometric matrix and **(b)** Kinetic vector for the AOB-mediated processes.

(a)

Stoichiometric matrix						
	S_{NHX}	S_{NO2}	S_{O2}	S_{NO}	S_{N2O}	X_{AOB}
Aerobic AOB growth	$-1/Y_{AOB}-i_{NXB}$	$1/Y_{AOB}$	$-(3.43-Y_{AOB})/Y_{AOB}$			1
Anoxic AOB growth on NO_2^-	$-1/Y_{AOB}-i_{NXB}$	$-1/Y_{AOB}$	$-(2.29-Y_{AOB})/Y_{AOB}$	$2/Y_{AOB}$		1
Anoxic AOB growth on NO	$-1/Y_{AOB}-i_{NXB}$	$1/Y_{AOB}$	$-(2.29-Y_{AOB})/Y_{AOB}$	$-2/Y_{AOB}$	$2/Y_{AOB}$	1

(b)

Kinetic vector	
Aerobic AOB growth	$\mu_{AOB,T} \cdot \frac{S_{O2}}{S_{O2}+K_{O2,AOB}} \cdot \frac{S_{FA}}{S_{FA}+K_{FA,AOB}+S_{FA}^2/K_{I9,FA}} \cdot \frac{K_{I9,FNA}}{K_{I9,FNA}+S_{FNA}} \cdot X_{AOB}$
Anoxic AOB growth on NO_2^-	$\mu_{AOB,T} \cdot \eta_{AnoxAOB} \cdot DO_{HaldaneFunc}{}^{*} \cdot \frac{S_{FA}}{S_{FA}+K_{FA,AOB}} \cdot \frac{S_{FNA}}{S_{FNA}+K_{FNA,AOB}} \cdot X_{AOB}$
Anoxic AOB growth on NO	$\mu_{AOB,T} \cdot \eta_{AnoxAOB} \cdot DO_{HaldaneFunc}{}^{*} \cdot \frac{S_{FA}}{S_{FA}+K_{FA,AOB}} \cdot \frac{S_{NO}}{S_{NO}+K_{NO,AOB}} \cdot X_{AOB}$

$$DO_{HaldaneFunc}{}^{*} = \frac{S_{O2}}{K_{SO2,AOBden} + \left(1 - 2 \cdot \sqrt{K_{SO2,AOBden}/K_{IO,AOBden}}\right) \cdot S_{O2} + S_{O2}{}^2/K_{IO,AOBden}}$$

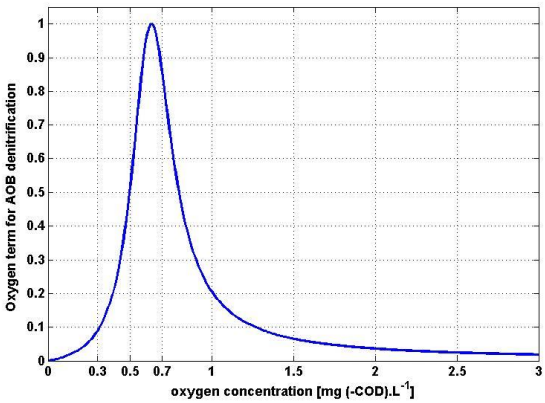

Figure 3.3: oxygen term for AOB denitrification by Guo and Vanrolleghem [37].

Table 3.2: **(a)** stoichiometric matrix and **(b)** kinetic vector for the NOB activity.

(a)

Stoichiometric matrix					
	S_{NHX}	***S_{NO2}***	***S_{O2}***	***S_{NO3}***	***X_{NOB}***
Aerobic NOB growth	$-i_{NXB}$	$-1/Y_{NOB}$	$-(1.14-Y_{NOB})/Y_{NOB}$	$1/Y_{NOB}$	1

(b)

Kinetic vector	
Aerobic NOB growth	$\mu_{NOB,T} \cdot \frac{S_{FNA}}{S_{FNA} + K_{FNA,NOB} + S_{FNA}^2/K_{I10,FNA}} \cdot \frac{S_{O2}}{S_{O2} + K_{O2,NOB}} \cdot \frac{K_{I10,FA}}{K_{I10,FA} + S_{FA}} \cdot X_{NOB}$

Table 3.3: **(a)** stoichiometric matrix and **(b)** kinetic vector for the HB-mediated processes.

(a)

Stoichiometric matrix								
	S_S	**S_{O2}**	**S_{NO3}**	**S_{NO2}**	**S_{NO}**	**S_{N2O}**	**S_{N2}**	**X_{HB}**
Aerobic HB growth	$-\frac{1}{Y_H}$	$\frac{1-Y_H}{Y_H}$						1
Anoxic HB growth on NO_3^-	$-\frac{1}{n_Y \cdot Y_H}$		-A	A				1
Anoxic HB growth on NO_2^-	$-\frac{1}{n_Y \cdot Y_H}$			-B	B			1
Anoxic HB growth on NO	$-\frac{1}{n_Y \cdot Y_H}$				-B	B		1
Anoxic HB growth on N_2O	$-\frac{1}{n_Y \cdot Y_H}$					-B	B	1

$$A = \frac{1 - Y_H \cdot n_Y}{1.143 \cdot Y_H \cdot n_Y}$$

$$B = \frac{1 - Y_H \cdot n_Y}{0.571 \cdot Y_H \cdot n_Y}$$

(b)

Kinetic vector	
Aerobic HB growth	$\mu_{HB,T} \cdot \frac{S_S}{S_S + K_{S1}} \cdot \frac{S_{O2}}{S_{O2} + K_{OH1}} \cdot \frac{S_{NH}}{S_{NH} + K_{NH,HB}} \cdot X_{HB}$
Anoxic HB growth on NO_3^-	$\mu_{HB,T} \cdot \eta_{AnoxHB,2} \cdot \frac{S_S}{S_S + K_{S2}} \cdot \frac{K_{OH2}}{S_{O2} + K_{OH2}} \cdot \frac{S_{NO3}}{S_{NO3} + K_{NO3}} \cdot X_{HB}$
Anoxic HB growth on NO_2^-	$\mu_{HB,T} \cdot \eta_{AnoxHB,3} \cdot \frac{S_S}{S_S + K_{S3}} \cdot \frac{K_{OH3}}{S_{O2} + K_{OH3}} \cdot \frac{S_{NO2}}{S_{NO2} + K_{NO2}} \cdot \frac{K_{I3,NO}}{K_{I3,NO} + S_{NO}} \cdot X_{HB}$
Anoxic HB growth on NO	$\mu_{HB,T} \cdot \eta_{AnoxHB,4} \cdot \frac{S_S}{S_S + K_{S4}} \cdot \frac{K_{OH4}}{S_{O2} + K_{OH4}} \cdot \frac{S_{NO}}{S_{NO} + K_{NO} + S_{NO}^2 / K_{I4NO}} \cdot X_{HB}$
Anoxic HB growth on N_2O	$\mu_{HB,T} \cdot \eta_{AnoxHB,5} \cdot \frac{S_S}{S_S + K_{S5}} \cdot \frac{K_{OH5}}{S_{O2} + K_{OH5}} \cdot \frac{S_{N2O}}{S_{N2O} + K_{N2O}} \cdot \frac{K_{I5,NO}}{K_{I5,NO} + S_{NO}} \cdot X_{HB}$

The model parameters were calibrated in order to have effluent concentration predictions similar to the ones given when the ASM1 is used. This was done because it is generally accepted in the literature that the ASM1 gives realistic predictions of the effluent quality. Additionally, it was assumed that the BSM2 with the ASMG1 would emit nitrous oxide according to an emission factor of 0.5% on the influent total nitrogen (TN) load [37]. The way the parameters have been calibrated makes the model parameters affected by strong uncertainties, especially the parameters related to the newly-introduced processes, i.e. AOB denitrification. The model can be considered to realistically predict the effluent concentrations of WWTPs and to reproduce - to some extent - correctly the dynamics of N_2O emissions with regards to different aeration regimes. However, the predicted amount of N_2O emitted has not to be taken as an absolute number, but more as a relative number for comparisons with different operation scenarios, which fits perfectly into the purpose of benchmarking control strategies.

3.2.2 Model Implementation

The model is used to describe the biological processes in the five biological tanks of the BSM2. Compared to the ASM1, the model splits S_{NOX} (i.e. the sum of NO_3^- and NO_2^-) into S_{NO3} and S_{NO2} and adds state variables like S_{NO}, S_{N2O} and S_{N2}. Furthermore, X_{AB} (i.e. the sum of AOB and NOB) is split up into X_{AOB} and X_{NOB}. The primary and secondary settler models were extended according to the new variables, assigning different dynamics according to whether the variable is soluble or particulate.

In the ASM-to-ADM interface, the nitrite, nitric oxide and nitrous oxide are used as electron acceptors for the anoxic oxidation of organic carbon, similarly to the ASM1 S_{NOX}. X_{AOB} and X_{NOB} are attributed the same fate as X_{AB}, i.e. they are assumed to decay instantaneously into X_{ND}, X_P and X_S and then to become part of the ADM1 proteins, lipids, and carbohydrates fractions.

As a result of this implementation and the extensions of the other treatment unit models, the BSM2Na is achieved.

3.3 Inclusion of the two-pathway model by Pocquet *et al.* [38] (2PM1) – the BSM2Nb

In this section, the inclusion of the two pathway model by Pocquet *et al.* [38] (2PM1) for the description of the biological processes in the activated sludge unit is presented.

3.3.1 The model

The model incorporates three main processes:

1) Aerobic AOB activity, where ammonium is oxidized into nitrite,
2) AOB denitrification, where nitrous oxide is produced as a result of nitrite reduction,
3) Incomplete hydroxylamine oxidation, where nitrous oxide is produced as a result of accumulation of NH_2OH oxidation intermediates.

Figure 3.4 shows how these three processes are modelled, whereas Table 3.4 shows their stoichiometry and kinetics. As can be seen, the aerobic AOB oxidation is modelled to occur according to three sequential steps: (I) aerobic oxidation of NH_4^+ to NH_2OH, (II) aerobic oxidation of NH_2OH to NO, and (III) aerobic oxidation of NO to NO_2^-. AOB are assumed to grow only during the second oxidation step. AOB denitrification is modelled as a one-step process where nitrite is directly reduced into N_2O during the oxidation of NH_2OH. This differs from the modelling of the same process according to the ASMG1, where AOB denitrification was modelled as a two-step process with NO as intermediate. It is thus assumed that the NO produced from nitrite reduction by AOB is quickly consumed subsequently for the production of N_2O. Furthermore, NH_2OH and not NH_4^+ is modelled as the substrate consumed. This is more in agreement with the biochemical observations, which show NH_2OH and not NH_4^+ as the true substrate used during AOB denitrification. Although the enhancing effect of NH_2OH accumulation on AOB denitrification is already taken into account with a usual Monod function, the oxygen function is still a Haldane function. By comparing the Haldane-type function for the oxygen used in the ASMG1 (see Figure 3.3) and the one used in the present model (see Figure 3.5), it can be noted that in both cases concentrations of oxygen between 0.5 mg (-COD).L^{-1} and 0.7 mg (-COD).L^{-1} are modelled as enhancing N_2O production by AOB denitrification. However, for oxygen concentrations higher than 0.7 mg (-COD).L^{-1}, AOB denitrification is more inhibited by oxygen in the ASMG1 than in the 2PM1. The N_2O production during incomplete NH_2OH oxidation is modelled as the oxidation of NH_2OH using the NO as electron acceptor. An accumulation of NO and/or NH_2OH due to incomplete NH_2OH oxidation can trigger this process. As no effect of oxygen is included in the rate of this process, the N_2O production according to this pathway can theoretically occur both in the aerobic and in the anoxic zone.

3.3.2 Model implementation

As can be noted, the model includes both the pathways according to which N_2O is known to be produced during AOB activity. However the model does not include the HB denitrification pathway. During the implementation in the BSM2 context, the HB denitrification by the ASMG1 is used. Similarly, all the other processes such as NOB activity, hydrolysis of entrapped organic nitrogen, hydrolysis of particulate organic substrate, ammonification and the decay of AOB, NOB and HB are used from the ASMG1.

As the model was calibrated using data obtained from a bioreactor operating at 27.9°C and a pH of 8.5, conversions of the free ammonia and the free nitrous acid half-saturation coefficient ($K_{FA,AOB}$ and $K_{FNA,AOB}$, respectively) were performed using the temperature and pH correlation summarized in Hiatt

and Grady [11]. Hence, the value of $K_{FA,AOB}$ was converted from 0.2 g $N.m^{-3}$ to 0.003 g $N.m^{-3}$, while the value of $K_{FNA,AOB}$ was converted from 0.004 g $N.m^{-3}$ to 0.178 g $N.m^{-3}$.

To the variables already included with the ASMG1, the model adds S_{NH2OH}. Primary and secondary settler models were updated to include the dynamics of this soluble component. With regard to its behaviour in the ASM-to-ADM interface, it was assumed that S_{NH2OH} would abiotically react with the NO_2^- leftover from HB denitrification to form N_2O. This last compound would then be added up to the S_{N2O} coming from the secondary settler and modelled to be consumed by HB according to the amount of organic biodegradable carbon available. If there is no NO_2^- leftover, NH_2OH is assumed to pass through the side-stream unchanged and is then partly recycled to the main stream.

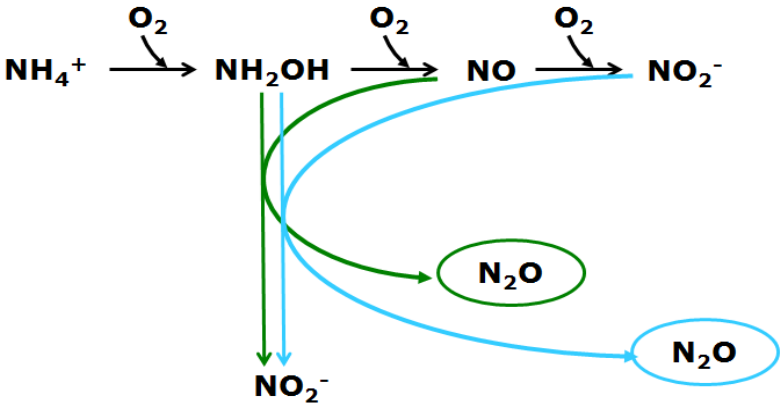

Figure 3.4: Processes modelled by Pocquet *et al.* [38] (2PM1).

Table 3.4: **(a)** Stoichiometric matrix and **(b)** kinetic vector describing the process model by Pocquet *et al.* [38].

(a)

Stoichiometric matrix							
	S_{NHX}	**S_{NH2OH}**	**S_{O2}**	**S_{NO2}**	**S_{NO}**	**S_{N2O}**	**X_{AOB}**
Aerobic oxidation of NH_X into NH_2OH	-1	1	-1.14				
Aerobic growth of AOB	$-i_{NXB}$	$-\frac{1}{Y_{AOB}}$	$-\frac{1.71-Y_{AOB}}{Y_{AOB}}$		$\frac{1}{Y_{AOB}}$		1
Aerobic oxidation of NO into NO_2^-			-0.571	1	-1		
N_2O production by Incomplete NH2OH oxidation		-1		1	-4	4	

N_2O production due to AOB denitrification		-1		-1		2	

(b)

Kinetic vector	
Aerobic oxidation of NH_X into NH_2OH	$\frac{\mu_{AOB,HAO}}{Y_{AOB}} \cdot \frac{S_{O2}}{S_{O2} + K_{O2,AOBAMO}} \cdot \frac{S_{FA}}{S_{FA} + K_{FA,AOB}} \cdot X_{AOB}$
Aerobic growth of AOB	$\mu_{AOB,HAO} \cdot \frac{S_{O2}}{S_{O2} + K_{O2,AOBHAO}} \cdot \frac{S_{NH2OH}}{S_{NH2OH} + K_{NH2OH,AOB}} \cdot X_{AOB}$
Aerobic oxidation of NO into NO_2^-	$\frac{\mu_{AOB,HAO}}{Y_{AOB}} \cdot \frac{S_{O2}}{S_{O2} + K_{O2,AOBHAO}} \cdot \frac{S_{NO}}{S_{NO} + K_{NO,AOBHAO}} \cdot X_{AOB}$
N_2O production via IncHydrOx	$\frac{\mu_{AOB,HAO}}{Y_{AOB}} \cdot \eta_{NN} \cdot \frac{S_{NH2OH}}{S_{NH2OH} + K_{NH2OH,AOB}} \cdot \frac{S_{NO}}{S_{NO} + K_{NO,AOBNN}} \cdot X_{AOB}$
N_2O production via AOBden	$\frac{\mu_{AOB,HAO}}{Y_{AOB}} \cdot \eta_{ND} \cdot \frac{S_{NH2OH}}{S_{NH2OH} + K_{NH2OH,AOB}} \cdot \frac{S_{FNA}}{S_{FNA} + K_{FNA,AOB}} \cdot DO_{HaldaneFunc}{}^{*} \cdot X_{AOB}$

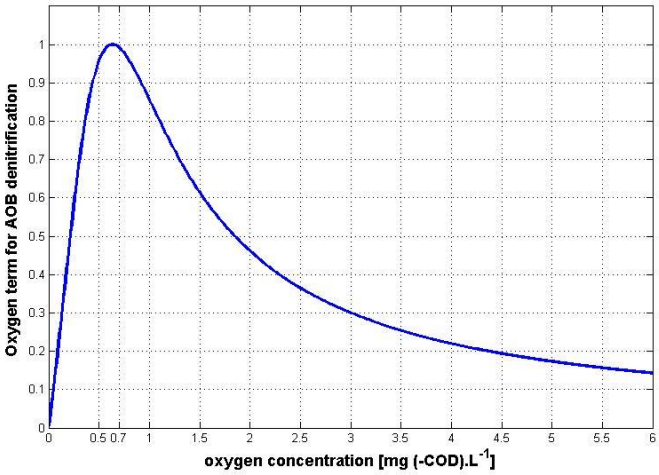

Figure 3.5: Haldane-type oxygen term for AOB denitrification by the 2PM1 [38].

3.4 Inclusion of the two-pathway model by Domingo-Felez *et al.* [39] (2PM2) – The BSM2Nc

3.4.1 The model

The model by Domingo-Felez *et al.* [39] includes the same processes as the 2PM1. However the modelling of these processes differs, as shown in Figure 3.6. More specifically, the aerobic activity of AOB is modelled as a two-step process, where only NH_2OH is the intermediate. There is however, in addition, the aerobic oxidation of NH_2OH to NO by AOB. AOB are modelled to grow during both the NH_2OH oxidation to NO_2^- and the NH_2OH oxidation to NO. This last compound is also produced as an intermediary component of the NO_2^- reduction to N_2O, i.e. AOB denitrification. This last pathway uses NH_2OH as substrate. As can be noted, there is essentially only one process which actually produces N_2O, namely the enzymatic reduction of NO, but there are two pathways from which this last compound is produced: (1) reduction of NO_2^- (i.e. AOB denitrification pathway), and (2) aerobic oxidation of NH_2OH (i.e. incomplete NH_2OH oxidation pathway). With regards to the kinetics used to model the rate of each process, it can be noted that, differently from the 2PM1, oxygen is assumed to only inhibit the AOB denitrification pathway. Table 3.5 shows the Petersen matrix of the processes modelled in the 2PM2.

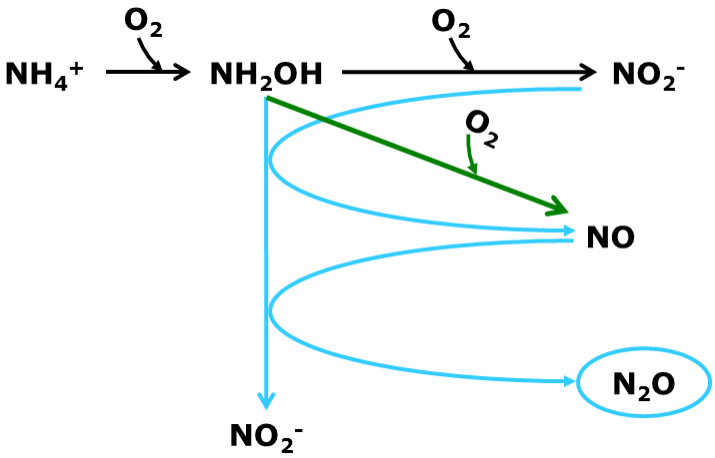

Figure 3.6: Processes modelled by Domingo-Felez *et al.* [39] (2PM2).

Table 3.5: Petersen matrix of the processes by Domingo-Felez et al. [39].

Stoichiometric matrix							
	S_{NHX}	S_{NH2OH}	S_{O2}	S_{NO2}	S_{NO}	S_{N2O}	X_{AOB}
Aerobic oxidation of NH_X into NH_2OH	-1	1	-1.14				
Aerobic growth of	$-i_{NXB}$	$-\frac{1}{Y_{AOB}}$	$-\frac{2.29 - Y_{AOB}}{Y_{AOB}}$	$\frac{1}{Y_{AOB}}$			1

AOB from NH_2OH to NO_2^-							
Aerobic grow of AOB from NH_2OH to NO	$-i_{NXB}$	$-\frac{1}{Y_{AOB}}$	$-\frac{0.57-Y_{AOB}}{Y_{AOB}}$		$\frac{1}{Y_{AOB}}$		1
AOB denitrification on NO_2^-		-1		-3	4		
AOB denitrification on NO		-1		1	-4	4	

Kinetic vector	
Aerobic oxidation of NH_X into NH_2OH	$\mu_{AOBAMO} \cdot \frac{S_{O2}}{S_{O2}+K_{O2,AOBAMO}} \cdot \frac{S_{NH}}{S_{NH}+K_{NH,AOBAMO}} \cdot X_{AOB}$
Aerobic growth of AOB from NH_2OH to NO_2^-	$\mu_{AOBHAO} \cdot (1-\eta_{NN}) \cdot \frac{S_{O2}}{S_{O2}+K_{O2,AOBHAO}} \cdot \frac{S_{NH2OH}}{S_{NH2OH}+K_{NH2OH,AOB}} \cdot X_{AOB}$
Aerobic grow of AOB from NH_2OH to NO	$\mu_{AOBHAO} \cdot \eta_{NN} \cdot \frac{S_{O2}}{S_{O2}+K_{O2,AOBHAO}} \cdot \frac{S_{NH2OH}}{S_{NH2OH}+K_{NH2OH,AOB}} \cdot X_{AOB}$
AOB denitrification on NO_2^-	$\mu_{AOBHAO} \cdot \eta_{ND} \cdot \frac{K_{IO,AOBden}}{K_{IO,AOBden}+S_{O2}} \cdot \frac{S_{NH2OH}}{S_{NH2OH}+K_{NH2OH,AOB}} \cdot \frac{S_{NO2}}{S_{NO2}+K_{NO2,AOB}} \cdot X_{AOB}$
AOB denitrification on NO	$\mu_{AOBHAO} \cdot \eta_{ND} \cdot \frac{S_{NH2OH}}{S_{NH2OH}+K_{NH2OH,AOB}} \cdot \frac{S_{NO}}{S_{NO}+K_{NO,AOB}} \cdot X_{AOB}$

3.4.2. Model Implementation

The implementation of the 2PM2 was performed according to the same procedure used for the 2PM1. In addition, the temperature dependency of the maximum specific growth rate of AOB (μ_{AOBHAO}) and on the maximum specific ammonium oxidation rate (μ_{AOBAMO}) was included by imposing the trends given by Hellinga *et al*. [49], taking into account that the model was calibrated for a reactor working at an operating temperature of 23ºC. Eqns. 3.1 and 3.2 show the variation of these two kinetic parameters in function of the temperature.

$$\mu_{AOBAMO}(T) = 4.38 \cdot 1.0947^{(T-23)} \quad (3.1)$$

$$\mu_{AOBHAO}(T) = 2.04 \cdot 1.0947^{(T-23)} \quad (3.2)$$

3.5 Inclusion of the Complete Autotrophic Nitrogen Removal

In this section, the inclusion of a new treatment unit at the end of the dewatering unit is described. As disclosed at the beginning of this chapter, a one-stage partial nitritation/Anammox (PN/A) reactor is used to reduce the amount of nitrogen recycled on top of the mainstream system. The model used to describe the physical and biological processes in this reactor is the Complete Autotrophic Nitrogen Removal model (CANRM) by Vangsgaard *et al.* [43]. This was done to allow plant-wide benchmarking and control strategies for this reactor, taken into account its increasing adoption to achieve more economically-efficient nitrogen removal [44]. The important feature to pay attention on when implementing this new treatment unit was the development of interfaces linking the state variables of the Activated Sludge Model framework, used in the dewatering unit, and the ones of the CANRM (and vice versa). The implementation is performed on the BSM2Na, namely the BSM2 extended with the ASMG1 as mathematical model for the mainstream. As a result, the BSM2NaPlusCANR, whose layout is shown in Figure 3.7, is obtained.

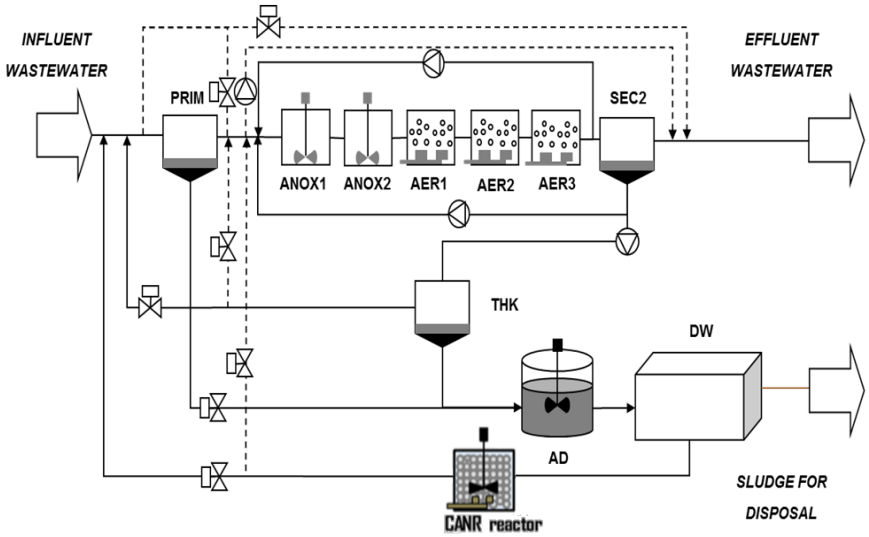

Figure 3.7: The BSM2NaPlusCANR layout.

3.5.1 CANR reactor model

The mathematical model employed describes a granular based single-stage PN/A reactor. The model developed and described in detail by Vangsgaard *et al.* [43] is shortly described here for the sake of completeness. It consists of mass balance equations for each soluble and particulate compound considered in the model. The main assumptions included are: (a) the transfer of soluble compounds within the granule occurs only by diffusion (Eqn. (3.3)) and (b) the transport of particulate compounds occurs only by advection (Eqn. (3.4)). The bulk of the reactor is assumed to be completely mixed, which results in Eqn. (3.5).

$$\frac{\partial S_i}{\partial t} = D_i \cdot \frac{1}{z^2} \cdot \frac{\partial}{\partial z}\left(z^2 \cdot \frac{\partial S_i}{\partial z}\right) + r_i \quad (3.3)$$

$$\frac{\partial X_i}{\partial t} = -\frac{\partial (X_i \cdot u_F)}{\partial z} + r_i \quad (3.4)$$

$$\frac{dC_i}{dt} = \frac{Q_{in} \cdot C_{i,in} - Q_{out} \cdot C_{i,bulk} - j_{bio,i} \cdot A_{bio}}{V} + r_i \quad (3.5)$$

In Eqns. (3.3-3.5) D_i is the diffusivity of compound i, z is the radial direction in spherical coordinates, S_i is the concentration of soluble compound i, r_i is the reaction rate for compound i, X_i is the concentration of particulate compound i, u_F is the biofilm net growth velocity, C_i is the concentration of generic compound i (it applies to both soluble and particulate compounds), Q_{in} and Q_{out} are the in- and outflow respectively, $j_{bio,i}$ is the flux in and out of the biofilm and V is the reactor volume. The reaction rate expression is deduced from the Petersen matrix reported in Vangsgaard *et al.* [43]. The model has 12 state variables, namely: AOB, AnAOB, NOB, HB, total ammonia nitrogen, total nitrite nitrogen, dissolved oxygen, nitrate, dinitrogen, readily biodegradable organic carbon, particulate organic material and particulate inert material. The modelled processes are: the growth and decay of AOB, NOB and AnAOB, the aerobic growth of HB and the anoxic growth of HB with both NO_2^- and with NO_3^- as electron acceptor, the decay of HB and the hydrolysis of organic suspended solids.

The PN/A reactor implemented in the BSM2 framework operates in continuous mode. The equipment of the reactor is represented in Figure 3.8. As can be seen, the reactor is modelled to have: (1) a mixer which guarantees perfect mixing of the bulk, (2) a heating jacket, which guarantees a constant temperature of 35ºC, and (3) a compressed air supplier. In addition to the temperature, also the pH is assumed to be ideally controller at 7.3.

Since the reactor was placed in a recycled stream, iterations were performed to know the right influent ammonium nitrogen to use for the calculation of the reactor volume. Using the value of 750 mg $N.L^{-1}.d^{-1}$, provided by Vangsgaard *et al.* [50], a volume of 400 m^3 for the one-stage PN/A reactor was identified as optimal. A nominal value of the oxygen mass transfer coefficient (k_La) of 164 d^{-1} was used according to the set point of the volumetric oxygen-to-ammonium loading rate (RO) equal to 1.66 g $O_2.g^{-1}$ N identified by Vangsgaard *et al.* [51].

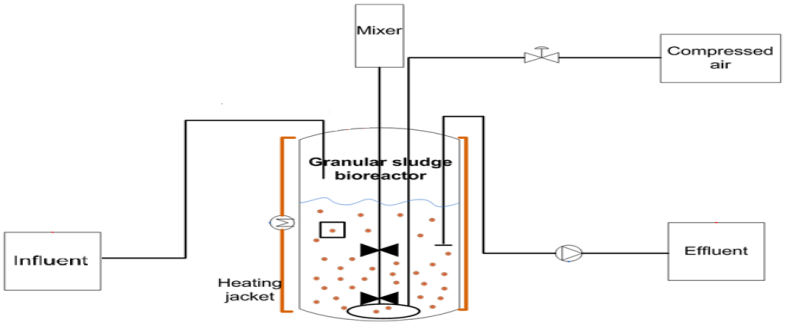

Figure 3.8: Reactor configuration for the CANR process [51].

3.5.2 Development of interfaces

Figure 3.9 shows how the interface linking the ASMG1 state variables (SVs) into the ones of the CARNM has been defined. The state variables in red are the ones added to the model. More in particular, X_{AnAOB} has been added to the pool of the ASMG1 SVs. Thus anaerobic AOB are allowed to build up in the mainstream activated sludge unit. A soluble inert component (S_I) was added as new state variable of the CANRM. The diffusivity used for this variable was the same as the one used for S_S, given the fact that both of them are soluble COD components. The alkalinity (S_{ALK}) was also added, defining its stoichiometry according to the ASM protocol, i.e. to close the electric charge balance of each process. With regard to the modelling of particulate inert components, the two models differ. In particular, in the ASMG1 framework there is a distinction between particulate inerts coming from the influent (X_I) and particulate inerts generated from biomass decay (X_P). This distinction is useful to track easily eventual phenomena of biomass decay. When, on the contrary, the two variables are merged together, the dynamics of one can be hindered by the dynamics of the other. In the CANRM this distinction was not made since the model was developed using a synthetic influent containing no particulate inerts. However, in full-scale real systems it is useful to keep the dynamics of the two components separated. Hence, the CANR model was added a so-called $X_{I,BIS}$, which would correspond to the X_I of ASMG1.

To be noted in addition is the fact that the CANRM does not contain organic nitrogen (soluble and particulate) as distinct state variables. However, in CANRM the particulate biodegradable COD component (X_S) has a nitrogen content whereas in the ASMG1 the same variable has no nitrogen content. This means that while in the ASMG1 X_{ND} and X_S are separately included, in the CARNM these two are now considered together. This difference in the state variables leads also to differences in the modelling of the biomass decay processes: in the CANRM the end products of biomass decay are X_S and X_P, whereas in the ASMG1 the end products are X_S, X_{ND} and X_P. To map the X_{ND} and X_S of the ASMG1 (from the dewatering unit) into X_S of CANRM, the loop described in Eqn. (3.4) was used.

$$\begin{cases} if\ X_{ND,ASMG1} \geq i_{N,XS,CANR} \cdot X_{S,ASMG1} \Rightarrow \begin{cases} X_{S,CANRM} = X_{S,ASMG1} \\ X_{ND,left} = X_{ND} - i_{N,XS,CANR} \cdot X_{S,ASMG1} \\ \Delta S_{S,CANRM} = 0 \\ \Delta S_{NH,CANRM} = X_{ND,left} \end{cases} \\ if\ X_{ND,ASMG1} < i_{N,XS,CANR} \cdot X_{S,ASMG1} \Rightarrow \begin{cases} X_{S,CANRM} = X_{ND}/i_{N,XS,CANRM} \\ X_{ND,left} = 0 \\ \Delta S_{S,CANRM} = X_{S,ASMG1} - X_{S,CANRM} \\ \Delta S_{NH,CANRM} = 0; \end{cases} \end{cases} \tag{3.4}$$

As can be seen, the amount of particulate organic nitrogen available is compared to the amount of nitrogen needed to merge all the X_S of the ASMG1 ($X_{S,ASMG1}$) into the X_S of the CANRM ($X_{S,CANRM}$). If this amount is enough, all the X_S of the ASMG1 is mapped as X_S of CANRM. If there is some particulate organic nitrogen left ($X_{ND,left}$), this is assumed to become ammonium assuming a fast hydrolysis and ammonification. In case the amount of particulate organic nitrogen is not enough, only the fraction of X_S equal to the ratio between X_{ND} and $i_{N,XS,CANR}$ (N content of $X_{S,CANRM}$) was mapped as the $X_{S,CANRM}$. The $X_{S,ASMG1}$ not mapped into $X_{S,CANRM}$ was assumed to become soluble organic carbon (S_S) of the CANRM, assuming fast hydrolysis.

The S_{ND} of the ASMG1 was modelled to become S_{NH} of CANRM, assuming a high ammonification rate.

With regard to the nitrogen oxides like nitric and nitrous oxide, following the approach by Volcke *et al.* [52], NO and N_2O were mapped into partially NO_2^- and partially N_2 by solving a system of two equations for the conservation of the COD and total nitrogen (see Eqns. (3.5) and (3.6) for NO and N_2O, respectively). However, this assumption does not have an effect on the results, since most of the times, these nitrogen components, originating from the last aerobic tank of the mainstream, are already depleted in the ASMG1-to-ADM1 interface.

$$\begin{cases} COD_{NO} = i_{NOtoNO2} \cdot COD_{NO2} + i_{NOtoN2} \cdot COD_{N2} \\ 1 = i_{NOtoNO2} + i_{NOtoN2} \end{cases} \tag{3.5}$$

$$\begin{cases} COD_{N2O} = i_{N2OtoNO2} \cdot COD_{NO2} + i_{N2OtoN2} \cdot COD_{N2} \\ 1 = i_{N2OtoNO2} + i_{N2OtoN2} \end{cases} \tag{3.6}$$

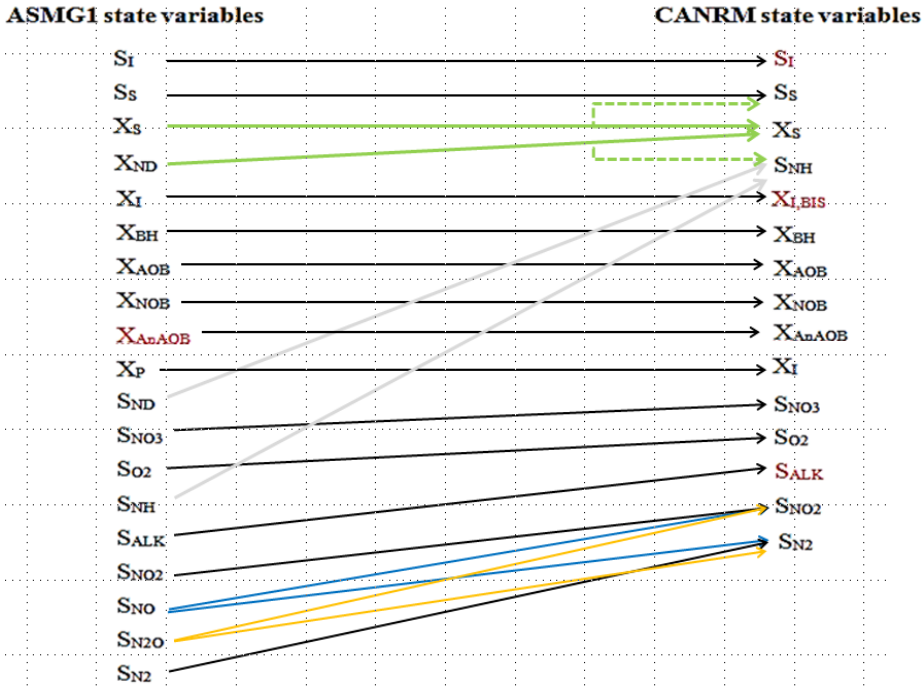

Figure 3.9: ASMG1-to-CANRM interface.

With regard to the interface linking the CANRM state variables to the ones of the ASMG1 (shown in Figure 3.10), the X_S of the ASMG1 was split up into X_{ND} and X_S of the ASMG1. Differently from what was proposed by Volcke *et al.* [52], the biomass was not modelled to decay, rather it was recycled unchanged to the mainstream.

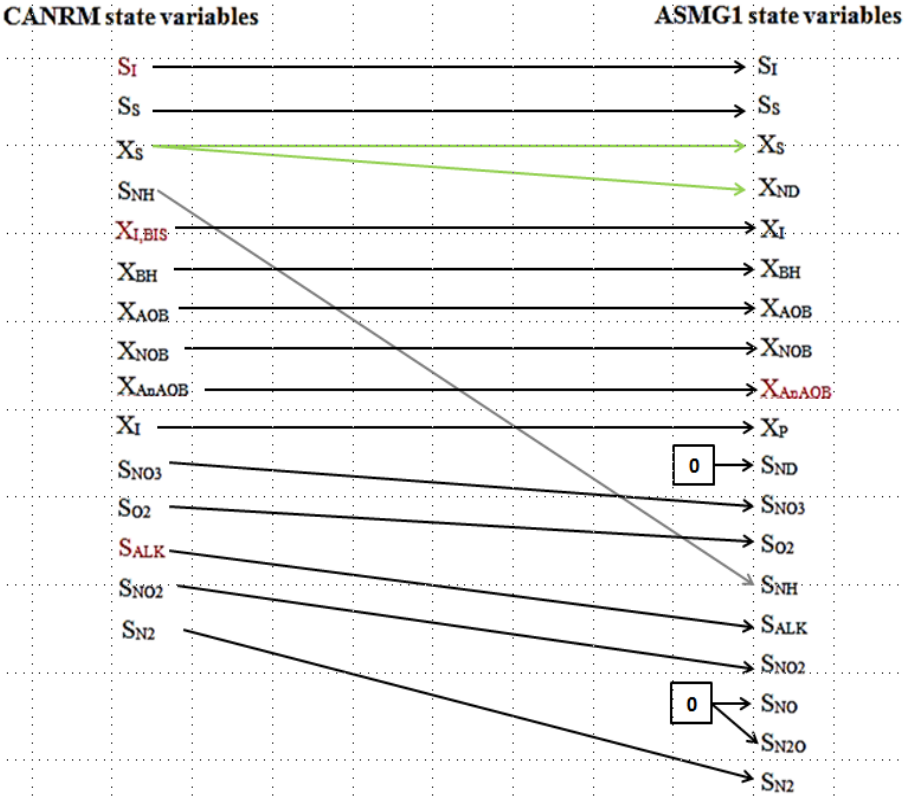

Figure 3.10: CANRM-to-ASMG1 interface.

3.6 Results and discussion

In this section, a comparison among the predictions given by the different models will be performed. In particular, the BSM2Na, BSM2Nb and BSM2Nc predictions in terms of both liquid and gaseous stream compositions are compared. In addition, a comparison between BSM2Na and BSM2NaPlusCANR is carried out to evaluate the advantages brought from the inclusion of the new PN/A reactor on a plant-wide basis.

For a more unbiased benchmarking of the results, steady-state simulations of the four BSMs are performed by controlling the oxygen concentration in three aerobic tanks at 1 mg (-COD).L^{-1}.

In the BSM2NaPlusCANR, the reject water from the dewatering unit was recycled to the activated sludge unit instead of the primary clarifier. This was in order not to waste the biomass formed during the PN/A processes by settling them in the primary clarifier. Thus potential improvements of the mainstream pollutant removal can be considered. For the sake of comparison, also the BSM2Na and the other BSMs had the water rejected from the dewatering unit recycled to the activated sludge unit.

3.6.1 Liquid concentrations predicted by the BSM2Na, BSM2b and BSM2c

Figure 3.11 shows the partition of the TN in the influent into the three main fluxes leaving the plant, namely the gaseous stream emitted from the activated sludge unit, the plant effluent and the sludge disposed. The values are expressed in percentage per unit of influent TN.

As can be seen, the three models predict the same amount of TN removed through sludge disposal (i.e. 16.5 % of the influent TN). With regard to the mainstream, the BSM2Nc, obtained by using the model by Domingo-Felez *et al.* [39], predict a higher conversion of nitrogen into gaseous components than the other two models, which predict the nitrogen conversion similarly. The reasons for these discrepancies have to be found in the kinetic parameters used to model the aerobic AOB activity, shown in Table 2. This is because all the other processes used are identical in the different models. The N_2O producing processes by AOB can only have a marginal effect on the effluent liquid concentrations. Although the parameters used in the BSM2Na are difficult to compare with the ones of the other two due to the fact that the aerobic AOB activity is modelled as a one-step process (whereas it is modelled as a two-step process in the other two models), a coarse comparison can still be made by considering the fact that most of the electrons of this process are exchanged during the oxidation of NH_2OH to NO_2^-. Furthermore, only during this process AOB are assumed to grow. Hence, this last process can be considered to have the most impact on the description of the AOB activity.

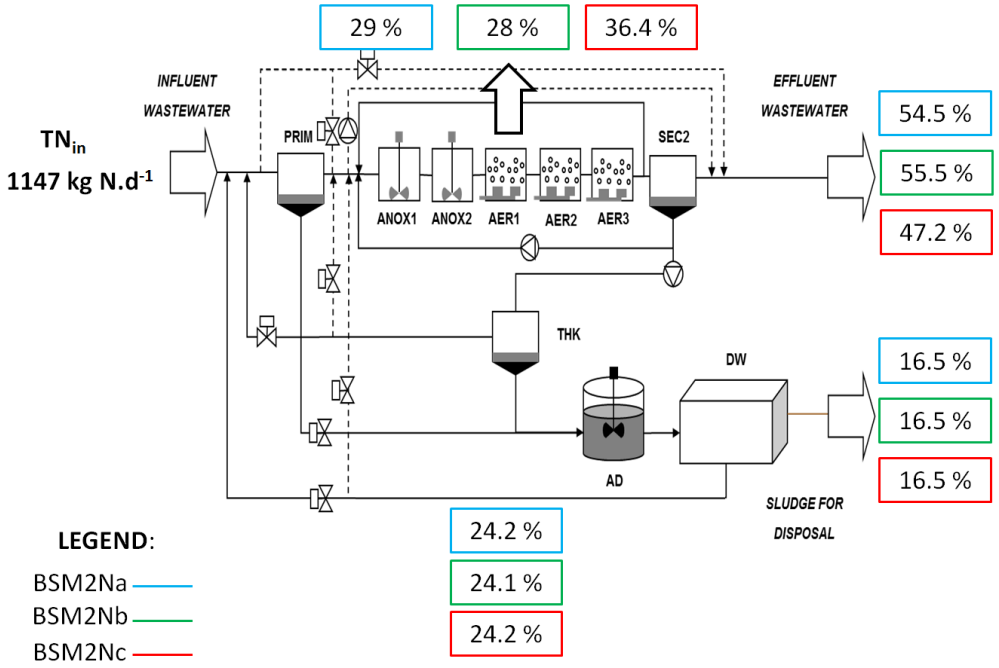

Figure 3.11: TN streams predicted by the BSM2Na (in light blue), BSM2Nb (in green) and BSM2Nc (in red) expressed as percentage of the influent TN.

As can be noted, the maximum specific growth rate of AOB is much higher in the BSM2Nc than in the other two models. Furthermore, the oxygen affinity constant for NH_2OH to NO_2^- used in the BSM2Nc is much lower. Finally, the free ammonia affinity constant used is largely lower in the BSM2Nc than the ones used by the other two BSMs. These modelling choices contribute significantly to speeding up the AOB oxidation process in the BSM2Nc, thus leading to lower TN in the effluent and more TN emitted.

Table 3.6: AOB activity model parameters.

Parameter	unit	**BSM2Na***	**BSM2Nb**	**BSM2Nc**
$\mu_{AOB,AMO}$ (20ºC)	d^{-1}	0.78	4.33	4.38
$\mu_{AOB,HAO}$ (20ºC)	d^{-1}		0.78	2.02
$K_{O,AOBAMO}$	g (-COD).m^{-3}	0.6	1	0.4
$K_{O,AOBHAO}$	g (-COD).m^{-3}		0.6	0.073
K_{FA}	g N.m^{-3}	0.004	0.003	0.00059
K_{NH2OH}	g N.m^{-3}		0.9	1

* The BSM2Na AOB activity is a one-step process.

3.6.2 Nitrous oxide predictions by the BSM2Na, BSM2Nb and BSM2Nc

Table 3.7a shows the emissions of N_2O predicted by the three benchmark simulation models. More specifically, emission factors per unit of influent TKN and per unit of TKN removed are used as indicators. Table 3.7b shows the N_2O produced according to the three different pathways, namely HB denitrification, AOB denitrification and incomplete NH_2OH oxidation. No distinction between N_2O produced by the two AOB pathways could be made for model BSM2Nc. The overall N_2O produced by the three BSMs is presented as well.

As can be noted, the BSM2Nb, using the model by Pocquet *et al.* [38], predicts the lowest emissions, whereas the other two models predict similar emissions. This occurs not only for the N_2O emissions per unit of influent TKN, but also per unit of removed TKN. By looking at the contributions by the different pathways, it emerges that the BSM2Nc has much higher N_2O production and consumption rates than the other models. However, when globally considered, the total N_2O production by BSM2Nc is similar to the one by BSM2Na. On the other side, the total N_2O production prediction by BSM2Nb is lower than predicted by the other two models. This explains the similarity in the emission factors between the BSM2Na and the BSM2Nc, and the dissimilarity with the prediction by the BSM2Nb. By looking at the contributions by the different pathways, it emerges that according to the BSM2Nb the contribution by AOB denitrification is quite low compared to the contribution by incomplete NH_2OH oxidation. The reason for this can be found in the kinetic parameters used to model AOB denitrification. As can be seen, the lower N_2O emissions by BSM2Nb can be attributed to a lower anoxic reduction factor (η_{ND}), which means that a lower percentage of total AOB are assumed to take part in the production of N_2O through denitrification. Furthermore, the affinity constant for free nitrous acid ($K_{FNA,AOB}$), which determines how the accumulation of nitrite enhances AOB denitrification, is much higher in the BSM2Nb than in the other models. This means that for the same amount of nitrite available, AOB denitrification will be slower in the BSM2Nb than in the other two BSMs. Despite the rather low value used for the reduction factor η_{NN}, the predicted contribution by the incomplete NH_2OH oxidation pathway is high. This has to be attributed to the large amount of HB-produced nitric oxide.

With regard to the heterotrophic contributions, the differences between the net N_2O production by HB cannot be ascribed to the different modelling approaches, which are indeed identical for the three BSMs, but to the different availability of AOB-produced N_2O. As a matter of fact, the highest N_2O consumption by HB occurs according to the BSM2Nc, where AOB are modelled to produce the largest amount of N_2O.

Finally, it is important to note that HB are always predicted to have a very small or negative contribution to the total N_2O emissions, while AOB are always the major N_2O producers. According to the BSM2Nb and BSM2Nc HB are found to be consuming part of the AOB-produced N_2O, while the BSM2Na predicts a positive but low contribution by HB on the total N_2O produced.

These preliminary results suggest that a control strategy for low N_2O emissions should be focusing on reducing the production of N_2O by AOB. More in-depth insights regarding the N_2O dynamics will be achieved through the sensitivity analyses described in Chapter 4.

Table 3.7: **(a)** Total N_2O emission per unit of influent TKN (N_2O emission factor 1), Total N_2O emission per unit of TKN removed (N_2O emission factor 2), and **(b)** net N_2O produced by HB, N_2O produced during AOB denitrification, N_2O produced during incomplete NH2OH oxidation, total N_2O produced by AOB, total N_2O produced predicted by the BSM2Na, BSM2Nb and BSM2Nc.

(a)

	unit	BSM2Na	BSM2Nb	BSM2Nc
N_2O emission factor 1	[% g $N_2O_{gas}.g^{-1}$ TKN_{in}]	0.0327	0.0174	0.0364
N_2O emission factor 2	[% g $N_2O_{gas}.g^{-1}$ TKN_{rem}]	0.033	0.018	0.037

(b)

		BSM2Na	BSM2Nb	BSM2Nc
N_2O net produced by HB	[g N_2O-N.d^{-1}]	94.56	-818.6	-13258.7
N_2O produced during AOB denitrification	[g N_2O-N.d^{-1}]	195.6	3.7	13486.6
N_2O produced during incomplete NH_2OH oxidation	[g N_2O-N.d^{-1}]	-	974.1	
Total N_2O produced by AOB	[g N_2O-N.d^{-1}]	195.6	977.8	13486.6
Total N_2O produced	[g N_2O-N.d^{-1}]	290.16	159.2	227.9

3.6.3 Comparison between predictions by the BSM2Na and predictions by the BSM2NaPlusCANR

Liquid predictions

In this section, the impact of the inclusion of the CANR reactor on the effluent quality is evaluated by comparing the steady-state results of the BSM2Na and the steady-state results of the BSM2NaPlusCANR achieved by controlling the oxygen concentration in the aerobic zone of the mainstream activated sludge unit at 1 mg (-COD).L^{-1}. Figure 3.12 reports the percentage per unit of influent TN of the nitrogen streams from the different outlets and the TN recycled to the mainstream activated sludge unit. Table 3.8 shows details on the main effluent nitrogen species (NH_4^+, NO_2^-, NO_3^-, N_2) in terms of both concentration and percentage with respect to the influent total nitrogen and the effluent biodegradable COD concentration (sum of S_S and X_S). The ratio between biodegradable COD and nitrate nitrogen in the influent to the first anoxic tank is presented as well.

As can be seen from Figure 3.12, the total amount of influent TN converted into nitrogen gas and subsequently stripped to the atmosphere increased from 29% to 40.5% through the inclusion of the new treatment unit. Furthermore, the TN recycled to the mainstream is reduced by approximately 22% through the inclusion of the new side-stream reactor. This affects the amount of nitrate produced by NOB in the mainstream. Consequently, the amount of NO_3^- reduced by heterotrophs in the anoxic zone is larger since the ratio between COD and nitrogen – influent to the anoxic zone - is drastically increased. This in turn leads to the drastic lowering of the effluent NO_3^- concentration and, hence, of the effluent total nitrogen from 54.5% to 40.9% of the TN (see Table 3.8b). As more influent COD is oxidized aerobically than anoxically, less biodegradable COD is found in the effluent (see Table 3.8a).

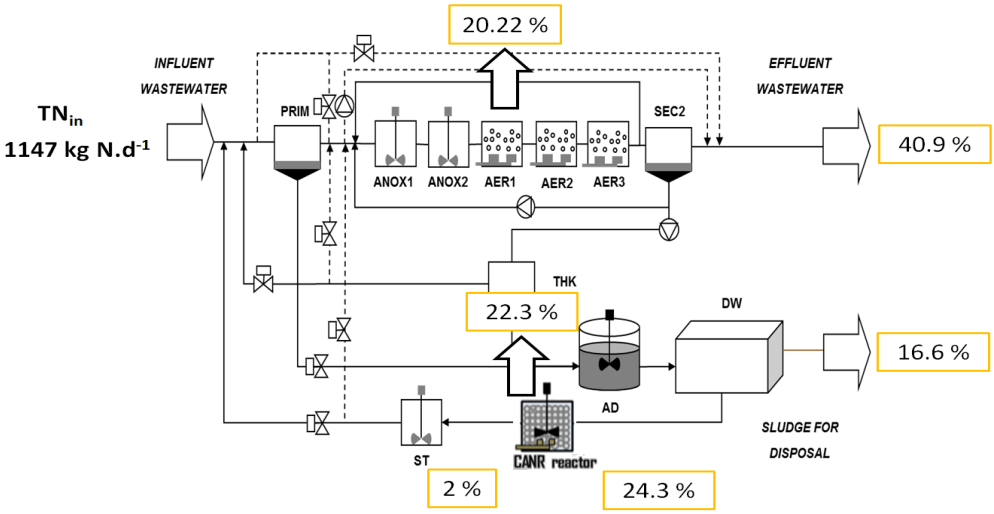

Figure 3.12: TN streams predicted by the BSM2NaPlusCANR.

Table 3.8: (a) Effluent concentrations of NH_4^+, NO_2^-, NO_3^-, biodegradable COD (sum of S_S and X_S) and TN predicted by the BSM2Na and BSM2NaPlusCANR

(a)

	$\left.\frac{COD_{biodeg}}{NO_3^- - N}\right\|_{in,AS}$	**Effluent variables**				
		NH_4^+	**NO_2^-**	**NO_3^-**	**TN**	**COD_{biodeg}**
Unit	g COD.g^{-1} N	g N.m^{-3}	g N.m^{-3}	g N.m^{-3}	g N.m^{-3}	g COD.m^{-3}
BSM2Na	7.5	0.13	0.00047	15	30.3	1.1
BSM2NaPlusCANR	15.5	0.1	0.00048	7.4	22.7	0.92

(b)

	Effluent variables				
	NH_4^+	**NO_2^-**	**NO_3^-**	**N_2**	**TN**
Unit	[% g N.g^{-1} TN_{in}]				
BSM2Na	0.24	0	27	24.1	54.5
BSM2NaPlusCANR	0.18	0	13.4	24.1	40.9

Nitrous oxide emission predictions in the mainstream

In this subsection, the impact on the nitrous oxide emissions from the mainstream due to the inclusion of the new reactor is investigated. Since the CANR model does not include any N_2O emissions, this study is limited only to seeing how much N_2O is emitted per unit of TN influent to the activated sludge unit ($TN_{in,AS}$). Extensions of the CANR model including N_2O production and emission dynamics should be carried out with the aim of evaluating globally the impact of the inclusion of the PN/A treatment unit on the total N_2O emissions.

Table 3.9 shows the steady-state amount of N_2O emitted from the five biological tanks in the mainstream per unit of TN influent to the first anoxic tank (ANOX1), predicted by the BSM2Na and the BSM2NaPlusCANR by controlling the oxygen concentrations in AER1, AER2 and AER3 at 1 mg (-COD).L^{-1}. As can be noted, the amount of N_2O emitted per unit of $TN_{in,AS}$ is sensibly reduced by including the new PN/A treatment unit (approximately 48%). As can be noted by looking at the N_2O production rates by HB and AOB per unit of influent TN, the production of N_2O by both HB and AOB drops down significantly as the new treatment unit is included. The reduction of the N_2O production by HB can be attributed to the fact that the COD-to-NO_3^- ratio of the influent to the anoxic zone, shown in Table 4, is largely increased with the inclusion of the new treatment unit, which allows a more complete heterotrophic denitrification. Furthermore, as can be noted from Table 3.9, the control system infers lower oxygen mass transfer coefficients for the aerobic zone when the new unit is included. This is thanks to the fact that, to obtain the same concentration of oxygen, less air needs to be supplied when a lower TN is fed in the reactor. The lower oxygen mass transfer coefficient leads to less N_2O stripping capability, which increases the residence time of the N_2O produced in the liquid phase and thus its possibility to be reduced into N_2 by HB. More relevant than the drop of N_2O production by HB (around 55%) is the one by AOB (around 63%). This can be attributed to the general lower presence of AOB in the system due to lower substrate, which decreases the AOB denitrification kinetics.

Table 3.9: steady-state TN load of the influent to the activated sludge unit, oxygen mass transfer coefficients of the three aerobic tanks, N_2O specific production rates by HB and AOB, and N_2O emitted per unit of TN_{inAS}.

	TN influent to AS	**Oxygen mass transfer coefficients**			**N_2O prod. rate by HB per unit of $TN_{in,AS}$**	**N_2O prod. rate by AOB per unit of $TN_{in,AS}$**	**N_2O emitted**
Unit	kg $N_{in,AS}.d^{-1}$	[d^{-1}]			[g N_2O-N.g^{-1} TN]	[g N_2O-N.g^{-1} TN]	[% g N_2O_{gas}-N.g^{-1} TN_{inAS}]
BSM2Na	$3.9 \cdot 10^4$	179.4	88.8	53.6	$2.43 \cdot 10^{-6}$	$5.02 \cdot 10^{-6}$	$7.51 \cdot 10^{-4}$
BSM2NaPlusCANR	$3.82 \cdot 10^4$	151.83	73.8	52.8	$1.1 \cdot 10^{-6}$	$1.85 \cdot 10^{-6}$	$3.91 \cdot 10^{-4}$
		AER1	*AER2*	*AER3*			

Oxygen consumption

In this subsection, the steady-state oxygen consumptions by the different microorganisms predicted by the BSM2Na and the BSM2NaPlusCANR with the oxygen concentration in the aerobic zone controlled at 1 mg (-COD).L^{-1} are compared with each other. Table 3.10 shows the total oxygen consumed, the percentages of oxygen taken up by the three different classes of microorganisms (HB, AOB and NOB) and the amount of oxygen consumed per unit of total nitrogen removed. As can be noted, the total amount of oxygen consumed decreases by about 29.3% when the PN/A reactor is included. With regard to the partition of oxygen consumed among the three classes of microorganisms, the lower the oxygen consumed by the autotrophic biomass, the higher is the oxygen consumption by HB when the new treatment unit is included. This is because, as less nitrogen is fed in the activated sludge unit, less nitrogen oxides are produced by the autotrophic biomass. This means that less organic carbon will be oxidized in the anoxic zone. A higher amount of organic biodegradable carbon will then be fed to the aerobic zone, thus triggering the oxygen consumption by HB. With regard to the amount of oxygen consumed per unit of TN removed, a drastic decrease can be observed when the new treatment unit is included, which proves the economical convenience of including side-stream PN/A reactors.

Table 3.10: Comparison between BSM2Na and BSM2NaPlusCANR configurations at steady-state: total oxygen consumption, partition of oxygen consumption among HB, AOB and NOB, specific amount of oxygen consumed (i.e. per unit of TN removed).

	OXYGEN CONSUMPTIONS				
	Total	**HB**	**AOB**	**NOB**	**Specific**
Unit	kg $O_2.d^{-1}$	[%]			kg $O_2.kg^{-1}$ N_{rem}
BSM2Na	8774.2	39.5	45.6	14.9	12.7
BSM2NaPlusCANR	6197.6	47.1	39.3	13.6	7.3

3.7 Conclusions

In conclusion, four different benchmark simulation models are made available. This way, testing of control strategies for N_2O emission minimization can be benchmarked against each other. While the simulation results obtained with the BSM2Na and BSM2Nc showed similar results suggesting AOB denitrification as the main N_2O producing pathway, the BSM2Nb has the incomplete-NH_2OH-oxidation process are the main N_2O producing pathway. Although this may look like a contradiction, the diversity in the predictions can be exploited, at this stage of research, for a more unbiased testing of future control strategies for N_2O emission mitigation. Nevertheless, for the future research, one of these model structures should be calibrated according to full-scale plant measurements at the aim of having the most reliable N_2O emission predictions.

CHAPTER 4
Understanding the N_2O formation mechanisms through sensitivity analyses using a benchmark plant-wide simulation model

4.1 Introduction

With the aim of reducing the carbon footprint of WWTPs, control strategies minimizing the emissions of this gas have to be developed, and understanding the main biological mechanisms responsible for N_2O production in the WWTP is essential. Performing sensitivity analyses (SAs) on a model describing the N_2O dynamics typically occurring in WWTPs can represent an efficient tool to capture these mechanisms. The ASMG1 was build up by extending the previously-developed Activated Sludge Model nº1 (ASM1) by Henze *et al.* [30] with processes for the production of N_2O by ammonia-oxidising and heterotrophic bacteria (AOB and HB, respectively). During the extension, the model parameters were calibrated by fitting the liquid concentrations predicted to the ones by the ASM1. Since the ASM1 is well-known to predict realistically the effluent concentrations of WWTPs [53,54], the ASMG1 can therefore be considered to reliably describe typical WWTP effluent concentrations while contextually incorporating most of the N_2O dynamics. However, the parameters of the ASMG1, and especially those describing the N_2O producing processes by HB and AOB, are affected by strong uncertainties. The latter necessitate using proper uncertainty analysis methods to make statistical inferences about model predictions [34].

The platform in which the model will be used is provided by the Benchmark Simulation Model nº2 (BSM2), developed by Jeppsson *et al.* [22]. The BSM2 is a simulation environment where plant performance at different operating conditions can be evaluated and compared with one another in an unbiased way. It represents a typical full-scale WWTP with a pre-denitrification configuration for the main stream and with a side stream for wastage sludge treatment. The ASMG1 is used here to describe the biological processes occurring in the main stream biological unit of this configuration.

During this work, to help understanding the complex mechanisms responsible for N_2O emissions, first a sensitivity analysis is carried out by systematically changing operating conditions such as the oxygen mass transfer coefficients (k_La) and the influent ammonium (NH_4^+) concentration. A second sensitivity analysis at key operational points is then performed by considering a wide range of model parameter uncertainties in order to verify and improve the insights obtained from the first sensitivity analysis. Thus the biological mechanisms responsible for N_2O emissions are elucidated independently from the model parameter uncertainties. Both the analyses will investigate the potential occurrence of changes in the mechanisms determining N_2O emissions as a function of seasonal variations since there are evidences suggesting significant variations in the quantities of N_2O emitted with operating temperature [55].

In addition to this, taking into account that controlling N_2O has to be performed in such a way that the effluent respects discharge limits, the sensitivity analyses mentioned before will also be carried out on the total nitrogen removal efficiency (η_{TN}) as output.

Finally, also the sensitivity to process parameters of the oxygen consumptions by the different microorganisms will be analysed.

4.2 Material and methods

In this section, the two sensitivity analyses are presented. The first will be to investigate the effect of operating conditions (subsection 4.2.1), while the second will investigate the effect of model parameter uncertainties (subsection 4.2.2) according to two procedures: the Monte Carlo procedure and the Morris screening procedure.

4.2.1. Sensitivity analysis for operating conditions

As disclosed in the introduction, the first sensitivity analysis is carried out by perturbing operating conditions as follows: the oxygen mass transfer coefficients of the three aerobic reactors (k_La_{AER}) and the influent ammonium concentration are varied between a lower and an upper boundary. In particular, the k_La_{AER} is varied between a minimal value of 5 d^{-1} and a maximal value of 360 d^{-1}, using a fixed interval of 5 d^{-1}, whereas the influent ammonium concentration was varied between a minimum value of 5 mg $N.L^{-1}$ and a maximum value of 70 mg $N.L^{-1}$, with a fixed interval of 5 mg $N.L^{-1}$. Full-factorial combinations between k_La_{AER} and NH_4^+ form the k_La_{AER}-NH_4^+ samples. For the sake of simplicity the same value of k_La_{AER} was here used for the three aerobic tanks. The k_La_{AER}-NH_4^+ samples identified are then used for steady-state simulations of the BSM2Na.

4.2.2. Sensitivity analysis for parameter uncertainties

Based on the fact that the ASMG1 parameter values are affected by variably-strong uncertainties, the observations from the first sensitivity analysis are attempted to be verified and improved through a secondary sensitivity analysis investigating the propagation of the model parameter uncertainties to the predicted outputs. In this regard, two different sensitivity analysis methods will be used: the Monte Carlo (MC) procedure and the Morris Screening (MS) procedure, which were presented in Section 2.2.

Parameter uncertainties

For both the Monte Carlo and the Morris screening sampling, following the examples by Sin *et al.* [34] and Vangsgaard *et al.* [43], the ASMG1 parameters are ranked according to the following uncertainty classes:

- CLASS 1: 5% uncertainty,
- CLASS 2: 25% uncertainty,
- CLASS 3: 50% uncertainty,
- CLASS 4: 100% uncertainty.

More in detail, yield coefficients for the different microbial groups and the half-saturation coefficient for hydrolysis of slowly-biodegradable organics (X_S) are assigned to CLASS 1; decay coefficients, N contents, maximal specific growth rates and reduction factors are assigned to CLASS 2; all the half-saturation coefficients are assigned to CLASS 3 apart from the parameters related to AOB denitrification to which the CLASS 4 uncertainty is given. Higher uncertainty is assigned to the parameters related to AOB denitrification in virtue of the fact that these parameters are related to newly-introduced processes, whose modelling is still subject to much higher uncertainties than the parameters related to the other processes coming from the better-established Activated Sludge Model for Nitrogen

(AMSN) by Hiatt and Grady [11]. Table 4.1 summarizes the assignment of uncertainty classes to each ASMG1 parameter.

Table 4.1: Uncertainty classes for the ASMG1 parameters grouped according to the processes that are described.

Parameters	Description	Default value at 15oC	Unit	CLASS
Aerobic AOB activity				
$\mathbf{Y_{A1}}$	growth yield of AOB	0.18	g COD_{BIO}.g-1 N	1
$\mathbf{\mu_{A1}}$	maximum specific growth rate of AOB	0.58	d-1	2
$\mathbf{K_{FA}}$	NH_3 half saturation parameter for aerobic AOB activity	0.004	g N.m-3	3
$\mathbf{K_{O,AOB}}$	O_2 half-saturation constant for AOB activity	0.6	g (-COD).m-3	3
$\mathbf{K_{I9,FA}}$	NH_3 inhibition constant for AOB activity	1	g N.m-3	3
$\mathbf{K_{I9,FNA}}$	HNO_2 inhibition constant for AOB activity	0.1	g N.m-3	3
$\mathbf{b_{A1}}$	decay coefficient of AOB	0.028	d-1	2
NOB activity				
$\mathbf{Y_{A2}}$	growth yield of NOB	0.06	g COD_{BIO}.g-1 N	1
$\mathbf{\mu_{A2}}$	maximum specific growth rate of NOB	0.68	d-1	2
$\mathbf{K_{O,NOB}}$	O_2 half-saturation constant for NOB activity	1.2	g (-COD).m-3	3
$\mathbf{K_{I10,FA}}$	NH_3 inhibition constant for NOB activity	0.5	g N.m-3	3
$\mathbf{K_{I10,FNA}}$	HNO_2 inhibition constant for NOB activity	0.1	g N.m-3	3
$\mathbf{K_{FNA}}$	HNO_2 half saturation parameter for NOB activity	10-6	g N.m-3	3
$\mathbf{b_{A2}}$	decay coefficient of NOB	0.028	d-1	2
Aerobic HB activity				
$\mathbf{Y_H}$	growth yield of HB	0.6	g COD_{BIO}.g-1 COD	1
$\mathbf{\mu_H}$	maximum specific growth rate of HB	4.78	d-1	2
$\mathbf{K_{S1}}$	S_S half-saturation coefficient for aerobic HB activity	15	g COD.m-3	3
$\mathbf{K_{OH1}}$	O_2 half saturation coefficient for aerobic HB activity	0.2	g (-COD).m-3	3
$\mathbf{b_H}$	decay coefficient of HB	0.3	d-1	2
HB denitrification				
$\mathbf{n_Y}$	anoxic reduction factor for HB yield	0.9	[-]	1
$\mathbf{K_{I3,NO}}$	NO inhibition constant of for HB-mediated NO_2- reduction	0.5	g N.m-3	3
$\mathbf{K_{I4,NO}}$	NO inhibition constant of for HB-mediated NO reduction	0.3	g N.m-3	3
$\mathbf{K_{I5,NO}}$	NO inhibition constant of for HB-mediated N_2O reduction	0.2	g N.m-3	3
$\mathbf{K_{N2O}}$	N_2O half-saturation for HB-mediated N_2O reduction	0.02	g N.m-3	3
$\mathbf{K_{NO}}$	NO half-saturation for HB-mediated NO reduction	0.04	g N.m-3	3
$\mathbf{K_{NO2}}$	NO_2- half-saturation for HB-mediated NO_2- reduction	0.3	g N.m-3	3
$\mathbf{K_{NO3}}$	NO_3- half-saturation for HB-mediated NO_3- reduction	1.5	g N.m-3	3
$\mathbf{K_{S2}}$	S_S inhibition coefficient for HB-mediated NO_3- reduction	20	g COD.m-3	3
$\mathbf{K_{S3}}$	S_S inhibition coefficient for HB-mediated NO_3- reduction	20	g COD.m-3	3
$\mathbf{K_{S4}}$	S_S inhibition coefficient for HB-mediated NO reduction	20	g COD.m-3	3
$\mathbf{n_{g2}}$	reduction factor for HB anoxic growth on NO_3-	0.3	[-]	2
$\mathbf{n_{g3}}$	reduction factor for HB anoxic growth on NO_2-	0.3	[-]	2
$\mathbf{n_{g4}}$	reduction factor for HB anoxic growth on NO	0.6	[-]	2
$\mathbf{n_{g5}}$	reduction factor for HB anoxic growth on N_2O	0.8	[-]	2
$\mathbf{K_{S5}}$	S_S inhibition coefficient for HB-mediated N_2O reduction	30	g COD.m-3	3
$\mathbf{K_{OH2}}$	O_2 inhibition coefficient for HB-mediated NO_3- reduction	0.2	g (-COD).m-3	3
$\mathbf{K_{OH3}}$	O_2 inhibition coefficient for HB-mediated NO_2- reduction	0.2	g (-COD).m-3	3
$\mathbf{K_{OH4}}$	O_2 inhibition coefficient for HB-mediated NO reduction	0.2	g (-COD).m-3	3
$\mathbf{K_{OH5}}$	O_2 inhibition coefficient for HB-mediated N_2O reduction	0.2	g (-COD).m-3	3
Hydrolysis of particulate organics				
$\mathbf{k_h}$	maximum specific hydrolysis rate	2.89	g COD.g-1 COD_{BIO}	2
$\mathbf{n_h}$	reduction factor for hydrolysis	0.8	[-]	2
$\mathbf{K_{OH}}$	O_2 half-saturation coefficient for hydrolysis	0.2	g (-COD).m-3	3
$\mathbf{K_X}$	Half-saturation coefficient for hydrolysis of X_S	0.1	g COD.m-3	1

Ammonification				
k_a	Rate constant for ammonification	0.07	m3. g-1 COD_{BIO}.d-1	3
AOB denitrification				
$K_{SNO,AOB}$	NO half saturation coefficient for AOB-mediated NO reduction	1	g N.m-3	4
$K_{SO,AOBden1}$	O_2 half saturation coefficient for AOB-mediated NO_2- reduction	11.4	g (-COD).m-3	4
$K_{IO,AOBden1}$	O_2 inhibition coefficient for AOB-mediated NO_2- reduction	0.0351	g (-COD).m-3	4
$K_{SO,AOBden2}$	O_2 half saturation coefficient for AOB-mediated NO reduction	11.4	g (-COD).m-3	4
$K_{IO,AOBden2}$	O_2 inhibition coefficient for AOB-mediated NO reduction	0.0351	g (-COD).m-3	4
n_{AOB}	reduction factor for AOB growth on NO_2-/NO	0.5	[-]	4
$K_{FNA,AOB}$	HNO_2 half saturation coefficient for AOB-mediated NO_2- reduction	6·10-4	g N.m-3	4
$K_{FA,AOB}$	NH_3 half saturation coefficient for AOB-mediated NO_2- and NO reduction	0.0027	g N.m-3	4
AnAOB activity				
Y_{AnAOB}	growth yield of AnAOB	0.16	g COD_{BIO}.g-1 N	1
μ_{AnAOB}	maximum specific growth rate of AnAOB	0.0173	d-1	2
$K_{NH3,AnAOB}$	NH_3 half saturation coefficient for AnAOB activity	0.0012	g N.m-3	3
$K_{HNO2,AnAOB}$	HNO_2 half saturation coefficient for AnAOB activity	2.81·10-6	g N.m-3	3
$K_{O2,AnAOB}$	O_2 inhibition coefficient for AnAOB activity	0.01	g (-COD).m-3	3
b_{AnAOB}	decay coefficient of AnAOB	6.19·10-4	d-1	2
Other parameters				
f_P	fraction of X_P generated from biomass decay	0.08	g COD_{XP}.g-1 COD_{BIO}	3
i_{XB}	N content in biomass	0.086	g N.g-1 (COD)	2
i_{XP}	N content in X_P	0.06	g N.g-1 (COD)	2

Monte Carlo and Morris screening samplings

For the LHS, a number of samples equal to 250 is chosen and no correlation between the parameters was taken into account. For the Morris sampling, the number of levels (*p*) in which the parameter space is split up was 8 and the number of points in the parameter space at which the elementary effects are to be calculated was decided to be 15. Given that the uncertain parameters are 61, a number of samples equal to 930 resulted for the Morris Screening analysis.

4.2.3. Performing simulations for the sensitivity analyses

For both the sensitivity analysis investigating the effect of operating conditions and the one investigating the effect of parameter uncertainties, steady-state simulations were performed by controlling the concentration of total suspended solids (TSSs) in the last aerobic tank (AER3) at a set point of 4000 mg (TSS).L^{-1} by manipulating the wastage flow rate. The sludge wastage is carried directly from AER3 to the thickener in the side stream. Furthermore, in order to check the effect of operating temperature on the biological mechanisms determining the TN removal efficiency and the N_2O emissions, additional sets of simulations were performed by setting the operating temperature in the biological system not only to 15ºC, but also to 10ºC and 20ºC. Thus mechanisms determining N_2O emissions, η_{TN} and oxygen consumptions in typical winter, autumn/spring and summer are investigated. For the sensitivity analysis investigating the effect of parameter uncertainties on the model predictions (i.e. Monte Carlo and Morris screening analyses), also the oxygen concentration in the three aerobic tanks is controlled at four key set points, identified according to the function describing the oxygen influence on the AOB denitrification process rate, depicted in Figure 4.1. The reason for this is that AOB have been extensively reported to be the most important contributors to the total N_2O emitted [42,56–59]. By plotting the Haldane function describing the direct correlation between AOB denitrification and oxygen in Figure 4.1, it appears clearly that small variations of oxygen can make a

huge difference on the rate of AOB denitrification rate and, consequently, on the N_2O emissions. The four oxygen set points were chosen as follows:

- 0.3 mg (-COD).L^{-1}, where oxygen has an enhancing effect,
- 0.65 mg (-COD).L^{-1}, where oxygen is maximizing the function,
- 1 mg (-COD).L^{-1}, where oxygen has a moderately-inhibiting effect, and
- 2 mg (-COD).L^{-1}, where oxygen has a strong inhibiting effect.

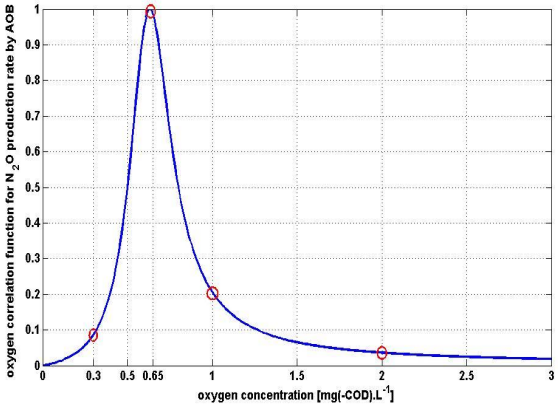

Figure 4.1: oxygen correlation function for the N_2O production rate by AOB.

Figure 4.2 shows the configuration of the BSM2Na used during the steady-state simulations for the SA investigating the propagation of ASMG1 parameter uncertainties on the predictions. As can be seen, the configuration is implemented with different Proportional Integral (PI) controllers: three oxygen concentration controllers for the three aerated tanks, which manipulate the respective oxygen mass transfer coefficients, and the TSS controller in AER3, which manipulates the wastage flow rate (Q_W). The configuration of the BSM2Na used during the steady-state simulations for the SA investigating the operating conditions is the same but without the three oxygen controllers. Table 4.2 summarizes the scenarios for the sensitivity analysis that was performed.

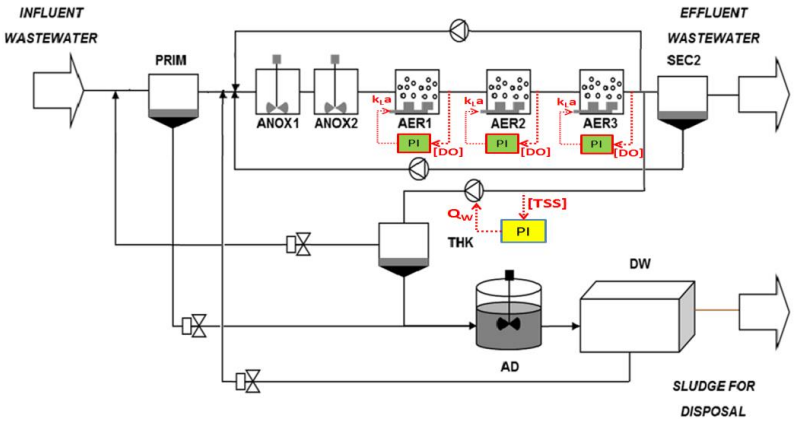

Figure 4.2: BSM2Na used during steady-state simulations for sensitivity analyses investigating ASMG1 parameter uncertainties.

Table 4.2: Scenarios of sensitivity analyses performed.

scenario	SENSITIVITY ANALYSIS	PLANT CONFIGURATION
1	PERTURBATION OF OPERATING CONDITIONS (FULL-FACTORIAL)	TSS CONTROL
2a	PERTURBATION OF MODEL PARAMETERS THROUGH MONTE CARLO REGRESSION PROCEDURE	OXYGEN AND TSS CONTROL
2b	PERTURBATION OF MODEL PARAMETERS THROUGH MORRIS SCREENING PROCEDURE	OXYGEN AND TSS CONTROL

4.3 Results and discussion

4.3.1 The total nitrogen removal efficiency

Sensitivity analysis perturbing the operating conditions

The TN removal efficiency resulting from the sensitivity analysis regarding the operating conditions is plotted against the influent oxygen-to-total-Kjeldahl-nitrogen ratio (RO) in Figure 4.3. RO is a parameter indicating the amount of oxygen supplied versus the amount of Total Kjeldahl Nitrogen (TKN) in the influent to the activated sludge unit, calculated according to Eqn. (4.1). This ratio was also used by Vangsgaard *et al.* [43] and typically indicates the aeration regime of the treatment plant.

$$RO = \frac{k_L a_{AER} \cdot V_{AER} \cdot \left(3 \cdot S_{O2,SAT} - S_{O2,AER1} - S_{O2,AER2} - S_{O2,AER3}\right)}{Q_{inAS} \cdot \left(S_{ND,inAS} + X_{ND,inAS} + S_{NH,inAS}\right)} \quad (4.1)$$

In Eqn. (4.1):

- k_La_{AER} is the oxygen mass transfer coefficient, equal for the three aerobic tanks,
- V_{AER} is the volume of one of the three tanks, corresponding to 3000 m3,
- $S_{O2,SAT}$ is the oxygen saturation concentration,
- $S_{O2,AER1}$, $S_{O2,AER2}$ and $S_{O2,AER3}$ are the oxygen concentrations in AER1, AER2 and AER3 respectively,
- Q_{inAS} is the inlet flow rate fed to top of the first anoxic tank (ANOX1),
- $S_{ND,inAS}$ is the inlet soluble organic nitrogen fed to ANOX1,
- $X_{ND,inAS}$ is the inlet particulate organic nitrogen fed to ANOX1,
- $S_{NH,inAS}$ is the inlet ammonium nitrogen fed to ANOX1.

As can be noted from Figure 4.3, independently from the operating temperature the TN removal efficiency increases with the increase of RO until a maximal value, after which it decreases with a rather scattered behaviour according to the amount of NH_4^+ in the influent. In particular, as the influent NH_4^+ increases, the decrease of η_{TN} gets steeper. The trend found suggests that for all the three temperatures there is a value for RO ($RO_{maxTNrem}$) at which the analysed output variable is maximized. In particular, as can be seen from Figures 4.4a and 4.4b depicting respectively the activity rates of AOB and NOB in the aerobic tanks, for values of RO lower than $RO_{maxTNrem}$ the NOB activity is at zero whereas AOB activity gradually grows up as RO increases. By looking at the removal efficiency of nitrogen oxides (namely, the sum of NO_3^- and NO_2^-) in the anoxic zone depicted in Figure 4.4c, for values of RO lower than $RO_{maxTNrem}$ HB denitrification works at its maximal efficiency since oxygen is not found in an inhibiting concentration. Furthermore, considering that influent NH_4^+ is converted into NO_2^- and not into NO_3^-, the NO_2^- reduction route for HB denitrification is followed rather than the NO_3^- reduction one, which requires a smaller amount of organic biodegradable carbon [49]. When RO is higher than $RO_{maxTNrem}$, NOB start growing. Due to the fact that HB denitrification requires more organic biodegradable carbon for the NO_3^- reduction route, the TN removal efficiency starts decreasing. As the amount of oxygen supplied per unit of TKN fed grows further, HB denitrification is more and more inhibited by the oxygen carried into the anoxic zone through the internal recycle. Hence, the removal efficiency drops significantly. As a result of HB denitrification inhibition, more organic carbon is oxidized by consuming oxygen. This leads to the higher HB activity shown in Figure 4.4d. The extra amount of oxygen consumed by HB for the oxidation of organic carbon is subtracted from AOB and NOB, whose activity rates decreases.

As can be additionally noted, the value of $RO_{maxTNrem}$ sensibly increases as the operating temperature increases. This means that, as temperature increases, for the same amount of TKN fed in the system, more oxygen is needed to maximize the TN removal efficiency. This is ascribed to the higher amount of oxygen consumed via endogenous respiration of biomass.

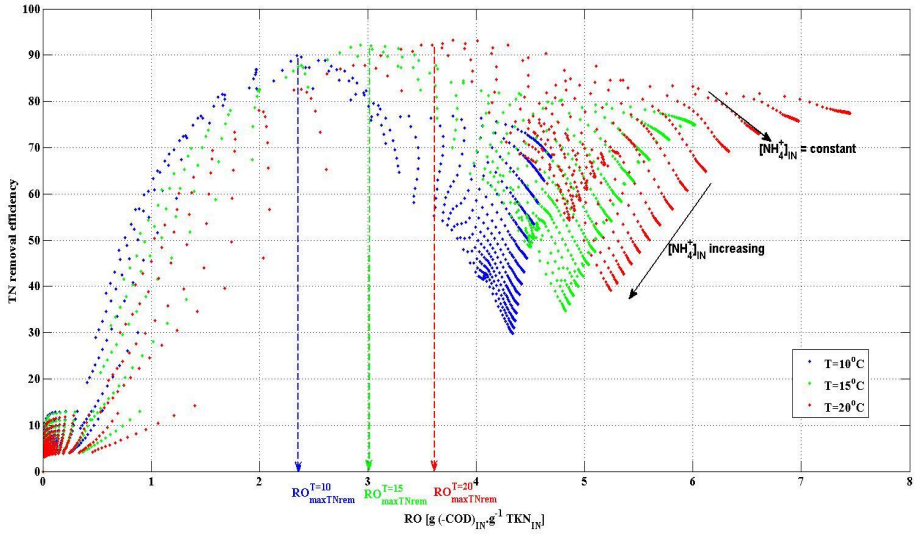

Figure 4.3: TN removal efficiencies in function of influent oxygen-to-total-Kjeldahl-nitrogen ratio (RO) at temperatures of 10ºC, 15ºC and 20ºC.

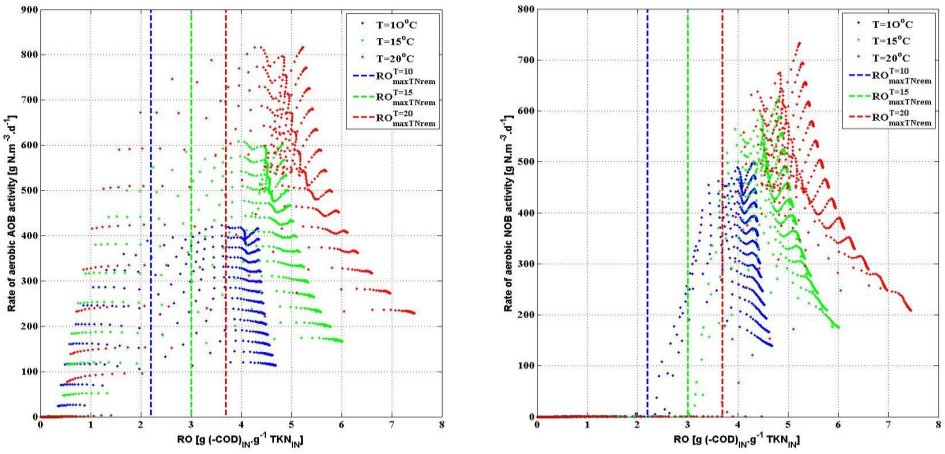

(a) **(b)**

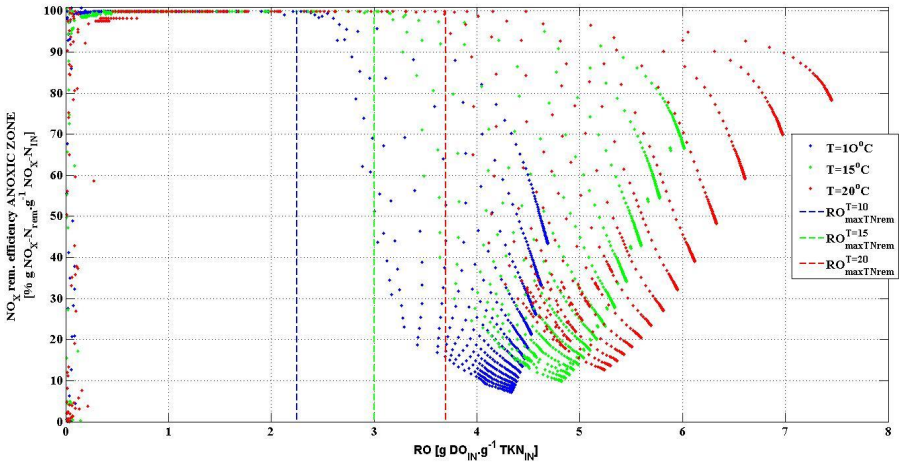

(c)

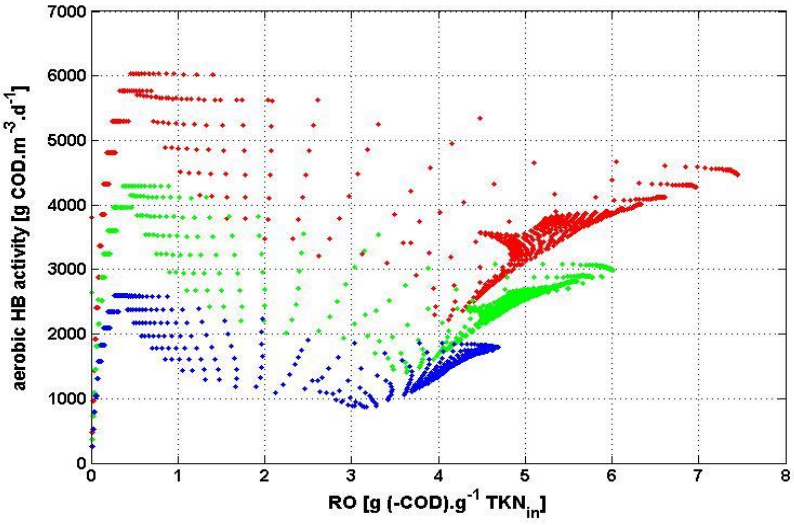

(d)

Figure 4.4: (a) AOB rates in the aerobic zone, **(b)** NOB rates in the aerobic zone, **(c)** nitrogen oxide removal efficiency in the anoxic zone, and **(d)** aerobic HB activity in the aerobic zone in function of influent oxygen-to-Total-Kjeldahl-Nitrogen ratio (RO) at temperatures of 10ºC, 15ºC and 20ºC.

Sensitivity analysis perturbing model parameters

As aforementioned, the presented biological mechanisms determining η_{TN} can change according to the parameter values of the ASMG1. Hence, the results of the sensitivity analysis investigating the impact of the parameter uncertainties on the model predictions are here considered. Table 4.3 shows a summary of the uncertainties of the TN removal efficiency at the different oxygen concentration set points in the aerobic zone (0.3, 0.65, 1 and 2 mg (-COD).L^{-1}) and at the three different temperatures (10, 15 and

20ºC). The sensitivities of the output variable analysed at these operating conditions with respect to the ASMG1 parameters, obtained according to the MC procedure, are represented in Table 4.4. ASMG1 parameters that have a standardized regression coefficient (β_i) value equal or higher than 0.1 are considered to have a significant impact on η_{TN}. The sensitivity of the outputs was analysed also according to the MS procedure and the results were similar. In Table 4.4 the parameters are reported in a decreasing order of importance, which is defined by the absolute value of β_i. The effect of the parameter on η_{TN} is given by the sign within the brackets: a positive sign means that an increase of the parameter value would increase the prediction of η_{TN} whereas a negative sign means that an increase of the parameter value would decrease the prediction of η_{TN}.

As can be noted from the ratio between standard deviation and mean value at all the operating conditions presented in Table 4.3, the propagation of parameter uncertainties on the predicted TN removal efficiency is low. η_{TN} increases as the temperature increases, since all the processes are generally sped up by temperature. On the other side, as oxygen increases, the removal of TN decreases, except for the case of winter temperatures where a slight increase of oxygen concentration from 0.3 to 0.65 mg (-COD).L^{-1} results in an improvement of the removal efficiency.

By looking the at Table 4.4, the main processes found to be affecting the TN removal efficiency are: (a) aerobic AOB activity, (b) NOB activity, (c) HB denitrification, and (d) anoxic hydrolysis of entrapped organics (X_S). In particular, the aerobic AOB activity has a positive effect, since it is the only process which converts the influent ammonium into a form of nitrogen which can be subsequently reduced into nitrogen gas. NOB activity has a negative effect, since it forces HB denitrification to work according to the NO_3^- reduction route. HB denitrification has a positive effect, since it improves the reduction of AOB and/or NOB -produced nitrogen oxides into nitrogen gas. Similarly, the anoxic hydrolysis of entrapped organics has an enhancing effect on η_{TN}, since it increases the availability of readily-biodegradable organic carbon to be used as electron donor during the nitrogen oxide reduction by HB.

As can be further observed, the relevance of the rates of these processes varies in function of operating oxygen concentrations and temperatures. In particular, for the DO concentration equal to 0.3 mg (-COD).L^{-1} at winter temperatures the parameters describing the rate of AOB activity are the most influencing ones whereas at other temperatures the parameters describing the rate of NOB activity emerge as the most influencing. This indicates that AOB activity is more limited by oxygen at lower temperatures. On the contrary, at higher temperatures NOB activity is more determining the TN removal efficiency. By looking at the parameters that are most affecting η_{TN} at other oxygen concentration set points, it can be noted that, independently from the temperatures, the most influencing processes switch from autotrophic activity to anoxic hydrolysis of entrapped organics (X_S) and HB denitrification. It is in this case evident that an increase of oxygen concentration in the aerobic zone enhances NOB activity while gradually limiting the anoxic hydrolysis of particulate organic carbon and heterotrophic denitrification via inhibition.

The responsible biological mechanisms found through the sensitivity analysis investigating the impact of operating conditions on the TN removal efficiency have been thus consolidated. However, the second sensitivity analysis has also showed that the TN removal efficiency in winter can be rather low due to the low AOB activity. Furthermore, the same sensitivity analysis showed, in addition to the previous one, the anoxic hydrolysis of X_S as limiting process for the complete reduction of nitrogen oxides in the anoxic zone, indicating that it is mainly the lack of organic biodegradable carbon availability which causes the TN removal efficiency to drop.

Table 4.3: mean (μ), standard deviation (σ) and ratio between them (σ/μ) for TN removal efficiency at oxygen concentrations in the aerobic zone of 0.3, 0.65, 1 and 2 mg (-COD).L^{-1} and at temperatures of 10, 15 and 20ºC.

			DO [mg (-COD).L-1]			
			0.3	**0.65**	**1**	**2**
η_{TN} [% g $TN_{rem}.g^{-1}$ TN_{IN}]	**T=10ºC**	**μ**	57.34	61.83	59.01	55.84
		σ	31.09	7.07	5	4.63
		σ/μ	0.54	0.11	0.08	0.08
	T=15ºC	**μ**	76.85	68.79	66.2	63.56
		σ	10.86	6.03	4.81	4.76
		σ/μ	0.14	0.09	0.07	0.08
	T=20ºC	**μ**	82.08	73.98	71.7	69.77
		σ	8.59	5.02	4.23	4.2
		σ/μ	0.10	0.7	0.06	0.06

Table 4.4: sensitivity analysis results with regard to the ASMG1 parameters for TN removal efficiency at oxygen concentrations in the aerobic zone of 0.3, 0.65, 1 and 2 mg (-COD).L^{-1} and at temperatures of 10, 15 and 20ºC.

		DO [mg (-COD).L^{-1}]			
		0.3	**0.65**	**1**	**2**
η_{TN}	**T=10ºC**	K_{OA1} (-), μ_{A1} (+), K_{OA2} (+), Y_{A1} (+), Y_H (-), i_{XP} (+).	n_h (+), K_{OA2} (+), n_Y (-), μ_{A2} (-), Y_H (-), μ_{A1} (+), K_{OA1} (-), $K_{FNA,AOB}$ (-), K_{NO2} (-), n_{AOB} (+), K_{NO3} (-).	n_h (+), n_Y (-), Y_H (-), k_h (+), K_{OA2} (+), K_{NO3} (-), μ_{A2} (-), K_{S1} (+), K_{NO2} (-), K_{S3} (-), μ_{A1} (+), b_H (+), K_{OA1} (-), n_{g3} (+), i_{XP} (+).	n_h (+), n_Y (-), Y_H (-), k_h (+), b_H (+), K_{S1} (+), K_{NO3} (-), i_{XB} (-), K_{S3} (-), K_{OA1} (-), i_{XP} (+), K_{OH1} (+).
	T=15ºC	K_{OA2} (+), μ_{A2} (-), b_{A2} (+), μ_{A1} (+), K_{OA1} (-), n_h (+), K_{S3} (-), K_{N2O} (-).	n_h (+), K_{OA2} (+), n_Y (-), μ_{A2} (-), Y_H (-), K_{NO3} (-), k_h (+), μ_{A1} (+), $K_{FNA,AOB}$ (-), K_{OA1} (-), K_{NO2} (-), μ_H (+), i_{XP} (+), n_{AOB} (+).	n_h (+), n_Y (-), k_h (+), Y_H (-), K_{NO3} (-), K_{OA2} (+), μ_{A2} (-), i_{XP} (+), K_{S1} (+), K_{S3} (-), i_{XB} (-), n_{g3} (+), K_{N2O} (-), K_{NO2} (-).	n_h (+), n_Y (-), Y_H (-), k_h (+), K_{NO3} (-), K_{S1} (+), i_{XB} (-), i_{XP} (+), K_{OA1} (-), K_{S3} (-), K_{OH1} (+), K_{I4NO} (+).
	T=20ºC	K_{OA2} (+), μ_{A2} (-), b_{A2} (+), K_{OA1} (-), μ_{A1} (+), k_h (+), n_h (+).	K_{OA2} (+), n_h (+), μ_{A2} (-), k_h (+), n_Y (-), K_{NO3} (-), b_{A2} (+), i_{XB} (-), K_{OA1} (-), n_{AOB} (+).	n_h (+), k_h (+), n_Y (-), K_{NO3} (-), K_{OA2} (+), i_{XB} (-), μ_{A2} (-), $K_{FNA,AOB}$ (-), K_{OA1} (-), n_{AOB} (+), b_H (-), μ_H (+).	n_h (+), n_Y (-), k_h (+), K_{NO3} (-), i_{XB} (-), Y_H (-), K_{S2} (-), μ_H (+), K_{OA1} (-), i_{XP} (+), n_{g2} (+), K_{OH1} (+), K_{S1} (+), K_{S3} (-).

4.3.2. The nitrous oxide emissions

Sensitivity analysis perturbing the operating conditions

The investigation of the effect of operating conditions on the N_2O emissions is performed by analysing the behaviour of the N_2O emission factors, calculated as ratio between the total amount of N_2O emitted from the biological tanks and the TKN loaded in the biological unit, with RO (see Figure 4.5). In order to know the contribution by the different microbial groups on the N_2O emissions reported, the N_2O produced by AOB and the net N_2O produced by HB, per unit of influent TKN, in function of RO are considered in Figures 4.6a and 4.6b, respectively. The specific net N_2O produced by HB represents the difference, in absolute values, between the actual N_2O produced by HB, resulting from NO reduction, and the N_2O consumed via reduction into dinitrogen (N_2). If the value of this output is negative, the N_2O consumed by HB is higher than the one produced, meaning that HB have consumed all the N_2O produced by themselves and an additional fraction of the N_2O produced by AOB. In addition to these, the average NO_2- in the aerobic zone per unit of influent TKN and the concentration of dissolved oxygen in the three aerobic tanks (AER1, AER2 and AER3), presented in Figures 4.7 and 4.8 respectively, are used to help understanding the N_2O dynamics.

As can be noted by observing the N_2O produced by AOB and HB in Figure 4.6 and the average NO_2^- in the aerobic zone per unit of influent TKN in Figure 4.7, at values of RO where nitrites accumulate (i.e. when the ratio between average NO_2^- and TKN_{IN} is significantly different from zero) due to null NOB activity, both HB and AOB denitrification contribute to total N_2O emissions.

As the amount of oxygen supplied per unit of influent TKN slightly increases, NOB activity starts getting enhanced (see Figure 4.4b) and both HB and AOB denitrification in Figure 4.6 decrease due to the consequent lower NO_2^- availability, depicted in Figure 4.7. As a result, the N_2O emissions drop down. However, a further increase of RO would trigger grossly AOB denitrification, thus increasing the N_2O emission factor rapidly. The present scenario is achieved at concentrations of dissolved oxygen in the first aerobic tank between 0.5 and 0.7 mg (-COD).L^{-1} (see Figure 4.8a), which represents the operating condition where the Haldane-function, depicted in Figure 4.1, maximises. In practical terms, this indicates a very high N_2O production and emission due to accumulation of the intermediate nitritation oxidation NH_2OH. Mere measurements of nitrites do not therefore constitute enough indication for high N_2O emissions, because it can be that part of the nitrite consumed is used by AOB for the oxidation of NH_2OH to produce N_2O and not entirely by NOB. In conclusion, low concentrations of nitrites do not constitute enough indication of low N_2O production and emissions.

Under the same operating conditions, as the liquid concentration of N_2O becomes particularly high, the N_2O-to-N_2 reduction by HB is enhanced, leading to negative net N_2O production by HB. The value of AOB denitrification rate under this condition is higher for higher temperatures, since AOB activity, similarly to other microbial processes, is enhanced by temperature. In virtue of this, AOB denitrification is generally lower in colder temperature; hence it is observed that at winter temperatures the contribution by HB denitrification is much more comparable to the one by AOB than at other seasonal conditions.

In general, N_2O emissions increase for higher temperatures.

Independently from the temperature, as oxygen concentration increases further, the operating conditions become inhibiting to both AOB and HB denitrification and the N_2O emissions drop consistently down to very low values.

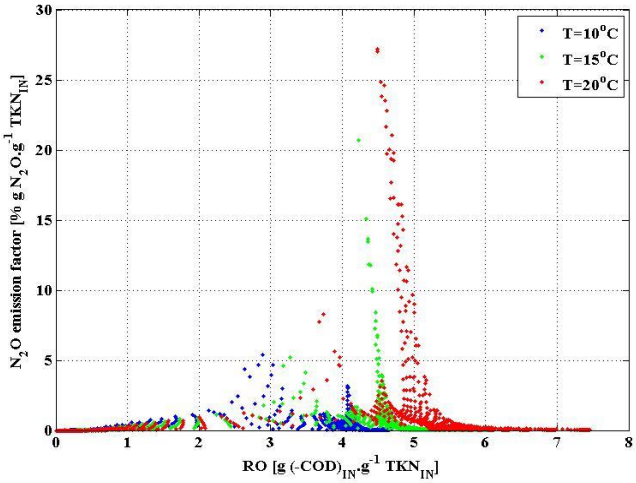

Figure 4.5: N_2O emission factors as function of influent oxygen-to-total-Kjeldahl-nitrogen ratio (RO) at temperatures of 10°C, 15°C and 20°C.

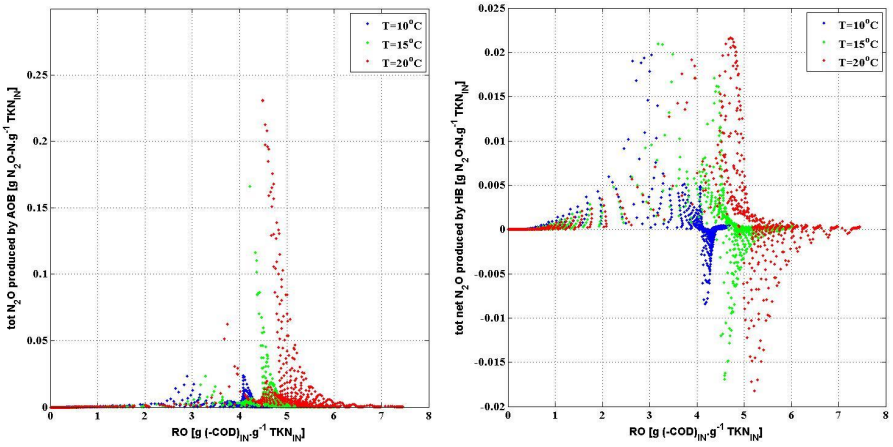

(a) **(b)**

Figure 4.6: **(a)** N_2O production by AOB, and **(b)** net N_2O production by HB.

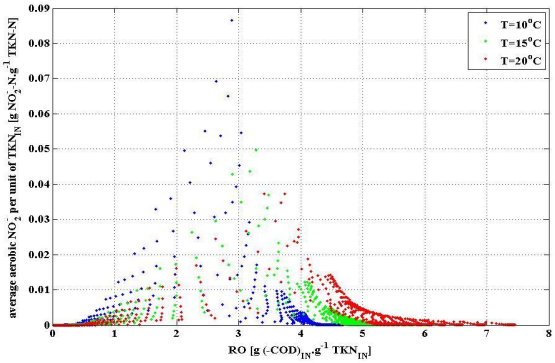

Figure 4.7: average NO_2^- concentration in the aerobic zone per unit of influent TKN.

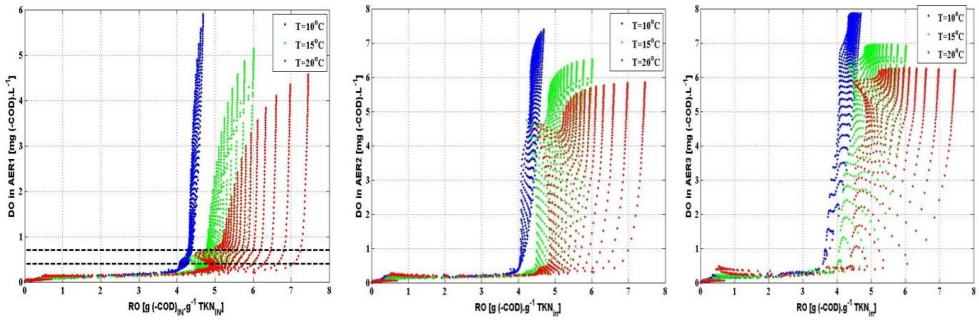

(a) **(b)** **(c)**

Figure 4.8: Oxygen concentrations in: **(a)** AER1, **(b)** AER2 and **(c)** AER3.

Sensitivity analysis perturbing the model parameters

Given the high uncertainty associated with the parameter values related to the processes describing N_2O production (see Table 4.5), the results of the sensitivity analysis investigating propagation of ASMG1 parameter uncertainties on N_2O emissions are considered. With regard to this, only the results from the Morris screening procedure could be reliably used due to the impossibility of finding reliably a linear relationship between N_2O emissions and the ASMG1 parameters during the Monte Carlo procedure. Among the ASMG1 parameters, those having a mean value of the standardized elementary effect (SEE) equal or larger than 0.01 are considered to have a significant effect on the N_2O emissions. These parameters are reported in Table 4.6 in a decreasing order: from the parameter having the highest SEE to the one having the lowest. Similarly to the parameters reported for η_{TN}, the effect of the parameter on the N_2O emitted is specified whether positive or negative within brackets. The fact that the N_2O emissions could not be linearly regressed with respect to the parameters could have been foreseen from the high nonlinear behaviour the N_2O emission factors have with respect to RO, as clearly depicted in Figure 4.5.

The ratios between standard deviations and mean values (σ/μ) reported in Table 4.5 result abundantly higher than the unit. For this reason, it can be stated that the propagation of parameter uncertainties to the N_2O emissions predicted by the model is very strong and significant. This does not allow identifying any general trend of N_2O emissions with oxygen concentration set point and with temperature. Hence, the aforementioned observation according to which N_2O emissions increase with temperature cannot be taken, for the moment, as reliable before a better identification of the kinetic parameters describing N_2O dynamics is performed. Nevertheless, the parameters most influencing N_2O emissions could be identified through the Morris screening procedure. This knowledge also allows detecting the changes in the biological mechanisms responsible for N_2O emissions according to operating oxygen concentration and temperature, which would be used as basis for the development of control strategies aiming at its minimization. The processes by which N_2O emissions result most affected are: (a) the last HB denitrification step, during which N_2O is converted into N_2, (b) the first HB denitrification step, during which NO_3^- is converted into NO_2^-, (c) AOB denitrification, and (d) NOB activity. In particular, the rate of the last HB denitrification step results having a negative effect on N_2O, since it consumes N_2O. Contrarily, the rate of the first HB denitrification step is revealed to have a positive effect, since it promotes accumulation of NO_2^-. AOB denitrification obviously affects positively N_2O emissions whereas NOB activity is found to have a negative effect, since it consumes NO_2^- in the aerobic zone, thus preventing its conversion into N_2O by both AOB and HB.
The results in Table 4.6 are analysed at different dissolved oxygen set points as follows:

- at very low DO concentrations (i.e. 0.3 mg (-COD).L^{-1}) while for winter temperatures the primary dominant process is the last HB denitrification step, at other temperatures NOB activity is the dominant process. This confirms the previous observation according to which HB denitrification plays a more compatible role with AOB at colder temperatures than at warmer temperatures;
- at DO concentrations equal to 0.65 and 1 mg (-COD).L^{-1}), NOB activity becomes among the dominant processes for all the temperatures together with the last HB denitrification step. With regard to this last, the fact that K_{N2O}, namely the N_2O half-saturation coefficient for N_2O-to-N_2 reduction by HB, is the most influencing parameter suggests that there is, as a consequence of high N_2O production by AOB, a very high N_2O liquid concentration which triggers the last denitrification step. For this reason, it can be said that AOB denitrification has become for all the temperatures the major contributors on total N_2O emissions at these oxygen concentrations. This confirms the observations taken previously. However, it is difficult to detect whether in this case the AOB denitrification is enhanced due to nitrite accumulation or due to hydroxylamine accumulation. On the basis of this it can be stated that the value of oxygen concentration maximizing the AOB denitrification can change quite a lot in function of the parameter values used to shape the function;
- at high oxygen concentrations (i.e. 2 mg (-COD).L^{-1}), the first HB denitrification step emerges among the contributing processes for N_2O emissions. This indicates that the first denitrification step leads to nitrite accumulation, which triggers the production of N_2O by HB. Contextually, the last denitrification step emerges as relevant process. Especially at high temperatures, oxygen is found to inhibit the last HB denitrification step. In addition, NOB growth rate is detected as contributing process able to reduce the N_2O emissions.

These considerations confirm the previous observations based on the results of the sensitivity analysis investigating the impact of aeration regime on N_2O emissions. However, the contribution by the first HB denitrification step was able to be detected only through the sensitivity analysis investigating the impact of parameter uncertainty. With regard to the temperature effect, it could be noted that the

availability of organic biodegradable substrates for the last HB denitrification step is more relevant under oxygen limiting conditions on the total N_2O emissions than nitrite accumulation when temperature is low.

Table 4.5: **(a)** mean, standard deviation and ratio between them for total N_2O emissions.

			DO [mg(-COD).L^{-1}]			
			0.3	**0.65**	**1**	**2**
N_2O_{tot} [g N_2O-N.d^{-1}]	**T=10ºC**	**μ**	10517.42	8958.24	4391.29	1483.22
		σ	34079.02	44391.61	19921.19	6084.5
		σ/μ	3.24	4.96	4.54	4.1
	T=15ºC	**μ**	9429.95	9170.1	4987.41	1710.62
		σ	30175.11	38767.79	21709.79	6927.47
		σ/μ	3.20	4.23	4.35	4.05
	T=20ºC	**μ**	10615.18	6159.86	2872.79	990.06
		σ	27252.99	19940.71	12885.05	5592.39
		σ/μ	2.57	3.24	4.49	5.65

Table 4.6: sensitivity analysis results with regard to the ASMG1 parameters for N_2O emissions at oxygen concentrations in the aerobic zone of 0.3, 0.65, 1 and 2 mg (-COD).L^{-1} and at temperatures of 10, 15 and 20ºC.

		DO [mg(-COD).L^{-1}]			
		DO=0.3	**DO=0.65**	**DO=1**	**DO=2**
Total N_2O emissions	**T=10ºC**	K_{S5} (+), n_{g5} (-), $K_{IO,AOBden1}$ (+), K_{N2O} (+), n_{g3} (+).	μ_{A2} (-), K_{N2O} (+).	K_{N2O} (+).	K_{N2O} (+), K_{S2} (-), n_{g2} (+), K_{FNA} (+), μ_{A2} (-), n_{AOB} (+).
	T=15ºC	K_{OA2} (+), $K_{FNA,AOB}$ (-), K_{S5} (+), $K_{SO,AOBden1}$ (-), K_{OH5} (-), n_{g5} (-), K_{S3} (-), K_{N2O} (+), K_{OA1} (-), b_{A1} (-), b_{A2} (+), .	μ_{A2} (-), K_{OA2} (+), K_{N2O} (+), f_P (+).	K_{N2O} (+), n_{g5} (-).	K_{S2} (-), n_{g2} (+), μ_{A2} (-), n_{AOB} (+).
	T=20ºC	K_{OA2} (+), K_{N2O} (+), K_{S3} (-), K_{FA} (-), f_P (+), b_{A1} (-), K_{NO2} (-).	K_{N2O} (+), K_{FNA} (+).	K_{OA2} (+), b_{A2} (+), μ_{A2} (-).	K_{N2O} (+), K_{OH5} (-), n_{g5} (-), K_{S2} (-), μ_{A2} (-).

4.3.3 The oxygen consumptions

In Table 4.7 the mean, standard deviation and ratio between them for the amount of oxygen consumed by the three different microbial groups (i.e. HB, AOB and NOB) and the specific oxygen consumption, namely the total oxygen consumed per total nitrogen removed, are presented. Table 4.8 shows the model parameters most influencing these uncertainties.

As can be noted from the uncertainty analysis results, the three oxygen consumptions have a low propagation of the model parameter uncertainties. However, NOB activity under oxygen-limited conditions has higher uncertainty than the other model outputs. Similarly, the specific oxygen consumed result quite uncertain under oxygen-limited conditions.

Looking at the mean values achieved for the oxygen consumed by HB, oxygen competition with autotrophic biomass emerges at low DO. More specifically, when DO is equal to 0.3 mg (-COD).L^{-1},

HB consumption is the lowest at temperature of 15ºC while AOB and NOB have their highest. From the sensitivity analysis results achieved at the same oxygen concentration and operating temperature, it emerges that NOB activity has a negative effect on HB activity. In addition, NOB activity is found to be playing a decisive role also on the oxygen consumption by AOB. At DO equal to 0.3 mg (-COD).L^{-1}, NOB has an increasingly-positive effect on the consumption of oxygen by AOB. This can be explained by the fact that at low oxygen concentrations, AOB denitrification is enhanced. This means that part of the influent ammonium will be oxidized using nitrite instead of oxygen. If NOB activity increases, nitrite availability will be reduced and thus AOB denitrification will be slowed down. More influent ammonium will be oxidized with oxygen, which in turn will increase the amount of oxygen consumed by AOB.

The competition between HB and NOB occurs also at higher oxygen concentrations. More specifically, as oxygen increases, NOB activity is observed to be limited by the presence of organic biodegradable carbon in the aerobic zone. As a matter of fact, the rate of the first HB denitrification step, where nitrate is reduced to nitrite, is found to positively influence NOB activity. This can be explained by the fact that, when the first reduction step by HB is slowed down, more organic carbon is fed into the aerobic zone, which increases the amount of oxygen consumed by HB and subtract it from NOB. As a matter of fact, the rate of aerobic HB activity is detected having a negative effect of NOB. This explains why, for the same operating temperature, when oxygen increases from 0.65 to 2 mg (-COD).L^{-1}, NOB activity decreases due to the prevalence of aerobic HB activity. This indicates that concentrations of oxygen higher than 1 mg (-COD).L^{-1} in the stream recycled from the last aerobic tank to the anoxic zone should be avoided to preserve high HB denitrification and preserve NOB activity, helpful for the prevention of N_2O formation.

The oxygen consumed by HB and AOB are found to be enhanced when oxygen concentration is increased from 1 to 2 mg (-COD).L^{-1}. Furthermore, from the sensitivity analysis results, similar are the most influencing parameters on these two outputs. Among these, the parameters linked to the biomass decay emerge. As more biomass is decayed and a larger fraction of these decay products can be reverted into biodegradable organic carbon and ammonium, higher is the consumption of oxygen by AOB and HB.

With regard to the oxygen consumed per unit of TN removed, excluding the value at DO equal to 0.3 mg (-COD).L^{-1} and temperature of 10ºC, whose uncertainty prevent from considering its mean value, it can be noted that this quantity increases as oxygen increases while it decreases at temperature increases. The oxygen effect is mainly linked to NOB activity. As a matter of fact, as oxygen is increased from 0.3 to 0.65 mg (-COD).L^{-1}, NOB activity increases, which in turn pushes up the total amount of oxygen consumed and contextually decreases the overall TN removal efficiency due to higher COD demand by heterotrophic denitrifiers. This thesis is confirmed by the sensitivity results which show at limited-oxygen conditions NOB-related model parameters as the most influencing. On the other side, the effect of temperature is due to the efficiency of HB denitrification. As temperature increases, HB denitrification gets more complete, which improves the TN removal efficiency for the same amount of oxygen consumed. This effect is deduced from the results of the sensitivity analyses performed, which shows the anoxic reduction factor for the hydrolysis of X_S (n_h) and the anoxic reduction factor for the heterotrophic yield (n_Y) as the main model parameters reducing the specific oxygen consumption.

Table 4.7: Mean value, standard deviation and ratio between them of oxygen consumptions by: **(a)** HB, **(b)** AOB, **(c)** NOB and **(d)** total oxygen consumption per unit of TN removed.

(a)

		O_2 consumed by HB			
units		[kg $(O_2)_{cons}.d^{-1}$]			
DO [mg (-COD).L^{-1}]		**0.3**	**0.65**	**1**	**2**
T=10ºC	**μ**	2636.1	2269.1	2343.4	2459
	σ	668.6	232.9	216.1	210.5
	σ/μ	0.25	0.1	0.09	0.09
T=15 ºC	**μ**	2587.4	2666.8	2745.7	2859.65
	σ	399.5	255	237.1	230.6
	σ/μ	0.15	0.1	0.09	0.08
T=20 ºC	**μ**	2960.6	2980.2	3052.3	3154.5
	σ	429	249.8	235.6	230.9
	σ/μ	0.14	0.08	0.08	0.07

(b)

		O_2 consumed by AOB			
units		[kg $(O_2)_{cons}.d^{-1}$]			
DO [mg (-COD).L^{-1}]		**0.3**	**0.65**	**1**	**2**
T=10ºC	**μ**	2186.2	2802.5	2885.9	2925.2
	σ	1231.7	316.9	123.3	57.6
	σ/μ	0.56	0.11	0.04	0.02
T=15 ºC	**μ**	2757	2864	2926.7	2955.8
	σ	355.3	303.3	128.3	633
	σ/μ	0.13	0.11	0.04	0.02
T=20 ºC	**μ**	2337.1	2888.2	2948.3	2976.7
	σ	327	234.04	141.7	65.5
	σ/μ	0.14	0.08	0.05	0.02

(c)

		O_2 consumed by NOB			
units		[kg $(O_2)_{cons}.d^{-1}$]			
DO [mg (-COD).L-1]		**0.3**	**0.65**	**1**	**2**
T=10ºC	**μ**	569.4	1132.5	1152.6	1112.7
	σ	570.95	173.3	130.9	115.8
	σ/μ	1	0.15	0.11	0.1
T=15 ºC	**μ**	1052.5	1204	1178.3	1125.4
	σ	527.15	182.5	140.1	124.5
	σ/μ	0.5	0.15	0.12	0.11
T=20 ºC	**μ**	1046.5	1193.4	1166	1107.3
	σ	571.3	172.7	122.2	90
	σ/μ	0.55	0.14	0.1	0.08

(d)

		Specific oxygen consumption			
units		[g $(O_2)_{cons}.g^{-1}$ TN_{rem}]			
DO [mg (-COD).L^{-1}]		**0.3**	**0.65**	**1**	**2**
T=10ºC	**μ**	476.7	10.86	11.56	12.43
	σ	6161.5	1.51	1.14	1.16
	σ/μ	12.93	0.14	0.1	0.09
T=15 ºC	**μ**	9.76	10.49	11.05	11.7
	σ	12.03	1.3	1.08	1.09
	σ/μ	1.23	0.12	0.1	0.09
T=20 ºC	**μ**	8.35	10.2	10.7	11.06
	σ	1.44	1.14	1	0.98
	σ/μ	0.17	0.11	0.09	0.09

Table 4.8: sensitivity analysis results with regard to the ASMG1 parameters for oxygen consumptions by HB, AOB and HB, and the total oxygen consumption per unit of TN removed at the temperatures of: **(a)** 10ºC, **(b)** 15ºC, and **(c)** 20ºC.

(a)

	T=10ºC			
	DO=0.3	**DO=0.65**	**DO=1**	**DO=2**
O_2 consumption by HB	K_{OA1} (+), μ_{A1} (-), K_{OA2} (+), μ_{A2} (-), f_P (-), b_H (+).	b_H (+), Y_H (-), f_P (-), K_{S2} (+), K_{S1} (-), n_h (-), K_{OH2} (-), n_{g2} (-), K_{NO3} (+).	b_H (+), Y_H (-), f_P (-), K_{S2} (+), n_h (-), K_{S1} (-), n_{g2} (-), K_{OH2} (-), K_{NO3} (+).	b_H (+), Y_H (-), f_P (-), n_h (-), K_{S2} (+), K_{S1} (-), n_{g2} (-).
O_2 consumption by AOB	K_{OA1} (-), μ_{A1} (+), Y_H (-).	$K_{FNA,AOB}$ (+), K_{OA2} (-), n_{AOB} (-), f_P (-), μ_{A2} (+).*	f_P (-), n_{AOB} (-), i_{XP} (-), i_{XB} (+), K_{OA2} (-), Y_H (-).*	f_P (-), i_{XP} (-), i_{XB} (+), Y_H (-), k_a (+), K_{FA} (-).
O_2 consumption by NOB	K_{OA2} (-), K_{OA1} (-), μ_{A2} (+), μ_{A1} (+), Y_H (-), K_{I3NO} (-), K_{FNA} (-).	K_{S2} (-), K_{OH2} (+), K_{S1} (+), K_{OA2} (-), n_{g2} (+), μ_{A2} (+), b_H (+), $K_{FNA,AOB}$ (+), f_P (-), K_{NO2} (+).	K_{S2} (-), K_{OH2} (+), K_{S1} (+), n_{g2} (+), K_{S4} (+), K_{I4NO} (-), n_Y (-), K_{OA2} (-), K_{NO2} (+).	K_{S2} (-), K_{OH2} (+), K_{I4NO} (-), n_{g2} (+), K_{S1} (+), K_{S4} (+), n_Y (-), K_{FA} (-).
Specific O_2 consumption	b_{A1} (+).*	n_h (-), K_{OA2} (-), n_Y (+), μ_{A2} (+), f_P (-), b_H (+), $K_{FNA,AOB}$ (+), n_{AOB} (-), μ_{A1} (-), K_{NO2} (+), n_{g3} (-), K_{OA1} (+), i_{XP} (-).	n_h (-), n_Y (+), f_P (-), k_h (-), K_{OA2} (-), μ_{A2} (+), K_{NO2} (+), K_{S1} (-), i_{XP} (-), n_{g3} (-), K_{NO3} (+), b_H (+), K_{S3} (+), i_{XB} (+), μ_{A1} (-).	n_h (-), n_Y (+), f_P (-), k_h (-), K_{S1} (-), i_{XB} (+), i_{XP} (-), Y_H (+), K_{NO3} (+), K_{S3} (+), K_{OH1} (-), K_{I4NO} (-), K_{S4} (+), K_{OA1} (+), K_{NO2} (+).

(b)

	T=15ºC			
	DO=0.3	**DO=0.65**	**DO=1**	**DO=2**
O_2 consumption by HB	K_{OA2} (+), μ_{A2} (-), f_P (-), K_{S2} (+), K_{S1} (-), b_H (+), Y_H (-), n_{g2} (-), K_{OH1}(-), b_{A2} (+).	f_P (-), b_H (+), Y_H (-), K_{S2} (+), K_{S1} (-), n_h (-), K_{OH2} (-), n_{g2} (-), K_{NO3} (+).	f_P (-), b_H (+), Y_H (-), K_{S2} (+), n_h (-), K_{S1} (-), n_{g2} (-), K_{OH2} (-), K_{NO3} (+), k_h (-).	f_P (-), b_H (+), Y_H (-), n_h (-), K_{S2} (+), K_{S1} (-), n_{g2} (-), k_h (-), K_{NO3} (+).
O_2 consumption by AOB	n_{AOB} (-), $K_{SO,AOBden1}$ (+), K_{OA2} (-).*	$K_{FNA,AOB}$ (+), f_P (-), K_{OA2} (-), n_{AOB} (-), $K_{IO,AOBDen1}$ (-), b_{A2} (-). *	f_P (-), i_{XP} (-), n_{AOB} (-), $K_{FNA,AOB}$ (+), i_{XB} (+), K_{I4NO} (+), Y_H (-), K_{S4} (-), K_{I3NO} (-), μ_H (-), $K_{IO,AOBDen1}$ (-).*	f_P (-), i_{XP} (-), i_{XB} (+), Y_H (-), k_a (+).
O_2 consumption by NOB	K_{OA2} (-), μ_{A2} (+), K_{S2} (-), b_{A2} (-), n_{g2} (+), K_{OH1} (+), K_{S1} (+), K_{OH2} (+).	K_{S2} (-), K_{OH2} (+), K_{S1} (+), K_{OA2} (-), μ_{A2} (+), n_{g2} (+), f_P (-), $K_{FNA,AOB}$ (+).	K_{S2} (-), K_{OH2} (+), K_{S1} (+), n_{g2} (+), f_P (-), K_{I4NO} (-), K_{S4} (+).	K_{S2} (-), K_{OH2} (+), K_{I4NO} (-), K_{S4} (+), n_{g2} (+), K_{S1} (+), K_{S5} (-), n_{g4} (-), n_Y (-), K_{I3NO} (+), f_P (-).
Specific O_2 consumption	K_{OA2} (-), n_{AOB} (-), μ_{A2} (+), $K_{SO,AOBDen1}$ (+),K_{NO3} (+), b_{A2} (-), K_{S1} (-), n_h (-).*	n_h (-), K_{OA2} (-), f_P (-), μ_{A2} (+), n_Y (+), b_H (+), $K_{FNA,AOB}$ (+), K_{NO3} (+), μ_{A1} (-), k_h (-), n_{AOB} (-), i_{XP} (-), μ_H (-), K_{NO2} (+), K_{OA1} (+).	n_h (-), f_P (-), n_Y (+), k_h (-), b_H (+), K_{NO3} (+), i_{XP} (-), μ_{A2} (+), n_{g3} (-), K_{OA2} (-), i_{XB} (+), K_{S1} (-), K_{N2O} (+).	n_h (-), n_Y (+), k_h (-), f_P (-), K_{NO3} (+), i_{XP} (-), K_{S1} (-), b_H (+), i_{XB} (+), K_{I4NO} (-), K_{S4} (+), K_{OA1} (+), K_{OH1} (-).

(c)

	T=20ºC			
	DO=0.3	**DO=0.65**	**DO=1**	**DO=2**
O_2 consumption by HB	K_{OA2} (+), μ_{A2} (-), f_P, Y_H (-), K_{S2} (+), K_{S1} (-), b_{A2} (+), b_H (+), K_{NO3} (+), K_{OH1} (-), K_{OH2} (-).	f_P (-), K_{S2} (+), b_H (+), Y_H (-), K_{S1} (-), K_{OH2} (-), n_{g2} (-), K_{NO3} (+), n_h (-).	f_P (-), b_H (+), Y_H (-), K_{S2} (+), K_{S1} (-), n_h (-), K_{OH2} (-), n_{g2} (-), K_{NO3} (+).	f_P (-), b_H (+), Y_H (-), K_{S2} (+), n_h (-), K_{S1} (-), K_{NO3} (+), k_h (-), n_{g2} (-).
O_2 consumption by AOB	μ_{A2} (+), K_{OA2} (-), $K_{SNO,AOB}$ (+), f_P (-).*	i_{XP} (-), i_{XB} (+), b_{A2} (-),Y_H (-), k_a (+), μ_{A1} (-), $K_{IO,AOBden1}$ (-), $K_{FA,AOB}$ (+), K_{FNA} (-), n_Y (-).*	f_P (-), i_{XB} (+), Y_H (-), n_{AOB} (-), K_{OA2} (-), i_{XP} (-), $K_{FNA,AOB}$ (+), b_{A2} (-), K_{OH4} (+), K_{S2} (-), $K_{FA,AOB}$ (+), $K_{SO,AOBDen1}$ (-).	f_P (-), i_{XP} (-), i_{XB} (+), Y_H (-), k_a (+).
O_2 consumption by NOB	K_{OA2} (-), μ_{A2} (+), b_{A2} (-), K_{S2} (-), f_P (-), K_{OA1} (+), K_{OH2} (+), K_{NO3} (-).	K_{S2} (-), K_{OH2} (+), K_{OA2} (-), K_{S1} (+), μ_{A2} (+), n_{g2} (+), f_P (-), $K_{FNA,AOB}$ (+), b_{A2} (-), K_{OA1} (+), Y_H (-).	K_{S2} (-), K_{S1} (+), K_{OH2} (+), n_{g2} (+), f_P (-), K_{OA2} (-), $K_{FNA,AOB}$ (+), μ_{A2} (+), Y_H (-), K_{OA1} (+).	K_{S2} (-), K_{OH2} (+), K_{S1} (+), n_{g2} (+), f_P (-), K_{S3} (+), K_{I4NO} (-), K_{NO3} (-), i_{XB} (+), K_{OA1} (+).
Specific O_2 consumption	K_{OA2} (-), μ_{A2} (+), f_P (-), K_{OA1} (+), b_{A2} (-), μ_{A1} (-), k_h (-), $K_{SO,AOBden1}$ (+), b_H (+).	K_{OA2} (-), f_P (-), n_h (-), μ_{A2} (+), k_h (-), $K_{FNA,AOB}$ (+), n_Y (+), b_H (+), Y_H (-), b_{A2} (-), K_{NO3} (+), i_{XB} (+), n_{AOB} (-), K_{OA1} (+).	n_h (-), f_P (-), k_h (-), n_Y (+), K_{OA2} (-), K_{NO3} (+), b_H (+), i_{XB} (+), $K_{FNA,AOB}$ (+), Y_H (-), μ_{A2} (+), n_{AOB} (-), K_{OA1} (+).	n_h (-), f_P (-), n_Y (+), k_h (-), K_{NO3} (+), i_{XB} (+), b_H (+), μ_H (-), i_{XP} (-), K_{S2} (+), K_{OA1} (+), K_{OH1} (-).

* results from sensitivity analysis according to MS procedure.

4.3.4 Comparison of the behaviours observed against measurements in literature

The present work uses a specific mathematical formulation of a biochemical wastewater model to derive the biological mechanisms determining the N_2O emission dynamics, the TN removal efficiency and the oxygen consumptions in pre-denitrification WWTPs. The investigation was carried out through two sensitivity analyses: one, performed by changing the operating conditions of the plant using the default parameter values by Guo and Vanrolleghem [37], and the other, performed by perturbing the default parameter values and fixing the oxygen concentration and the TSS concentration. Although the observations achieved can be considered independent from parameter uncertainties, there can be still discrepancies from the reality of the WWTPs due to the mathematical structure of the model and the plant configuration. Therefore, to assess the reliability of the identified biological mechanisms determining the TN removal efficiency, the oxygen consumptions and the N_2O emissions, it becomes important to consider the WWTP data collected from real experiences, especially the ones coming from full-scale applications. Table 4.9 shows the confirmations of some of the observations obtained through the present work from wastewater treatment plant experiences.

Table 4.9: Feedback on the observations obtained during the sensitivity analyses on N_2O emissions from real plant experiences.

OBSERVATIONS FROM SENSITIVITY ANALYSES	REAL PLANT EXPERIENCES
TN removal efficiency increases with temperature	Zhang *et al.* [55] Kim *et al.* [60]
TN removal efficiency limited at cold temperatures by AOB activity	Kim *et al.* [60]
N_2O emissions triggered by low oxygen concentrations and/or nitrite accumulation	Daelman *et al.* [40] Tallec *et al.* [61] Aboobakar *et al.* [41] Rassamee *et al.* [17] Kampschreur *et al.* [62]

With regard to the temperature effect on N_2O dynamics, the sensitivity analysis performed with the default ASMG1 parameter values has showed that the amount of N_2O emitted significantly increases with the temperature, although the high propagation of the parameter value uncertainties does not allow identifying a sure correlation between N_2O and temperature. Experiences by Daelman *et al.* [40] and Ahn *et al.* [58] have shown a similar challenge. However, the same Ahn *et al.* [58] would expect that N_2O emissions would increase with temperature due to the higher microbial kinetics, which is compatible with the predictions of the BSM2Na using the default parameter values.

Finally, important to consider can appear the fact that the present observations are taken by exploiting predictions by a model which does not include the production of N_2O according to the pathway related to the incomplete oxidation of hydroxylamine (NH_2OH). At this regard, it is first relevant to note that there have not been found strong-enough evidences suggesting that N_2O is produced in a large amount as a consequence of incomplete oxidation of hydroxylamine from full-scale WWTPs. For instance, the Kralingseveer WWTP has been suggested to produce N_2O as a result of AOB denitrification and not of incomplete NH_2OH oxidation [40]. Also Kampschreur *et al.* [62], Tallec *et al.* [61] and Rassamee *et al.* [17] have identified AOB denitrification as the main contributors for N_2O emissions. Only the experimental work performed by Peng *et al.* [19] suggests that, although AOB denitrification remains the N_2O major contributor, incomplete NH_2OH oxidation can contribute non-negligibly on the N_2O emissions for very high DO levels. In this last contribution, it was observed that high DO levels conjunctly with high AOB activity can make NH_2OH oxidation incomplete and thus trigger N_2O emissions. However, for control purposes the results achieved during the present work have suggested that the wastewater system should not operate at too high DO levels because this would inhibit both HB denitrification and the hydrolysis of entrapped organics and thus would reduce the plant TN removal efficiency. Furthermore, for the mere purpose of minimizing N_2O emissions, high DO levels promote accumulation of HB-produced NO_2^- in both the aerobic and anoxic zone.

In virtue of these considerations, although the parameter uncertainty has to be reduced in order to better quantify the emissions of N_2O, the biological mechanisms identified are compatible with the reality of the majority of the full-scale WWTPs. The information obtained during the present work can be therefore reliably used for the development of control strategies aiming at reducing the N_2O emission factors of WWTPs while contextually maintaining a good effluent quality.

4.3.5 Perspectives for the development of operation and control strategies for N_2O minimization

The results from the sensitivity analyses performed can be used to figure out some optimal operating windows for the achievement of high TN removal efficiency and low N_2O emissions.

Values of the RO maximizing the TN removal efficiency were found at the different temperatures. The results indicate that the way to maximize the TN removal efficiency of a plant consists simply in having a trade-off aeration regime that maximizes AOB activity and minimizes NOB activity. Thus all the influent NH_4^+ would be converted by AOB into NO_2^- and HB denitrification would then be able to work at its maximal efficiency by following NO_2^- reduction route rather than the NO_3^- route. However, these results have been obtained at fixed influent biodegradable organic carbon, which is the limiting factor preventing HB denitrification following NO_3^- route to work at its maximal efficiency. With regard to the influence of the operating temperature, it emerges that more oxygen is needed to be supplied in order to maximize the TN removal efficiency when the temperature is higher, due to a higher oxygen endogenous consumption by the biomass. Furthermore, as suggested by the uncertainty analysis results in Table 4.3, winter temperatures may drastically limit the TN removal efficiency due to low AOB activity and manipulating the aeration regime may not be anyhow enough to respect ammonium and total nitrogen effluent limits. Feedforward controllers imposing, according to the temperature, the $RO_{maxTNrem}$ identified in Figure 4.3 could be beneficial for the achievement of the maximal η_{TN}. However, having on-line sensors for organic nitrogen can be a challenge.

Another idea, in case NOB activity is allowed, would be to have a feedback controller using the removal efficiency of nitrogen oxides (η_{NOX}) as controlled variable and the flow rate adding readily-biodegradable organic carbon as manipulated variable, given the clear correlation between η_{TN} and η_{NOX}. It is in fact well-known that η_{NOX} is in correlation with the ratio between readily-biodegradable organic matter and NO_X in the inlet to the anoxic zone. However, for the sake of N_2O emission minimization also in this case the strategy has to be properly studied because in predenitrification the leftover organic carbon non-oxidized in the anoxic zone is carried in the aerobic zone where it enhances the consumption of oxygen by HB and thus it subtracts oxygen from NOB. As a matter of fact, NOB activity has been found out to be able to reduce N_2O production, and consequently emissions, by picking up the AOB-produced nitrites.

More specifically, the sensitivity analyses performed have shown that N_2O is being produced under those operating conditions at which oxygen is insufficiently supplied. An insufficient oxygen supply is found to:

- directly trigger nitrite pick-up by AOB,
- slow down the activity of NOB and consequently promoting nitrite accumulation, and
- trigger accumulation of NH_2OH.

During all of these circumstances AOB will consume part of the nitrite produced by themselves as electron acceptor to produce nitric and nitrous oxide. This amount of nitrite will not be used by NOB for the production of nitrate. At the aim of slow down AOB denitrification, oxygen availability has to be carefully increased at the aim of inhibiting nitrite-pickup by AOB and avoiding accumulation of nitrite and hydroxylamine. The nitrate produced by NOB should be compared against the amount of ammonium consumed by AOB. If the latter is higher than the former, oxygen availability should be increased. At the same time, excessive oxygen concentrations are found to inhibit the last HB denitrification step at high temperature, trigger accumulation of HB-produced nitrite and eventually slowing down NOB activity due to higher amount of organic carbon - non-oxidized in the anoxic zone – carried to the aerobic zone. A controller has to be built up in order to establish a trade-off oxygen

regime slowing down N_2O production from AOB denitrification and allowing a complete HB denitrification in function of the influent Total Kjedhal Nitrogen (TKN). The ratio between nitrate net produced and the ammonium net consumed in the aerobic zone (R_{NatAmm}) could be considered as controlled variable, since it approximates with a good correlation factor the ratio between NOB and aerobic AOB activity, as shown in Figure 4.9.

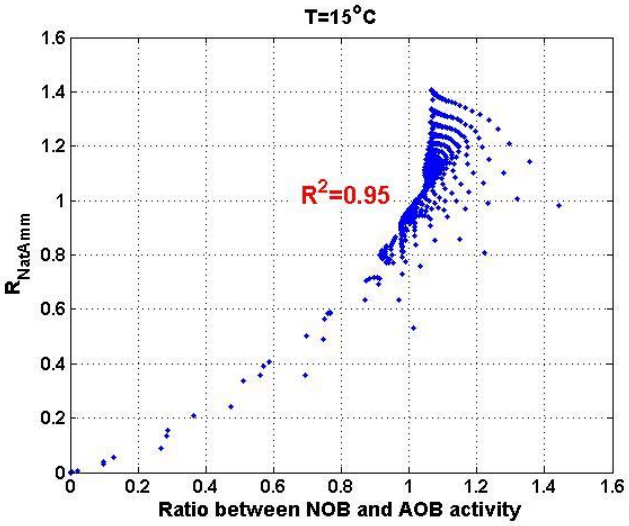

Figure 4.9: Ratio between NOB and AOB activity against R_{NatAmm} at temperature of 15°C.

Values of R_{NatAmm} larger than 1 come partly from the conversion of influent organic nitrogen into nitrate when the autotrophic bacteria are provided abundantly with oxygen. However, values of R_{NatAmm} largely higher than one can be ascribed to a loss of heterotrophic biomass. More specifically, looking at Figure 4.10 depicting the difference between the concentration of heterotrophs influent and effluent the aerobic zone, it can be noted that this quantity increases with RO. This means that as RO increases there is an overall decay of heterotrophs in the aerated zone, which frees nitrogen. This last is easily converted into nitrate by the autotrophic biomass.

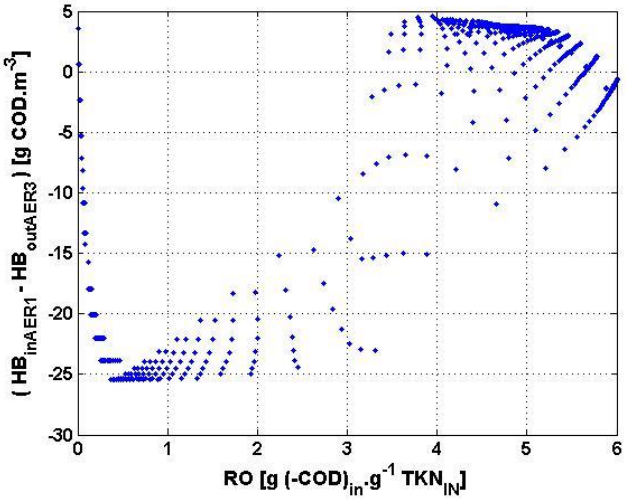

Figure 4.10: Difference between HB concentration influent and effluent to the aerobic zone.

The need for a control loop limiting the amount of oxygen carried from the aerobic to the anoxic zone could be contemplated as well.

While minimizing N_2O emissions and respecting the effluent limits, operating costs have also to be considered for real applications. The specific oxygen consumption, indicating the amount of oxygen consumed per unit of TN removed, has identified NOB activity to worsen the economic efficiency of the plant and reduce the TN removal efficiency by making more organic carbon required for heterotrophic denitrification. However, having high NOB activity is identified as the key for preventing N_2O production. In this case, choices have to be taken in virtue of the objectives which the WWTP managers want to privilege. In any case, aeration supply is of benefit on both the emissions and the effluent until a threshold, above which effluent quality gets worse and N_2O emissions do not further reduce.

4.4 Conclusions

The present work has been carried out with the aim of deriving the biological mechanisms determining N_2O emissions , TN removal efficiency, the competitions among the main microbial groups on oxygen and the trade-offs between oxygen consumption and effluent quality of a full-scale wastewater treatment plant on the basis of sensitivity analyses based on a published wastewater treatment model. The information achieved can then be exploited for the systematic development of control strategies aiming at minimizing the N_2O emissions from WWTPs while at the same time keeping the TN removal efficiency, and hence the effluent quality, at high levels. A large number of full-scale and lab-scale experiences have qualitatively confirmed the observations achieved from the two sensitivity analyses. However, more work would be needed to reduce the uncertainty of the kinetic parameters in order to better quantify the N_2O emissions.

The results from the sensitivity analyses performed have indicated the ratio between NOB and AOB activity as the key variable deciding the microbial balance leading to N_2O production. Controlling this ratio within its optimal range would ensure that all the AOB-produced NO_2^- will be consumed by NOB

and prevent heterotrophic denitrification being inhibited. Avoiding oxygen inhibition in the anoxic zone has been found important not only to avoid higher N_2O production by HB and low TN removal efficiency, but also at the aim of ensuring high activity of NOB, who can have their oxygen depleted by too high aerobic HB activity. Cold temperatures however were observed to hinder the aerobic AOB activity drastically. Due to the large uncertainty recorded, the effect of temperature on N_2O emissions observed with the default model parameters, suggesting higher N_2O production for higher temperatures, could not be confirmed.

CHAPTER 5
Development of a systematic methodology for the design of fuzzy logic based controllers applied to process systems

5.1 Introduction

In biological wastewater treatment the key to achieve high process performance is ensuring optimal environmental conditions, which allow the bacteria to work at the desired efficiency. These conditions can be accomplished by means of proper design of WWT systems. Nevertheless, since the influent to these systems – the main disturbance – is rather dynamic both in terms of flow rate and in terms of composition, the environmental conditions tend to move away from the optimal ones required by the microbial community. In order to cope with these fluctuations, on-line control strategies have to be implemented in the system. More specifically, Proportional Integrative Derivative (PID) control has been the type of controller commonly developed and tested for biological WWT systems [51,63–66] till now. However, as remarked by Aoi *et al.* [67], given their non-linear behaviour, biological WWT systems may perform poorly when controlled by linear controllers such as PID. Non-linear approaches such as non-linear Model Predictive Control (NLMPC), although they are able to take into account the non-linearity of the processes, rely on the descriptive capability of a model. For complex biological systems where different microbial groups coexist and interact, developing such a model may not be straightforward. As a matter of fact, a model may result able to realistically describe a very specific biological system but cannot be adopted in similar systems with different design and operation modes. Therefore, a NLMPC can perform well only when applied to the particular biological system used for the development of the model but can perform poorly when applied to other biological systems having different operational and design configurations, which the model is not able to describe accurately. Fine-tuning the controller may not be enough to obtain the desired process performance. On the contrary, as fuzzy-logic controllers (FLCs) can incorporate the non-linear nature of such bioprocesses and do not need to rely on the descriptive capability of models, they represent good candidates to overcome the challenges typically met with interactive biological systems, such as the wastewater treatment systems. . Furthermore, FLCs can make use of process engineering knowledge gained from observations and experiences with operating biological systems which is otherwise hard to be described mechanistically. Thus mechanistic knowledge can be easily integrated with additional insights on the processes to control, allowing a better control performance. Furthermore, control objectives for biological applications are often affected by some degree of fuzziness where, for the same controlled variable, a range of set points rather than a single value can be identified as optimal [68]. In such situations, FLCs offer the flexibility to include for the same variable a range of set points rather than a single value to be tracked.

Additionally, FLCs typically require a large number of design decisions, which makes them very flexible in function of specific requirements on control response. As matter of fact, design parameters can be easily changed in order to adapt the control system to specific requirements. However, this large number of degrees of freedom also comes with the challenge of making proper design choices in

a systematic way [69]. This in turn can limit the application range of FLCs for complex systems such as WWT plants. As described in Lababidi and Baker [70], the generic work of a fuzzy-logic inference system (FIS) consists of three main subsequent operations: "fuzzification", "fuzzy inference" and "defuzzification". More in detail, the fuzzification converts numerical (crisp) values of the input variables into fuzzy inputs, on the basis of which the fuzzy inference deduces the corresponding fuzzy outputs. The latter are then converted into crisp values through the defuzzification. While the "fuzzy inference" operation basically relies on linguistic rules, "fuzzification" and "defuzzification" are performed according to so-called membership functions (MFs). As stated by Seborg *et al.* [71], the definition of the MFs plays a major role in determining the FLC performance. Nevertheless, a systematic procedure for this MF definition has not been established yet, which in turn can hinder the good performance of FLCs and lead to unexpected behaviours. For this reason, during the present work a generic systematic methodology for tuning fuzzy-logic control will be deduced on the basis of an application case regarding a one-stage partial nitritation/Anammox (PN/A) system.
More specifically, a first-attempt control strategy for high and stable TN removal efficiency in a lab-scale sequencing-batch PN/A reactor is first developed intuitively on the basis of the available expert-knowledge. In a second instance, the control strategy will be finely-tuned according to a systematic approach. A generic systematic methodology for FLC design applied to process systems will then be proposed on the basis of the experience on the PN/A system.
For this reason, the present chapter is structured into the three following subsections:

1) Intuitively-designed control strategy for high TN removal efficiency in a lab-scale sequencing-batch PN/A reactor (Section 5.2),
2) Fine-tuning of the fuzzy-logic control presented in the previous section (Section 5.3), and
3) Definition of a generic systematic methodology for design of FL controllers applied to process systems (Section 5.4).

Section 5.2 will present mostly the work by Boiocchi *et al.* [72], while the work by Boiocchi *et al.* [73] is entirely used in Section 5.3.

5.2 Knowledge-based intuitive development and testing of a fuzzy-logic controller for high TN removal efficiency in a lab-scale sequencing-batch PN/A system.

This section describes the work by Boiocchi *et al.* [72], where a fuzzy-logic control strategy for high TN removal efficiency in one-stage PN/A system is intuitively developed on the basis of expert knowledge about the system itself and subsequently tested. The work is here presented to introduce some of the basic concepts needed to understand in order to achieve high process performance in this kind of reactors. The controller is successfully tested in a model representing a lab-scale sequencing-batch PN/A reactor. Fuzzy-logic controller is developed intuitively on the basis of acquired expert-knowledge. The control actions are inferred on the basis of the balance among the different microbial communities co-existing the system. The same logical concept will be adopted to define the structure of the fuzzy-logic controller presented in Section 5.3.

5.2.1. Introduction

Monitoring microbial activity is essential for achieving high control performances in biological reactors. Advances in molecular tools based on omics technology (genomics, metabolomics, etc...) provide a qualitative assessment of the activated sludge microbial community structure with its diverse functions [74]. These measurements are however off-line, tedious, time-intensive, expensive and not able to fulfil the actual needs of most monitoring and control applications. In addition, due to the presence of interacting microbial groups many challenges arise when trying to estimate the microbial activity in a mixed-culture bioreactor. Hence the information given by the few sensors usually implemented in a bioreactor needs to be expanded with observers or other state-estimation tools in order to infer the state of the microbial groups. When first principles models of the microbial kinetics are not available or mismatch significantly with the reality, expert-knowledge about a process system can represent a useful alternative for the development of control strategies. The so-called "fuzzy-logic inference system" (FIS) is a means of exploiting this knowledge for control strategy development [70,75]. Since its control laws are expressed in linguistic rather than mathematical expressions, FISs are intrinsically easy to understand and to adapt in function of control performance requirements. Moreover, FISs have been shown to enable integrating quantitative mechanistic knowledge with qualitative expert knowledge, making it suitable for processes that are still under development. Previous applications of FISs in wastewater treatment (WWT) include the control of activated sludge processes [4, 13] and anaerobic digesters [11] or improving disturbance rejection [6].

The so-called PN/A is a novel process that has shown its usefulness for the side-stream treatment of reject water from anaerobically-treated sludge dewatering or landfill leachate [44,76,77]. The CANR process performs the conversion of ammonium (NH_4^+) to dinitrogen (N_2) through the activity of ammonia-oxidizing bacteria (AOB) and anaerobic ammonia-oxidizing bacteria (AnAOB) [76,77]. AOB partially convert NH_4^+ to nitrite (NO_2^-) with oxygen (O_2) as electron acceptor and AnAOB oxidize the remaining fraction of NH_4^+ by reducing the AOB-produced NO_2^- [76,78–80]. In this last process, a minor fraction of nitrate (NO_3^-) is produced. Well-known advantages of the PN/A process are: reduction of O_2 supply, no need for organic biodegradable carbon addition and negligible sludge production [77]. CANR can be accomplished in a single reactor, where AOB and AnAOB work simultaneously, or in a two-stage configuration designed to have the aerobic AOB-mediated process, namely nitritation, preceding the AnAOB-mediated process. The performance of a single-stage CANR can be seriously compromised due to disturbances as well as operating conditions leading to unbalanced activity of the biomass. For example, a significant activity of nitrite-oxidizing bacteria (NOB), a class of autotrophic microorganisms converting NO_2^- to nitrate (NO_3^-), reduces the total nitrogen (TN) removal efficiency, since NO_3^- requires a significant amount of readily degradable organic carbon and a high activity of heterotrophic bacteria (HB) to be converted into N_2.

Ensuring a balanced microbiological activity when operating PN/A systems is therefore a key issue in order to achieve a good and stable performance. Since many microbial processes take place simultaneously resulting in dependencies and competition among the microbial groups, linear controllers using constant set point values for dissolved oxygen, O_2 reduction potential, N species or pH alone may not be enough to ensure balanced microbial community activities and therefore performance stability [81–83]. Too high O_2 concentrations inhibit the AnAOB activity and enhance the undesired activity of NOB. On the other hand, too low O_2 supply leads to low aerobic AOB activity [76,79]. Therefore, a diagnosis of the microbiological operation is needed to establish the appropriate control action.

The present work is a comprehensive extension and analysis of the work presented at the CAB/DYCOPS conference in 2013 [84]. The main additions made are: (i) a structured methodology and in-depth description of the work flows underlying the development of a fuzzy-logic diagnosis and fuzzy-logic controller. In addition, the control block diagram indicating the data-flow and information flow hierarchy is presented, (ii) detailed analysis and validation of the diagnosis tool with experimental data and process engineering insights, (iii) control performance evaluation under more challenging disturbances and conditions. The objective of this work is to develop a fuzzy-logic diagnosis (FLD) and a fuzzy-logic control (FLC) with the aim of achieving high and steady TN removal in a single-stage PN/A reactor with granular sludge. The FLD will provide information regarding the activity of the biomass as an input to the FLC. Diagnosis and control will be developed independently in order to achieve transparency on the input information given to the controller, and flexibility in case of needed control performance improvement and feasibility for the implementation of the knowledge by the operator.

The paper is organised as follows: first the mathematical model of a lab-scale PN/A reactor and the modelling of a generic FIS are presented. Afterwards, the development of the FLD and FLC tools is explained. The fuzzy-logic diagnosis performance will first be evaluated on the basis of the consistency of the outputs produced and of their capability of realistically describing the actual situation of the biomass during 100 days of a lab-scale CANR operation. Finally, both the FLD and the FLC are evaluated by simulation of a disturbance in the nitrogen load to the reactor, in the form of a change in the incoming ammonium concentration.

5.2.2. Materials and method

The FLD and FLC system developed are implemented using the fuzzy logic toolbox of MATLAB R2013 (The MathWorks, Natick, MA). The developed FLD and FLC are then coupled to a process model built in Simulink. The process model consists of the description of the physical and biochemical processes occurring in a one-stage PN/A granular reactor. In this section, first a brief description regarding the mathematical model used and the physical configuration of the reactor are provided. Afterwards an overview of the generic work done by a fuzzy-logic inference system will be shown.

Fuzzy-logic Inference System Modelling

In this subsection a brief description about the generic operation of a FIS is presented.

Figure 5.1 shows the procedure according to which a generic FIS deduces the numerical values of its outputs (i.e. crisp outputs) starting from a set of crisp inputs. As can be seen, this procedure can be divided into three main subsequent operations:

I) Fuzzification: a crisp input (u) is converted into fuzzy inputs (U) by the so-called "Fuzzifier",

II) Fuzzy Inference: The "Fuzzy Inference Engine" infers the fuzzy outputs (Y) on the basis of the values of U through the rules from the "Fuzzy rule base",

III) Defuzzification: the so-called "Defuzzifier" converts Y into a crisp output (y).

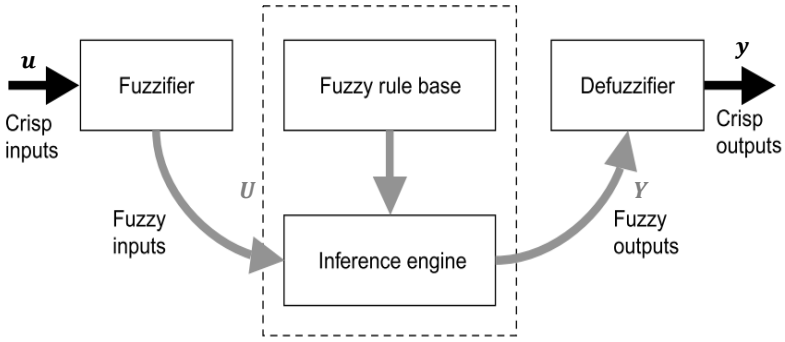

Figure 5.1: Simplified scheme of a fuzzy system [70].

For in-depth analyses about fuzzy system modelling, the work of Lababidi and Baker [70] should be consulted.

5.2.3. Development of fuzzy-logic diagnosis and control

As disclosed in the introduction to this section, the aim of the present work is to develop a process-insight based control strategy for a PN/A system to achieve a high and stable TN removal efficiency by adjusting the plant operation on the basis of the activity of the biomass. During the development of the control system, transparency and flexibility have also been considered as important features to be achieved. With the term "transparency", it is meant that the task of describing the microbiological activity of the biomass can be carried out independently from the task of deciding the control actions to be carried out. By delegating these two operations to two different tools it is possible to identify the underlying cause - a bottleneck - that compromises the performance of the entire control system. Thus the design of the tool giving a low performance can be changed without conceptually modifying the design of the other tool. For this reason, the following two fuzzy-logic tools have been developed separately: a fuzzy-logic diagnosis (FLD), in charge of diagnosing the current activity of the biomass in the system, and a fuzzy-logic control (FLC), in charge of deciding, on the basis of the diagnosis results, the appropriate control actions to be taken.

Development of Fuzzy-Logic Diagnosis

Identification of the input and output variables. Based on stoichiometric analysis of PN/A performance and on knowledge including a relationship between process performance and the microbiological state of the system, a decision tree for facilitating start-up of single-stage PN/A systems was developed by Mutlu *et al.* [85]. As can be seen in Figure 5.2, the tree provides a screening of the activity of the PN/A system on the basis of the values of the following parameters (defined in Figure 5.2 within rhombus-shaped boxes):

Total nitrogen variation: $$\Delta TN = TN_{eff} - TN_{in} \quad (5.1)$$

Ratio of NH_4^+ consumed to TN removed: $$R_{AmmTot} = \left|\frac{\Delta(NH_4^+ - N)}{\Delta TN}\right| \quad (5.2)$$

Ratio of NO_2^- produced to NH_4^+ consumed: $$R_{NitAmm} = \left|\frac{\Delta(NO_2^- - N)}{\Delta(NH_4^+ - N)}\right| \quad (5.3)$$

Ratio of NO_3^- produced to TN removed: $$R_{NatTot} = \left|\frac{\Delta(NO_3^- - N)}{\Delta TN}\right| \quad (5.4)$$

NH_4^+ removal efficiency: $$R_{eff} = 1 - \frac{(NH_4^+ - N)_{eff}}{(NH_4^+ - N)_{in}} \quad (5.5)$$

Ratio between NO_2^- and NH_4^+ in the effluent: $$R_{NitAmm,eff} = \frac{(NO_2^- - N)_{eff}}{(NH_4^+ - N)_{eff}} \quad (5.6)$$

The variations used in the above equations refer to the difference between the specific nitrogen compound concentration in the effluent at the end of the cycle and the one in the influent at the beginning of the same cycle. Total nitrogen (TN) is given by the sum of nitrate, nitrite and ammonium nitrogen. Thus ΔTN in equation (5.1) is representing the nitrogen gas produced and the nitrogen contained in the biomass in the reactor [85].

An in-depth description of the meaning of the diagnosis variables in Eqns. (5.2-5.6) and of their role in diagnosing the activity of the system biomass is provided in Mutlu *et al.* [85]. However, for the sake of completeness, a brief overview is presented:

In Eqn. (5.2) R_{AmmTot} represents the amount of ammonium consumed with respect to the amount of TN removed.

1) In case R_{AmmTot} is low, which means high conversion of ammonium into dinitrogen with respect to the amount of ammonium removed, the balance of the microbial activity is further checked by the value of R_{eff} which enables knowing if there is a fair activity of AOB.
    a. If R_{eff} is higher than 80%, the activity of the biomass is considered to be balanced.
    b. Otherwise, a low AOB activity is detected.
2) If the value of R_{AmmTot} is too high, i.e. ΔTN is too low with respect to NH_4^+ removed, the activity is defined as unbalanced. As a matter of fact, it is possible that, although NH_4^+ is significantly removed, the activity of AnAOB is compromised and/or excessive NOB concentrations are formed and/or the activity of AOB is too high. All these three conditions can be the cause of low ΔTN over ΔNH_4^+. To discriminate whether the imbalanced activity detected through R_{AmmTot} is given by NOB presence or not, the ratio of NO_3^- produced over ΔTN, represented in Eqn. (5.4), is used. As a matter of fact, the parameter quantifies the amount of NO_3^- produced over the total nitrogen removed. The higher NOB activity is, the larger R_{NatTot} is. According to the values of R_{NatTot}, two scenarios can be identified:

a. if R_{NatTot} is lower than 0.16 g NO_3^--N.g^{-1} N-TN (meaning no significant presence of NOB), R_{NitAmm} is then used to ascertain whether a nitrite accumulation is occurring or not as follows:
    i. If R_{NitAmm} is zero, then a limited activity of AOB is diagnosed because the variable represents the ratio between nitrite produced and the ammonium consumed.
    ii. if R_{NitAmm} is positive, then a problem of nitrite accumulation is detected because in a single-stage CANR reactor the nitrite produced by AOB should be subsequently consumed by AnAOB. In this case either too much nitritation or a limited activity of AnAOB would be the cause. To discriminate between these two situations the value of $R_{NitAmm,eff}$ (Eqn. (5.6)), which defines the ratio between the NO_2^- and NH_4^+ in the effluent, is used. In particular, in case (ii.a) $R_{NitAmm,eff}$ is larger than 1.32, the fault of the imbalance is addressed to an excessive activity of AOB, otherwise (ii.b) to a limitation in the AnAOB activity, being that AOB produce NO_2^- while AnAOB consume it.

b. If R_{NatTot} is higher than 0.16 g NO_3^--N.g^{-1} N-TN, NOB activity is high.

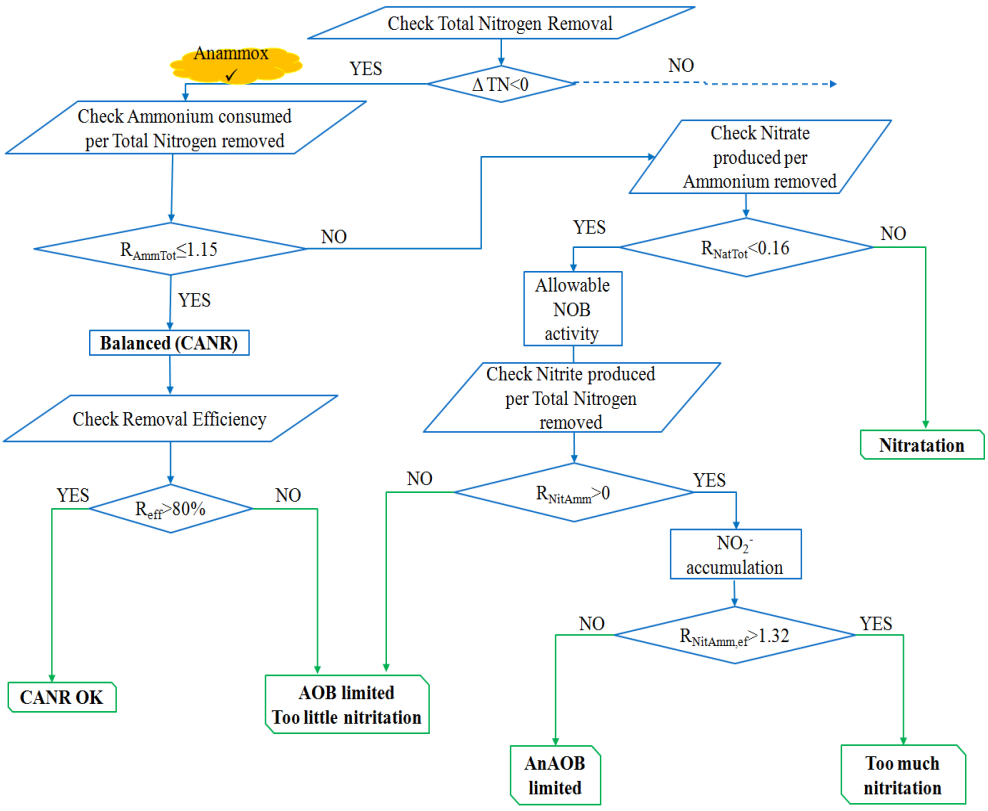

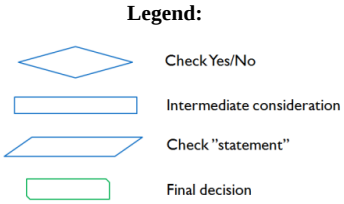

Figure 5.2: Diagnosis tree, adapted from Mutlu *et al.* [85].

Input variable centring and scaling. Before passing the inputs to the fuzzifier, the variables calculated through equations (5.2-5.6) were first centred and subsequently scaled. These two variable-handling procedures were performed in order to help defining the membership functions (MFs) shown in the subsequent paragraph more intuitively, thus allowing an easy implementation of the experience-acquired knowledge. As a matter of fact, centring the diagnosis inputs by subtracting their respective cut-off values used in the diagnosis tree (within the rhombus-shaped boxes in Figure 5.2) switches to "zero" the new cut-off value for all the variables. This is valid expect for $R_{eff,}$ which was not centred in order to preserve its own physical meaning of efficiency. Once centred, each variable was divided by a scaling factor. This served the purpose of making the numerical distributions of the input values uniform. Thus the MFs of the different variables could have been defined symmetrically. As resulted from these two operations, the variation range for all the crisp FIS inputs became [-1 1], apart from R_{eff} whose range remained [0 1].

Fuzzification. The membership functions for the input variables were chosen intuitively based on expert knowledge. Following as example the successful applications by Comas *et al.* [86], Garcia *et al.* [87] and Yong *et al.* [88], trapezoidal and triangular shapes were here chosen for the MFs for the sake of simplicity, as can be seen in Figure 5.3.
In order to illustrate the generic methodology adopted to define the MFs for the diagnosis inputs, the definition of membership functions for the ammonium removal efficiency (R_{eff}) is here shown as an example in Figure 5.3e.
Relying on process knowledge acquired during experiments, R_{eff} can be considered with 100% probability to belong to the linguistic set:

- "low" for values lower than 0.3,
- "medium" when it is equal to 0.5, and
- "high" when it is equal to 1.

With 100% degree R_{eff} is considered NOT belonging to the linguistic set:

- "low" when it is equal or higher than 0.5,
- "medium" for values equal or lower than 0.2 and equal or larger than 0.8, and
- "high" for values below 0.5.

To all the values of $R_{eff,}$ when 100% is the probability that the variable itself belongs to a linguistic set (i.e. 100% degree the R_{eff} is "low", "medium" and "high"), then one is the value assigned on the y-axis. To all the values of $R_{eff,}$ when 100% is the probability that the variable itself does not belong to a linguistic set (i.e. 100% degree the R_{eff} is "non-low", "non-medium" and "non-high"), zero is the value

assigned on the y-axis. To those values whose degree of membership to a certain fuzzy set is between 0% and 100%, the degree of membership varies linearly between these two values.

The decision of having a more or less smooth transition between two fuzzy sets of an input variable is based on experiences with process operation and understanding as well as on the desired behavior of the controller. In particular, for the definition of the membership functions (MFs) of each input variable the following property was taken into account: the higher the slope of a membership function of a control input variable is, the faster (relatively) the control action will be in response to changes in the input itself. For example, in the case of R_{AmmTot}, (scaled and centered) values with a degree to be classified as "Very High" are highly undesired from process operation point of view, while values in the range of "CANR" and/or "High" are considered to be fine. This is because, as can be deduced from the diagnosis tree in Figure 5.2, too high values of this variable would surely mean an imbalanced activity of the biomass (too high/low AOB activity and/or limited AnAOB activity and/or too much nitratation). This implies that, when R_{AmmTot} grows towards the region of the fuzzy set "Very High", the control action should be very fast in taking a control action to which a rapid decrease of R_{AmmTot} would correspond. By setting the slopes of MFs steeper in the region between the fuzzy sets "High" and "Very High", the transition between these two fuzzy sets is sensitized more and therefore emphasized more. Thus when R_{AmmTot} increases in that region (within the range [0.6 1]), the transition from the fuzzy set "High" to the fuzzy set "Very High" goes more rapidly and, in response to this, the controller will react faster.

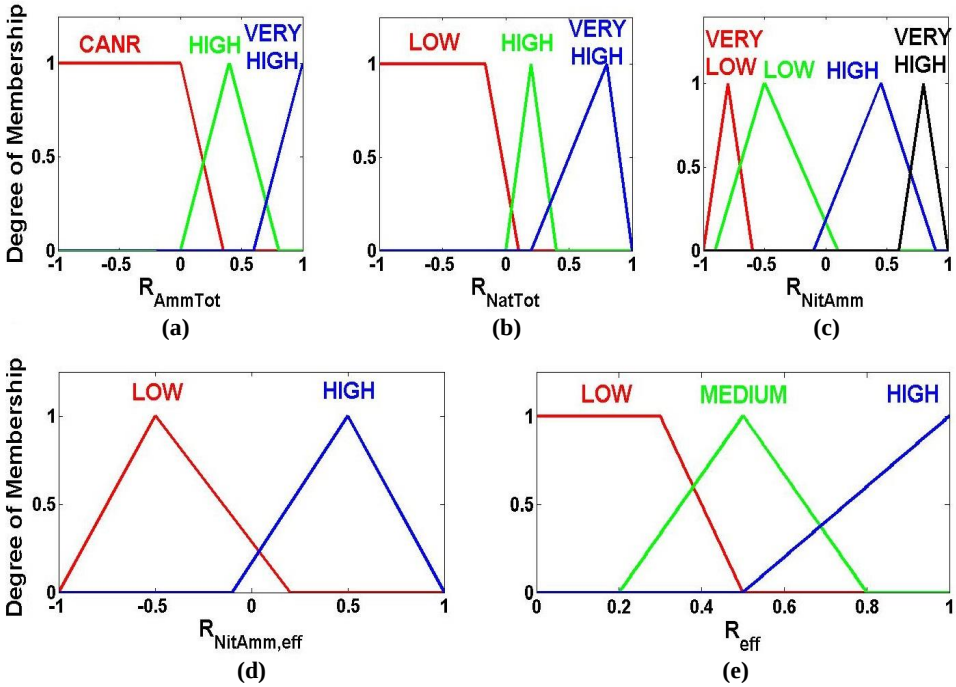

Figure 5.3: Membership functions of FLD inputs: **(a)** R_{AmmTot}, **(b)** R_{NatTot}, **(c)** R_{NitAmm}, **(d)** $R_{NitAmm,eff}$ and **(e)** R_{eff}.

Fuzzy inference. The IF-THEN rules were deduced from the diagnosis tree in Figure 5.2. Look-up tables including these rules are presented altogether in Table 5.1. The Mamdani-type inference was chosen for the sake of simplicity as the definition of Sugeno-type inference rules requires too specific knowledge for the consequent part of the rule. The rules have the same degree of importance with one another. Hence the same weights were assigned to all the rules. The implication method used when inferring from each rule a degree of membership for the related output variables was the correlation-minimum while disjunctive was the aggregation method chosen in order to sum up all the degrees of membership for the same output variables into one.
As outputs from this module, degrees of membership for each fuzzy set of each output are found.

Table 5.1: Fuzzy-logic diagnosis rules: **(a)** Output 1 = CANR performance index, **(b)** Output 2 = Nitritation, **(c)** Output 3 = AnAOB activity and **(d)** Output 4 = Nitratation.

Legend: VH=Very High, H=High, M=Medium, L=Low VL=Very Low, NL=Non-Limited, L=Limited and AZ=Almost Zero.

(a)

$\downarrow R_{eff}$ /R_{AmmTot} →	L	H	VH
H	***VH***	***H***	***L***
M	***OK***	***OK***	***L***
L	***L***	***L***	***L***

(b)

IF [R_{AmmTot} not Low] AND [R_{NatTol} Low] AND

$\downarrow R_{NitAmm,ef}$ /R_{NitAmm} →	VL	L	H	VH
L	***VL***	***L***	***OK***	***OK***
H	***VL***	***L***	***H***	***VH***

IF [R_{AmmTot} =Low] AND

$\downarrow R_{AmmTot}$ / R_{Eff} →	H	F	L
L	***OK***	***L***	***VL***

(c)

IF [R_{AmmTot} not Low] AND [R_{NatTol} = Low] AND

$\downarrow R_{NitAmm,ef}$ /R_{NitAmm} →	VL	L	H	VH
L	***NL***	***NL***	***L***	***L***
H	***NL***	***NL***	***NL***	***NL***

IF [R_{AmmTot} is Low] OR [R_{NatTol} not Low], THEN [AnAOB activity= NL]

(d)

$\downarrow R_{NatTot}$ /R_{AmmTot} →	L	H	VH
L	***AZ***	***AZ***	***AZ***
H	***AZ***	***L***	***H***
VH	***AZ***	***H***	***VH***

Defuzzification. The MFs shown in Figure 5.4 have been used for the FLD outputs. Similarly to those used for fuzzification, these functions were also defined with trapezoidal and triangular shapes. Theoretically the definition of these MFs could be done arbitrarily since the output variables at issue do not have a physical meaning but a quality-descriptive one. However, to check the performance of the FLD, its outputs have to be interpreted easily. For this purpose, low numerical values of CANR performance index, nitritation and nitratation (x-axis) belong to linguistic sets indicating low performance and/or low activity. On the other hand, high numerical values of the same variables were assigned to linguistic sets indicating high performance and/or high activity. The exception is the variable "AnAOB activity" to which an intrinsic meaning of "AnAOB activity limitation" was attributed. In this case, high numerical values are representative of higher limitation whereas low values represent low limitation. By defining the membership functions for the FLD outputs in this way, the resulting interpretation of the diagnosis performance could be done more intuitively.
The conversion of the degrees of membership (y-axis) for each FLD output found through the rules into a single numeric (crisp) value (x-axis) was chosen to be performed according to the Centre-Of-Area method. This choice was made in virtue of its characteristics of continuity and non-ambiguity mentioned in Helledoorn and Thomas [89].

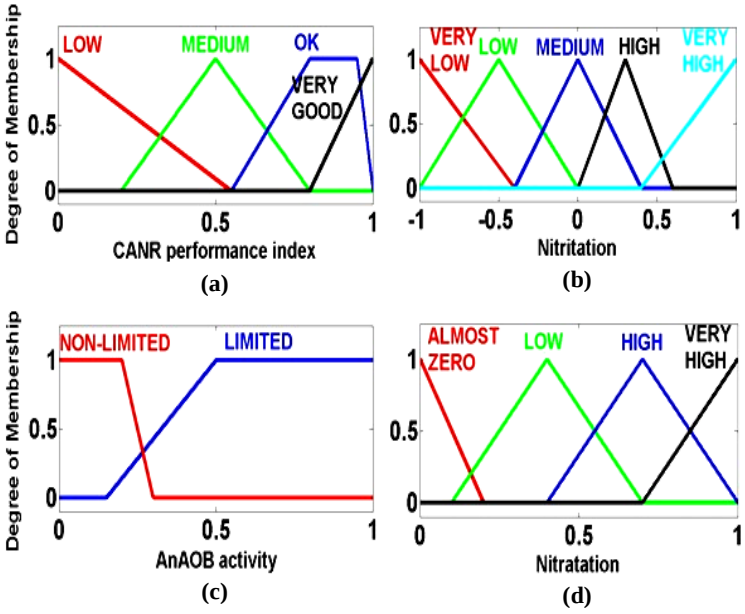

Figure 5.4: Membership functions for fuzzy-logic diagnosis outputs: **(a)** CANR performance index, **(b)** Nitritation, **(c)** AnAOB activity and **(d)** Nitratation.

Development of Fuzzy-Logic Control

Identification of the input and output variables. The fuzzy-logic control input variables correspond to the fuzzy-logic diagnosis output variables as its work is to infer control actions on the basis of the diagnosed biological activity. Thus the variables "*activity of aerobic AOB", "activity of AnAOB"* and "activity of *NOB"* and *"CANR performance index"* are identified as inputs. On the basis of their values, the fuzzy-logic control will infer the deviation of the manipulated variables (MVs) chosen from their respective nominal values. In order to identify the MVs a degree of freedom analysis was performed according to Larsson and Skogestad [90]. On the basis of this analysis the following four manipulated variables were considered as potential candidates: the mixer, the electrical heating jacket, the air supply and the exchange ratio (ER). The heating jacket is assumed to perfectly control the temperature. The mixer was not considered as a suitable MV due to a lack of mechanistic knowledge relating the mixing conditions to the process performance. ER was controlled at 0.5. For this reason the only MV chosen to control the process performance metric was the air supply, modelled as the oxygen mass transfer coefficient (k_La). The deviation of this MV (Δk_La) represents therefore the actual output of the FLC.

Fuzzification. The same MFs used for the defuzzification in FLD (shown in Figure 5.4) were used to find the probability of membership to the fuzzy sets for each input.

Fuzzy inference. Similarly to the FLD, also for this tool the Mamdani-type inference was used. The same importance degree was attributed to all of the IF-THEN rules. Correlation-minimum and disjunction were the methods chosen for the implication and aggregation operations respectively. Since the AnAOB activity is intrinsically linked with balanced nitritation and nitratation, ensuring a balanced activity of AOB and NOB implies ensuring a balanced AnAOB activity. Hence including rules for changes of the k_La in order to have balanced nitritation and nitratation can be considered sufficient to avoid AnAOB limitation. Thus, in order not to overload the control system with additional and superfluous rules, no direct rule linking k_La variation with AnAOB activity was taken into account. In the following look-up table the list of control rules used is presented.

Table 5.2: Fuzzy-logic control rules.

Legend: Z=zero; PL=Positive Large, P=Positive, N=Negative; NL=Negative Large, VG=Very Good;

↓Nitritation/CANR index →	VG	OK	M	LOW
VL	***P***	***P***	***PL***	***PL***
L	***Z***	***Z***	***P***	***P***
M	***Z***	***Z***	***Z***	***Z***
H	***Z***	***Z***	***N***	***N***
VH	***N***	***N***	***NL***	***NL***

↓Nitratation/CANR index→	VG	OK	M	LOW
AZ	***Z***	***Z***	***Z***	***Z***
L	***N***	***N***	***N***	***N***
H	***N***	***NL***	***NL***	***NL***
VH	***NL***	***NL***	***NL***	***NL***

Defuzzification. The MFs of the k_La deviation were shaped as trapezoidal and triangular as the MFs in the diagnosis. In Figure 5.5 the MFs of this variable are depicted. Similarly to the FLD, the method used to deduce a crisp value on the basis of the degrees of membership for each fuzzy sets of "k_La deviation" was the Centre-Of-Area.

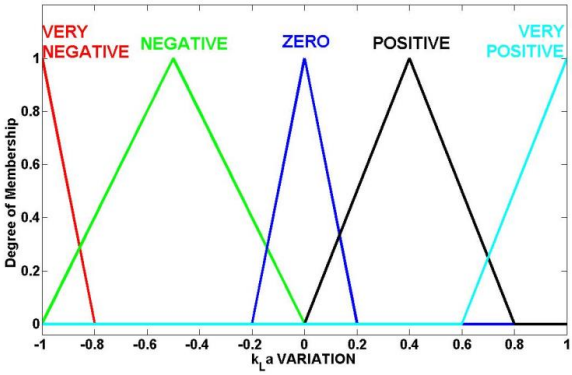

Figure 5.5: Membership functions of fuzzy-logic control output (k_La variation).

Output variable scaling. The crisp values obtained for k_La deviation from defuzzification are then scaled by multiplying the values by 150 d^{-1}.

5.2.4. Results and discussion

The block diagram of the fuzzy logic diagnosis and control system implementation to control the PN/A system is given in Figure 5.6.

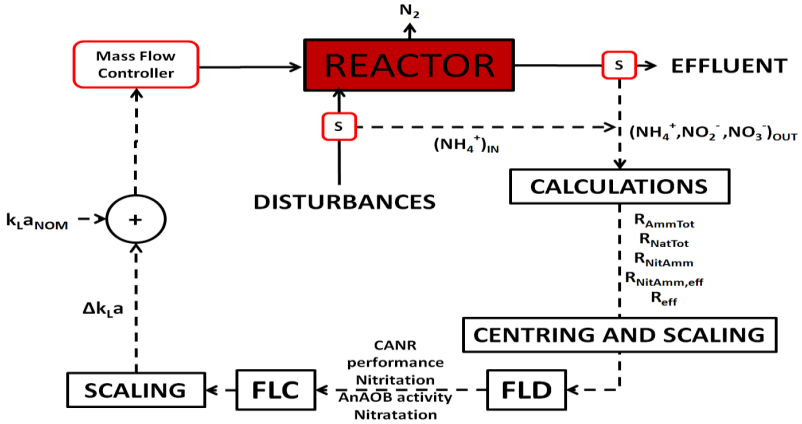

Figure 5.6: Structure of the fuzzy logic diagnosis and control system (FLD=Fuzzy-Logic Diagnosis, FLC=Fuzzy-Logic Control, S=Sensors).

As can be seen in Figure 5.6, the concentration of ammonium is measured both in the influent and in the effluent along with the effluent nitrite and nitrate concentrations. The sampling was done at the beginning of each cycle for the compounds in the influent and at the end of each cycle for those in the effluent. At this stage, measurement noises were not taken into account assuming their negligible influence in the context of a fuzzy-logic control where the measured (crisp) variables are handled in a fuzzified environment. The measured values obtained were then used to calculate the FLD inputs, namely R_{AmmTot}, R_{NitAmm}, R_{NatTot}, R_{eff} and $R_{NitAmm,eff}$. These inputs, after preliminary centring and scaling, were then handed over to the FLD tool which inferred the CANR performance index, Nitritation, AnAOB activity and Nitratation. At this point it is worth noting that the FLD outputs are called variables, although they have a quality-descriptive meaning rather than a physical meaning. As a matter of fact, they depict altogether the microbiological activity of the biological system. On the basis of their crisp values deduced by the FLD, the FLC is then able to infer the variations of the manipulated variable (k_La) from their respective nominal values. This control action takes place at the beginning of the reaction phase of the next cycle.

More in detail, the procedure according to which the proper control actions are calculated on the basis of the measurements is summarized in the following sequential steps:

I. Calculation of the crisp values for the diagnosis input variables: parameters R_{AmmTot}, R_{NatTot}, R_{NitAmm}, $R_{NitAmm,eff}$ and R_{eff} are calculated through Eqns. (5.2-5.6) by using the measured concentration of nitrogen species in the liquid phase,

II. Centring and scaling of the diagnosis input variables: the parameters calculated in I are centred according to their respective cut-off values given in the tree-like scheme of Figure 5.2 and scaled,

III. Fuzzy-logic Diagnosis: crisp values for CANR performance index, Nitritation, AnAOB activity and Nitratation are inferred on the basis of the crisp values of the centred and scaled R_{AmmTot}, R_{NatTot}, R_{NitAmm}, $R_{NitAmm,eff}$ and R_{eff},

IV. Fuzzy-logic Control: crisp values for Δk_La are inferred on the basis of crisp values for CANR performance index, Nitritation, AnAOB activity and Nitratation given by III,

V. Scaling of Fuzzy-logic Control outputs: the crisp values of Δk_La are multiplied by their respective nominal values.

VI. Calculation of the actual k_La as input to the reactor: Addition of the scaled Δk_La to their respective nominal values (i.e. $k_La(t) = k_La_0 + \sum_{i=0,\ldots\ldots t} (\Delta k_La(t))$).

Step III, namely fuzzy logic diagnosis, can be further split up into the following sub-steps:

IIIA. Diagnosis fuzzification: the crisp scaled and centred inputs R_{AmmTot}, R_{NatTot}, R_{NitAmm}, $R_{NitAmm,eff}$ and R_{eff} are converted into input fuzzy sets by means of the MFs shown in Figure 5.3,

IIIB. Diagnosis inference: the fuzzy outputs are generated from the corresponding input fuzzy sets on the basis of the rules in Table 5.1,

IIIC. Diagnosis defuzzification: the fuzzy outputs (CANR performance index, Nitritation, AnAOB activity and Nitratation) obtained in IIIB are then translated into numerical values for

CANR performance index, Nitritation, AnAOB activity and Nitratation through the Centre-of-Area method applied on the MFs shown in Figure 5.4.

Step IV, namely fuzzy logic control, can be further split up into the following sub-steps:

IVA. Controller fuzzification: the crisp values for CANR performance index, Nitritation, AnAOB activity and Nitratation obtained from sub-step IIIC are converted into input fuzzy sets by means of the same MFs used for IIIC,

IVB. Controller inference: the fuzzy inputs obtained in IVA are transformed into control fuzzy outputs according to the set of rules in Table 5.2,

IVC. Controller defuzzification: the controller fuzzy outputs (variation of k_La) are converted into their respective crisp values by applying the Centre-of-Area method on the MFs shown in Figure 5.5.

Table 5.3 sums up the input and output variables of the diagnosis and control tools.

Table 5.3: **(a)** Fuzzy-logic diagnosis input, **(b)** Fuzzy-logic diagnosis outputs and **(c)** control outputs.

(a)

FLD INPUT 1	FLD INPUT 2	FLD INPUT 3	FLD INPUT 4	FLD INPUT 5
R_{AmmTot}	R_{NitAmm}	R_{NatTot}	$R_{NitAmm,eff}$	R_{eff}

(b)

FLD OUTPUT 1	FLD OUTPUT 2	FLD OUTPUT 3	FLD OUTPUT 4
CANR performance index	Nitritation	AnAOB activity	Nitratation

(c)

FLC OUTPUT
Δk_La

Since FLD and FLC are independent tools, it is possible to separately evaluate the performance of each model.

Evaluation of the diagnosis tool

Since the control actions are based on the FLD outputs, a first check on the reliability of the outputs generated by the FLD is performed. To this end, data obtained from 100-day experimentation on the lab-scale reactor described in Vangsgaard *et al.* [50] were used. It is noted that the data were obtained from a period where the system was operated in a manual operating mode following the operation protocol given by Mutlu *et al.* [85]. Hence these data serve for the purpose of evaluating the performance diagnosis module alone. In Figure 5.7, the effluent concentrations of the three nitrogen species (i.e. ammonium, nitrate and nitrite) collected during the experiments and the related total

nitrogen removal efficiency are depicted. By using these data as inputs to the diagnosis module, the FLD outputs plotted in Figure 5.8 are obtained.

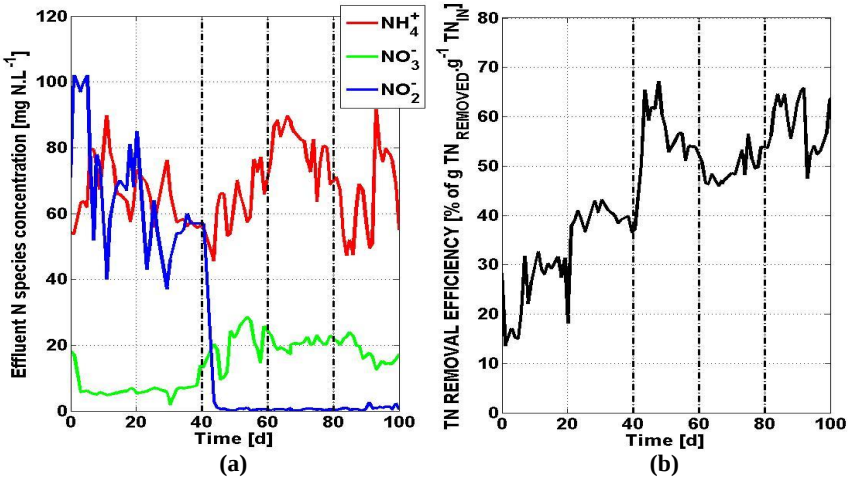

Figure 5.7: Input data set to FLD module: **(a)** effluent nitrogen species concentration (on the left: NH_4^+ (red), NO_3^- (green) and NO_2^- (blue)) and **(b)** TN removal efficiency (on the right).

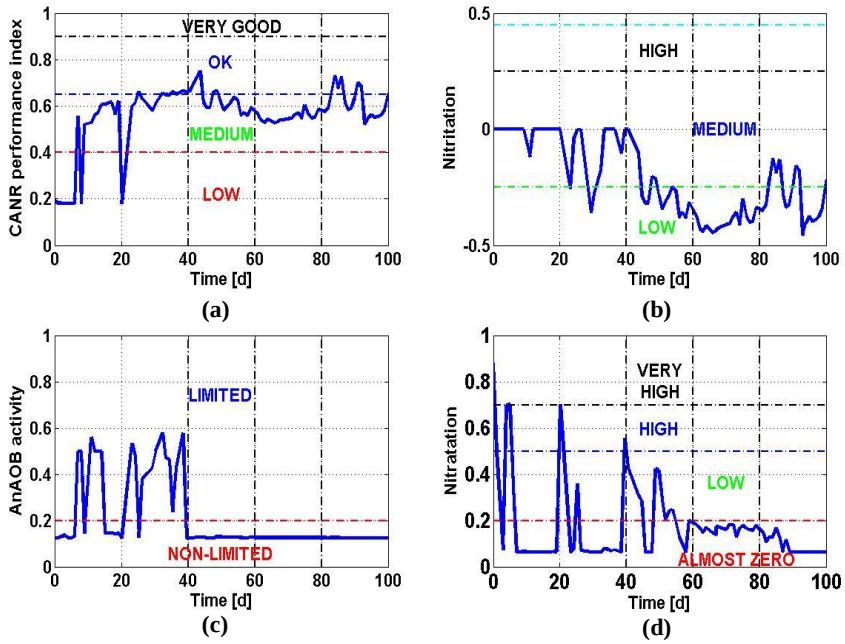

Figure 5.8: Output from FLD module: results of the fuzzy-logic diagnosis for 100 days.

As can be seen in Figures 5.7 and 5.8, the total duration of the experiment can be split up into four subsequent periods identified on the basis of the different behaviours of the biomass: from the beginning of the experiment till day 40, from day 40 till day 60, from day 60 till day 80 and from day 80 till the end.

By looking at Figure 5.8, the activity of the AnAOB is limited by high nitratation during the first period. This is because, as revealed in Figure 5.8d, the NOB activity is so high that the availability of NO_2^- for AnAOB is significantly reduced. As a result of this undesired imbalance (i.e. the NO_2^--to-NH_4^+ ratio), the performance is mostly unsatisfactory, which can be seen from the CANR performance index. By following the operation protocol in manual mode, during the second period the O_2 supply rate to the system was decreased. This operation helped AOB to successfully outcompete or reduce the NOB activity in the system – a desirable condition for promoting AnAOB activity and therefore achieving higher performance [85], as described by the CANR performance index. During the subsequent period of time, as a consequence of low oxygen availability due to a continuous decrease of air supply, NOB activity became negligible which in turn allowed AnAOB activity. However, also AOB activity got compromised and consequently the performance of the system decreased, as diagnosed by the CANR performance index. In the last period, a higher oxygen supply temporarily re-established nitritation to medium levels. In response to a higher ammonium oxidation, the system performance became satisfactory.

In order to evaluate the reliability of the diagnosis results, a comparison is made between the scenario described by the diagnosis outputs on the one hand, and the effluent concentrations of the nitrogen species measured and the calculated TN removal efficiency on the other hand. As can be seen in Figure 5.7a, NO_2^- in the first period is high (40-100 mg $N.L^{-1}$) compared to its concentration in the other periods. This is the result of its lacking consumption by AnAOB. As a matter of fact, when the nitrite concentration drops down to negligible values, the AnAOB activity is diagnosed as non-limited. Hence the FLD tool can be said to describe the activity of AnAOB in a realistic way.

The effluent NO_3^- concentrations measured during the first period are low (around 8 mg $N.L^{-1}$) compared to the concentration of the same compound in the other periods (around 20 mg $N.L^{-1}$). Although this may appear to be inconsistent with the diagnosed NOB activity, it has to be pointed out that the qualitative description of the different classes of biomass is in function of the purpose of the system, which is to remove a high percentage of nitrogen. Thus the qualitative description of NOB activity is a function of the capability of their interference with the system performance. For this reason, since the diagnosis results regarding AnAOB limitation and NOB activity are consistent with each other (i.e. for high NOB activity, AnAOB are limited and vice versa), nitratation can be considered to be described correctly by the FLD.

Particularly evident is the correlation between effluent ammonium concentrations and the aerobic activity of AOB diagnosed. As can be noted in Figure 5.8b and Figure 5.7a, an increase of effluent NH_4^+ concentration corresponds to a decrease in AOB activity. Hence the FLD tool realistically describes the aerobic activity of AOB.

The tool performs reliably, also in terms of overall system performance description, as the CANR performance index follows the TN removal efficiency time dynamics throughout the experimentation period.

Given these considerations, the results of the diagnosis can be considered reliable enough for the FLC to infer proper control actions.

Evaluation of the control tool

The system shown in Figure 5.6 was implemented in Simulink in order to test its capability to achieve the control objective, namely high and steady TN removal efficiency. The control performance evaluation was done by simulating the implemented model with a step input disturbance on the ammonium concentration in the feed for a period of 18 days. The change was imposed to occur when the batch cycles were approximately steady, that is after 10 days counting from the beginning of the simulation. The initial conditions were taken from a steady state solution of an equivalent continuous reactor. In Figure 5.9 the microbiological state of the system biomass diagnosed is screened by plotting the dynamics of the FLD outputs. The difference between the concentrations of total nitrogen fed at the beginning of the cycle and at the end of the same cycle was divided by the concentration of TN fed at the beginning of the cycle to obtain the TN removal efficiency plotted in Figure 5.10. Since the production of nitrogen gas is indicative of the removal efficiency, the nitrogen gas concentration in the reactor is also shown. Figure 5.11a depicts the dynamics of the nitrogen species concentration in the reactor effluent at the end of each cycle. The change of the manipulated variable, i.e. oxygen mass transfer coefficient, throughout the simulation period is shown in Figure 5.11b.

As can be noted in Figure 5.10, the system gets approximately stabilized within 4 days. The TN removal efficiency prior to the step change was already at a very high level at around 93%. As a result of the immediate increase of ammonium in the feed at the 10^{th} day, the concentration of NH_4^+ in the effluent increases (Figure 5.11a) and, consequently, the CANR performance index drops down (Figure 10a). Corresponding to this, the TN removal efficiency drops down to a minimum of 86%. The controller reacts to this scenario by increasing the k_La (Figure 5.11b) to a value at around 250 d^{-1}. Thus the removal efficiency performance is increased and established at a higher stable value of 89% and returns to the area where the CANR performance index is very good. Given that, according to the diagnosis, the system operates in the desired range, the controller then stops changing the aeration flow.

In order to further increase the removal efficiency, the definition of the linguistic variable “very good CANR performance index” must be restricted to higher values. However, trying to operate at so high removal efficiencies despite disturbances comes with a disadvantage, since it increases the risk of occurrence of nitratation. Hence, the controller is able to reject the disturbance on the ammonium influent loading while keeping the microbial activity balanced.

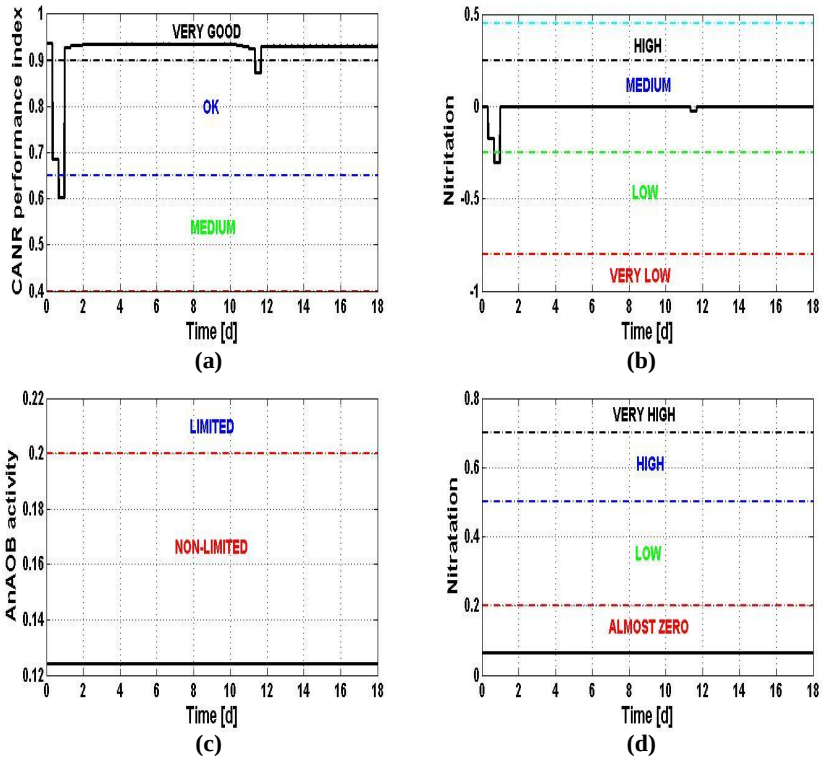

Figure 5.9: Diagnosis outputs from the simulation of a controlled system with a +10%-step-change disturbance in the influent ammonium concentration 10 days after the start of the simulation.

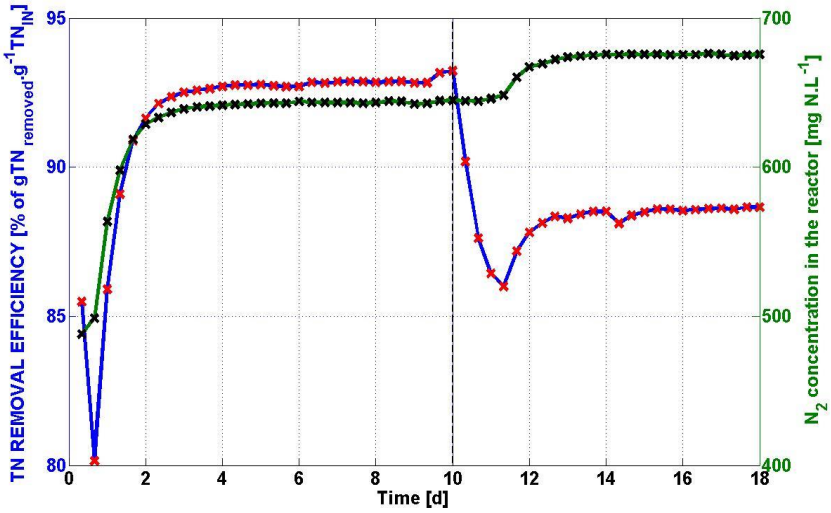

Figure 5.10: Dynamics of total nitrogen removal efficiency (blue line, red crosses) and N_2 concentration in the reactor (dark-green line, black crosses) with a +10%-step-change disturbance in the influent ammonium concentration at day 10.

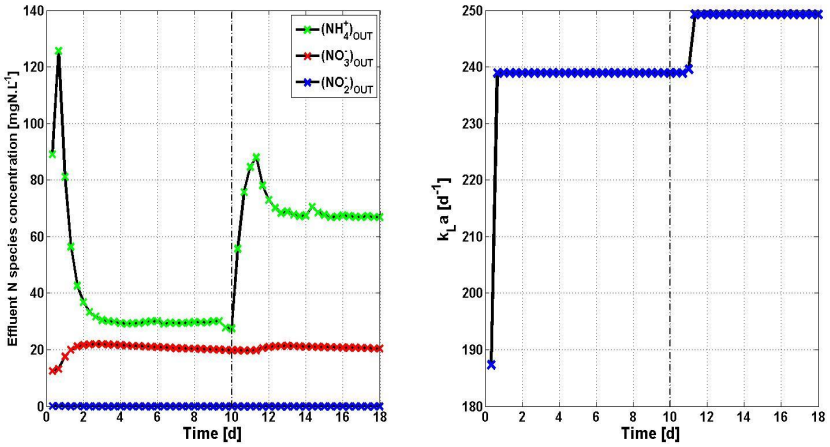

(a) **(b)**

Figure 5.11: **(a)** Dynamics of nitrogen species concentration in the effluent (left graph: NH_4^+ (green crosses), NO_3^- (red crosses) and NO_2^- (blue crosses)) and **(b)** dynamic trend of oxygen mass transfer coefficient (k_La) (right graph) with a +10%-step-change disturbance in the influent ammonium concentration at day 10.

5.2.5 Conclusions

In this section, the performance of a granular PN/A system has been upgraded through the implementation of a fuzzy-logic control aided by a fuzzy-logic diagnosis. The long term real process data obtained from operation of a lab-scale reactor was used to verify the fuzzy-logic diagnosis module. Next, the fuzzy-logic control module was tested and evaluated using dynamic simulations and has shown to achieve high and stable total nitrogen removal efficiency (around 90%). The originality of the control structure is that the fuzzy-logic control uses the valuable information about the microbiological state of the system that has been deduced from macro-measurements using process stoichiometry contributions by different microbial groups.

The fact that the fuzzy-logic diagnosis tool is developed and used separately from the fuzzy-logic control augments the value of the work in terms of transparency and flexibility. Transparency is gained because the user can see the diagnosis output as well as controller outputs. The performance of the FLD can therefore be checked independently from the actions of the FLC. For the users, this in turn allows easy maintenance and further enhancement of the diagnosis and control modules in case the control performance needs improvement.

Fine-tuning has to be considered as the next task. The present control strategy is not able to achieve high TN removal efficiency gained prior to applying the step change. This can be attributed to the fact that the membership functions for the input variables to the fuzzy-logic diagnosis module and the output variable of the fuzzy-logic control model were not defined in direct link to the control objectives. As a consequence, the new set point achieved is not exactly the one desired. For the reason, in the next section the present controller will be finely-tuned according to a systematic methodology.

5.3. Systematic design of membership functions for fuzzy-logic control: a case study on one-stage partial nitritation/Anammox treatment systems

In this section a fuzzy-logic controller with the same objective as the one presented in Section 5.2 is presented in order to provide a systematic methodology according to which membership functions for input and output variables are designed in function of pre-specified control objectives. On the basis of this example, a generic formulation of the methodology will be given in Section 5.4. The current section is presented the work published in Boiocchi *et al.* [73].

5.3.1. Introduction

As disclosed in Section 5.1, fuzzy-logic control design needs to have a systematic procedure at the aim of avoiding undesired behaviour of the control system itself. The systematic procedure will allow connecting easily control objectives to the parameters determining the control performance and thus will be useful in case of need for fine-tuning. Without such a systematic approach, the performance of a fuzzy-logic controller may result unexpectedly low and this can hinder taking advantages from the typical benefits of the fuzzy-logic approach, such as the possibility of incorporating knowledge-based control actions, the detachment from the reliability of dynamic models, whose calibration can be often case specific, and the chance of controlling highly non-linear process systems. The fuzzy-logic controller presented in Section 5.2 will be fine-tuned with the aim of exploring the possibility of linking pre-defined control objectives to the main design parameters of fuzzy-logic controllers. The definition

of the membership functions (MFs) will be the focus of the work since, as stated by Seborg *et al.* [71], their definition plays a major role in determining the FLC performance.
Once implemented, the performance of the novel controller is evaluated on the basis of the results from simulations of the PN/A reactor model by Vangsgaard *et al.* [43] with different types of disturbances. In particular, step increase and decrease in influent ammonium and readily-biodegradable carbon are used first to understand the general behaviour of the controller. In a second instance, a long-term realistic dynamic influent scenario is used to benchmark the systematically-designed FLC against a number of other control strategies (CSs) from the literature [51,72]. Finally, since there is a large number of PN/A applications working in sequencing batch reactors (SBRs) [44], the performance of the systematically-designed FLC strategy is tested in a lab-scale SBR with realistic influent dynamics. The performance is additionally evaluated by incorporating measurement noise and an actuator model.

5.3.2. Materials and methods

The systematically-developed control strategy will be tested in two reactor configurations for one-stage PN/A treatment process: a full-scale continuous reactor and the sequencing-batch reactor. Both the reactors are modelled to have the equipment described in subsection 3.5.1. Here these two reactor configurations are presented.

Continuous configuration

The continuous PN/A reactor used corresponds to the one modelled as described in Section 3.5. During the biological processes, pH and temperature are assumed to be ideally controlled at their optimal values of 7.3 and 35ºC, respectively. A reactor volume of 400 m^3 was identified as ideal. As a first evaluation of the control performance on this system, the dynamic responses to step changes in both NH_4^+ and S_S loads are used. In particular, within an overall simulation time of 2000 days, the step was imposed at the 150th day, namely once the steady-state was ensured. In a second instance, the control strategy is benchmarked across open-loop and other CSs with a 609-day long realistic dynamic influent obtained from the Benchmark Simulation Model nº2 (BSM2) by Jeppsson *et al.* [22]. A nominal value of the oxygen mass transfer coefficient (k_La) of 164 d^{-1} was used according to the set point of the volumetric oxygen-to-ammonium loading rate (RO) equal to 1.66 g $O_2.g^{-1}$ N selected by Vangsgaard *et al.* [51]. The nominal value chosen has only a limited effect on the overall performance in the long term. In this simulation environment, the capability of the novel control strategy (*CS1*) in rejecting the disturbances will be benchmarked against:

- open-loop,
- a configuration corresponding to *CS1* with measurement noises and actuator delay (*CS2*), whose modelling is reported in the Appendix (Sections A.2 and A.3 respectively),
- the feedforward control strategy developed by Vangsgaard et al. [51] (*CS3*),
- a feedforward-feedback controller (*CS4*) built up by using the newly-developed fuzzy-logic control strategy to update the RO set point (RO_{sp}) of the feedforward CS3,
- the intuitively-developed fuzzy-logic control strategy by Boiocchi et al. [72] (*CS5*).

Following the BSM2 protocol defined for the performance evaluation of control strategies by Jeppsson *et al.* [22], the full-scale continuous reactor is simulated for 609 days with a sampling time of 15 minutes. The simulation results of the last 52 weeks are then used to calculate evaluation criteria such as: the average total nitrogen removal efficiency ($\overline{\eta_{TN}}$), the standard deviation of η_{TN} ($\sigma(\eta_{TN})$), the integral absolute error (*IAE*) and the total variation of the k_La (*TV*). The IAE is used to quantify the ability of the controller in keeping the removal efficiency equal or above the minimal target of 92%

without differentiating between deviations occurring at the beginning or at the end of the evaluation period of time. On the other hand, the TV is used to quantify the manipulation of the manipulated variables. An ideal controller would require lower variation to maintain a set-point tracking. In addition, TV is a useful performance indicator (qualitatively) for actuator maintenance: a high TV – a sign of aggressively tuned controllers, means frequent and significant changes in actuators which implies increased need for equipment maintenance. Therefore, all other things being equal, a lower TV would be desirable when benchmarking several controller candidates. In addition, in order to evaluate the economic feasibility of the control strategies, the average aeration energy (AAE) consumed is considered. This quantity is calculated by assuming that 1.8 kilos of oxygen is transferred per kWh consumed, according to the BSM2 protocol [91], as expressed in Eqn. (2.6).
The measurement noise signals introduced for *CS2* are modelled by transforming the actual value of the controlled variable by a linear transfer function, through which the delay is implemented.

Sequencing batch configuration

With regard to the performance evaluation in a lab-scale PN/A SBR, the reactor is the same as the one used in Section 5.2. The dynamic influent by Mauricio-Iglesias *et al.* [92], depicted in Figure 5.12, is used to test the newly-developed control strategy. In addition, the performance obtained will be compared against the performance of the control strategy *CS5* in order to quantify the importance of using a systematic methodology for FLC design.

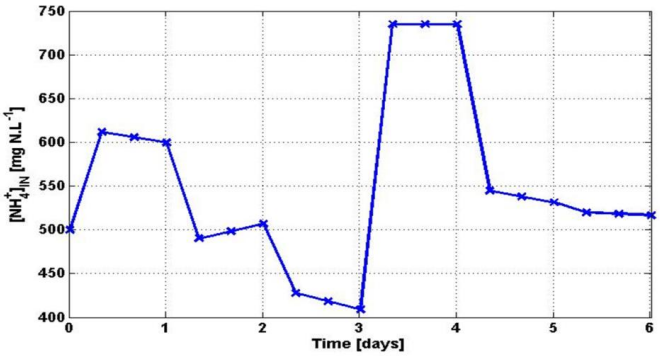

Figure 5.12: Influent ammonium concentration dynamics for the lab-scale sequencing batch reactor [92].

5.3.3. Design of the fuzzy-logic controller for the single-stage Partial Nitritation/Anammox system

In this work, the design of the FLC applied to a single-stage PN/A system is performed according to the following sequential steps:

1) specification of the optimization problem,
2) identification of so-called "critical points" for the controlled variables,
3) definition of membership functions of input and output variables,
4) implementation of the linguistic rules, and

5) tuning of additional design parameters.

In-depth descriptions regarding each of these steps will be presented in the next subsections.

1) Specification of the optimization problem

1a. *Specification of the control objectives*

In general, a controller is required to behave in such a way that, when the control objectives are met, i.e. the variable to be optimized (VAR_{OPT}) takes the desired value, no change in control action is taken. In biological system applications there is a single value or, more likely, a range of values for VAR_{OPT} which can be considered satisfactory. This situation is here defined as the so-called "optimal system operation". In fuzzy-logic control an additional value or set of values for VAR_{OPT} defining a so-called "worst system operation", which describe the system to be in a highly-undesired state, needs to be identified. When the system is found in this range, the controller will be designed such that the maximal control action is taken. Thus the system is moved away from the "worst system operation" as fast as possible. Between these two system operation modes, there is a third mode, the so-called "suboptimal system operation". In view of this, the control objectives can be generally stated for biological applications according to the following formulation of constraints for VAR_{OPT} (lower and upper bound of each operation mode):

$$\begin{cases} \text{OPTIMAL SYSTEM OPERATION: } LB_{OPT} \leq VAR_{OPT} \leq UB_{OPT} \\ \text{SUBOPTIMAL SYSTEM OPERATION: } UB_{WORST} < VAR_{OPT} < LB_{OPT} \\ \text{WORST SYSTEM OPERATION: } LB_{WORST} \leq VAR_{OPT} \leq UB_{WORST} \end{cases} \quad (5.7)$$

In Eqn. (5.7) LB_{OPT} and UB_{OPT} are the lower and upper boundaries defining the range for the "optimal system operation" whereas LB_{WORST} and UB_{WORST} are the lower and upper boundaries defining the range for the "worst system operation", respectively. Assuming that the control objectives are meant to maximize VAR_{OPT}, UB_{OPT} represents the absolute best operation while LB_{WORST} is the absolute worst operation. UB_{OPT} and LB_{WORST} are respectively the minimal and the maximal value that VAR_{OPT} can possibly take. In case a single value of VAR_{OPT} identifies the optimal system operation, LB_{OPT} and UB_{OPT} will have the same value.

For the present case study, a controller has to be built for high and stable TN removal efficiency (η_{TN}) (i.e. VAR_{OPT}) into a single-stage PN/A system. 100% is the theoretical maximal value for η_{TN} that can be achieved in a single-stage PN/A system. However, since the effluent of the side-stream reactor is supposed to be recycled to the mainstream activated sludge treatment units and thus further treated, there is no need to keep the system at such a high performance level, meaning that lower efficiencies of the PN/A reactor can be tolerated as well. A minimal acceptable value for η_{TN} equal to 92%, representing LB_{OPT} in Eqn. (5.7), is here chosen. Thus, when TN removal efficiency is found between a lower boundary of 92% and an upper boundary of 100%, no change in control action is taken. With regard to the "worst system operation", values of η_{TN} equal and below 75% are considered highly undesired, hence requiring the maximal control action. Thus, the control objectives can be mathematically expressed through the following set of constraints:

$$\begin{cases} \text{OPTIMAL SYSTEM OPERATION: } 92\% \leq \eta_{TN} \leq 100\% \\ \text{SUBOPTIMAL SYSTEM OPERATION: } 75\% < \eta_{TN} < 92\% \\ \text{WORST SYSTEM OPERATION: } 0 \leq \eta_{TN} \leq 75\% \end{cases} \quad (5.8)$$

1b. *Definition of the control structure*

The FLC will have the same input and output variables as the control strategy previously developed by Boiocchi *et al.* [72]. In particular, the controlled variables used are: ratio between NH_4^+ consumed and TN removed (R_{AmmTot}), ratio between NO_2^- produced and NH_4^+ consumed (R_{NitAmm}), ratio between NO_3^- produced and TN removed (R_{NatTot}), ratio between NO_2^- and NH_4^+ in the effluent ($R_{NitAmm,eff}$) and NH_4^+ removal efficiency (R_{eff}). The only manipulated variable used is the oxygen supply, here represented by the oxygen mass transfer coefficient (k_La). For issues related to ease of implementation of the expert knowledge and flexibility illustrated in Boiocchi *et al.* [72], the control structure is decomposed using the following four empirical indicators of the microbiological balance into the reactor as intermediary variables: "CANR performance index", "AOB activity", "AnAOB activity" and "NOB activity". Typical influent variables such as the concentrations of ammonium (NH_4^+), readily-biodegradable organic carbon (S_S), slowly-biodegradable organic carbon (X_S) and volumetric flow rate (Q) are considered as representative of the system disturbances. The state variables considered for the PN/A systems are the concentration of: ammonium, nitrite, nitrate, readily biodegradable organic material, slowly biodegradable organic carbon, AOB, NOB, AnAOB and HB. Eqns. (5.9-5.12) summarize the control system structure in terms of disturbance, manipulated, state and controlled variables.

$$\underline{y} = [R_{AmmTot}, R_{NitAmm}, R_{NitAmmEff}, R_{NatTot}, R_{eff}] \quad (5.9)$$

$$\underline{u} = [k_L a] \quad (5.10)$$

$$\underline{d} = [d_{NH_4^+}, d_{S_S}, d_{X_S}, d_Q] \quad (5.11)$$

$$\underline{x} = [x_{NH_4^+}, x_{NO_2^-}, x_{NO_3^-}, x_{S_S}, x_{X_S}, x_{X_{AOB}}, x_{X_{NOB}}, x_{X_{AnAOB}}, x_{X_{HB}}] \quad (5.12)$$

The overall structure of the controlled system is represented in Figure 5.13. As can be seen, from the PN/A system, the vector of controlled variables is measured and given directly as input to the first fuzzy-inference system FLC_1, which infers information about the biological state of the system. On the basis of this last, the second fuzzy-inference system FLC_2 deduces the unitary variation of the oxygen mass transfer coefficient ($\Delta_U k_L a$), which can take values between -1 and 1. $\Delta_U k_L a$ is then given a physical dimension by multiplication with a scaling factor (K_{SF}). By integration in time, the difference between the actual k_La to be applied to the system and the corresponding nominal value (k_La_0) is found. By addition of k_La_0 to this difference, the value of k_La is known.

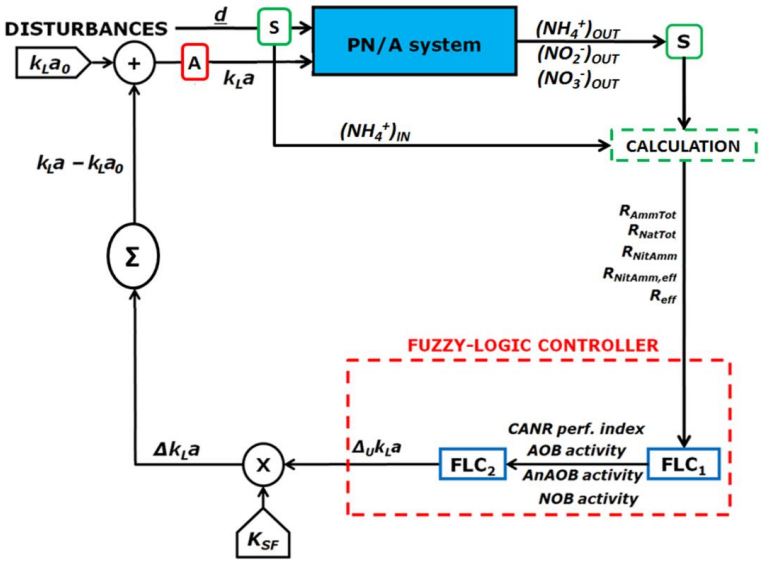

Figure 5.13: Structure of the control strategy implemented in the single-stage PN/A system.

1c. *Specification of the physical constraints*

The disturbance variables of Eqn. (5.11) are non-negative for physical reasons.

The manipulated variable, namely the oxygen mass transfer coefficient, is limited by a maximum value, i.e. a saturation limit of 300 d^{-1}.

The constraints on the state variables are used to enable the controller identifying the biological scenarios leading the system far from the control objectives. On the basis of the identified biological scenario, the controller is able to decide whether to infer a positive deviation of the manipulated variable or a negative deviation.

The first step for the definition of these constraints consists of the identification of the main microbiological scenarios leading to suboptimal and worst system performance and the ones leading to the best system performance. This is done on the basis of the findings from a sensitivity analysis performed by Vangsgaard *et al.* [43]. According to the observations reported, the best system operation can occur when: (a) no NOB are present in the system, (b) all the AOB-produced NO_2^- is consumed by AnAOB, and (c) both AOB and AnAOB co-operate to achieve a complete oxidation of all the influent NH_4^+. The microbiological scenarios leading the system far from the optimality are summarized in Table 5.4. As can be seen, the activities of AOB, AnAOB and NOB are considered as markers for the identification of the four key scenarios leading the system far from the achievement of the control objectives whereas HB activity is assumed constant. This implies that the FLC will be designed in such a way that the manipulation of the operating conditions will occur only when the activities of AOB, AnAOB and NOB will be compromised but not for mere changes of the HB activity. Thus, variations of the latter will require manipulation of the k_La only in case they change the activity of the other classes of microorganisms. This choice was taken because HB activity is generally low given the poor amount of biodegradable organic carbon in the influent.

Table 5.4: The four microbiological scenarios leading the system far from the control objectives.

SCENARIO ↓	AOB activity	AnAOB activity	NOB activity	HB activity
1	Low	Ok	Zero	Constant
2	Low	Low	Zero	Constant
3	High	Low	Zero	Constant
4	Ok	Ok	High	Constant

The identified microbiological scenarios can now be translated into physical constraints on state variables. In particular, the best system operation (i.e. VAR_{OPT}=UB_{OPT}) can be represented by having steady-state concentrations of NH_4^+, NO_2^- and NOB in the system at zero, as shown in Eqn. (5.13). It is assumed that only one microbiological situation can lead the system to the absolute best performance.

$$\begin{cases} (NH_4^+)_{lb}^{LBOPT} = 0 \\ (NH_4^+)_{ub}^{LBOPT} = 0 \\ (NO_2^-)_{lb}^{LBOPT} = 0 \\ (NO_2^-)_{ub}^{LBOPT} = 0 \\ (X_{NOB})_{lb}^{LBOPT} = 0 \\ (X_{NOB})_{ub}^{LBOPT} = 0 \end{cases} \tag{5.13}$$

On the other hand, the microbiological scenarios leading to bad system performance can in general be imposed using the general constraints on the state variable expressed in Eqn. (5.14).

$$\forall l = 1, \dots \dots, s \begin{cases} (NH_4^+)_{lb}^{l} \leq NH_4^+ \leq (NH_4^+)_{ub}^{l} \\ (NO_2^-)_{lb}^{l} \leq NO_2^- \leq (NO_2^-)_{ub}^{l} \\ (X_{NOB})_{lb}^{l} \leq X_{NOB} \leq (X_{NOB})_{ub}^{l} \end{cases} \tag{5.14}$$

In Eqn. (5.14) *l* is the microbiological scenario moving the system away from the optimality and *s* is the total number of microbiological scenarios moving the system away from the optimality. The values for the lower and upper boundaries of Eqn. (5.14) (*lb* and *ub*, respectively) are summarized in Table 5.5. All the other non-specified state variables have a lower boundary of 0 and do not have a specified upper boundary.

Table 5.5: Physical constraints on steady-state ammonium, nitrite and NOB concentrations for each scenario.

SCENARIO ↓	$[NH_4^+]$		$[NO_2^-]$		$[X_{NOB}]$	
	lb	**ub**	**lb**	**ub**	**lb**	**ub**
1	0.01*	TN_{IN}	0	0	0	0
2	0.01*	TN_{IN}	0.01*	TN_{IN}	0	0
3	0	0	0.01*	TN_{IN}	0	0
4	0	0	0	0	0.01*	10^{10}**

*0.01 is here indicative of a value for the lower boundary different from zero.

**10^{10} is here indicative of a very large value for the upper boundary.

The constraints on the controlled variables are defined in Eqn. (5.15).

$$\begin{cases} 0 \leq R_{eff} \leq 1 \\ 0 \leq R_{AmmTot} < +\infty \\ 0 \leq R_{NitAmm} \leq 1 \\ 0 \leq R_{NitAmm,eff} < +\infty \\ 0 \leq R_{NatTot} < 1 \end{cases} \tag{5.15}$$

1d. *Specification of the system of equations to be solved*

The identification of so-called critical points (CPs) is here performed by assuming the system is at steady state. Hence, a stoichiometry-based approach can be used. Capturing knowledge of the process from a stoichiometry-based model rather than a dynamic model to calculate the CPs would avoid failures of the controller itself since stoichiometry does not rely on model parameter estimations which are often subject to identifiability issues and case specific. In particular, reactions (5.16-5.19) are used to describe the biological reactions mediated by the four main classes of microorganisms present in the PN/A system, namely AOB, NOB, AnAOB and HB, respectively. As the controller has to be designed in order to maintain a high TN removal efficiency despite influent fluctuations, reactions (5.16-5.19) can be simplified by neglecting all the compounds which do not contain nitrogen. Furthermore, since the performance of the system is strictly dependent on the interactions among the different classes of microorganisms [43], the reactions are virtually multiplied by a constant coefficient describing the rate of a particular process in relation to the rate of AOB activity. From these two simplifications, reactions (5.20-5.23) result.

$$1.34NH_4^+ + 1.86O_2 + 2.66HCO_3^- \rightarrow 0.024C_5H_7NO_2 + 1.32NO_2^- + 1.06H_2O + 2.54H_2CO_3 \tag{5.16}$$

$$NO_2^- + 0.0025NH_4^+ + 0.4875O_2 + 0.0025HCO_3^- + 0.01H_2CO_3 \rightarrow 0.0025C_5H_7NO_2 + NO_3^- + 0.0075H_2O \tag{5.17}$$

$$NH_4^+ + 1.32NO_2^- + 0.066HCO_3^- + 0.13H^+ \rightarrow 0.26NO_3^- + 1.02N_2 + 0.066CH_2O_{0.5}N_{0.15} + 2H_2O \tag{5.18}$$

$$0.167CH_3OH + 0.156NO_3^- + 0.156H^+ \rightarrow 0.0095C_5H_7O_2N + 0.073N_2 + 0.378H_2O + 0.12CO_2 \tag{5.19}$$

$$1.34NH_4^+ \rightarrow 0.02N_{biom} + 1.32NO_2^- \tag{5.20}$$

$$(NO_2^- + 0.0025NH_4^+ \rightarrow 0.0025N_{biom} + NO_3^-) \cdot \boldsymbol{r_{NOB}} \tag{5.21}$$

$$(NH_4^+ + 1.32NO_2^- \rightarrow 0.26NO_3^- + 1.02N_2 + 0.02N_{biom}) \cdot \boldsymbol{r_{AnAOB}} \tag{5.22}$$

$$(0.156NO_3^- \rightarrow 0.0095N_{biom} + 0.073N_2) \cdot \boldsymbol{r_{HB}} \tag{5.23}$$

In Eqns. (5.20-5.23) r_{NOB}, r_{AnAOB} and r_{HB} represent the rate of respectively NOB, AnAOB and HB activity with respect to the rate of AOB activity. N_{biom} is the nitrogen stored into the biomass cells.

Reactions in Eqns. (5.20-5.23) are then directly used to derive the equations describing the single-stage PN/A system at steady state as follows:

$$\begin{cases} \dfrac{(NO_2^-)_{OUT}}{(NH_4^+)_{REM}} = \dfrac{1.32 - r_{NOB} - 1.32 \cdot r_{AnAOB}}{1.34 + r_{AnAOB} + 0.0025 \cdot r_{NOB}} \\ \dfrac{(NO_3^-)_{OUT}}{(NH_4^+)_{REM}} = \dfrac{r_{NOB} + 0.26 \cdot r_{AnAOB} - 0.156 \cdot r_{HB}}{1.34 + r_{AnAOB} + 0.0025 \cdot r_{NOB}} \\ \dfrac{(N_2)_{OUT}}{(NH_4^+)_{REM}} = \dfrac{0.073 \cdot r_{HB} + 1.02 \cdot r_{AnAOB}}{1.34 + r_{AnAOB} + 0.0025 \cdot r_{NOB}} \\ NH_4^+ = (NH_4^+)_{OUT} \\ NO_2^- = (NO_2^-)_{OUT} \\ NO_3^- = (NO_3^-)_{OUT} \\ N_2 = (N_2)_{OUT} \end{cases} \tag{5.24}$$

Similarly, the system of equations describing the relationship between controlled variables and manipulated, disturbance and state variables is specified for the PN/A system as follows:

$$\begin{cases} R_{eff} = \dfrac{NH_{4,IN}^+ - NH_{4,OUT}^+}{NH_{4,IN}^+} \\ R_{AmmTot} = \left| \dfrac{NH_{4,IN}^+ - NH_{4,OUT}^+}{TN_{IN} - TN_{OUT}} \right| \\ R_{NitAmm} = \left| \dfrac{NO_{2,OUT}^-}{NH_{4,IN}^+ - NH_{4,OUT}^+} \right| \\ R_{NitAmm,eff} = \left| \dfrac{NO_{2,OUT}^-}{NH_{4,OUT}^+} \right| = \dfrac{R_{NitAmm}}{\dfrac{1}{R_{eff}} - 1} \\ R_{NatTot} = \left| \dfrac{NO_{3,OUT}^-}{TN_{IN} - TN_{OUT}} \right| \end{cases} \tag{5.25}$$

The objective function, i.e. the TN removal efficiency (η_{TN}), can be specified for the PN/A system as follows:

$$0 = (\eta_{TN})_{b,r} - R_{eff} \cdot \left(1 - \frac{1.32 - 1.06 \cdot r_{AnAOB} - 0.156 \cdot r_{HB}}{1.34 + 0.0025 \cdot r_{NOB} + r_{AnAOB}}\right) \quad (5.26)$$

Eqn. (5.26) expresses the relationship between the variable to be optimized (i.e. η_{TN}) and the rates of AnAOB, NOB and HB activities related to the rate of AOB activity and the ammonium removal efficiency (R_{eff}).

2) Identification of so-called "critical points" for the controlled variables

In the present work, critical points (CPs) can be defined as those numerical values describing the four boundaries for optimal and worst system operation in Eqn. (5.8) resulting from specific microbiological scenarios. Their identification is essential for the successful performance of the controller. On the basis of their values, the membership functions are defined. This in turn will allow FLC_1 to identify correctly what the microbial activity in the system is like, on the basis of which FLC_2 will decide whether to infer a positive or a negative unitary deviation of the k_La.

The system consisting of Eqns. (5.24-5.26) and constrained by Eqns. (5.13-5.15) for each of the four key values for η_{TN} in Eqn. (5.8) (i.e. LB_{OPT}, UB_{OPT}, LB_{WORST} and UB_{WORST}) was solved using the optimization algorithm *fmincon* in Matlab (R2013b), whose objective was to find the values for the five CVs minimizing the difference between the TN removal efficiency and each of the four set point values in Eqn. (5.8). Worth noting is that the optimization is not based on dynamic models but is based on process stoichiometry and process insights. This ensures that the critical points identified can be valid not only for few specific cases, but also for a larger range of reactors where a single-stage PN/A process operates. The following critical points for the vector of controlled variables of Eqn. (5.9) are identified:

$$\eta_{TN} = 100\% \Rightarrow \underline{y}_{UB,OPT} = [1\ 0\ 0\ 0\ 1] \quad (5.27)$$

$$\eta_{TN} = 92\% \Rightarrow \begin{cases} \underline{y}^1_{LB,OPT} = [1.0362\ 0\ 0\ 0.0362\ 0.953] \\ \underline{y}^2_{LB,OPT} = [1.043\ 0.0081\ 0.1944\ 0.0351\ 0.96] \\ \underline{y}^3_{LB,OPT} = [1.087\ 0.0543\ +\infty\ 0.028\ 1] \\ \underline{y}^4_{LB,OPT} = [1.087\ 0\ 0\ 0.087\ 1] \end{cases} \quad (5.28)$$

$$\eta_{TN} = 75\% \Rightarrow \begin{cases} \underline{y}^1_{UB,WORST} = [1.0362\ 0\ 0\ 0.04\ 0.78] \\ \underline{y}^2_{UB,WORST} = [1.043\ 0.0042\ 0.0149\ 0.0357\ 0.78] \\ \underline{y}^3_{UB,WORST} = [1.33\ 0.26\ +\infty\ 0\ 1] \\ \underline{y}^4_{UB,WORST} = [1.33\ 0\ 0\ 0.333\ 1] \end{cases} \quad (5.29)$$

$$\eta_{TN} = 0\% \Rightarrow \begin{cases} \underline{y}^1_{LB,WORST} = [\text{ind.}\ 0\ 0\ 0\ 0] \\ \underline{y}^2_{LB,WORST} = [\text{ind.}\ 0\ 0\ 0\ 0] \\ \underline{y}^3_{LB,WORST} = [+\infty\ 1\ +\infty\ 0\ 1] \\ \underline{y}^4_{LB,WORST} = [+\infty\ 0\ 0\ +\infty\ 1] \end{cases} \quad (5.30)$$

3) Definition of membership functions of input and output variables

After having found the critical points for each key value of η_{TN} and at each microbiological scenario, the MFs for the variables of Eqn. (5.9) can be defined. More specifically, the first step consists of the identification of the key CVs whose variation clearly indicates the microbiological imbalance typical for the scenario itself for each microbiological scenario. The following table shows which are the key CVs identified for each scenario:

Table 5.6: Key CVs representing the microbiological imbalance typical for each scenario.

SCENARIO ↓	R_{AmmTot}	R_{NitAmm}	$R_{NitAmm,eff}$	R_{NatTot}	R_{eff}
1					X
2		X	X		
3	X	X	X		
4	X			X	

Based on this selection, the following fuzzy sets were able to be identified for each of the CVs:

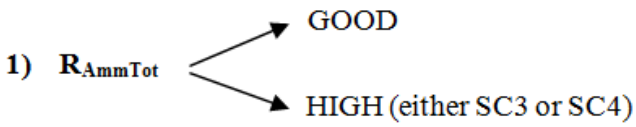

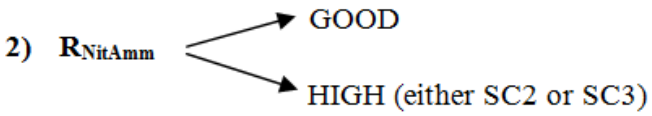

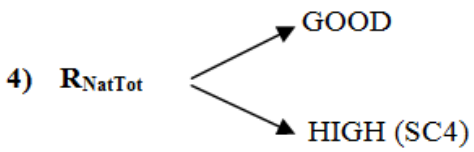

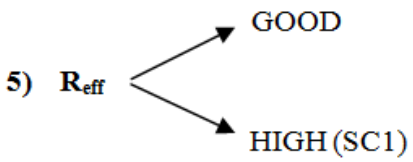

With regards to the shape, literature shows that many authors have used a Gaussian bell shape for the membership functions of the variables of fuzzy-logic controllers applied to biological systems [67,94,95]. This is because the non-linear behaviour required by the controller, which has to deal with highly non-linear processes such as the biological ones, would thus be incorporated. However, as pointed out by Jager [96], the non-linearity of the controller is already achieved through the implementation of the linguistic rules, which replicate the non-linear behaviour of the biological processes. Hence, given their higher simplicity (meaning that fewer parameters are needed to be specified for their definition), rigid shapes such as the triangular-trapezoidal shape have been preferred over the non-linear ones.

The last step to complete the definition of the membership functions is to assign the degree of membership to the fuzzy sets for each numerical value of the CVs. In order to do this, the critical points will be assigned a degree of membership equal to 1 as expressed in Eqns. (5.31-5.34). The same critical points will be assigned a degree of membership to the other fuzzy sets equal to 0.

$$\eta_{TN} = 100\% \Rightarrow \begin{cases} (R_{AmmTot})_{GOOD} = y_{UB,OPT,1} = 1 \\ (R_{NitAmm})_{GOOD} = y_{UB,OPT,2} = 0 \\ (R_{NitAmm,eff})_{LOW} = y_{UB,OPT,3} = 0 \\ (R_{NatTot})_{GOOD} = y_{UB,OPT,4} = 0 \\ (R_{eff})_{GOOD} = y_{UB,OPT,5} = 1 \end{cases} \tag{5.31}$$

$$\eta_{TN} = 92\% \Rightarrow \begin{cases} (R_{AmmTot})_{GOOD} = y^{3}_{LB,OPT,1} = y^{4}_{LB,OPT,1} = 1.087 \\ (R_{NitAmm})_{GOOD} = \min\left(y^{2}_{LB,OPT,2}, y^{3}_{LB,OPT,2}\right) = 0.0081 \\ (R_{NitAmm,eff})_{LOW} = \dfrac{(R_{NitAmm})_{GOOD}}{\left(\dfrac{1}{(R_{eff})_{GOOD}} - 1\right)} = 0.164 \\ (R_{NatTot})_{GOOD} = y^{4}_{LB,OPT,4} = 0.087 \\ (R_{eff})_{GOOD} = y^{1}_{LB,OPT,5} = 0.953 \end{cases} \tag{5.32}$$

$$\eta_{TN} = 75\% \Rightarrow \begin{cases} (R_{AmmTot})_{HIGH} = y^{3}_{UB,WORST,1} = y^{4}_{UB,WORST,1} = 1.33 \\ (R_{NitAmm})_{HIGH} = \max\left(y^{2}_{UB,WORST,2}, y^{3}_{UB,WORST,2}\right) = 0.2592 \\ (R_{NitAmm,eff})_{HIGH} = \dfrac{(R_{NitAmm})_{HIGH}}{\left(\dfrac{1}{(R_{eff})_{LOW}} - 1\right)} = 0.9 \\ (R_{NatTot})_{HIGH} = y^{4}_{UB,WORST,4} = 0.33 \\ (R_{eff})_{LOW} = y^{1}_{UB,WORST,5} = 0.78 \end{cases} \tag{5.33}$$

$$\eta_{TN} = 0\% \Rightarrow \begin{cases} (R_{AmmTot})_{HIGH} < +\infty \\ (R_{NitAmm})_{HIGH} = 1 \\ (R_{NitAmm,eff})_{HIGH} < +\infty \\ (R_{NatTot})_{HIGH} < +\infty \\ (R_{eff})_{LOW} = 0 \end{cases} \tag{5.34}$$

The resulting membership functions for the input variables are shown in Figure 5.14.

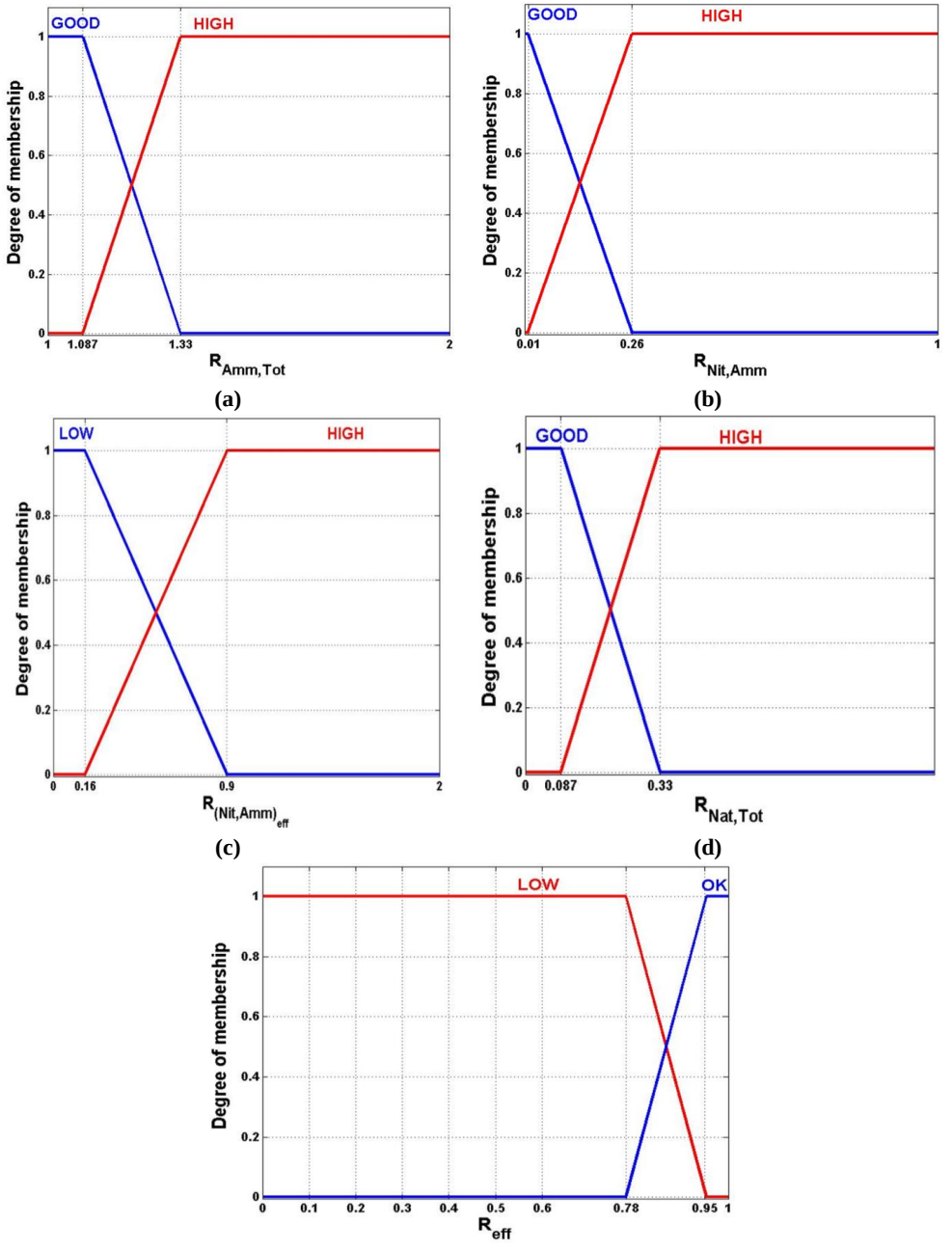

Figure 5.14: Membership functions defined for FLC input variables: **(a)** R_{AmmTot} , **(b)** R_{NitAmm}, **(c)** $R_{NitAmm,eff}$, **(d)** R_{NatTot}, and **(e)** R_{eff}.

Assuming that the defuzzification method chosen is the Center-of-Area method, the membership functions defined for the unitary deviation of the k_La are defined as shown in Figure 5.15.

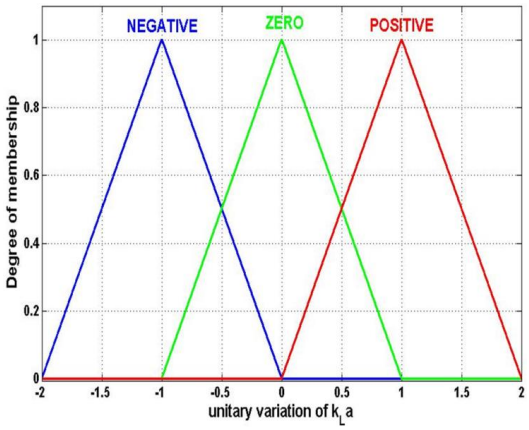

Figure 5.15: Membership functions defined for the FLC output variable ($\Delta_U k_L a$).

Thus, when the PN/A system is found in the range "optimal system operation", namely that η_{TN} is comprised between 92% and 100%, k_La is not varied (i.e. $\Delta_U k_L a=0$) whereas, when η_{TN} is equal or below 75%, either maximal positive or maximal negative variation of the k_La is inferred. Assuming that the Center-of-Area method is used for the defuzzification, +1 and -1 will be the maximal positive and the maximal negative values, respectively, that $\Delta_U k_L a$ can take.

With regards to the MFs for the four intermediary variables indicating the state of the biomass in the system (namely: "CANR performance index", "AOB activity", "AnAOB activity" and "NOB activity") no particular rule was followed. The fuzzy sets used for each of these variables were determined in order to be able to uniquely identify the cause leading to microbiological imbalance of the system and thus to infer the proper variation of k_La. The membership functions shown in Figure 5.16 were thus defined.

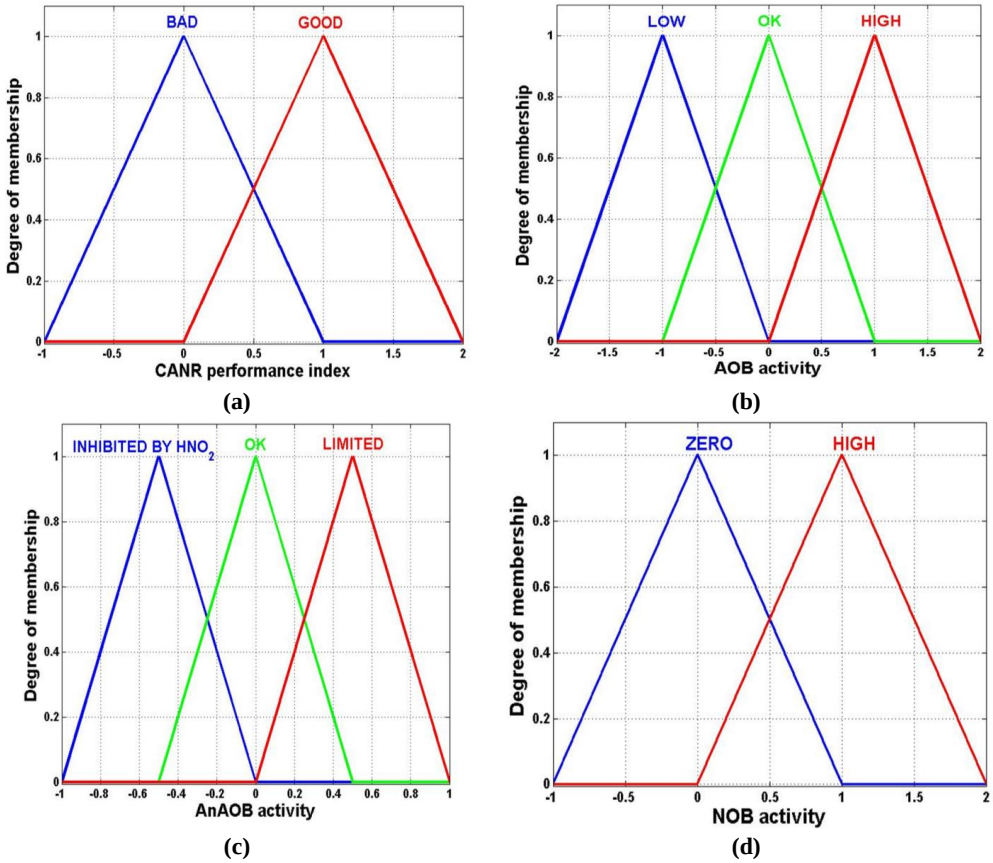

Figure 5.16: Membership functions defined for the FLC intermediary variables: **(a)** CANR performance index, **(b)** AOB activity, **(c)** AnAOB activity, and **(d)** NOB activity.

4) Implementation of the linguistic rules

On the basis of the diagnosis tree adapted from Mutlu *et al.* [85] and represented in Figure 5.2, the linguistic IF-THEN rules shown in Table 5.7 were implemented for FLC1.

Table 5.7: Linguistic rules for FLC1.

	IF					THEN			
	R_{AmmTot}	R_{NatTot}	R_{NitAmm}	$R_{NitAmm,eff}$	R_{eff}	CANR perf. index	AOB activity	AnAOB activity	NOB activity
1	GOOD	GOOD	GOOD	GOOD	GOOD	GOOD	OK	OK	ZERO
2	HIGH	HIGH				BAD			HIGH
3	HIGH		HIGH	HIGH		BAD	HIGH	INHIB. by HNO_2	ZERO
4	HIGH		HIGH	LOW		BAD	LOW	LIMITED	ZERO
5					LOW	BAD	LOW		

6		GOOD							ZERO

Thus, the FLC1 infers the microbiological scenarios occurring into the system, on the basis of which the FLC2, whose rules are represented in Table 5.8, decides on the control action to be taken.

Table 5.8: Linguistic rules for FLC2.

	IF				THEN
	CANR perf. index	**AOB activity**	**AnAOB activity**	**NOB activity**	**$\Delta_U k_L a$**
1	BAD	HIGH	INHIB. by HNO_2		NEGATIVE
2	GOOD	OK	OK	LOW	ZERO
3	BAD			HIGH	NEGATIVE
4	BAD	LOW			POSITIVE
5	BAD		LIMITED		POSITIVE

5) Setting of additional design parameters

Additional design parameters to choose are the implication and aggregation methods and the scaling factor for the oxygen mass transfer coefficient. The implication method chosen is the correlation-minimum whereas the aggregation method used is the disjunctive method. With regard to the scaling factor, a value equal to 136 d^{-1} - corresponding to the difference between the value of oxygen mass transfer coefficient at saturation and the corresponding nominal one - was considered as a good candidate to obtain a sufficient speed of the control response.

5.3.4 Performance evaluation of the novel controller

As disclosed in the introduction, the control strategy developed as described in Section 5.3.3 is implemented both in a full-scale continuous reactor and in a lab-scale sequencing batch single-stage PN/A reactor. In this section, the simulation results will be presented and discussed for both reactors.

Evaluation Case Study 1: Responses to influent ammonium concentration step changes by a continuous PN/A system

Figure 5.17 shows the dynamics of the effluent ammonium and nitrate nitrogen, the TN removal efficiency and the manipulation of the oxygen mass transfer coefficient obtained by simulating the continuous full-scale reactor with the influent ammonium step changes previously described. It can be observed that the controller increases the k_La as the influent ammonium increases whereas it decreases the k_La as the influent ammonium decreases. As a matter of fact, when more NH_4^+ is fed into the system, more oxygen is required by AOB to oxidize it whereas, when less NH_4^+ is fed, the higher oxygen concentrations led by lower uptake by AOB inhibit the activity of AnAOB. The different values of η_{TN} achieved after the step changes are due to the activity of HB, which is influenced by the oxygen concentration. In particular, as the oxygen supply is increased (i.e. for NH_4^+ step increase), the anoxic HB activity, responsible for the reduction of AnAOB-produced NO_3^-, is inhibited and this in turn leads to lower TN removal efficiency compared to the case when oxygen supply is reduced (i.e. for NH_4^+ step

decrease). In both cases, the TN removal efficiencies are quickly re-established above the minimal target of 92% after the step changes occur.

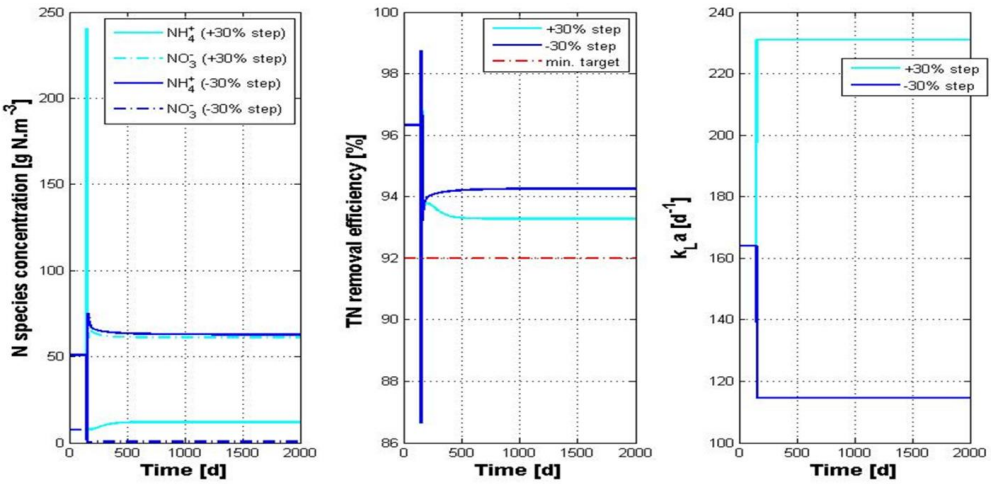

Figure 5.17: Simulated dynamic responses to step increases and decreases in influent ammonium concentration.

Evaluation Case Study 2: Responses to influent soluble carbon concentration step changes by a continuous PN/A system

Figure 5.18 shows the dynamic response of the biological system to a 100%-step increase and decrease in the readily biodegradable organic carbon (S_S). As can be observed, the control strategy is able to overcome these disturbances. In particular, when the S_S concentration in the feed is decreased, the HB concentration decreases and the reduction of AnAOB-produced NO_3^- to N_2 performed by this class of microorganisms is therefore compromised, thus leading to a higher concentration of NO_3^- (and hence higher TN) in the effluent. However, as can be noted, since the TN removal efficiency does not decrease below the minimal target, no change in control action is taken. When the feeding of S_S is increased, the oxygen uptake by HB increases, thus reducing the amount of oxygen available for AOB and consequently reducing the AOB activity. Consequently, despite a much lower NO_3^- concentration due to higher heterotrophic reduction, the amount of ammonium in the effluent increases such that the TN removal efficiency decreases. The control system reacts to this situation by increasing the k_La, thus providing more oxygen for AOB. In both cases (i.e. step increase and decrease) the control system has shown its capability to ensure a TN removal efficiency equal to or higher than the minimal target fixed of 92% removal determined during the formulation of the control objectives.

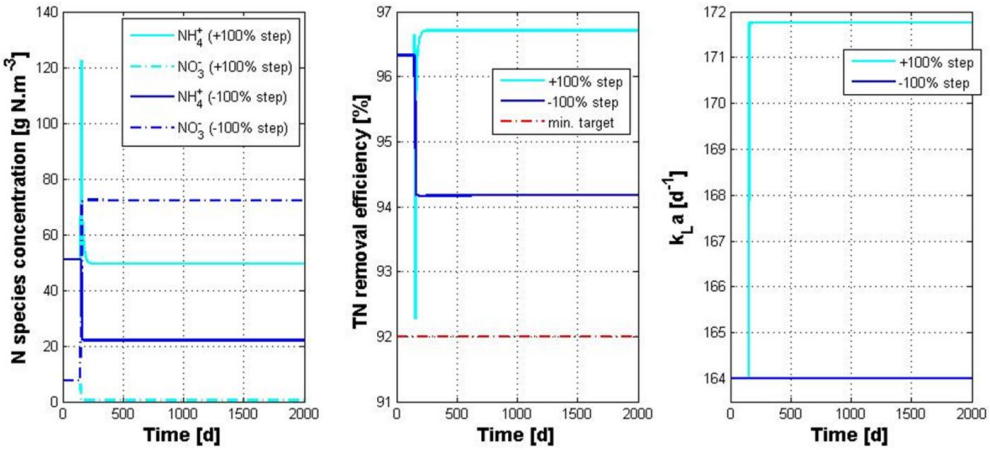

Figure 5.18: Dynamic responses to step increases and decreases in influent readily biodegradable organics concentration.

Evaluation Case study 3: Responses to BSM2 realistic dynamic influent by a continuous PN/A system

The disturbance rejection capability of the novel control strategy is analysed on the plant-wide BSM2, and is compared to performance of other control strategies. Table 5.9 summarizes the results obtained by simulating the full-scale reactor with the following five control strategies:

1) fuzzy-logic control strategy developed in this study according to the new methodology *(CS1*),
2) CS1 with sensor and actuator dynamics (*CS2*),
3) feedforward (FF) controller by Vangsgaard *et al.* [51] (*CS3*),
4) feedforward-feedback controller, built up by using the output of CS1 to updated the RO set point of the FF controller of point 3) and K_{SF} equal to 1 g $O_2.g^{-1}$ N (*CS4*) (see Figure 5.19),
5) fuzzy-logic control strategy previously developed according to an intuitive approach by Boiocchi *et al.* [72] (*CS5*).

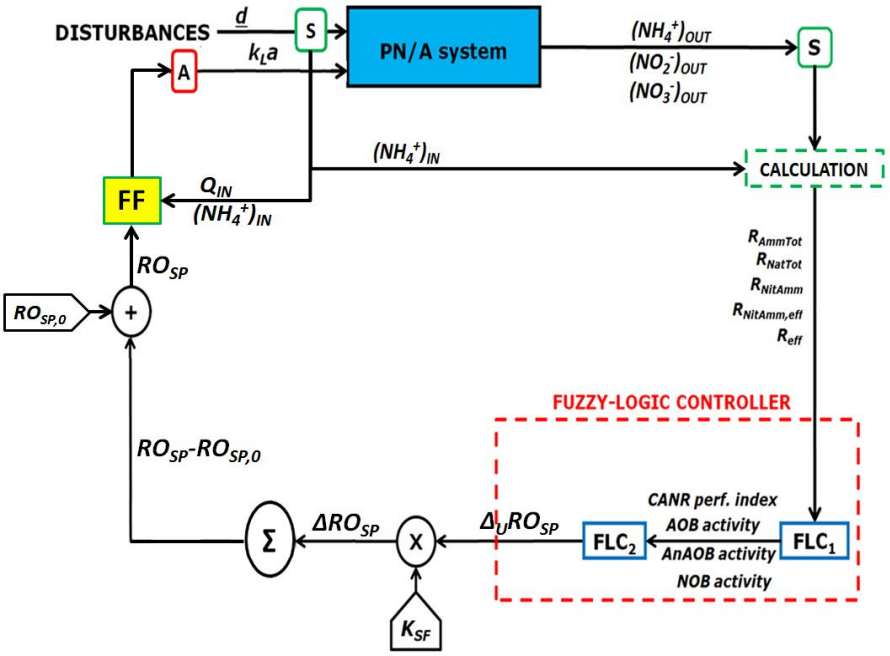

Figure 5.19: Implementation of the feedforward-fuzzy-logic controller (*CS4*) in the continuous PN/A system.

In addition, the dynamic results of the open-loop are used in order to evaluate the value of these five control structures in terms of their capability of enhancing the TN removal efficiency of the reactor. As can be seen from Table 5.9 showing the four evaluation criteria, the novel control strategy (*CS1*) enables achieving an average TN removal efficiency which is above the minimal target of 92% removal. From the standard deviation of the η_{TN}, it can be deduced that the systematically-tuned controller is successfully able to fully avoid the predefined "area of worst system operation", by keeping the system above 75% removal efficiency. The standard deviation of η_{TN} is drastically reduced through the controller, which means that higher stability of the reactor performance has been enabled. A slightly better performance (i.e. 93.2%) is achieved through the feedforward-feedback loop (*CS4*) leading to a lower IAE. In this case, the standard deviation of η_{TN} is reduced compared to the CS2, meaning that a higher stability of the system is achieved. However, the advantage in terms of performance efficiency obtained with CS4 comes at the expense of a much higher value of the TV obtained. The reason for having this higher TV by CS4 is due to the fact that the feedforward part of the controller changes the k_La by following the strong dynamics of the influent nitrogen load. For the same reason, also the feedforward controller (*CS3*) gave a very high TV, but in this case a very low average TN removal efficiency is achieved, mainly due to the non-optimality of the RO_{sp} used.

The advantage in terms of average TN removal efficiency by comparing CS1 against CS5 is almost 10%. Furthermore, compared to the open-loop case, CS5 does not show any improvement that can warrant its implementation in real systems, since it gives a TN removal efficiency worse than the open-loop case. The reason for this is that, although CS5 incorporates insights on the processes and is able to

handle influent step changes as demonstrated in Boiocchi *et al.* [72], its membership functions were not systematically defined with respect to the control objectives. A rather intuitive approach was adopted instead without any rationale for consistency check. The control performance results of CS5 thus demonstrate the importance of adopting the systematic approach presented for the design of membership functions of fuzzy-logic controllers applied to biological systems.

Furthermore, by including actuator delay and sensors noises (see *CS2*), it can be noted that there is only a slight decrease of the performance of CS1, which indicates robustness (i.e. low sensitivity) of the present fuzzy-logic controller to sensor and actuator dynamics. This can clearly be seen from the dynamic results of CS1 compared to the results of CS5, shown in Figure 5.20.

From an economic point of view, it can be noted that the implementation of the new control strategy increases the average aeration consumptions by only 5-6%, which can be considered marginal given the greater advantage in terms of TN removal efficiency. On the other hand, the intuitively-designed fuzzy-logic control strategy increases the energy consumption by 19%. This is considered quite a lot given also the relatively poor performance of this strategy in reducing the effluent nitrogen. On the basis of its low aeration energy consumption, the poor performance of the feedforward controller (*CS3*) can be attributed to the low amount of oxygen supplied.

Table 5.9: Evaluation criteria for open-loop and the control strategies CS1, CS2, CS3, CS4 and CS5.

	$\overline{\eta}_{TN}$	$\sigma(\eta_{TN})$	**IAE**	**TV**	**AAE**
Units	**[% of g $TN_{REM}.g^{-1}$ TN_{IN}]**	**[% of g $TN_{REM}.g^{-1}$ TN_{IN}]**	**[% of g $TN_{REM}.g^{-1}$ TN_{IN}]**	**[d^{-1}]**	**[$kWh.d^{-1}$]**
OPEN-LOOP	88.86	9.4	1343.6	0	258.9
CS1	92.5	5.4	343.7	21001	270.7
CS2	92.3	5.9	536.1	18569	273.2
CS3	86.5	2.8	1938.9	26022	239.8
CS4	93.2	5	258.3	30865	287.5
CS5	83.64	11.7	3257.5	11250	308.5

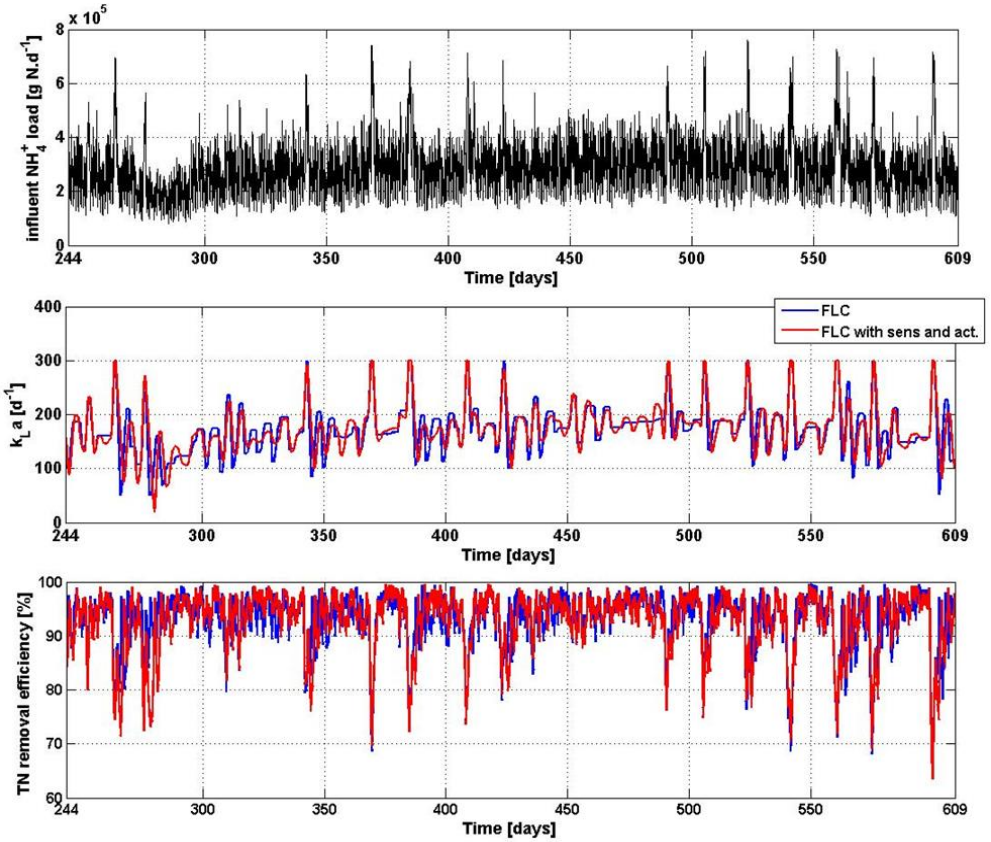

Figure 5.20: Long-term disturbance rejection evaluation (the last 52 weeks of BSM2 benchmark simulation) influent ammonium load, oxygen mass transfer coefficient (k_La) and TN removal efficiency obtained for a continuous PN/A system with novel FLC (in blue line) and novel FLC evaluated considering sensor noise and actuator delays (in red line).

Evaluation Case Study 4: Responses to realistic dynamic influent by the sequencing batch PN/A system

Figure 5.21 shows the dynamic response of the SBR to the realistic dynamic influent variations given by the implementation of CS1 and CS5. Both controllers show their capability in keeping a removal efficiency above 80%, which is considered an acceptable value. However, the TN removal efficiency dynamics confirm the conclusion drawn before from the continuous application results, which highlight the importance of designing the FLC according to the systematic methodology. As a matter of fact, CS1 keeps the removal efficiency at a stable value above 92% whereas CS5 tends to allow the system to reach a considerably lower TN removal efficiency. Increasing the scaling factor of CS5 would only slightly increase the speed of the control response, but not the capability of achieving the control objectives. As can be noted in Figure 5.21, the k_La value for CS5 does not change anymore after 1.25 days from the beginning of the simulation. This means that the controller has identified its own optimal value for the k_La at this point of time. Increasing the gain would only slightly reduce the time at which

this value is reached but not the TN removal efficiency obtained, which is significantly lower than the minimal target (92 %).
These results emphasize the importance of the present contribution in providing a systematic methodology for the design of fuzzy-logic controllers for biological systems.

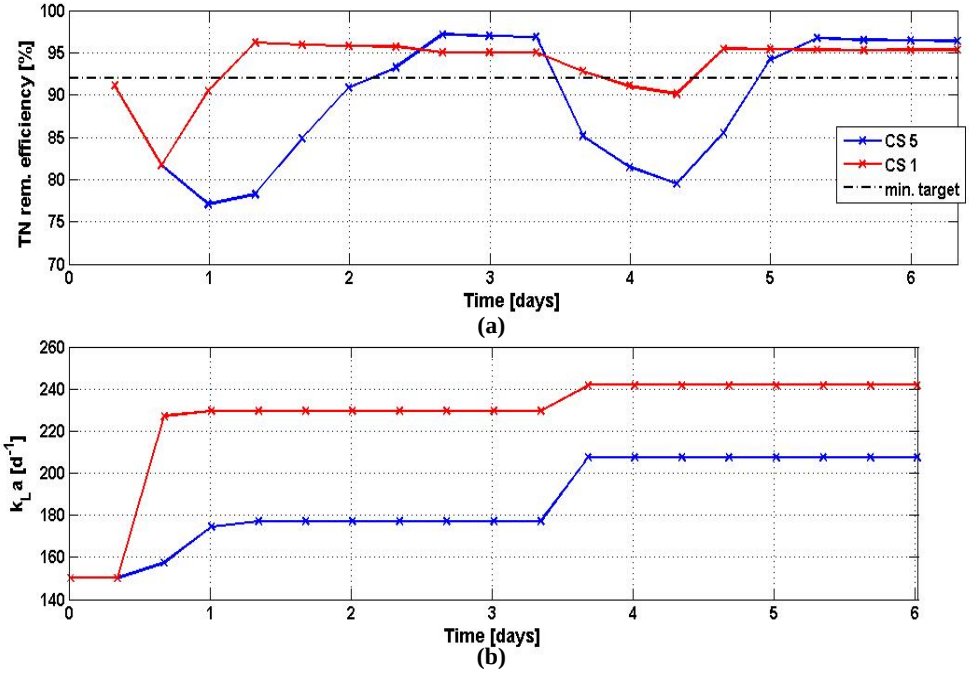

Figure 5.21: SBR dynamic responses of: **(a)** TN removal efficiency, and **(b)** oxygen mass transfer coefficient by CS1 (in red) and CS5 (in blue). The black dashed line represents the minimum TN removal target.

5.3.4. Discussion

The performance evaluation of the control strategy developed during this work has shown the clear advantage of using a systematic methodology to define the membership functions in a multiple-variables control systems rather than using an intuitive approach. This has been proven not only in a continuous but also in a sequencing batch reactor configuration with realistic dynamic influent. The implementation of the control strategy leads to higher operating costs due to a higher aeration required. For real implementations, the control strategy showed its capability in achieving the control objectives despite the measurement and actuator noises. The controller developed can therefore be considered ready for use in real full-scale single-stage PN/A reactors as aeration control module. Adjustments of the speed of the control response can be easily implemented by manipulating the scaling factor. Furthermore, the successful performance of the controller adds credit to the methodology employed for its design. Therefore the systematic methodology is also expected to be useful for the systematic development of other fuzzy-logic controllers applied to other biological systems. Among these, the

emerging urgency of developing control strategies for the minimization of the emissions of N_2O produced during biological wastewater treatment is one obvious application [15,26]. Also fermentation systems, where FLCs are barely used in practice [97,98], can have their performance enhanced through the application of FLCs designed according to the present methodology. In summary, the results presented here feature two significant contributions: (a) a systematic methodology to tune a FL controller (the previous contribution like all others in the field used an intuitive trial and error method which leads to suboptimal results); and (b) a new and improved FL control technology, as a direct result of improving the tuning and design methodology in (a).

5.3.6. Conclusion

A systematic methodology is developed for the design of fuzzy-logic controllers applied to biological systems. The key feature of the methodology is that for each operation objective, a corresponding constrained optimisation problem is formulated and solved to identify the cut-off values of the membership functions for different measured controlled variables. The methodology was then used to develop a fuzzy logic controller for high and stable total nitrogen removal in a single-stage side-stream partial nitritation/Anammox system. The resulting controller is implemented in a dynamic reactor model and benchmarking simulations are performed in other to evaluate its capability in rejecting the disturbances. The results with a realistic dynamic influent show that the fuzzy-logic controller improved the open-loop TN removal efficiency by approximately 4%, leading to a total nitrogen removal efficiency of about 92.5%, and importantly prevented the system performance from falling below 75%. Furthermore, benchmarking the systematically-designed control strategy against the fuzzy-logic controller developed intuitively based on available process knowledge by Boiocchi *et al.* [72] in both continuous and sequencing batch reactors confirms the importance of adopting a systematic methodology for the design of fuzzy-logic controllers rather than using an intuitive approach. Also, the newly-developed fuzzy-logic controller showed its capability in filtering sensor noise and actuator delay time, which are promising for its future successful operation in a real system.

The methodology can be further adopted as a supporting tool for the development of other fuzzy-logic controllers for other process systems. We feel that the methodology would be particularly needed for the design of membership functions in multivariable control systems to ensure consistency between the membership functions of measured variables.

In the next section, the methodology will be formulated generically in order to ease its application.

5.4. Formulation of the generic methodology for the design of fuzzy-logic control applied to process systems

In this section, a generic formulation of a methodology for the design of FLCs is extrapolated on the basis of the approach adopted for the development of the FLC used in Section 5.3. In the first subsection, the reference architecture for control implementation will be given. Afterwards, the design of the fuzzy-logic controller implemented according to the described reference architecture will be illustrated.

5.4.1. Reference control implementation architecture

In this subsection, the description of the reference architecture for the fuzzy-logic controller is presented. As can be seen in Figure 5.22, the methodology can be applied for FLCs implemented as feedback systems using the measurements ($\underline{y}_m$) of the controlled variables ($\underline{y}$) directly as input variables and deducing the required variations of the manipulated variables ($\Delta_S\underline{u}$) - scaled from a minimal value of -1 to a maximal value of +1 - as outputs. These deviations are then given a physical dimension by multiplication with a scaling factor ($\underline{K}_{SF}$). The variations of the MVs are integrated in time to get the difference between the value of the MV to be actuated ($\underline{u}$) and its corresponding nominal value ($\underline{u}_0$).

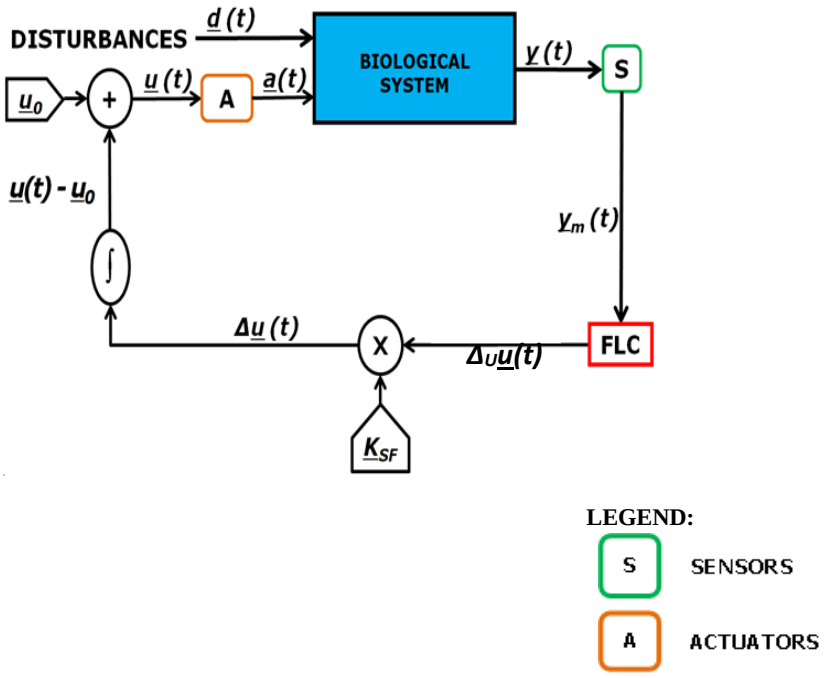

Figure 5.22: Reference architecture of the fuzzy-logic based control strategy implementation as feedback controller for biological systems.

The symbols used in Figure 5.22 are described as follows:

$\underline{d}$	vector of disturbances
$\underline{u}$	vector of manipulated variables (MVs)
$\underline{y}$	vector of controlled variables (CVs)
$\underline{y_m}$	vector of measured CVs
$\Delta_U\underline{u}$	vector of scaled deviations of MVs
$\Delta\underline{u}$	vector of deviations of MVs
$\underline{K_{SF}}$	vector of scaling factors
$\underline{a}$	vector of actuated MVs
$\underline{u_0}$	vector of nominal MVs

The operations performed by the closed-loop system represented in Figure 5.22 can be mathematically expressed by the following sequence of equations:

$$\frac{d\underline{x}}{dt} = f(t, \underline{d}, \underline{u}, \underline{x}) \tag{5.35}$$

$$\underline{y}(t) = g(t, \underline{d}, \underline{u}, \underline{x}) \tag{5.36}$$

$$\underline{y_m}(t) = \underline{y}(t) + \underline{v}(t) \tag{5.37}$$

$$\Delta_U\underline{u}(t) = f_{FIS}\left(\underline{y_m}(t)\right) \tag{5.38}$$

$$\Delta\underline{u}(t) = \underline{K_{SF}} \cdot \Delta_U\underline{u}(t) \tag{5.39}$$

$$\underline{u}(t) - \underline{u_0} = \int_0^t \Delta\underline{u}(t) \cdot dt \tag{5.40}$$

$$\underline{a}(t) = G_A \cdot \underline{u}(t) \tag{5.41}$$

Eqn. (5.35) represents the system dynamics. The time dependency of CVs on disturbances, manipulated variables and states is expressed in Eqn. (5.36) by the function g. The measurement of the CVs is represented by Eqn. (5.37) whereas the operation of the fuzzy-logic controller is generically represented through the function f_{FIS} (Eqn. (5.38)) which uses directly the measurements as input variables and generates scaled deviations of the MVs as output variables. The latter are then multiplied by $\underline{K_{SF}}$ as shown in Eqn. (5.39). Finally an integrator is used to obtain the current value of the MV (Eqn. (5.40)) which the actuator should apply to the system (Eqn. (5.41)).

5.4.2. The generic systematic procedure for tuning the FLC applied to process systems

The general procedure for tuning FLC consists of the following five main subsequent steps:

I. Specification of the optimization problem, which the controller has to accomplish, mathematically represented as follows

$$\underset{\underline{x}}{\text{argmin}}\ \text{OBJ} = h(t, \underline{d}, \underline{u}, \underline{x}, \underline{y}) \tag{5.42}$$

subject to:

$$\frac{d\underline{x}}{dt} = f(t, \underline{d}, \underline{u}, \underline{x}) \tag{5.43}$$

$$\underline{y} = g(t, \underline{d}, \underline{u}, \underline{x}) \tag{5.44}$$

$$t \in R \tag{5.45}$$

$$\underline{x}, \underline{u}, \underline{d}, \underline{y} \in R^n \tag{5.46}$$

$$\underline{d}_{lb} \leq \underline{d} \leq \underline{d}_{ub} \tag{5.47}$$

$$\underline{u}_{lb} \leq \underline{u} \leq \underline{u}_{ub} \tag{5.48}$$

$$\underline{x}_{lb} \leq \underline{x} \leq \underline{x}_{ub} \tag{5.49}$$

$$\underline{y}_{lb} \leq \underline{y} \leq \underline{y}_{ub} \tag{5.50}$$

In Eqn. (5.42) OBJ is the optimization objective function to be minimized, which is a function *h* of time, state, controlled, manipulated and disturbance variables. Physical constraints can be imposed on these variables through Eqns. (5.47-5.50).

II. Identification of the so-called critical points (CPs) by solving the optimization problem,

III. Definition of the membership functions for input and output variables,

IV. Implementation of the linguistic rules linking input to output variables,

V. Setting of additional design parameters.

Specification of the optimization problem

In this section, indications about how to specify the optimization objective for the development of fuzzy-logic controllers applied to biological systems are given.

Specification of the control objectives

In biological system applications, a FLC can be designed in such a way that, when the optimization objective of Eqn. (5.42) is in the ideal range, which defines a so-called "optimal system operation", no control action is taken. On the contrary, an additional value or set of values defining a so-called "worst system operation", where the system is in a highly-undesired state, has to be identified. Thus the fuzzy-logic controller will be designed in such a way that, when *OBJ* is found in this range, the maximal control action will be applied. Between these two system operation modes, there can be identified a third mode, the so-called "suboptimal system operation". As a result of this, the optimization problem in Eqn. (5.42) can be specified for the biological applications according to the following formulation of constraints (lower and upper bound of acceptable operation for each mode):

$$\begin{cases} \text{OPTIMAL SYSTEM OPERATION: } LB_{OPT} \leq OBJ \leq UB_{OPT} \\ \text{SUBOPTIMAL SYSTEM OPERATION: } UB_{WORST} < OBJ < LB_{OPT} \\ \text{WORST SYSTEM OPERATION: } LB_{WORST} \leq OBJ \leq UB_{WORST} \end{cases} \tag{5.51}$$

In Eqn. (5.51) LB_{OPT} and UB_{OPT} are the lower and upper boundaries defining the range for the "optimal system operation" whereas LB_{WORST} and UP_{WORST} are the lower and upper boundaries defining the range for the "worst system operation", respectively.

Thus the definition of the control objectives to be achieved consists in identifying the vector OBJ_b in Eqn. (5.52).

$$\underline{OBJ_b} = [LB_{OPT}\ UB_{OPT}\ LB_{WORST}\ UB_{WORST}] \tag{5.52}$$

Definition of the control structure

After having defined the control objectives, the control structure is defined in terms of manipulated, controlled, disturbance and state variables.

Specification of the physical constraints

With regard to the specification of the physical constraints, a particular attention has to be paid to the state variables. As previously described, the controller has to be designed in such a way that, when OBJ is in the worst system operation, the maximal control action is applied, namely a unitary variation of the manipulated variable equal to either +1 or -1 is applied. In order for the controller to decide on the sign of the variation of the manipulated variables, it is crucial to correctly identify the occurring microbiological scenario (MS) to be corrected. This has to be done on the basis of the numerical values of the CVs. To enable the controller doing so, membership functions for the CVs have to be designed on the basis of so-called critical points (CPs) for the controlled variables, namely those numerical values which describe the four boundaries for optimal and worst system operation in Eqn. (5.52) led by specific MSs. In order to find these CPs, the optimization problem has to be solved for each of the four elements of $\underline{\text{OBJ}_b}$ by imposing specific physical constraints on the state variables. As a matter of fact, by constraining the state variables a particular microbiological scenario is selected. For this reason, the first step to take consists in the identification of the potential microbiological scenarios leading the system away from the specified optimality. This can be typically done on the basis of knowledge acquired during operation, literature study and sensitivity analyses about the biological system itself. The key state conditions describing each of the identified microbiological scenarios are then defined accordingly. Thus for each microbiological scenario a set of lower and upper boundaries for the state variables (SVs) corresponds. Eqn. (5.49) can then be specified as follows:

$$\begin{cases} \text{for r} = 1 \quad \underline{x}_{lb}^{LBOPT} \leq \underline{x} \leq \underline{x}_{ub}^{LBOPT} \\ \text{for r} = 2,3,4 \quad \underline{x}_{lb}^{s} \leq \underline{x} \leq \underline{x}_{ub}^{s} \quad \forall s = 1, \dots \dots, q \end{cases} \tag{5.53}$$

where:

- $\underline{x}_{lb}^{LBOPT}$ and $\underline{x}_{ub}^{LBOPT}$ are the lower and upper boundaries for the SVs identifying the microbiological situation leading to the best system operation (i.e. OBJ=LB_{OPT}),
- $\underline{x}_{lb}^{s}$ and $\underline{x}_{ub}^{s}$ are the lower and upper boundaries for the SVs identifying the microbiological scenarios (*s*) leading the system away from the optimality (i.e. OPT=UP_{OPT},LB_{WORST},UP_{WORST}),
- q is the total number of potential microbiological scenarios leading to poor system performance,
- r indicates the elements of OBJ_b.

As can be noted from Eqn. (5.53), for the same value of OBJ different from LB_{OPT} multiple scenarios can be selected by constraining the state variables and thereby different CPs result. Thus the identification of the microbiological scenarios on the basis of the values of the CVs is enabled. Furthermore, it is reasonably assumed that only one microbiological scenario can lead the system to the absolute best performance (OPT=LB_{OPT}).

Specification of system of equations to be solved for the identification of CPs

At this stage, functions *f*, *g* and *h* have to be identified.

Identification of the so-called "critical points" for the controlled variables

By inverting the function *h*, taking into consideration the physical constraints imposed, the following results will be achieved:

$$\begin{cases} \underline{y}_{LB,OPT} \ s.t. \ LB_{OPT} - h\left(t, \underline{x}, \underline{y}, \underline{d}, \underline{u}\right) = 0 \\ \underline{y}_{UB,OPT}^{s} \ s.t. \ UB_{OPT} - h\left(t, \underline{x}, \underline{y}, \underline{d}, \underline{u}\right) = 0 \ \ \forall s = 1, \dots\dots, q \\ \underline{y}_{LB,WORST}^{s} \ s.t. \ LB_{WORST} - h\left(t, \underline{x}, \underline{y}, \underline{d}, \underline{u}\right) = 0 \ \ \forall s = 1, \dots\dots, q \\ \underline{y}_{UB,WORST}^{s} \ s.t. \ UB_{WORST} - h\left(t, \underline{x}, \underline{y}, \underline{d}, \underline{u}\right) = 0 \ \ \forall s = 1, \dots\dots, q \end{cases} \tag{5.54}$$

Each vector $\underline{y}$ in Eqn. (5.54) uniquely describes a particular microbiological scenario which leads the system performance to having an OBJ equal to one of the four elements in Eqn. (5.52).

Definition of the membership functions for input and output variables

The definition of the membership functions for FLC input variables consists of four sequential steps:

I) Identification of the key CVs whose variation from the ideal operation zone clearly indicates a particular microbiological imbalance,

II) Identification of the fuzzy sets according to which the universe of discourse of each CV is to be divided,

III) Choice of the shape of the MF,

IV) Assignment of degrees of membership to each fuzzy set.

Step I

For each microbiological scenario, the key controlled variables (y_i) whose variation clearly indicates the particular microbiological imbalance typical of the scenario itself are identified. Thus the numerical values of these CVs will be used for the identification of a particular microbiological scenario on the basis of which the proper control action is taken.

Step II

For each of the CVs, the following generic fuzzy sets can be found:

- one to which numerical values describing the microbiological balance of the system belong. The linguistic term "GOOD" will be used in this section to refer to this fuzzy set,
- one or more fuzzy sets to which numerical values describing one or more microbiological scenarios leading the system far from the control objectives belong. The generic linguistic term "BAD led by SCENARIO (SC) *l*" will be used in this section to refer to each of these fuzzy sets.

Step III

The choice of the shape is made in virtue of the same motivations given in subsection 5.3.3.

Step IV

To those critical points of a CV describing the "optimal system operation", a value of 1 is assigned as degree of membership to the fuzzy set "GOOD" and a 0 degree of membership to the other fuzzy sets is assigned. To the critical points describing the occurrence of a microbiological scenario *l* leading the system far from the control objectives, a value of 1 is assigned to the degree of membership to the fuzzy set "BAD led by SCENARIO *l*" and degrees of membership to the other fuzzy sets equal to zero are assigned.

To the remaining numerical values the assignment of the degree of membership to each fuzzy set is carried out as follows:

- those numerical values comprised between two critical points to which the same degree of membership to the same fuzzy set is assigned will be given the same degree of membership to that fuzzy set,
- those numerical values comprised between a point to which a degree of membership equal to 1 is assigned to a certain fuzzy set, and the adjacent one to which a degree of membership equal to 0 is assigned to the same fuzzy set, are assigned a degree of membership by interpolation according to the chosen shape of the MF.

For the FLC output variables, namely the deviations of the manipulated variables ($\Delta_U \underline{u}$), the definition of the membership functions is more standardized as these variables have always a maximum value of 1 and a minimum value of -1. However, it is important to note that the definition of MFs for these variables is strictly dependent on the defuzzification method chosen during the previous step.

In particular, the following are the fuzzy sets which always have to be included:

- “ZERO” for cases when the control objectives are achieved,
- “NEGATIVE” for cases when the microbiological scenario leading the system to bad performance needs to be corrected by negative variations of the MV,
- “POSITIVE” for cases when the microbiological scenario leading the system to bad performance needs to be corrected by positive variations of the MV.

The critical points for the output variables will always be -1, 0 and 1. To these points the previously mentioned assignment of the membership values to the fuzzy sets has to be carried out as shown in Table 5.10.

Table 5.10: Assignment of degrees of membership to the fuzzy sets for FLC output variable ($\Delta_U u$).

CRITICAL POINTS↓ FSs→	**NEGATIVE**	**ZERO**	**POSITIVE**
-1	1	0	0
0	0	1	0
1	0	0	1

The assignment of membership values to the fuzzy sets for the numerical values different from the critical points will be performed by interpolation, similarly to what was done for the MFs of the CVs. It is important to take into account the way the crisp values are inferred on the basis of the fuzzy outputs found by the Inference Engine. The MFs will have to be designed in such a way that when the optimization objective is detected in the area of “worst system operation” either -1 or +1 will be the crisp values resulting from the defuzzification whereas when the optimization objective is detected to be in the area of “optimal system operation”, 0 will be the crisp value resulting from the defuzzification. As an example, the triangular membership functions should be defined for the output variables, taking into account “Center-of-Area” as the defuzzification method chosen, as represented in Figure 5.23.

The controller, through the implementation of the linguistic rules, will infer a scaled variation of the manipulated variable equal to:

- 0, when the optimization objective is within the predefined “optimal system operation” range,
- +1, when the optimization objective is within the predefined “worst system operation” range and the microbiological scenarios identified have to be corrected by increasing the manipulated variable,
- -1, when the optimization objective is within the predefined “worst system operation” range and the microbiological scenarios identified have to be corrected by decreasing the manipulated variable.

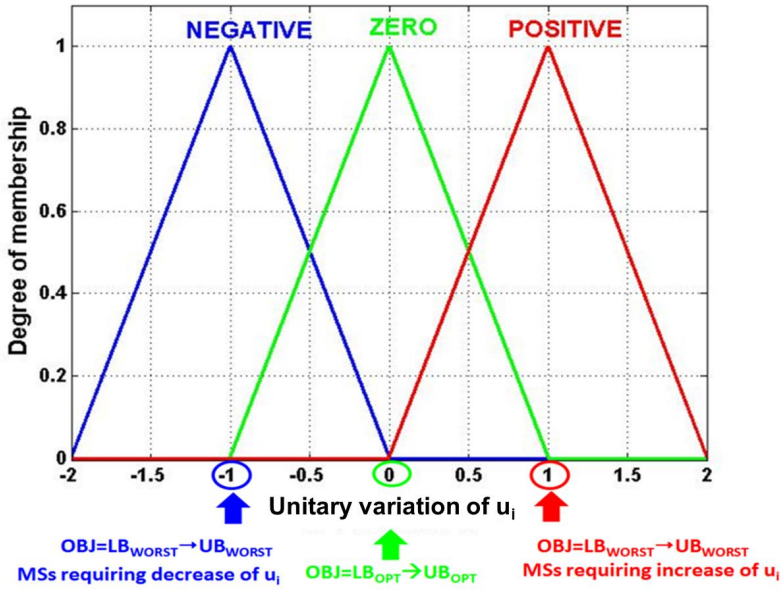

Figure 5.23: Generic MFs for a FLC output variable using "Center-of-Area" as defuzzification method.

CHAPTER 6
A novel fuzzy-logic control strategy minimizing N_2O emissions

6.1. Introduction

On-line process control is a tool widely used to automatically manipulate operating conditions of a process system in function of measured disturbances with the aim of achieving predefined targets on the system itself. In wastewater treatment plants, several objectives need to be satisfied, among which the respect of the legal effluent discharge limits and the minimization of the operational costs are some of the most important objectives. There is however also an emerging objective which needs to be tackled through the use of on-line process control, i.e. the minimization of N_2O emissions. It has in fact been found that the amount of greenhouse gases emitted from WWTPs has increased constantly over the last decades [1] and, in order to limit the carbon footprint of WWTPs, N_2O emissions need to be minimized. As explained in Chapter 4, AOB denitrification is ascribed to be the major contributor to the total N_2O produced. Establishing those environmental conditions slowing down AOB denitrification turns out as the key for the prevention of N_2O formation. AOB denitrification is a biological process during which AOB use nitrites and nitric oxides as electron acceptors instead of oxygen for the oxidation of ammonium. Microbiological and experimental experiences have found that AOB denitrification is triggered by low availability of dissolved oxygen and high availability of nitrites. More specifically, low availability of oxygen forces AOB to use alternative nitrogen oxides for the oxidation of their substrate. In addition, high levels of nitrites have been found to trigger AOB denitrification. In a laboratory experience by Peng *et al.* [19], it has been found that sludge rich in nitrite-oxidizing bacteria (NOB) is able to suppress AOB denitrification. This can be ascribed to the fact that NOB consume the nitrites formed by the AOB. Moreover, the full-scale experience by Sun *et al.* [26] showed that ensuring oxygen availability in a full-scale WWT system to achieve complete nitrification, namely complete conversion of ammonium into nitrate, is the key for preventing N_2O formation and therefore for minimizing N_2O emissions. This is because in this way AOB denitrification, consuming the nitrification intermediates like nitrites, is prevented. However, the N_2O minimizing effect of oxygen is only observed until a certain threshold, above which supplying more oxygen does not further reduce the N_2O production and emissions. Excessive oxygen levels can actually inhibit heterotrophic denitrification, and in particular trigger the accumulation of nitrite in the anoxic zone and slow down its last reduction step, where N_2O is converted into dinitrogen (N_2). A worse quality of the effluent, richer in unreduced nitrogen oxides, and higher N_2O production, are expected when oxygen is supplied in excess. For this reason, a balanced oxygenation level has to be accomplished such that all the AOB-produced nitrite is consumed by NOB and at the same time HB denitrification is not inhibited.

Till now, on-line control strategies aiming at accomplishing this balance among the different microbial communities (AOB, NOB and HB) so that the N_2O production is minimized have not yet been developed. The present work will focus on developing an on-line control strategy establishing the optimal oxygen availability in the aerated zone with the aim of preventing N_2O formation in continuously-aerated WWT systems. The control strategy will use the measured ratio between nitrate generated and ammonium depleted in an aerobic zone to identify the microbiological imbalance

between the different microorganisms and, on the basis of this, infer the proper control action to take. The control action will have to be decided also on the basis of the concentration of effluent ammonium, which needs to respect the effluent law limits.
Several approaches can be adopted for the development of such a control strategy, among which model-predictive, Proportional-Integrative-Derivative (PID) and fuzzy-logic control (FLC). The control actions taken according to the model-predictive control approach rely on a mathematical model and on its capability of describing the processes to be controlled. This approach is considered not to fit the control objectives of the present work, since models accurately describing N_2O emissions are not available at the moment. Controllers minimizing the N_2O emissions predicted by a model can fail to reduce the N_2O emissions when applied in real plants. Similarly, the multiple control objectives and the highly non-linear behaviour typical of WWT processes can hinder the good performance of a controller designed according to the PID approach. On the other hand, the fuzzy-logic (FL) approach is able to easily incorporate the process non-linearity and the multiple objectives of WWT systems. This makes the FL approach the most suitable to address the control objectives of the present work.
The novel control strategy will be developed on the basis of the systematic methodology by Boiocchi *et. al.* [73] (given in Chapter 5) and then tested in three simulation environments where different models describing N_2O emissions are used. In this way the robustness of the control strategy against different N_2O modelling approaches will be thoroughly evaluated. Furthermore, to address the asset of the novel control strategy to WWTPs, the performance of the control strategy will be compared against another typical control strategy which has as its only objective the maintenance of a low effluent ammonium concentration. Finally, the robustness of the control strategy against the sensor and actuator noises commonly occurring in WWTPs will be evaluated.

The present work is also used in the patent application whose reference number is P81602701DK00, titled "Control of N_2O-emissions by aeration".

6.2. Design of the control strategy

Following the systematic development of the membership functions used by Boiocchi *et al.* [73], the fuzzy-logic control strategy involved the following main steps:

I) Specification of the optimization problem,
II) Identification of the critical points,
III) Definition of the membership functions for input and output variables,
IV) Definition of additional design parameters.

6.2.1 Specification of the optimization problem

This section is split up into the following sub-steps:

- Definition of the control objectives,
- Definition of the control structure,
- Definition of the physical constraints,
- Identification of the key scenarios leading the system away from the optimality,
- Identification of the relationship between optimization variables and controlled variables.

Definition of the control objectives

The controller is required to achieve the lowest N_2O emissions possible while respecting the effluent ammonium concentration $[NH_4^+]_{eff}$. In addition, lowering down $[NH_4^+]_{eff}$ has to be prioritized to the minimization of N_2O emissions because meeting the effluent requirements is generally more important than reducing the carbon footprint.

Contrarily to what has been done for the controller developed by Boiocchi *et al.* [73], the objectives for N_2O emissions cannot be expressed numerically because – different compared to the TN removal efficiency – the minimum amount of N_2O possibly emitted varies quite a lot from one plant to another according to many operating and design parameters. Instead, the control objectives are here defined qualitatively as follows: "the controller has to establish those generic environmental conditions which give the least N_2O production and subsequent emission suited for the particular WWTP, while respecting legal effluent NH_4^+ limitations". In this way, the strategy will be able to be applied for a large number of WWTPs, without a need for strong adaptations to specific cases. More specifically, control objectives will be defined on the basis of the trends of the steady-state N_2O emission factors and of the effluent ammonium concentration with respect to the oxygen-to-TKN loading ratio (RO), found through the sensitivity analysis described in Chapter 4 at the temperature of 15ºC. Temperature adjustments will follow in a secondary instance.

Figure 6.1 summarizes the so-called "best and worst system operations" identified. The best system operation is found when the minimal N_2O emission factor is achieved and the effluent ammonium is below the typical law limit of 4 mg $N.L^{-1}$. As can be seen, at RO equal to zero, N_2O emission factors are zero. However, this scenario is not considered desirable since the conversion of ammonium is zero. On the other hand, for values of RO equal or higher than 5.2 g (-COD).g^{-1} TKN, N_2O is minimized while at the same time having the highest ammonium conversion. However, N_2O production by HB in the anoxic zone sensibly increases after 5.2 g (-COD).g^{-1} TKN. Although according to the model used, the contribution of HB from the anoxic zone to N_2O emissions is almost negligible, it is still relevant to avoid this scenario due to the uncertainty in the model parameters. As a matter of fact, it can be that for some plants this contribution will emerge to be more relevant than predicted according to the BSM2Na. Besides this, working at ROs higher than this value means increasing aeration energy consumption without any advantage in terms of N_2O emission reduction. In addition, higher oxygen availability would have only the effect of inhibiting overall nitrogen oxides reduction by HB in the anoxic zone, thus worsening the effluent quality. In view of this, the best system operation is identified for RO equal to 5.2. With regard to the "worst system operation", this is identified to occur according to two different scenarios: (a) excessive oxygen availability, at RO equal to 6 ($RO_{worst,a}$), and (b) insufficient oxygen availability, at RO equal to 4.8 ($RO_{worst,b}$). In both cases, the control action will have to be the maximal possible in order to re-establish the system operation to its best as soon as possible. The value at $RO_{worst,a}$ was chosen since it was the maximal possible indicating the excessive oxygen supply. The value at $RO_{worst,b}$ was chosen when the curve for the N_2O emission factor started increasing towards rather high N_2O emissions. In addition to this, regardless the N_2O emission factors, the maximum control action will have to be taken when the effluent ammonium is above the typical legal limit of 4 mg $N.L^{-1}$.

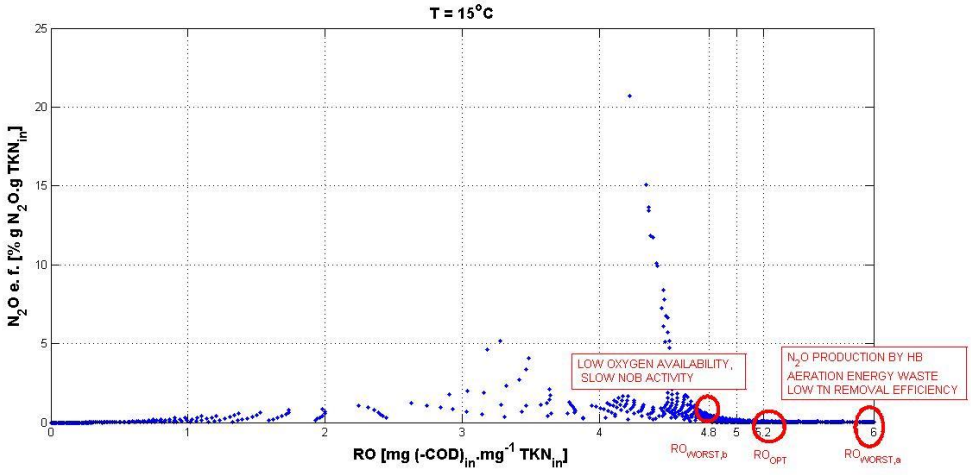

(a)

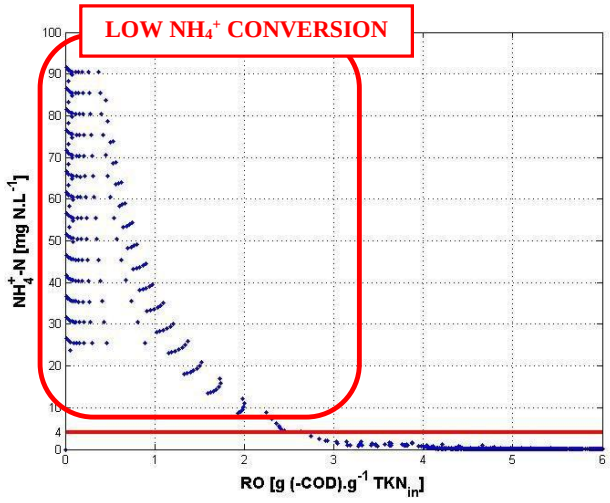

(b)

Figure 6.1: **(a)** N_2O emission factors against oxygen-to-nitrogen loading ratio, and (**b)** effluent NH_4^+ concentration.

Definition of the control structure

On the basis of the observations from the sensitivity analyses in Chapter 3, most of N_2O emitted from continuously-aerated systems is found to originate during AOB denitrification occurring in the aerobic zone, where the AOB-produced nitrites are consumed as electron acceptors for the oxidation of hydroxylamine instead of being consumed as electron donor by NOB and turning to nitrates. If all the ammonium oxidized by AOB in the aerobic zone is converted into nitrate, this indicates that all the AOB-produced nitrites have been oxidized by NOB and not reduced by AOB to originate N_2O. On the

basis of this reasoning, the ratio between nitrate produced by NOB and ammonium consumed by AOB in an aerated zone can be considered as an indicator of the production of N_2O during AOB denitrification. When the entire ammonium consumed by AOB is subsequently consumed by NOB, the production of N_2O during AOB denitrification is zero. Hence, guaranteeing this turns out to be the key for the minimization of N_2O emissions from continuously-aerated systems. For this reason, the ratio between overall nitrate produced and overall ammonium nitrogen depleted in an aerobic zone (R_{NatAmm}), expressed in Eqn. (6.1), is used here as candidate controlled variable.

$$R_{NatAmm} = \frac{NO_3^-|_{OUT,AER} - NO_3^-|_{IN,AER}}{NH_4^+|_{IN,AER} - NH_4^+|_{OUT,AER}} \tag{6.1}$$

As a matter of fact, the difference between ammonium concentrations at the inlet and the outlet of the aerobic zone is supposed to quantify the amount of ammonium consumed by AOB whereas the difference between nitrate out and in the aerobic zone quantifies the amount of nitrate produced by NOB. It is important that the measurements are taken from the inlet and the outlet of an aerobic zone and not of an entire wastewater treatment plant. This is because the difference between nitrate out and in the plant would not represent only the NOB activity, since NO_3^- consumption by heterotrophs would be involved as well. Given these considerations, the theoretical value of R_{NatAmm} indicating complete nitrification should be around 1, which indicates that all the ammonium consumed is equal to the amount of nitrate produced and no nitrification intermediate is used to produce N_2O. Nevertheless, the difference between ammonium in and out the aerobic zone does not entirely incorporate all the ammonium consumed by AOB. As a matter of fact, especially at high oxygen levels when most of the ammonium is depleted, AOB start using the influent organic nitrogen, quickly hydrolysed and ammonified, as electron donor. The nitrite produced thereby is subsequently converted into nitrate by NOB, which is added to the amount of nitrate produced from the oxidation of influent ammonium. For this reason, it can be that the difference between nitrate in the outlet and the inlet to the aerobic zone is slightly higher than the difference between ammonium in the inlet and the outlet. Thus the optimal value of R_{NatAmm} should be expected to be higher than its theoretical value of 1.

Since ensuring complete nitrification means that all the NO_2^- produced by AOB is consumed by NOB, this control strategy is expected to slow down not only AOB but also HB denitrification occurring in the aerobic zone. As a matter of fact, it can occur due to low presence of oxygen and nitrite build-up that HB will start using AOB-produced nitrites as electron acceptors for the oxidation of organic carbon and thus produce N_2O, which, contrarily to what would happen in an anoxic zone, is likely to strip fast to the atmosphere given the higher stripping capability.

The same R_{NatAmm} can also be used to identify excessive aeration conditions. It is in fact found in the previously-performed sensitivity analysis (see Chapter 4) that excessive oxygen supply comes along with biomass decay in the aerobic zone, which releases organic nitrogen that is quickly converted by the autotrophic biomass into nitrate. Values of R_{NatAmm} drastically higher than 1 indicate that this scenario took place.

By setting R_{NatAmm} at its optimal set point, N_2O production is expected to be automatically minimized while at the same time avoiding wasting aeration energy and inhibiting HB denitrification.

Since the conversion of organic nitrogen into nitrate is sped up by an increased operating temperature, the optimal value for R_{NatAmm} increases in function of operating temperature. To take this into account, temperature adaptation of the set points for R_{NatAmm} is included using a separate fuzzy-logic module.

While keeping R_{NatAmm} at its optimal value and thus reducing N_2O production, it is important is to ensure a sustained ammonium conversion with the aim of respecting its effluent limits. For this reason,

the effluent ammonium concentration is used as additional input to the control system for the decision of the proper control action.

On-line measurements of N_2O liquid concentrations in the aeration zone are not considered useful for the achievement of the control objectives. As a matter of fact, the N_2O liquid concentrations can be quite low in an aerated zone, given the high stripping capability typical of this zone. These very low concentrations are much more subject to measurement errors, which in turn would hinder the good performance of a controller using N_2O measurements. Furthermore, mere N_2O measurements do not help the controller decide whether an increase or a decrease in the control action has to be inferred. On the contrary, measurements of nitrites in the aerobic zone would help detect an incomplete nitrification and, hence, decide the proper action to take. However, as presented in Chapter 3, not the entire N_2O is produced as a consequence of nitrite accumulation. There is in fact a high production of N_2O due to NH_2OH accumulation. The nitrite measured would be able to quantify the nitrite left over from all the reactions consuming it and it can happen that, as in the case of NH_2OH accumulation due to insufficient oxygen availability, low nitrite concentrations can result from a very high rate of AOB denitrification, when a high amount of N_2O is produced and emitted. The typical low concentrations of nitrites in continuously aerated systems can, similarly to N_2O measurements, compromise the performance of a controller using NO_2^- measurements.

With regard to the manipulated variable used to achieve the control objective, either the air supply, here represented by the oxygen mass transfer coefficient (k_La), or the oxygen concentration set point (DO_{SP}) of a Proportional Integral (PI) controller, will be adopted to regulate the oxygen availability in the aerobic zone. It will be evaluated which one of the two manipulated variables is more effective in adapting the oxygen demand to achieve the optimal value of R_{NatAmm} and thus reducing N_2O emissions and keeping low $[NH_4^+]_{eff}$.

Eqns. (6.2-6.5) summarize the fuzzy-logic control structure in terms of disturbances ($\underline{d}$), states ($\underline{x}$), manipulated ($\underline{u}$) and controlled variables ($\underline{y}$) around an aerated zone.

$$\underline{d} = [NH_{4,in}^+, S_{S,in}, T_{in}, X_{S,in}, X_{P,in}, NO_{2,in}^-, NO_{3,in}^-, Q_{in}, NO_{in}, N_2O_{in}, N_{2,in}, X_{I,in}, S_{I,in}] \quad (6.2)$$

$$\underline{x} = [NH_4^+, S_S, T, X_S, X_P, NO_2^-, NO_3^-, NO, N_2O, N_2, X_I, S_I] \quad (6.3)$$

$$\underline{y} = [R_{NatAmm}, NH_{4,eff}^+] \quad (6.4)$$

$$\underline{u} = [k_La] \; or \; [DO_{SP}] \quad (6.5)$$

According to the two manipulated variables of Eqns. (6.5), two generic control structures are implemented in an aerobic zone for the minimization of N_2O emissions, as shown in Figure 6.2. As can be seen, the measured ammonium and nitrate nitrogen in the inlet and outlet of the aerated zone are used for the calculation of R_{NatAmm}. The influent temperature to the system is used to update the set point for R_{NatAmm} ($R_{NatAmm,SP}$) through a fuzzy-logic module. The difference between $R_{NatAmm,SP}$ and R_{NatAmm}, along with effluent NH_4^+ concentration, is given as input to the fuzzy-logic control, which infers the unitary variation for the manipulated variable (either $\Delta_U k_La$ or $\Delta_U DO_{SP}$). This variation is named unitary because it is comprised between a minimal value of -1 and maximal value of +1. The quantity is therefore an indicator of whether the manipulated variable has to be increased or decreased. To attribute a physical dimension to this quantity, a scaling factor (either SF_{kLa} or SF_{DOsp}), of the same order of magnitude as the nominal value of the corresponding manipulated variable, is multiplied with this quantity. Summed up in time, the variations Δk_La or ΔDO_{SP} constitute the difference between the value of the actual manipulated variable and its corresponding nominal value (either k_La_{nom} or $DO_{SP,nom}$). The exact setting of the manipulated variable is thus known by adding its corresponding nominal value. In

the configuration where the set point for dissolved oxygen is used as manipulated variable (Figure 1b), the DO_{SP} inferred through the fuzzy-logic controller is then used in a PI controller exploiting the DO measurements.

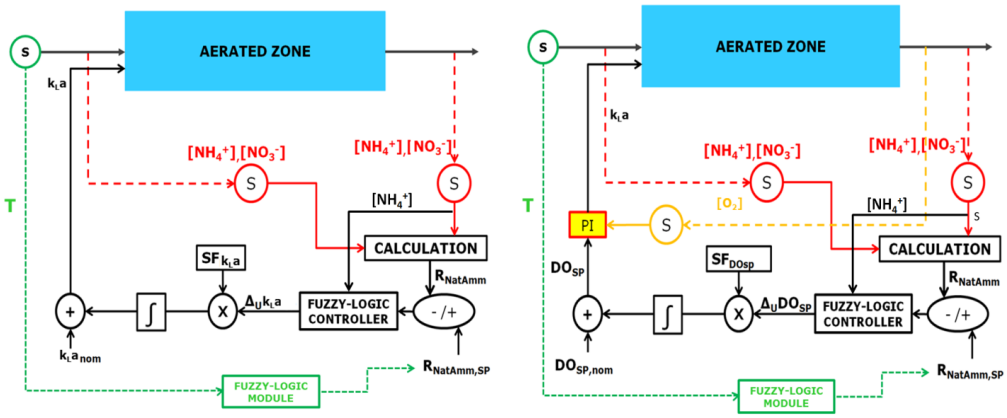

(a) **(b)**

Figure 6.2: Control system implementation using as manipulated variable: **(a)** oxygen mass transfer coefficient, and **(b)** set point of dissolved oxygen concentration.

Definition of the physical constraints

In line with the BSM2, k_La is kept between 0 and 360 d^{-1}. The values for DO are kept between 0.5 and 3 mg (-COD).L^{-1} while the oxygen concentration in the stream recycled to the anoxic zone is kept between 0.5 and 1 mg (-COD).L^{-1}. The choice of the minimal oxygen concentration equal to 0.5 mg (-COD).L^{-1} was taken to prevent compromising biomass settleability. The maximum oxygen concentration of 3 mg (-COD).L^{-1} value was chosen to avoid wasting aeration energy without improving process performance. It is also well-known that WWTPs working with continuous aeration do not usually surpass this threshold. The upper limit in the stream carried to the anoxic zone (1 mg (-COD).L^{-1}) was chosen to avoid direct oxygen inhibition of HB denitrification, which causes a higher amount of non-oxidized organic carbon to be fed in the aerobic zone. This in turn subtracts oxygen from NOB (due to competition with heterotrophs) who are in charge to avoid nitrite accumulation.

The physical constraints on the controlled variables R_{NatAmm} and $[NH_4^+]_{eff}$ are expressed in Eqn. (6.6). As can be seen, both of them have a lower limit of zero. The upper limit for R_{NatAmm} is given by the unit, which is achieved when all the influent ammonium is converted into nitrate, plus the ratio between the total amount of influent organic nitrogen ($N_{org,inAER}$) and the amount of influent ammonium consumed. As a matter of fact, as previously described, the organic nitrogen influent to the aerobic zone can be, under high oxygenation regimes, quickly hydrolysed and ammonified, oxidized into nitrite and finally converted into nitrate by NOB. Thus R_{NatAmm} can have values higher than the unit. $TKN_{in,AER}$ is the Total Kjeldahl Nitrogen in the influent to the aerobic zone which is used to represent the maximal amount of effluent ammonium that could potentially be released. As a matter of fact, at rather poor oxygen levels, the influent ammonium is not consumed and, in addition, the influent organic nitrogen is hydrolysed and ammonified.

$$\begin{cases} 0 \leq R_{NatAmm} \leq \left(1 + \frac{N_{org,inAER}}{\Delta NH_4^+}\right) \\ 0 \leq [NH_4^+]_{eff} \leq TKN_{inAER} \end{cases} \quad (6.6)$$

All disturbances and state variables others than the oxygen concentrations in the aerobic zone can have theoretically values comprised between 0 and <+∞.

Identification of the key scenarios leading the system away from the control objectives

The best system operation is decided to be achieved when both N_2O emissions are minimized and effluent ammonium concentration respects effluent law limits. On the other hand, situations when N_2O emissions are not minimized and/or effluent ammonium concentrations do not respect legal effluent limits are considered to represent a biological system away from the optimality. Table 6.1 summarizes all of these conditions. The parameters used as indicators of the system's proximity to the control objectives are: N_2O emissions and effluent NH_4^+ concentration.

Table 6.1: Summary of scenarios leading the biological system away from optimality.

Scenario↓	**N_2O emissions**	**$[NH_4^+]_{eff}$**
1	LOW	HIGH
2	HIGH due to excess O_2 availability	LOW
3	HIGH due to low O_2 availability	LOW
4	HIGH due to excess O_2 availability	HIGH
5	HIGH due to low O_2 availability	HIGH

Relationships between optimization and controlled variables

Differently from Boiocchi et al. [73], in this case study the relationship between control objectives and controlled variables is not calculated on the basis of mathematical expressions but is qualitatively derived from the steady state results achieved during the sensitivity analysis on the BSM2Na. This is basically due to the high degree of uncertainty linked to the calculation of N_2O emissions, where too many biological and physical processes are involved

Figure 6.3 shows the relationships between N_2O emission factors and RO while Figure 6.3b shows the relationships between R_{NatAmm} and RO at three different operating temperatures of 10°C, 15°C and 20°C. Figure 6.3b will be used to derive the critical points for R_{NatAmm} on the basis of which its membership functions are defined. The membership functions for $E_{RNatAmm}$ will be derived from this. Figures 6.3a and 6.3c will be used to build up the fuzzy-logic module adjusting the set points for R_{NatAmm} in function of temperature.

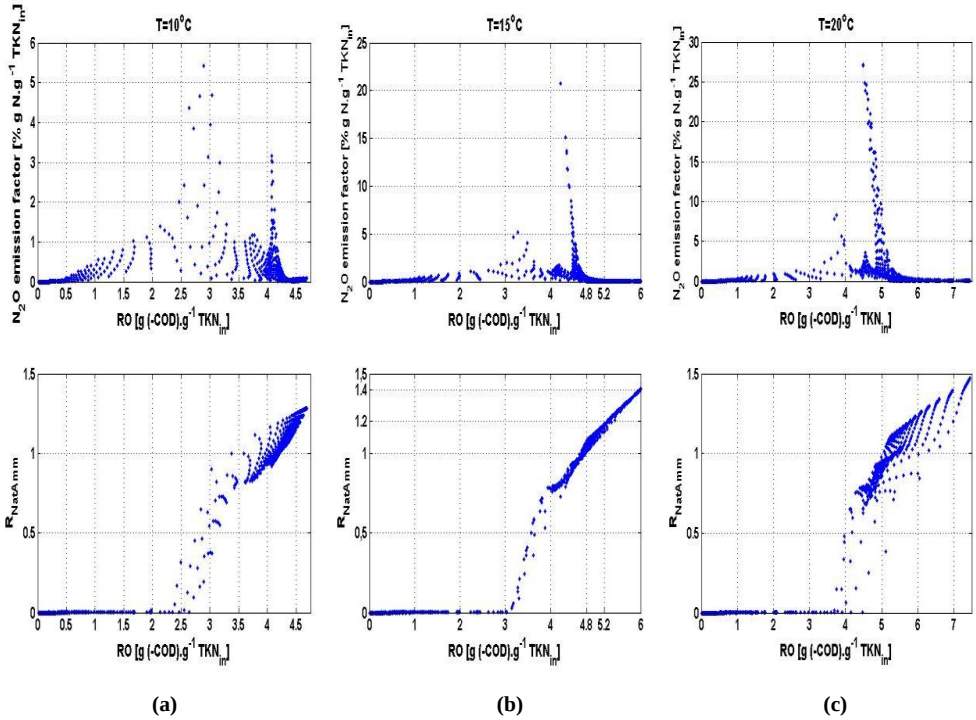

(a) **(b)** **(c)**

Figure 6.3: steady-state N_2O emission factors and R_{NatAmm} in function of RO at the operating temperatures of **(a)** 10 °C, **(b)** 15 °C, and **(c)** 20°C.

In real applications, historical measurements of nitrogen concentrations and N_2O emissions could be used instead of sensitivity analyses results obtained from model simulations. As an alternative, a model can be calibrated according to the full-scale WWTP where there is a desire for minimizing N_2O emissions and then exploited for sensitivity analyses to achieve the same relationships used in this case. In general, it expected that the minimal value of R_{NatAmm} to achieve with the aim of having a balanced activity between AOB and NOB should not go below unity in any case. On the other hand, the value of R_{NatAmm} indicating the worst system operation due to excessive oxygen supply could be more subjective and case-specific.

6.2.2. Identification of the critical points for the controlled variables

Critical points for the controlled variable R_{NatAmm} are retrieved from Figure 6.3b. As can be seen, the value of R_{NatAmm} minimizing N_2O emissions is equal to 1.2. However, to incorporate potential error in the measurements, negative and positive variations of 0.05 around this set point where considered to be completely acceptable. The value of R_{NatAmm} which describes the so-called "worst operation system" due to insufficient oxygen availability is found to be equal to 1 while the value of R_{NatAmm} which describes the same operation of the system due to excessive oxygen supply is found to be equal to 1.4.

With regards to the effluent ammonium concentration, although a typical legal limit for effluent ammonium concentrations is 4 mg $N.L^{-1}$, in order to stay on the safe side, it was decided for the

controller to identify values higher than 2 mg $N.L^{-1}$ as the worst system operation requiring maximal control action. Optimal values for $[NH_4^+]_{eff}$ are chosen to be equal or lower than 1.5 mg $N.L^{-1}$.
Eqns. (6.7-6.10) express the critical points for the vector of controlled variables identified at each system operation, optimal and worst, for each scenario of Table 6.1.

$$UB \text{ for } OPTIMAL\ SYSTEM\ OPERATION \Rightarrow \underline{y}_{UB,OPT} = [1.2 \quad 0] \tag{6.7}$$

$$LB \text{ for } OPTIMAL\ SYSTEM\ OPERATION \Rightarrow \begin{cases} y^1_{LB,OPT} = [1.2 \quad 1.5] \\ y^2_{LB,OPT} = [1.25 \quad 0] \\ y^3_{LB,OPT} = [1.15 \quad 0] \\ y^4_{LB,OPT} = [1.25 \quad 1.5] \\ y^5_{LB,OPT} = [1.15 \quad 1.5] \end{cases} \tag{6.8}$$

$$UB \text{ for } WORST\ SYSTEM\ OPERATION \Rightarrow \begin{cases} y^1_{UB,WORST} = [1.2 \quad 2] \\ y^2_{LB,OPT} = [1.4 \quad 0] \\ y^3_{LB,OPT} = [1 \quad 0] \\ y^4_{LB,OPT} = [1.4 \quad 2] \\ y^5_{LB,OPT} = [1 \quad 2] \end{cases} \tag{6.9}$$

$$LB for\ WORST\ SYSTEM\ OPERATION \Rightarrow \begin{cases} y^1_{UB,WORST} = \left[1.2 \quad TKN_{in,AER}\right] \\ y^2_{UB,WORST} = \left[\left(1 + \frac{N_{org,inAER}}{\Delta NH_4^+}\right) \quad 1.5\right] \\ y^3_{UB,WORST} = [0 \quad 1.5] \\ y^4_{UB,WORST} = \left[\left(1 + \frac{N_{org,inAER}}{\Delta NH_4^+}\right) \quad TKN_{in,AER}\right] \\ y^5_{UB,WORST} = \left[0 \quad TKN_{in,AER}\right] \end{cases} \tag{6.10}$$

6.2.3. Definition of the membership functions for input and output variables

The first step for the definition of the membership functions (MFs) for the input variables consists of the identification of the key CVs whose variation clearly indicates the moving away from optimality. In this case, both R_{NatAmm} and effluent NH_4^+ are key for the identification of the different scenarios presented in Table 1.
The following fuzzy sets were able to be identified for R_{NatAmm} and $(NH_4^+)_{eff}$:

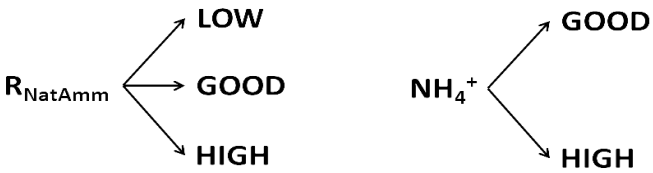

With regards to the shape of the membership functions for input and output variables, triangular and trapezoidal shapes were chosen for the sake of simplicity.
The last step consists in the assignment of the degree of membership to fuzzy sets previously identified for each numerical value of R_{NatAmm} and $(NH_4^+)_{eff}$. A degree of membership to the identified fuzzy sets equal to 1 will be assigned to the critical points defined in subsection 6.2.2 as expressed in Eqns. (6.10-6.13). A degree of membership equal to 0 to the other fuzzy sets will be assigned to the same critical points.

$$UB \text{ for } OPTIMAL\ SYSTEM\ OPERATION \Rightarrow \begin{cases} (R_{NatAmm})_{GOOD} = 1.2 \\ \left(NH_{4,eff}^{+}\right)_{GOOD} = 0 \end{cases} \tag{6.10}$$

$$LB \text{ for } OPTIMAL\ SYSTEM\ OPERATION \Rightarrow \begin{cases} (R_{NatAmm})_{GOOD} = 1.15\ and\ 1.25 \\ \left(NH_{4,eff}^{+}\right)_{GOOD} = 1.5 \end{cases} \tag{6.11}$$

$$UB \text{ for } WORST\ SYSTEM\ OPERATION \Rightarrow \begin{cases} (R_{NatAmm})_{LOW} = 1 \\ (R_{NatAmm})_{HIGH} = 1.4 \\ \left(NH_{4,eff}^{+}\right)_{HIGH} = 2 \end{cases} \tag{6.12}$$

$$LB \text{ for } WORST\ SYSTEM\ OPERATION \Rightarrow \begin{cases} (R_{NatAmm})_{LOW} = 0 \\ (R_{NatAmm})_{HIGH} = \left(1 + \dfrac{N_{org,inAER}}{\Delta NH_4^+}\right) \\ \left(NH_{4,eff}^{+}\right)_{HIGH} = TKN_{in,AER} \end{cases} \tag{6.13}$$

Figure 6.4 shows the resulting membership functions for R_{NatAmm} and $(NH_4^+)_{eff}$.

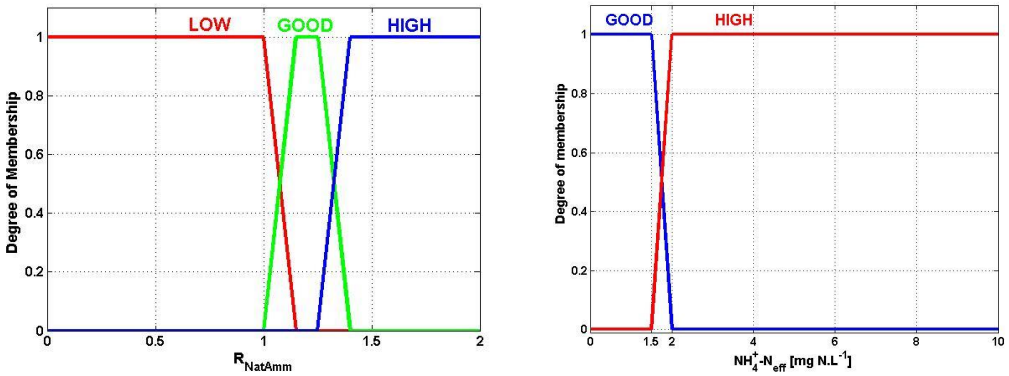

Figure 6.4: membership functions for: **(a)** R_{NatAmm} and **(b)** $[NH_4^+]_{eff}$.

As disclosed in the Section "control structure definition", the difference between the $R_{NatAmm,SP}$ and R_{NatAmm} ($E_{RNatAmm}$=$R_{NatAmm,SP}$-R_{NatAmm}), and not R_{NatAmm}, is used as input variable. This makes the external change of the set point easier, which is in this case needed to incorporate the temperature effect. To obtain the membership functions for $E_{RNatAmm}$ from the ones for R_{NatAmm}, the numerical values of the membership function (on the x-axis) in Figure 4a will be multiplied by -1 and then added the value of 1.2, which is the set point at 15ºC for R_{NatAmm}. The membership functions in Figure 6.5 are thereby obtained as a result.

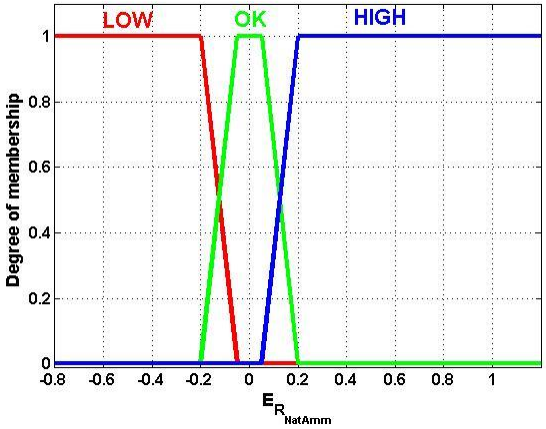

Figure 6.5: Membership functions for $E_{RNatAmm}$.

Similarly to Boiocchi *et al.* [73], the membership functions for the unitary variation of k_La or of DO_{SP} are defined such that the maximum positive value that this quantity will get is +1 and the maximum negative value that this quantity will get is -1. Taking into account the Center-of-Area as the chosen defuzzification method, the membership functions depicted in Figure 6.6 are defined accordingly.

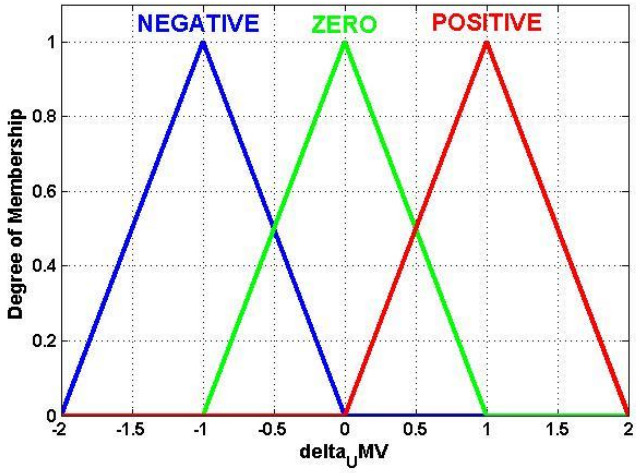

Figure 6.6: Membership functions for the unitary variation of the manipulated variable (Δ_UMV).

Fuzzy logic module for temperature adaptation

As previously disclosed, the set point for R_{NatAmm} is adapted in function of the temperature. This is because temperature increases the amount of influent organic nitrogen overall converted into nitrate and thus it sensibly increases the optimal set point for R_{NatAmm} at which N_2O emissions are minimized. The present fuzzy-logic module uses as input the influent temperature and as output $R_{NatAmm,SP}$. The membership functions were decided on the basis of the values of R_{NatAmm} minimizing N_2O emissions at the three different temperatures from Figure 6.3. Specifically, the set points of Table 6.2 were found.

Table 6.2: Set points for R_{NatAmm} in function of temperature.

TEMPERATURE [ºC]	**$R_{NatAmm,SP}$**
10	1.1
15	1.2
20	1.4

Extrapolating, the $R_{NatAmm,SP}$ for temperature of 5 degree was assumed to be 1 while the set point for temperature of 25 was assumed to be 1.6.
Choosing as default defuzzification method the Center-of-Area method, the membership functions for its input and output variables shown in Figure 6.7 were designed.

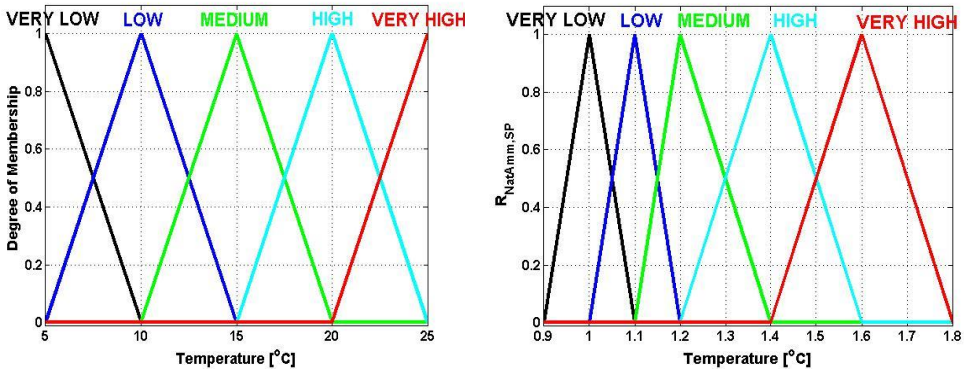

(a) **(b)**

Figure 6.7: **(a)** membership functions for the influent temperature, and **(b)** membership functions for $R_{NatAmm,SP}$.

6.2.4. Implementation of the linguistic rules

The following look-up table (Table 6.3) shows the IF-THEN linguistic rules connecting the inputs ($E_{RNatAmm}$ and the effluent NH_4^+) to the output variable ($\Delta_U k_L a$ or $\Delta_U DO_{SP}$). As can be noted, when the effluent NH_4^+ is found to belong to the fuzzy set "HIGH", the controller increases the manipulated variable, regardless $E_{RNatAmm}$. Otherwise, the controller will: (a) increase the oxygen availability if $E_{RNatAmm}$ belongs to the fuzzy set "HIGH" (i.e. when R_{NatAmm} is lower than the set point), which indicates suboptimal NOB activity rate, or (b) decrease it if $E_{RNatAmm}$ belongs to the fuzzy set "LOW" (i.e. when R_{NatAmm} is higher than the set point), which indicates waste of oxygen supply, enhancement of N_2O production by HB in the anoxic zone and worsening of effluent quality. If both the effluent NH_4^+ and $E_{RNatAmm}$ belong to the fuzzy set "GOOD", no control action is taken.

Table 6.3: Look-up table for the linguistic rules linking $E_{RNatAmm}$ and $(NH_4^+)_{eff}$ to Δ_UMV (either $\Delta_U k_L a$ or $\Delta_U DO_{SP}$).

		$E_{RNatAmm}$		
		LOW	**GOOD**	**HIGH**
$(NH_4^+)_{eff}$	**GOOD**	**N**	**Z**	**P**
	HIGH	**P**	**P**	**P**

Legend: P=POSITIVE, N=NEGATIVE, Z= ZERO.

‘

The linguistic rules for the temperature adaptation fuzzy-logic module are shown in Table 6.3.

Table 6.4: linguistic rules linking the temperature to $R_{NatAmm,SP}$.

IF	THEN
TEMPERATURE	**$R_{NatAmm,SP}$**
VERY LOW	VERY LOW
LOW	LOW
MEDIUM	MEDIUM
HIGH	HIGH
VERY HIGH	VERY HIGH

6.2.5 Setting of additional design parameters

The additional design parameters to be decided were the implication and the aggregation method. Correlation-minimum was chosen as the implication method whereas disjunctive was chosen as the aggregation method.

The scaling factor used for the controller was chosen to be equal or below the difference between the saturation limit for the manipulated variable used and its nominal value.

6.3. Controller implementation and performance evaluation

Once designed, the control strategies will be implemented and tested in the three benchmark simulation models (BSM2Na, BSM2Nb and BSM2Nc) described in Chapter 3. Figure 6.8a shows the implementation of the novel control strategy using R_{NatAmm} and effluent ammonium as controlled variables and the oxygen mass transfer coefficient as direct manipulated variable while Figure 6.8b shows the same implementation using the DO set point as direct manipulated variable.

(a)

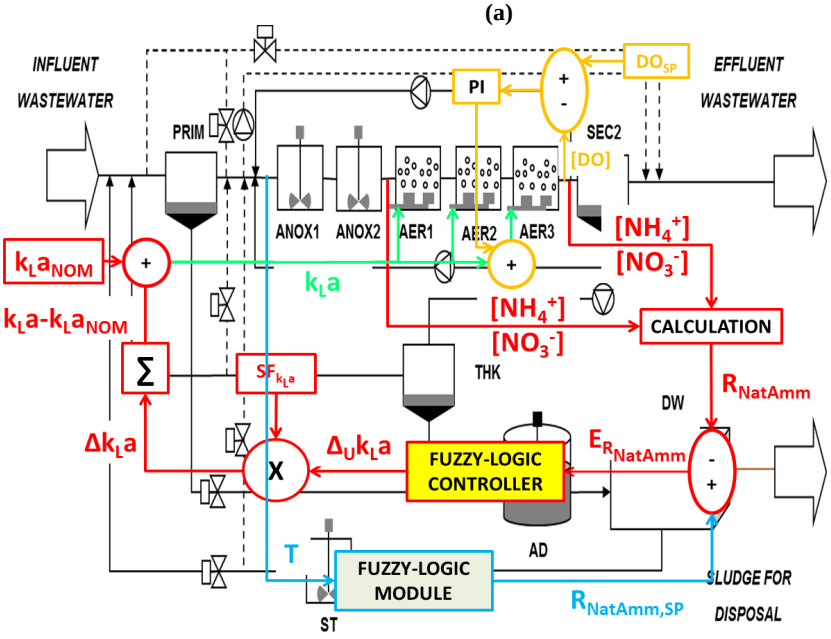

(a)

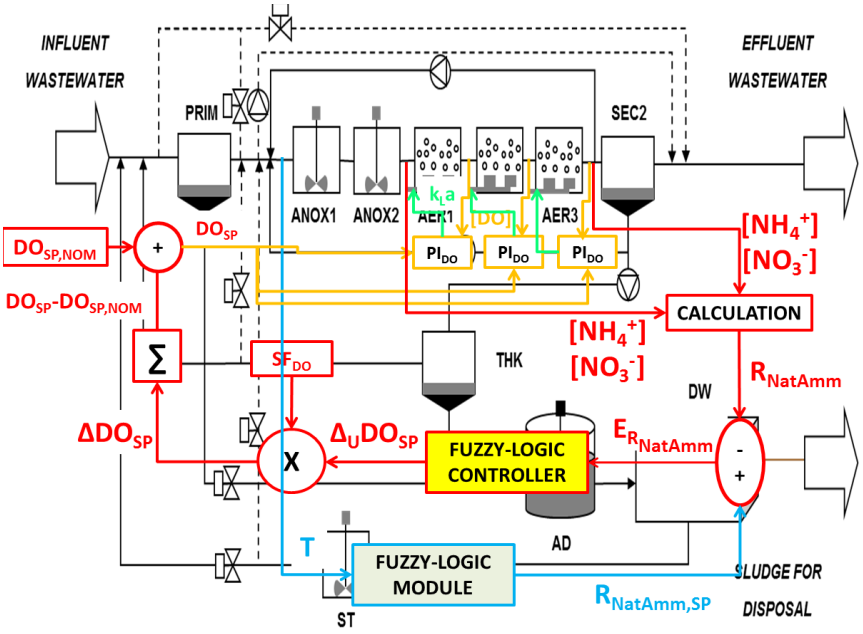

(b)

Figure 6.8: **(a)** Implementation of the regulatory control strategy, **(b)** implementation of the cascade control strategy.

As explained in Chapter 3, the simulation models describe different dynamics according to which N_2O is produced. More specifically, the BSM2Na describes N_2O production during HB and AOB denitrification, but not during the incomplete oxidation of hydroxylamine (NH_2OH) while the BSM2Nb and the BSM2Nc incorporate additionally the N_2O production during the incomplete NH_2OH oxidation but according to different mathematical expressions and assumptions. HB denitrification is modelled the same for all the three models. As a consequence of the different N_2O modelling approaches, the models predict N_2O dynamics differently and, since there is no consensus on which model is the most reliable, all of them should be used in order to test the robustness of the controllers against different modelling approaches. The testing and evaluation procedure will follow Jeppsson *et al.* [22] described in Chapter 2. The performance criteria used to evaluate the control strategies will be:

- Average R_{NatAmm},
- Integral Absolute Error for R_{NatAmm} ($IAE_{RNatAmm}$),
- Integral Square Error for R_{NatAmm} ($ISE_{RNatAmm}$),
- Total Variation (TV) of k_La, calculated by summing the TV of the three k_La in the aerobic zone,
- N_2O emission factor, calculated per unit of influent TKN (N_2O_{ef1} [g N_2O-N.g^{-1} TKN_{in}]),
- N_2O emission factor, calculated per unit of removed TKN (N_2O_{ef2} [g N_2O-N.g^{-1} TKN_{rem}]),
- Average N_2O production rates according to the different pathways [g N_2O-N.d^{-1}],
- Average TKN removal efficiency (η_{TKN}),

- Average TN removal efficiency (η_{TN}),
- Average effluent nitrate ($[NO_3^-]_{eff}$),
- Percentage of total time when effluent ammonium violations occur (V_{NH}),
- Percentage of total time when effluent total nitrogen violations occur (V_{TN}),
- Effluent quality index (EQI [kg pollutant.units.d^{-1}]),
- Average aeration energy consumed (AEC [kWh.d^{-1}]).

Using each simulation model, these parameters will be calculated for the closed-loop configurations and compared against a corresponding open-loop configuration which represents the reference scenario. In addition to these, a third configuration, regulating the set point of the oxygen concentrations in the three aerobic tanks on the basis of the effluent ammonium concentration, is considered in order to evaluate the added value of the novel control idea. Finally, the robustness of the novel control strategy against sensor and actuator dynamics was evaluated by implementing the models for sensors and actuators suggested by Alex *et al.* [21]. More specifically, the continuous sensors of type A, working without delay, were chosen for temperature and oxygen concentrations while sensors type B1 (photometric with normal filtration) were modelled for the measurements of ammonium and nitrate concentrations. Type-A actuators were used for the manipulation of the oxygen mass transfer coefficients.
The reference scenario for the three benchmark simulation models is identified by optimizing the oxygen mass transfer coefficients of the three aerobic biological tanks to have the highest TKN conversion and contextually the lowest N_2O emissions per unit of TKN removed predicted by the BSM2Na. The solutions were further selected by limiting the concentration of oxygen in the last aerobic tank between 0.5 and 1 mg (-COD).L^{-1}. The following optimal k_La values were identified: 156.1 d^{-1} for AER1, 100.7 d^{-1} for AER2 and 55.7 d^{-1} for AER3. It can be observed that the steady-state N_2O emissions are minimized by supplying more oxygen into the first aerobic tank and less into the last. This is explained by the fact that when more NH_4^+ comes into a tank, more oxygen is required for its complete oxidation into NO_3^-, which agrees with the basic idea that complete nitrification is the key for N_2O emission minimization in continuously-aerated systems.
The reference scenarios for the three BSMs were obtained by simulating each model with the dynamic influent and these constant k_La values.

6.4. RESULTS

In this section, the simulation results obtained using the BSM2Na, BSM2Nb and BSM2Nc are presented and discussed. This section will be split up into three main subsections: one analyzing the N_2O dynamics (subsection 6.4.1), another one focusing on the effluent quality (subsection 6.4.2) and a third one discussing the energy consumptions linked to aeration (subsection 6.4.3). The control strategies tested and benchmarked against the open-loop reference scenario are:

1) R_{NatAmm} and NH_4^+ regulatory controller, using directly k_La as manipulated variable (*CS1*),
2) R_{NatAmm} and NH_4^+ cascade controller, using directly the set point for dissolved oxygen (DO_{SP}) as manipulated variable (*CS2*),
3) NH_4^+ cascade controller, using directly the set point for dissolved oxygen (DO_{SP}) as manipulated variable (*CS3*) using 1.5 mg $N.L^{-1}$ as set point for the effluent ammonium nitrogen,
4) Control strategy *CS2* with sensor and actuator noises (*CS4*).

6.4.1. Control performance on the N_2O emissions

Tables (6.4-6.6) show the emission factors for N_2O, R_{NatAmm}, and the N_2O contributions by the different pathways according to the BSM2Na, BSM2Nb and BSM2Nc, respectively. The Integral Absolute Error and the Integral Square Error for R_{NatAmm} ($IAE_{RNatAmm}$ and $ISE_{RNatAmm}$) are included as well in order to evaluate how the tracking of the set point for R_{NatAmm} affects the N_2O emissions. The total variation of the k_La is considered to understand the aggressiveness of the control response.

As can be deduced by comparing the results in open-loop and with *CS1* and *CS2*, the controller is able for all the three models to drastically reduce the average rate of AOB denitrification by increasing the average value of R_{NatAmm}. More specifically, for each model as the tracking of the set point for R_{NatAmm} - indicated by the IAE and the ISE - improves, the higher is the reduction of the amount of N_2O produced by AOB. The production of N_2O according to the incomplete hydroxylamine pathway according to the BSM2Nb was also able to be reduced through the R_{NatAmm} controller. This is because the controller attempts to achieve complete nitrification in the aerobic zone, which means that accumulation of NH_2OH and NO are avoided. However, the reduction of the N_2O produced according to this pathway is lower than the reduction achieved on AOB denitrification since this last process is inhibited by oxygen while the N_2O production from the other AOB pathway is not. Besides the reduction of AOB-mediated N_2O production, a contextual decrease in the amount of N_2O consumed by HB can also be observed in all the three models. This can be largely assigned to the overall lower N_2O accumulation in the liquid phase, which triggers the last HB denitrification reduction step. Since the decrease of N_2O produced by AOB is more than the decrease of N_2O consumed by HB, both the total N_2O emitted per unit of influent TKN (N_2O_{ef1}) and the total N_2O emissions per unit of TKN removed (N_2O_{ef2}) result drastically reduced. The fact that also N_2O emissions per unit of TKN removed are reduced demonstrates the fact that N_2O has not been reduced by diminishing the overall TKN conversion, but by reducing the rates of those specific processes producing it.

Adaptability to temperature changes

The capability of the controller to adapt to the temperature variations is checked by observing Figure 6.8, showing the dynamics of the N_2O production in the aerobic zone by the different processes and the total N_2O emitted predicted by the BSM2Nc in open-loop, with *CS1* and with *CS2*. As can be noted from the open-loop configuration, N_2O emissions (Figure 6.8a) are in phase with N_2O produced by AOB (Figure 6.8b). More specifically, in the open-loop configuration, as the temperature increases, N_2O production by AOB increases and N_2O emissions follow the same trend. The behaviour of AOB production is to be attributed to the balance between the aerobic growth of AOB and the aerobic growth by NOB. According to Hellinga *et al.* [49], NOB growth is disadvantaged over the growth of AOB as temperature increases. This is in fact one of the reasons why the nitritation systems, like the SHARON, are able to work efficiently. As a matter of fact, by keeping the operating temperatures high (30-35^{o}C), NOB can be washed out. In activated sludge systems like the one considered here, this behaviour leads to higher nitrite accumulation at warm temperatures (see Figure 6.8c) which, in turn, triggers AOB denitrification and, consequently, N_2O emissions. From Figure 6.8d it can be noted that, similarly to AOB denitrification, HB-mediated N_2O production is high when temperature increases due to higher availability of AOB-produced nitrites. As expected, both *CS1* and *CS2* are able to reduce drastically the N_2O produced by HB. However, also the consumption of N_2O by HB during the last reduction step is reduced drastically when the controllers are applied (see Figure 6.8e). Overall, the net N_2O production by HB in the aerobic zone is always negative (see Figure 6.8f), which means that the amount of N_2O consumed by HB overcomes the amount of N_2O produced by HB and that a fraction of AOB-produced

N_2O is consumed by HB. This overall N_2O consumption by HB decreases when the controllers are implemented. This fact can be explained by the lower availability of N_2O in the liquid phase partly due to lower AOB denitrification and partly due to higher N_2O stripping.
To cope with the imbalance between AOB and NOB activity observed for high temperatures, both *CS1* and *CS2* increase the oxygen supply when temperature increases, as depicted in Figures 6.9a and 6.9b.

Comparison between regulatory and cascade controllers

By comparing more in detail the results obtained with *CS1* and *CS2*, it can be noted that slightly higher N_2O is emitted when *CS1* is used according to all the three models. This is due the fact that the oxygen supply is better regulated according to the influent ammonium dynamics through *CS2* than through *CS1*. Such behaviour can be clearly observed in Figure 6.10a, which shows the dynamics of k_La of ammonium concentration in the first aerobic tank in the time span between the 350^{th} and the 360^{th} days according to the BSM2Nc. As can be observed, the k_La manipulated by the cascade controller is increased faster when the influent ammonium increases and is decreased faster when the influent ammonium decreases, compared to the k_La manipulated by the regulatory controller. Thus a more complete nitrification is achieved, which in turn allows a better tracking of the set point for R_{NatAmm} (see $IAE_{RNatAmm}$ values in Table 6.6), a consequent higher reduction of the rate of AOB denitrification (see Figure 6.10b) and, finally, lower N_2O emitted.
Interestingly, according to the BSM2Na and the BSM2Nb, the amount of net N_2O consumed by HB is higher when *CS2* instead of *CS1* is used. This is the consequence of a different stripping regime of N_2O. As a matter of fact, *CS2* allows a larger residence time of N_2O in the liquid phase, which in turn increases its chances of being reduced into N_2 by HB. This property could not be clearly found in the BSM2Nc, probably due to the fact that the controllers have to push up the aeration supply more to overcome the higher AOB denitrification rate.
Nevertheless, the better performance of *CS2* comes at the expenses of higher aggressiveness of the control response, which is clearly indicated by the higher value of TV.

Added value of novel control strategy: comparison against the cascade controller for effluent NH_4^+

As can be noted by comparing the N_2O emission factors achieved from the open-loop configurations and *CS3* according to the three BSMs, it can be noted that, although the controller was not designed to reduce N_2O emissions, a decrease in the N_2O emission factors could be achieved with such a control strategy. As a matter of fact, *CS3* is designed in order to keep the oxygen concentration to a significant level in order to ensure high AOB activity, and consequently low effluent ammonium. By doing so, the controller triggers contextually the activity of NOB and this in turn reduces nitrite accumulation and the AOB denitrification rate. Thus, as can be noted, the average R_{NatAmm} is increased. Nevertheless, the reduction of the N_2O emission factors, both N_2O_{ef1} and N_2O_{ef2}, compared to the open-loop, is lower than the reduction achieved through the implementation of the controllers specifically designed for low N_2O emissions (*CS1* and *CS2*) according to the BSM2Na and BSM2Nc. The reason for having higher N_2O emissions according to the BSM2Na and BSM2Nc with *CS3* is to be found in the manipulation of the oxygen supply actuated at warm temperatures (see Figure 6.11d). As a matter of fact, while *CS1* and *CS2* tend to drastically increase the oxygen supply in the aerobic zone to cope with the increased imbalance between AOB and NOB growth rates typical of high temperatures, *CS3* does not. This leads to higher generation of N_2O from AOB denitrification at high temperatures for *CS3* (see Figure 6.11b). In turn, N_2O emissions are higher in summer with *CS3* activated (see Figure 6.11a).

On the other hand, according to the BSM2Nb, the reduction of N_2O emissions obtained with CS3 is more comparable to *CS2*. Analysing the N_2O produced according to the three different pathways, AOB denitrification and incomplete NH_2OH oxidation pathways aremore slowed down with *CS2* than with *CS3*. However, the HB-mediated N_2O consumption resulting from using *CS3* is larger than the one resulting from using *CS2*. This leads to slightly lower emission factors with *CS3*.

Robustness against sensor and actuator noises

As can be noted by comparing the average N_2O emitted per unit of influent TKN and unit of TKN removed with *CS2* and *CS4* according to each model, the novel control strategy *CS2*, and presumably *CS1*, can be considered robust against the sensor and actuator noises. *CS4* is in fact able to achieve a drastic reduction of the N_2O emissions compared to the open-loop. According to all the three models, the IAE and ISE values achieved using *CS4* are slightly higher than the ones achieved with *CS2*, which in turn leads to slightly higher N_2O emissions with *CS4*. Nonetheless, the manipulation of the oxygen mass transfer coefficient needed to cope with sensor and actuator noises imposed results that seem to be much more aggressive, as can be noted from the value of TV calculated.

Table 6.4: N_2O emission factors, average R_{NatAmm} and average N_2O produced by HB and AOB predicted by the BSM2Na in open-loop and with the four control strategies (*CS1*, *CS2*, *CS3* and *CS4*).

BSM2Na						
	units	**OL**	**CS1**	**CS2**	**CS3**	**CS4**
Average R_{NatAmm}	$\frac{g\ NO_3^- - N}{g\ NH_4^+ - N}$	1.065	1.25	1.26	1.207	1.26
$IAE_{RNatAmm}$	[-]	98.45	73.84	73.62	79.3	74.06
ISE	[-]	40.95	24	23.68	26.84	23.94
TV	[d^{-1}]	0	1543.2	3021.2	2733.4	5668.5
N_2O_{ef1}	$\%\ \frac{g\ N_2O - N_{gas}}{g\ TKN - N_{in}}$	0.191	0.066	0.045	0.16	0.047
N_2O_{ef2}	$\%\ \frac{g\ N_2O - N_{gas}}{g\ TKN - N_{rem}}$	0.203	0.068	0.047	0.166	0.049
Average N_2O produced by HB	$\frac{g\ N_2O - N_{liq}}{d}$	290.8	-52.5	-213.65	-1917.6	-44.87
Average N_2O produced by AOB	$\frac{g\ N_2O - N_{liq}}{d}$	1718.7	731.42	679.92	3558.4	528

Table 6.5: N_2O emission factors, average R_{NatAmm} and average N_2O produced by HB and AOB predicted by the BSM2Nb in open-loop and with the four control strategies (*CS1*, *CS2*, *CS3* and *CS4*).

BSM2Nb						
	units	**OL**	**CS1**	**CS2**	**CS3**	**CS4**
Average R_{NatAmm}	$\frac{g\ NO_3^- - N}{g\ NH_4^+ - N}$	1.15	1.28	1.28	1.265	1.28
$IAE_{RNatAmm}$	[-]	83.95	77.56	76.82	83.5	77.16
$ISE_{RNatAmm}$	[-]	29.47	26.19	25.51	29.71	25.65
TV	[d^{-1}]	0	1685.4	2985.3	2909.8	5688.2
N_2O_{ef1}	$\% \frac{g\ N_2O - N_{gas}}{g\ TKN - N_{in}}$	0.0481	0.0248	0.0208	0.0176	0.0226
N_2O_{ef2}	$\% \frac{g\ N_2O - N_{gas}}{g\ TKN - N_{rem}}$	0.0524	0.026	0.0217	0.0184	0.0234
Average N_2O produced by HB	$\frac{g\ N_2O - N_{liq}}{d}$	-2545.9	-958.05	-997.54	-1574.8	-902.04
Average N_2O produced from AOB denitrification	$\frac{g\ N_2O - N_{liq}}{d}$	78.8865	6.21	4.74	10.051	3.88
Average N_2O produced from incomplete NH_2OH oxidation	$\frac{g\ N_2O - N_{liq}}{d}$	2980.2	1208.3	1208.7	1747.1	1131.9

Table 6.6: N_2O emission factors, average R_{NatAmm} and average N_2O produced by HB and AOB predicted by the BSM2Nc in open-loop and with the four control strategies (*CS1*, *CS2*, *CS3* and *CS4*).

BSM2Nc						
	units	**OL**	**CS1**	**CS2**	**CS3**	**CS4**
R_{NatAmm}	$\frac{g\ NO_3^- - N}{g\ NH_4^+ - N}$	0.9	1.24	1.2615	1.17	1.256
$IAE_{RNatAmm}$	[-]	153.5302	84.23	83	92.97	85.1
$ISE_{RNatAmm}$	[-]	101.6277	30.74	29.78	35.84	31.21
TV	[d^{-1}]	0	1681.9	3331.8	2779.8	6309.7
N_2O_{ef1}	$\% \frac{g\ N_2O - N_{gas}}{g\ TKN - N_{in}}$	0.39	0.067	0.047	0.167	0.049
N_2O_{ef2}	$\% \frac{g\ N_2O - N_{gas}}{g\ TKN - N_{rem}}$	0.413	0.069	0.048	0.172	0.051
Average N_2O produced by HB	$\frac{g\ N_2O - N_{liq}}{d}$	-97387	-26844	-20370	-48113	-21937
Average N_2O produced by AOB	$\frac{g\ N_2O - N_{liq}}{d}$	117490	34464	25637	57402	27692

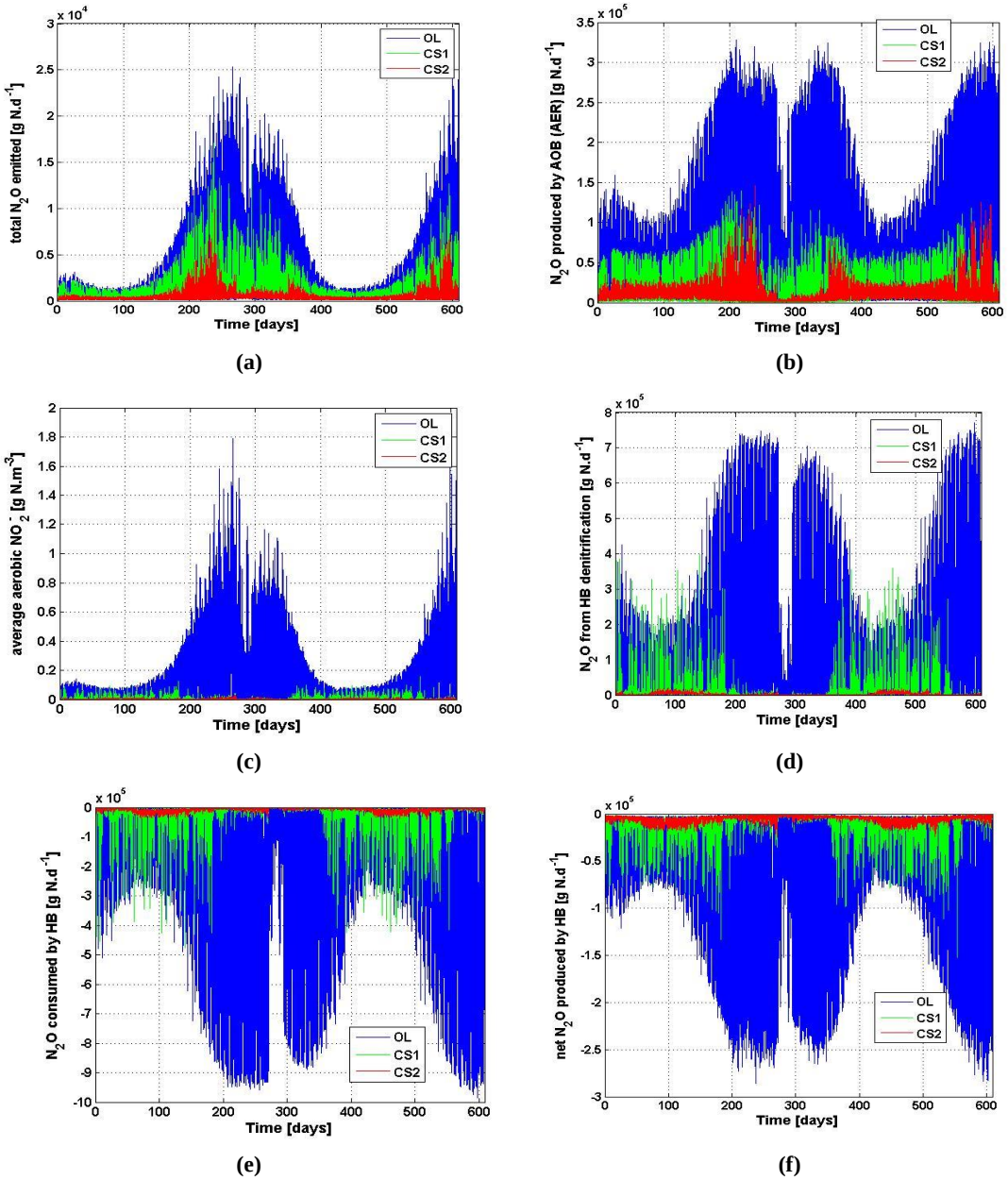

Figure 6.8: **(a)** total N_2O emitted, **(b)** N_2O production by AOB, **(c)** average NO_2^- concentration in the aerobic zone, **(d)** N_2O produced by HB in the aerobic zone (third HB denitrification step), **(e)** N_2O consumed by HB in the aerobic zone (forth HB denitrification step), and **(f)** net N_2O produced by HB in the aerobic zone (third plus forth denitrification steps), predicted by the BSM2Nc in open-loop and with *CS1* and *CS2*.

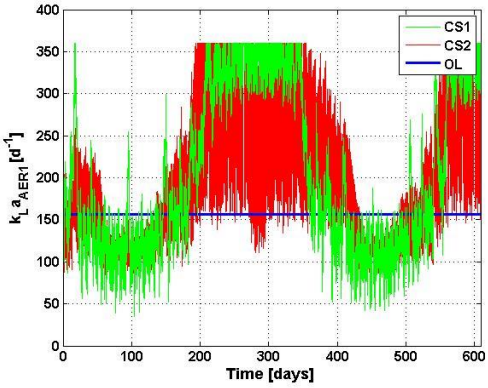

(a)

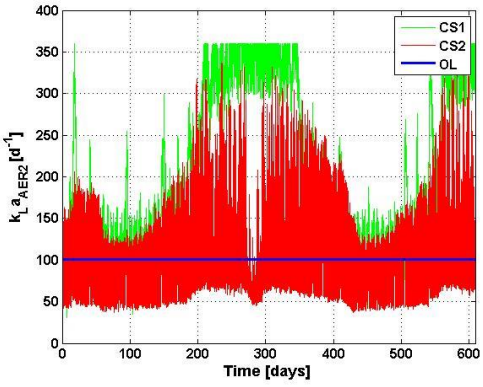

(b)

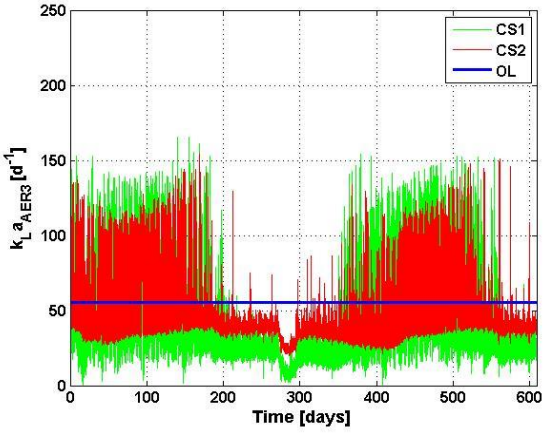

(c)

Figure 6.9: k_La according to the BSM2Nc in open-loop and with CS1 and CS2 in: **(a)** first aerobic tank (k_La_{AER1}), **(b)** second aerobic tank (k_La_{AER2}), and **(c)** third aerobic tank (k_La_{AER3}).

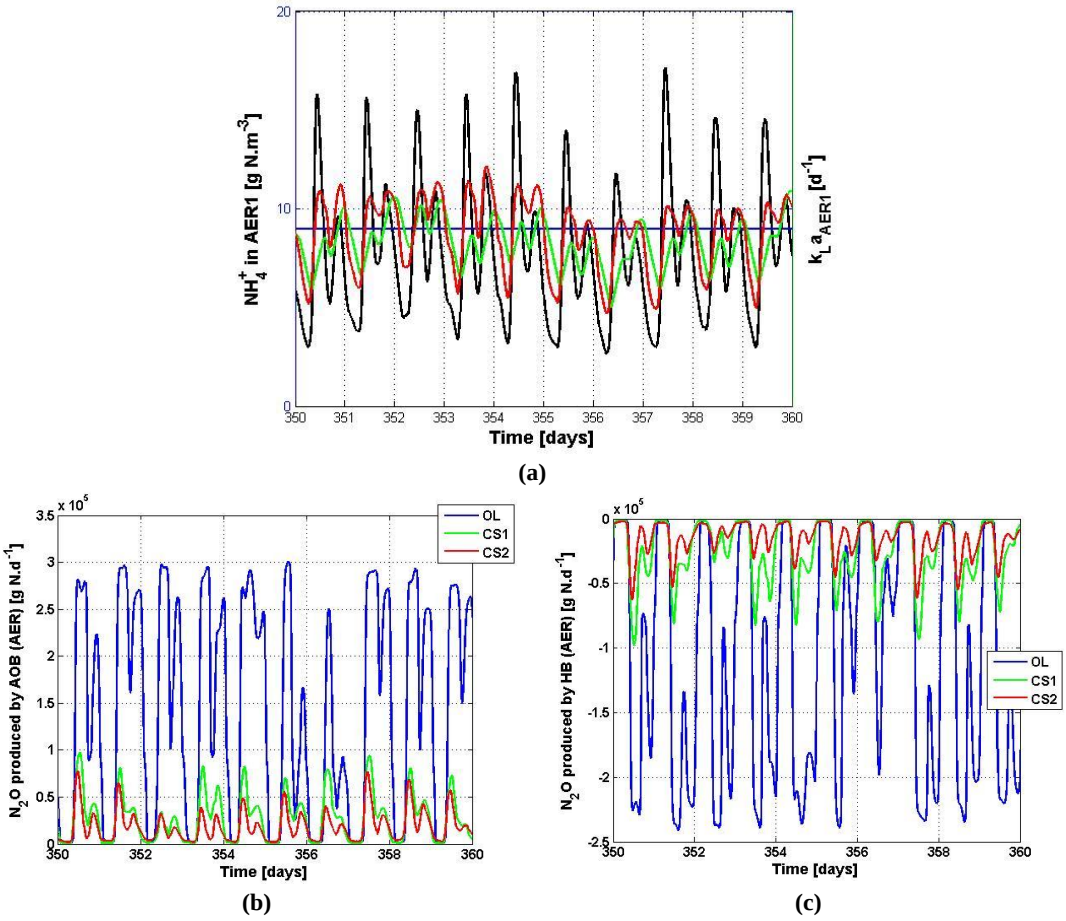

Figure 6.10: **(a)** influent ammonium and k_La to the first aerobic tank, **(b)** N_2O produced by AOB and **(c)** net N_2O produced by HB according to the BSM2Nc in open-loop, with *CS1* and *CS2*.

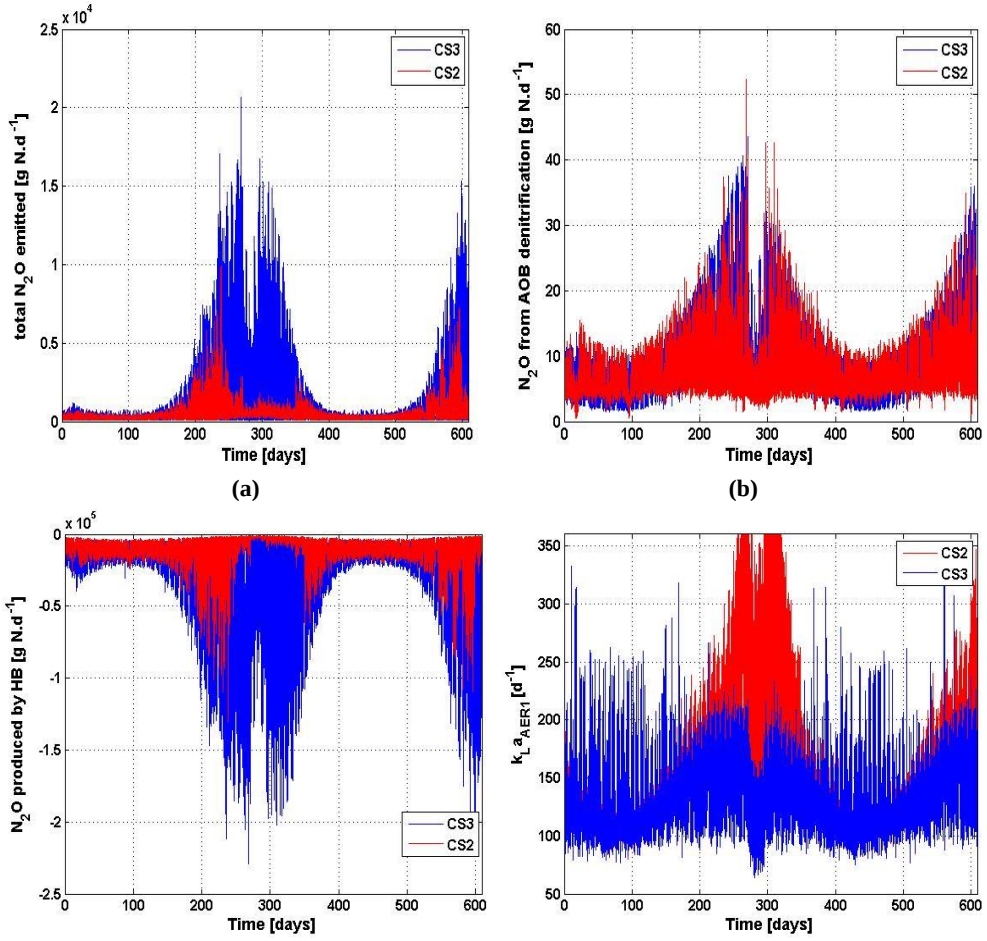

Figure 6.11: **(a)** total N_2O emissions, **(b)** N_2O produced by AOB, **(c)** N_2O net produced by HB, and **(d)** k_La of the first aerobic tank according to the BSM2Nc with *CS2* and *CS3*.

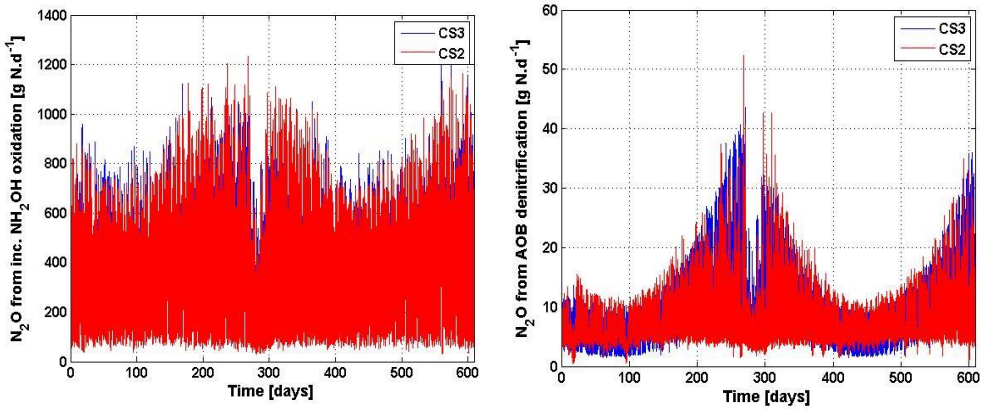

(a) **(b)**

Figure 6.12: **(a)** N_2O generated from incomplete NH_2OH oxidation pathway, and **(b)** N_2O generated from AOB denitrification according to the BSM2Nb with *CS2* and *CS3*.

6.4.2. Control performance on the effluent quality

Within the context of mitigation of N_2O emissions, the effluent quality has to be considered. Tables (6.9-6.11) show the average TKN removal efficiency, TN removal efficiency, ammonium and total nitrogen violations and effluent quality index according to the BSM2Na, BSM2Nb and BSM2Nc, respectively, in open-loop, and with *CS1*, *CS2*, *CS3* and *CS4*. As can be noted, according to all the three models, *CS1* and *CS2* are able to increase the overall TKN removal efficiency compared to the corresponding open-loop scenario. Furthermore, by observing the frequency of violations of the effluent ammonium limit (4 mg $N.L^{-1}$), it can be easily demonstrated that the controllers are able to drastically reduce the ammonium violations and to re-establish the ammonium concentration within acceptable values. As a matter of fact, V_{NH} in the open-loop configurations according to the BSM2Nb and BSM2Nc resulted particularly high and CS1 and CS2 were able to reduce them to reasonable values. *CS2* performed considerably better in reducing the ammonium violations than *CS1*. This can be ascribed to the fact that the k_La is increased more rapidly when influent ammonium increases when *CS2* is used, as previously shown in Figure 10a.

The effluent ammonium violations obtained by *CS3* are negligible. The controller is able to keep respecting the effluent ammonium limits throughout the entire simulation period and performs in this regard better than *CS1* and *CS2*. The reason for this can be due to the fact that *CS1* and *CS2* have also to cope with N_2O emissions and the objectives can be sometimes conflicting. While in hot seasons aeration has to be increased to work out the lower NOB activity rate compared to AOB activity rate, in winter the controller, while keeping the nitrification complete, attempts to avoid aeration energy waste and high N_2O production by HB denitrifiers. Thus there will be instances in cold temperatures when CS1 and CS2 will infer negative variations of the oxygen supply. As a consequence, this will cause a temporary increase of effluent ammonium, which can become higher than the effluent limit. Anyhow, *CS1* and especially *CS2* are able to ensure high TKN conversion, which means that they are able to cope with the slightly-higher frequency of ammonium violations. To be noted is also that the TKN removal efficiency is higher when using *CS2* than when using *CS3*. As a drawback of *CS1*, *CS2* and *CS3*, the effluent TN violations are variably increased. This has to be attributed to the higher COD demand by

heterotrophic denitrifiers to perform the complete reduction of autotrophically-produced nitrogen oxides (such as nitrates and nitrites) into dinitrogen gas (N_2). As a matter of fact, since the controllers achieve a more complete oxidation of ammonium into nitrate and thus avoid nitrite leftovers, HB denitrification will receive a higher load of nitrates in the anoxic zone, which requires more biodegradable COD than nitrites to be reduced into N_2 [49]. Consequently, more unreduced nitrates will be in the effluent and higher violation of effluent TN limit will occur, as shown in Tables (6.7-6.9). For the same reason, the EQI significantly increases. Since *CS2* was more able to achieve complete nitrification than *CS1*, the EQI is worse when *CS2* is used.

Table 6.7: TKN and TN removal efficiencies, effluent average nitrate, ammonium and TN violations and effluent quality index predicted by the BSM2Na in open-loop and with the four control strategies (*CS1*, *CS2*, *CS3* and *CS4*).

BSM2Na						
	units	**OL**	**CS1**	**CS2**	**CS3**	**CS4**
η_{TKN}	$\%\frac{g\ TKN_{rem}}{g\ TKN_{in}}$	94.25	96.3	96.35	96.1	96.5
η_{TN}	$\%\frac{g\ TN_{rem}}{g\ TN_{in}}$	73.6	67.3	66.76	69.8	66.64
NO_3^-	$g\ N.m^{-3}$	10.21	14.42	14.72	13.07	14.84
V_{NH}	% of operating time	6.42	1.71	0.58	0.054	0.4
V_{TN}	% of operating time	7.56	29.94	35.13	22.8	36.3
EQI	kg pollutant.units.d^{-1}	5700	5928.32	5967	5713.8	5957.2

Table 6.8: TKN and TN removal efficiencies, effluent average nitrate, ammonium and TN violations and effluent quality index predicted by the BSM2Nb in open-loop and with the four control strategies (*CS1*, *CS2*, *CS3* and *CS4*).

BSM2Nb						
	units	**OL**	**CS1**	**CS2**	**CS3**	**CS4**
η_{TKN}	$\%\frac{g\ TKN_{rem}}{g\ TKN_{in}}$	91.716	95.7	95.9	95.5878	96.24
η_{TN}	$\%\frac{g\ TN_{rem}}{g\ TN_{in}}$	68.2194	67	66.73	67.2831	66.88
NO_3^-	$g\ N.m^{-3}$	11.51	14.18	14.52	14.08	14.61
V_{NH}	% of operating time	28.6344	4.6	2.44	0.11447	0.95
V_{TN}	% of operating time	23.9269	35.7	36.84	30.7606	34.63
EQI	kg pollutant.units.d^{-1}	6769.3554	6081.4237	6060.04	6069.0539	5979.07

Table 6.9: TKN and TN removal efficiencies, effluent average nitrate, ammonium and TN violations and effluent quality index predicted by the BSM2Nc in open-loop and with the four control strategies (*CS1*, *CS2*, *CS3* and *CS4*).

BSM2Nc						
	units	**OL**	**CS1**	**CS2**	**CS3**	**CS4**
η_{TKN}	$\%\frac{g\ TKN_{rem}}{g\ TKN_{in}}$	94.8057	96.8	97.14	96.9594	97
η_{TN}	$\%\frac{g\ TN_{rem}}{g\ TN_{in}}$	79.8498	74.32	73.63	76.1982	74.4
NO_3^-	$g\ N.\ m^{-3}$	7.2454	11.19	11.7	10.32	11.24
V_{NH}	% of operating time	24.9062	1.54	0.38	0.077266	0.44
V_{TN}	% of operating time	0.49794	1.45	2.05	1.2363	1.3
EQI	kg pollutant.units.d^{-1}	4930	5087	5089	2864.88	5042.86

6.4.3. Control performance on aeration energy consumptions

To evaluate the economic feasibility of the control strategies, the aeration energy consumptions are evaluated. Tables (6.10-6.12) show the average aeration energy consumed according to the predictions by the BSM2Na, BSM2Nb and BSM2Nc. As can be noted, *CS1* and *CS2* have led to a variable increment of the average aeration energy consumed according to all the three models. This was expected since more oxygen was needed to ensure higher NOB activity. However, as can be noted, the variation is only between 3 and 6 %. More in detail, given the better regulation of the oxygen supply, some aeration energy was managed to be saved by using the cascade configuration rather than the regulatory one. This is because k_La is manipulated the same with *CS1* in the first two aerobic tanks while is manipulated according to the amount of influent ammonium to the tanks with *CS2*. As can be noted from Figure 6.9, the oxygen supplied to the two aeration tank is lower when CS2 is used. This enables avoiding aeration energy wastes and leads to less energy consumptions.

The lower aeration energy consumptions by *CS3* indicate less oxygen supply, which caused higher AOB-mediated N_2O production according to the three models. However, this lower oxygen supply was found to be beneficial on the total N_2O emissions according to the BSM2Nb, because it allowed a higher HB-mediated N_2O consumption compared to the closed-loop configurations with CS1 and CS2.

Table 6.10: Average aeration energy consumptions according to the BSM2Na in open-loop and with the four control strategies (*CS1*, *CS2*, *CS3* and *CS4*).

BSM2Na						
	units	**OL**	**CS1**	**CS2**	**CS3**	**CS4**
AEC	kWh.d^{-1}	2877.3	3276.7	3133.6	2935.1	3172.6

Table 6.11: Average aeration energy consumptions according to the BSM2Nb in open-loop and with the four control strategies (*CS1*, *CS2*, *CS3* and *CS4*).

BSM2Nb						
	units	**OL**	**CS1**	**CS2**	**CS3**	**CS4**
AEC	$kWh.d^{-1}$	2978.896	3194.62	3068.3	2827.139	3129.95

Table 6.12: Average aeration energy consumptions according to the BSM2Nc in open-loop and with the four control strategies (*CS1*, *CS2*, *CS3* and *CS4*).

BSM2Nc						
	units	**OPEN LOOP**	**CS1**	**CS2**	**CS3**	**CS4**
AEC	$kWh.d^{-1}$	2940.2759	3209.53	3167.38	2930.2025	3134.72

6.5. Discussion

The novel controller for low N_2O emissions and low effluent ammonium concentration has shown its ability in drastically reducing the N_2O emissions through a better tracking of the set points fixed for R_{NatAmm}. This proves the concept according to which R_{NatAmm} is the true controlled variable to be used with the aim of mitigating the N_2O emissions. In fact, as the IAE and the ISE decreased, lower were the N_2O emissions achieved. The controllers on average increase the value of R_{NatAmm} so that all the TKN in the influent is converted into nitrate. The reduction of average amount of N_2O produced by AOB shows that AOB denitrification has been managed to be reduced through the formulated control concept. The fact that the emission factor calculated as the sum of the N_2O emitted per unit of TKN removed is a proof of the fact that N_2O emissions are not reduced by lowering the conversion of TKN, but by merely slowing down the N_2O production by the different processes. Furthermore, the control strategy showed its ability in reducing the N_2O even when sensors and actuator dynamics were included. Together with the fact that the N_2O emissions were able to be mitigated despite the different N_2O modelling approaches, this should encourage the application of the control strategy in real full-scale wastewater treatment plants where nitrifying microorganisms coexist.

With regard to the effluent quality, the conversion of TKN achieved through the novel controllers was higher, which in turn drastically decreased the number of violations of the effluent ammonium limits. However, a significant increase of the number of violations of the effluent total nitrogen was also observed. This was because, when a more complete nitrification is achieved, the COD demand for the complete reduction of nitrogen oxides into dinitrogen is higher. Hence, the controller for low N_2O emissions and effluent NH_4^+ has to be coupled with other control strategies ensuring a more complete HB denitrification through the addition of organic carbon and/or regulation of the internal recycle flow rate.

Since the way to achieve complete nitrification was to speed up NOB activity by increasing oxygen availability, aeration energy consumptions increased. However, a more efficient air supply would be able to limit this increase.

Compared then to the performances achieved through the cascade controller keeping low effluent NH_4^+, the results showed that, when AOB denitrification is the dominant pathway according to which N_2O is

produced, the novel controllers give a much more drastic reduction of N_2O emissions than the nominal cascade controller of low effluent NH_4^+. The slightly higher ammonium violations achieved with the novel controllers can be deemed in any case acceptable for future applications in WWTPs since they are very low. Furthermore, the novel control strategies achieve an overall higher TKN conversion compared to the default cascade controller for low effluent NH_4^+. If the dominant N_2O-producing pathway is the incomplete NH_2OH oxidation, slightly better is the performance of the NH_4^+ cascade controller. As a matter of fact, the N_2O emissions are slightly higher when the cascade novel control configuration is used. Furthermore, higher would be the operational costs due to aeration and the TN violations. These results indicate that, although the novel controller using R_{NatAmm} as additional controlled variable enables a drastic reduction of the N_2O emissions, the NH_4^+ cascade controller may result preferable for the sake of aeration energy demand and the effluent quality when the incomplete NH_2OH oxidation process is the main N_2O-producing pathway.

6.6. Conclusion

The work presented the development and testing of a novel control idea minimizing N_2O emissions while at the same time keeping low ammonium concentrations in full-scale continuously-aerated WWTPs. The strategy is based on the concept that accumulation of intermediates like nitrites has to be avoided in order to prevent N_2O production, and its consequent emission. In continuously-aerated WWT systems, this can be done by triggering the activity of nitrite-oxidizing bacteria (NOB), which are in charge of consuming the nitrites produced by ammonia-oxidizing bacteria in aerobic environments. Nitrite accumulation has been in fact found to trigger the production of N_2O from ammonia-oxidizing bacteria (AOB) denitrification, which has been identified as the main pathway for several WWTPs. The control strategy is designed to receive as measurement an indicator of the relationship between AOB and NOB. On the basis of this measured variable, the controller is able to infer the proper deviation of either the oxygen supply or the oxygen set point of a default oxygen controller.

In three different benchmark simulation environments the novel control strategies was found to enable achieving a drastic reduction of the total N_2O emissions despite the different modelling approaches. The control concept was able to successfully cope with the measurements and actuator dynamics imposed. It was also found that when AOB denitrification is the main N_2O-producing pathway the novel control approach performs largely better than a default control loop using only ammonium as controlled variable, while, when the incomplete NH_2OH oxidation pathway is the dominant N_2O producer, the mere use of ammonium as controlled variable enables the drastic reduction in N_2O emissions.

These preliminary results should suggest the implementation of the control strategy in full-scale WWTPs with the aim of drastically reducing their carbon footprint. However, there is a side effect of the controller which may lead to increase in the effluent total nitrogen and especially the nitrate concentrations. Therefore appropriate analysis and corresponding adaptations to plant operations – such as enhancing complete heterotrophic denitrification – are need.

CHAPTER 7
Development and testing of novel control strategies for complete heterotrophic denitrification

7.1. Introduction

As demonstrated in Chapter 6, at the aim of drastically reducing the emissions of nitrous oxide from continuously-aerated systems, complete nitrification needs to be accomplished. However, this requires among others increasing the amount of biodegradable COD under anoxic conditions to enable complete HB denitrification. This may need to be coped with in order to comply with the effluent requirements for nitrate and total nitrogen discharge limits. In this chapter, a novel control strategy adapting the COD demand of the system to achieve complete HB denitrification is developed and tested. The control strategy is a feedback fuzzy-logic based controller which uses the measured nitrate removal efficiency in an anoxic zone to infer the variation of the flow rate adding a concentrated solution of ethanol to the same anoxic zone. While accomplishing a complete HB denitrification in the anoxic zone, the accumulation of nitrite and the net production of N_2O in the anoxic zone are expected to get reduced. At the same time, excesses of organic carbon supply have to be avoided to contain operational costs due to the ethanol solution. As shown in Chapter 4, these excesses in a predenitrification configuration have in addition a negative effect on the activity of NOB in the aerobic zone, where the leftover carbon supplied subtracts oxygen to NOB by triggering the aerobic activity of HB.

The novel control strategy will be developed following the approach by Boiocchi *et al.* [73]. Once developed, it will be implemented and tested in the three benchmark simulation models developed as described in Chapter 3. Testing the controller in the three BSMs will allow a better overview of the controller effect on the total nitrous oxide emissions.

7.2. Development of the novel control strategy for complete HB denitrification

Following the methodology developed in Chapter 5, the main steps according to which the fuzzy-logic control strategy for complete HB denitrification is developed are:

I) Specification of the optimization problem,
II) Identification of the critical points for input variables,
III) Definition of the membership functions for input and output variables,
IV) Implementation of the linguistic rules linking input to output variables,
V) Setting of additional design parameters.

7.2.1. Specification of the optimization problem

Specification of the control objectives

The objectives needed to be achieved through the implementation of the controller consist of respecting the effluent TN violations within contained operational costs.

Control structure definition

The control strategy will attempt to minimize the violations of effluent total nitrogen by maximizing the measured nitrate removal efficiency ($\eta_{NO3,ANOX}$) in the anoxic zone. The flow rate for the external addition of a solution of ethanol (Q_S) will be used as manipulated variable, while the concentration of COD in the solution is assumed constant, equal to 400000 mg COD.L^{-1}. The control structure is defined in terms of disturbance, state, manipulated and controlled variables according to Eqns. (7.1-7.4).

$$\underline{d} = [NH_{4,in}^{+}, S_{S,in}, T_{in}, X_{S,in}, X_{P,in}, NO_{2,in}^{-}, NO_{3,in}^{-}, Q_{in}, NO_{in}, N_2O_{in}, N_{2,in}, X_{I,in}, S_{I,in}] \quad (7.1)$$

$$\underline{x} = [NH_4^{+}, S_S, T, X_S, X_P, NO_2^{-}, NO_3^{-}, NO, N_2O, N_2, X_I, S_I] \quad (7.2)$$

$$\underline{y} = \eta_{NO3} \quad (7.3)$$

$$\underline{u} = [Q_S] \quad (7.4)$$

The generic control implementation is showed in Figure 7.1.

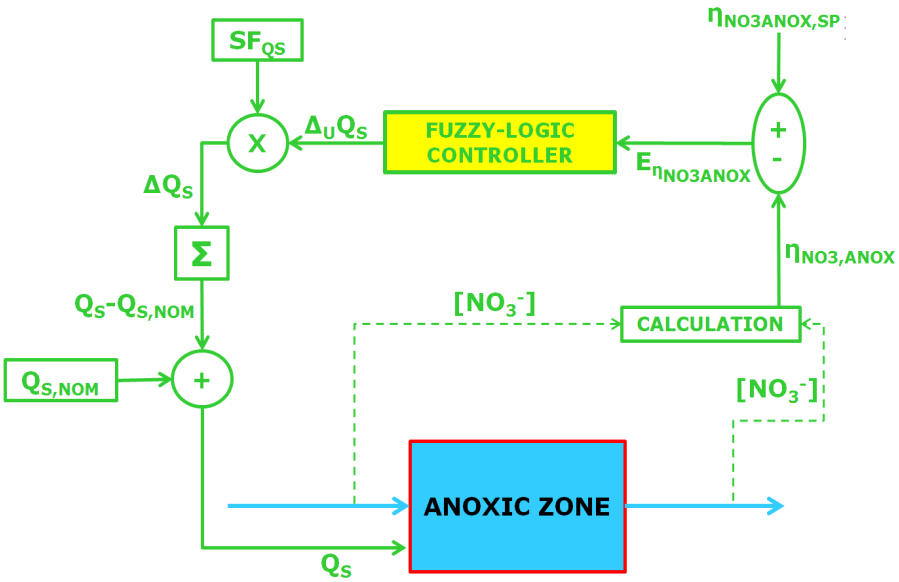

Figure 7.1: Implementation of the controller for complete HB denitrification in anoxic zone.

According to Figure 7.1, the measured nitrates in the inlet and outlet of the anoxic zone are used for the calculation of the anoxic nitrate removal efficiency, which subtracted from the set point, gives the input

($E_{\eta NO3ANOX}$) handed over to the fuzzy-logic controller as input variable. According to the linguistic rules implemented, the fuzzy-logic controller infers the unitary deviation of the flow rate for carbon addition ($\Delta_U Q_S$), which is in turn multiplied by a scaling factor (SF_{QS}) to get a physical dimension. The variation of Q_S (ΔQ_S) obtained is summed to the ones obtained at the previous time steps to obtain the overall variation between Q_S and the nominal value of Q_S ($Q_{S,NOM}$), which will be used to know the value of Q_S to be actuated to the biological anoxic system.

Definition of the physical constraints

With regard to the controlled variable, the maximum value which can be possibly obtained is equal to 100% while the minimum is 0%. All the disturbances and state variables have a lower limit of zero and a finite undefined upper limit. The manipulated variable, the Q_S, cannot be negative and has an upper limit depending on the context where the controller is implemented. In general, the upper limit has to be chosen in such a way that Q_S should not upset the hydraulics of the reactor.

Identification of the key scenarios leading the system away from the optimality

The indicators for the system optimality are here identified, according to the control objectives, in two variables: (a) the violations of the effluent total nitrogen limitations (V_{TN}), and (b) operational costs due to carbon addition (OC_{carb}). Table 7.1 screens the two possible scenarios leading the systems away from optimality.

Table 7.1: Key scenarios leading the system away from the optimality.

	V_{TN}	OC_{carb}
1	HIGH	LOW
2	LOW	HIGH

7.2.2. Identification of the critical points for the input variable

Although the actual input variable to the system is $E_{\eta NO3ANOX}$, for the sake of simplicity the membership functions will be first defined for $\eta_{NO3,ANOX}$ and subsequently translated to have the ones for $E_{\eta NO3ANOX}$. Consequently, here the critical points will be identified for $\eta_{NO3,ANOX}$. In this case, the value of the nitrate anoxic removal efficiency representing the optimality is arbitrarily chosen, i.e. 95%. However, oscillations of 0.5% around this value are considered to represent in any case the optimality. This allows filtering out measurement errors easily. Values of $\eta_{NO3,ANOX}$ equal to 100% are, on the contrary, considered to be avoided since these unrealistically high values require an extra amount of organic carbon to be fed in the system, which unnecessarily increases the operational costs. When the system is found to have such a value, the controller will have to infer the maximum negative control action (i.e. maximum decrease of Q_S). On the other side, values of $\eta_{NO3,ANOX}$ equal or lower than 92.5% are arbitrarily chosen to be highly avoided. In this case, the maximum positive control action (i.e. increase of Q_S) will have to be inferred.

Eqns. (7.5-7.8) summarize the identified critical points.

$$\text{UB for OPTIMAL SYSTEM OPERATION} \Rightarrow \underline{y}_{UB,OPT} = [95] \tag{7.5}$$

$$\text{LB for OPTIMAL SYSTEM OPERATION} \Rightarrow \begin{cases} \underline{y}^1_{LB,OPT} = [94.5] \\ \underline{y}^2_{LB,OPT} = [95.5] \end{cases} \tag{7.6}$$

$$\text{UB for WORST SYSTEM OPERATION} \Rightarrow \underline{y}_{UB,WORST} = [92.5] \tag{7.7}$$

$$\text{LB for OPTIMAL SYSTEM OPERATION} \Rightarrow \begin{cases} \underline{y}^1_{LB,WORST} = [0] \\ \underline{y}^2_{LB,WORST} = [100] \end{cases} \tag{7.8}$$

7.2.3. Definition of the membership functions for input and output variables

The following fuzzy sets were identified for $\eta_{NO3,ANOX}$:

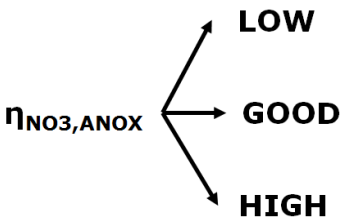

Trapezoidal shapes were adopted for the membership functions, for the same reasons given by Boiocchi *et al.* [73]. The critical points in Eqns. (7.9-7.12) will be assigned a degree of membership equal to 1 to the fuzzy sets they are related to. The same critical points will be assigned a degree of membership to the other fuzzy sets equal to 0.

$$\text{UB for OPTIMAL SYSTEM OPERATION} \Rightarrow y_{UB,OPT} = 95 \tag{7.9}$$

$$\text{LB for OPTIMAL SYSTEM OPERATION} \Rightarrow \begin{cases} y^1_{LB,OPT} = [94.5] \\ y^2_{LB,OPT} = [95.5] \end{cases} \tag{7.10}$$

$$\text{UB for WORST SYSTEM OPERATION} \Rightarrow \underline{y}_{UB,OPT} = [92.5] \tag{7.11}$$

$$\text{LB for OPTIMAL SYSTEM OPERATION} \Rightarrow \begin{cases} y^1_{LB,OPT} = [0] \\ y^2_{LB,OPT} = [100] \end{cases} \tag{7.12}$$

The membership functions represented in Figure 7.2 are thus defined for $\eta_{NO3,ANOX}$.

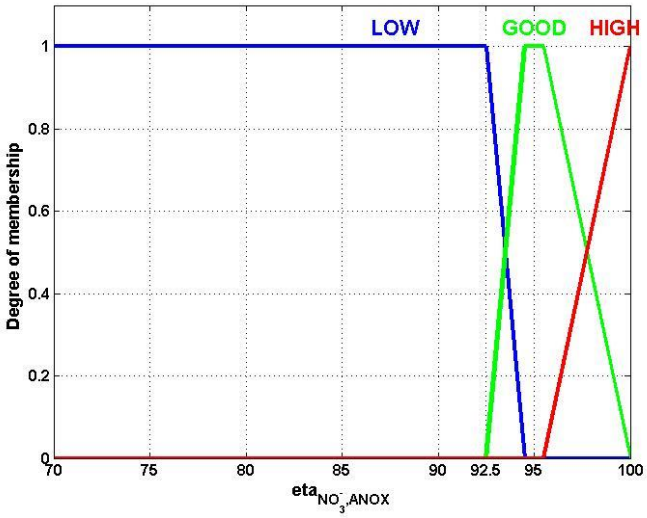

Figure 7.2: Membership functions for the removal efficiency of nitrate in the anoxic zone.

Similarly to what was done to obtain the MFs of $E_{RNatAmm}$ in Chapter 6, the membership functions in Figure 7.2 are translated to obtain the ones for $E_{\eta NO3ANOX}$. The membership functions depicted in Figure 7.3 were thus obtained.

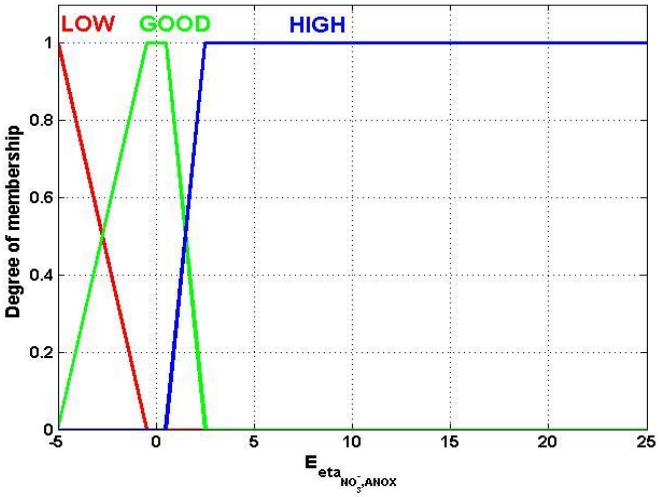

Figure 7.3: Membership functions for the error between set point and measured removal efficiency of nitrate in the anoxic zone.

With regard to the output variable $\Delta_U Q_S$, the membership functions in Figure 7.4 were defined, opting for the Center-of-Area as defuzzification method.

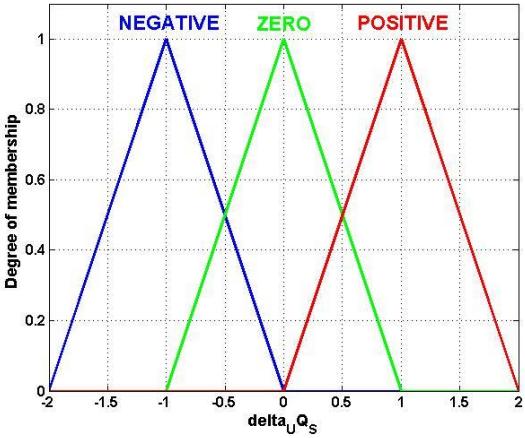

Figure 7.4: Membership functions for the unitary variation of the manipulated variable Q_S.

7.2.4. Implementation of the linguistic rules

To connect the input to the output variables, the following IF-THEN linguistic rules were used:

	IF	THEN
	$E_{\eta NO3ANOX}$	$\Delta_U Q_S$
1	LOW	NEGATIVE
2	GOOD	ZERO
3	HIGH	POSITIVE

7.2.5. Setting of additional design parameters

As for the implication and aggregation methods, correlation-min and disjunctive were, chosen respectively.

7.3. Implementation and testing of the control strategy

The designed controller such designed is implemented in the layout of the BSMs (i.e. BSM2Na, BSM2Nb and BSM2Nc) as shown in Figure 7.5.

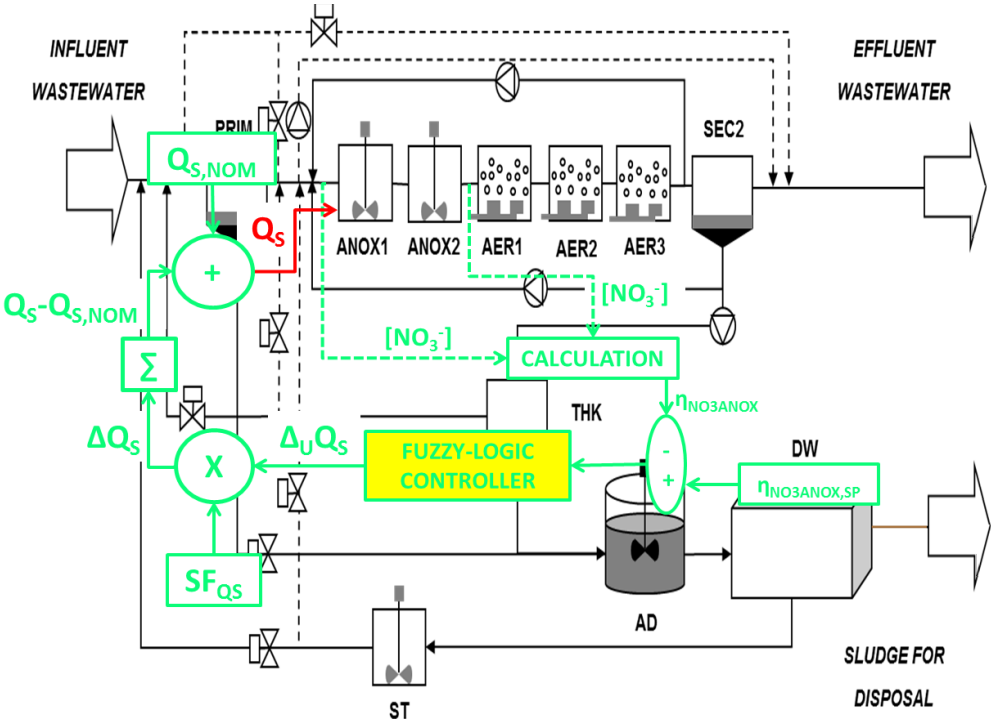

Figure 7.5: Implementation of the controller for high nitrate removal efficiency in the anoxic zone in the three benchmark simulation models.

The nominal value for Q_S used ($Q_{S,NOM}$) is taken equal to the one used in the default BSM2 by Jeppsson *et al.* [22], i.e. 2 $m^3.d^{-1}$. A saturation limit for the flow rate was taken equal to 10 $m^3.d^{-1}$, which can be considered not to disturb the hydraulics of the plant. On the basis of these two values, the scaling factor could be chosen between a value higher than 0 and lower than 8. A first attempt for the scaling factor (SF_{QS}) equal to 2 $m^3.d^{-1}$ was chosen to avoid aggressive behaviour of the controller, eventual waste of organic carbon and too much disturbance in the aerobic zone. In the real application, the value of this scaling factor could be increased once the behaviour of the controller is known.

The $\eta_{NO3,ANOX}$ controller is tested with different aeration control regimes of the three aerated tanks (AER1, AER2 and AER3):

- Constant oxygen mass transfer coefficients, equal to the ones found from the optimization Section 6.3 (k_La_{AER1}=156.1 d^{-1}, k_La_{AER2}=100.7 d^{-1}, and k_La_{AER3}= 55.7 d^{-1}) (*CS5*),
- R_{NatAmm} and $[NH_4^+]_{eff}$ regulatory controller developed in Chapter 6 (*CS6*),
- R_{NatAmm} and $[NH_4^+]_{eff}$ cascade controller developed in Chapter 6 (*CS7*),

In this way, not only the improvement achieved through the implementation of this controller is analysed in terms of effluent nitrogen, but also the impact of the controller on the N_2O emissions is evaluated. Furthermore, the interaction between the previously developed control strategy for low N_2O emissions and low effluent ammonium with the present one is thoroughly examined.

The parameters used for the evaluation will be all the ones calculated in Section 6.3 with the addition of:

- the average removal efficiency of nitrate in the anoxic zone,
- the Integral Absolute Error for $\eta_{NOX,ANOX}$ ($IAE_{\eta NOX,ANOX}$),
- the Integral Square Error for $\eta_{NOX,ANOX}$ ($ISE_{\eta NOX,ANOX}$),
- Total variation of QS (TV_{QS}),
- Average external carbon consumption (CC).

7.4. Results

The present section is structured in two different analyses: (a) impact of the novel controller on the effluent predictions (Subsection 7.4.1), and (b) impact of the novel controller on the total N_2O emitted (Subsection 7.4.2).

The present results can be fully understood by taking into account the results presented in Tables (6.4-6.12) presenting the evaluation of the corresponding configurations without the $\eta_{NOX,ANOX}$ controller (i.e. open-loop (*OL*), *CS1* and *CS2* control configurations). The values of $IAE_{\eta NO3}$, $ISE_{\eta NO3}$ and $\eta_{NO3,ANOX}$ for these three configurations according to the three models (BSM2Na, BSM2Nb and BSM2Nc) are presented in Tables (7.2-7.5) below.

Table 7.2: $IAE_{\eta NO3}$, $ISE_{\eta NO3}$ and $\eta_{NO3,ANOX}$ according to the BSM2Na.

BSM2Na				
	units	**OL**	**CS1**	**CS2**
$IAE_{\eta NO3}$	[-]	10996	16020	16348
$ISE_{\eta NO3}$	[-]	476190	771240	797510
$\eta_{NO3,ANOX}$	$\%\frac{g\,(NO_3^-)_{rem,ANOX}}{g\,(NO_3^-)_{in,ANOX}}$	64.9	51.11	50.21

Table 7.3: $IAE_{\eta NO3}$, $ISE_{\eta NO3}$ and $\eta_{NO3,ANOX}$ according to the BSM2Nb.

BSM2Nb				
	units	**OL**	**CS1**	**CS2**
$IAE_{\eta NO3}$	[-]	12621	15479	15961
$ISE_{\eta NO3}$	[-]	585220	739730	771180
$\eta_{NO3,ANOX}$	$\%\frac{g\,(NO_3^-)_{rem,ANOX}}{g\,(NO_3^-)_{in,ANOX}}$	60.4	52.6	51.3

Table 7.4: $IAE_{\eta NO3}$, $ISE_{\eta NO3}$ and $\eta_{NO3,ANOX}$ according to the BSM2Nc.

BSM2Nc				
	units	**OL**	**CS1**	**CS2**
$IAE_{\eta NO3}$	[-]	5123.3	7977.2	8837
$ISE_{\eta NO3}$	[-]	179900	264070	305540
$\eta_{NO3,ANOX}$	$\% \frac{g\,(NO_3^-)_{rem,ANOX}}{g\,(NO_3^-)_{in,ANOX}}$	83.44	73.3	70.86

7.4.1. Impact of the controller on the effluent quality

Tables (7.5-7.7) show the results in terms of $IAE_{\eta NO3}$, $ISE_{\eta NO3}$, TV_{Qs}, CC, V_{TN}, η_{TN}, V_{TKN}, η_{TKN}, NO_3^-, $\eta_{NO3,ANOX}$, CC, and EQI according to the BSM2Na, BSM2Nb and BSM2Nc.

As can be noted, in all the three models the novel controller for high nitrate removal efficiency in the anoxic zone has shown its capability in tracking the set point. The controller is able in all the cases to improve the nitrate removal efficiency and thus reduce the flow-weighted average effluent nitrate concentrations. This occurs not only when *CS5* is used, but also when *CS6* and *CS7* are implemented. In these two last configurations, the carbon consumptions (*CC*) are much higher since in these cases oxygen supply was regulated to achieve complete nitrification, which increases oxygen demand by heterotrophic denitrifiers. This demonstrates the controller is able to adapt to the increase of the influent nitrate. Figure 7.6 shows how the controller is able to cope with temperature fluctuations. As can be noted, the controller keeps the nitrate removal efficiency around the constant set point value by increasing the carbon solution flow rate more during winter time when HB are disfavoured.

Interestingly, the controller tracks better the set point for $\eta_{NO3,ANOX}$ and it achieves slightly higher anoxic removal efficiency when the controllers for low N_2O and effluent ammonium are implemented. This can be explained by the fact that the controllers used in the aerobic zone (*CS6* and *CS7*) limit the oxygen concentration of the last aerobic zone between 0.5 and 1 mg (-COD).L^{-1}. Thus the carbon added is more effective on HB denitrification because it is more consumed anoxically, while a fraction of carbon added in the models implemented with *CS5* is consumed aerobically and does not immediately trigger HB denitrification. The fact that TV_{Qs} is higher according to the models implemented with *CS5* than with *CS6* and *CS7* confirms that *CS5* has to overcome the higher oxygen concentration coming from the aerobic zone while *CS6* and *CS7* do not have to.

Despite the slightly higher removal efficiency of nitrate in the anoxic zone, the concentration of nitrate in the effluent is higher when *CS6* and *CS7* are implemented. This is because the system used is in a predenitrification configuration, where the effluent nitrate concentration is roughly given by sum of nitrate leaving the anoxic zone and the one produced in the aerobic zone, while in postdenitrification configurations the amount of nitrate in the effluent is roughly the same as the amount of nitrate leaving the anoxic zone. In the case at issue, *CS6* and *CS7* include control actions to have complete nitrification, which in turn increases the amount of nitrate produced in the aerobic zone.

As a drawback of the present control strategy on the effluent quality, the AOB activity is slowed down. This can be clearly seen by comparing the TKN removal efficiency and the frequency of violations of effluent ammonium of *CS5*, *CS6* and *CS7* against open-loop, *CS1* and *CS2*, respectively. Such is the result of the higher amount of organic carbon fed from the last anoxic zone into the first aerobic tank (see Figure 7.7), which triggers oxygen consumption by HB and thus slows down the activity of the autotrophic biomass. This difference is more notable by comparing the results with *CS5* against the ones obtained in open-loop, than by comparing the results with *CS6* and *CS7* against the ones obtained with *CS1* and *CS2*, respectively. This is because the controllers used in the aerobic zone enable - to a certain extent - coping with the lack of oxygen availability for the autotrophic biomass while the constant oxygen supply in *CS5* cannot. As a result of this, the effluent quality index is higher in *CS5* than in open-loop while it decreases with *CS6* and *CS7* compared to *CS1* and *CS2* respectively.

Table 7.5: IAE and ISE for η_{NO3}, TV for Qs, average carbon consumption, violations of effluent ammonium and total nitrogen, TKN and TN removal efficiency, flow-weighted average of effluent nitrate concentration, average η_{NO3} and EQI according to the BSM2Na with *CS5*, *CS6* and *CS7*.

BSM2Na				
	units	**CS5**	**CS6**	**CS7**
$IAE_{\eta NO3}$	[-]	1522	947.7	861.03
$ISE_{\eta NO3}$	[-]	13099	4358	3341.4
TV_{Qs}	[d^{-1}]	4.65	3.7	3.51
CC	[kg COD.d^{-1}]	5526.43	8986.14	9148.06
V_{NH}	% of operating time	24.6	3.51	0.92
V_{TN}	% of operating time	0.5	1.02	1.18
Average η_{TKN}	$\%\frac{\text{g TKN}_{\text{rem}}}{\text{g TKN}_{\text{in}}}$	91.75	94.76	94.88
Average η_{TN}	$\%\frac{\text{g TN}_{\text{rem}}}{\text{g TN}_{\text{in}}}$	80.85	77.82	77.53
Average NO_3^-	g N.m^{-3}	5.3	8.42	8.42
Average $\eta_{NO3,ANOX}$	$\%\frac{\text{g } (NO_3^-)_{\text{rem,ANOX}}}{\text{g } (NO_3^-)_{\text{in,ANOX}}}$	94.2	95.15	95.15
EQI	[kg poll.units.d^{-1}]	5641.1	5659.91	5698.54

Table 7.6: IAE and ISE for η_{NO3}, TV for Qs, average carbon consumption, violations of effluent ammonium and total nitrogen, TKN and TN removal efficiency, flow-weighted average of effluent nitrate concentration, average η_{NO3} and EQI according to the BSM2Nb with *CS5*, *CS6* and *CS7*.

BSM2Nb				
	units	**CS5**	**CS6**	**CS7**
$IAE_{\eta NO3}$	[-]	1489.5	1078	884.21
$ISE_{\eta NO3}$	[-]	12971	5402	3374.6
TV_{Qs}	[d^{-1}]	4.5	4.1	3.63
CC	[kg COD.d^{-1}]	2084.23	9034.89	8961.95
V_{NH}	% of operating time	65.5	9.3	3.2
V_{TN}	% of operating time	4.96	1.4	1.12
Average η_{TKN}	$\%\frac{g\ TKN_{rem}}{g\ TKN_{in}}$	85.4	93.52	94.3
Average η_{TN}	$\%\frac{g\ TN_{rem}}{g\ TN_{in}}$	72.8	76.6	77.03
Average NO_3^-	$g\ N.m^{-3}$	6.08	8.43	8.57
Average $\eta_{NO3,ANOX}$	$\%\frac{g\ (NO_3^-)_{rem,ANOX}}{g\ (NO_3^-)_{in,ANOX}}$	94.31	95.04	95.3
EQI	[kg poll.units.d^{-1}]	7749.8	6075.65	5862.9

Table 7.7: IAE and ISE for η_{NO3}, TV for Qs, average carbon consumption, violations of effluent ammonium and total nitrogen, TKN and TN removal efficiency, flow-weighted average of effluent nitrate concentration, average η_{NO3} and EQI according to the BSM2Nc with *CS5*, *CS6* and *CS7*.

BSM2Nc				
	units	**CS5**	**CS6**	**CS7**
$IAE_{\eta NO3}$	[-]	2296.8	1077.8	1023.1
$ISE_{\eta NO3}$	[-]	37483	7029.7	6071
TV_{Qs}	[d^{-1}]	5.04	3.72	3.63
CC	[kg COD.d^{-1}]	3311.4	5534.74	5645.86

V_{NH}	% of operating time	13.73	1.41	0.32
V_{TN}	% of operating time	0.186	0.3	0.35
Average η_{TKN}	$\%\frac{g\ TKN_{rem}}{g\ TKN_{in}}$	94	96.7	96.9
Average η_{TN}	$\%\frac{g\ TN_{rem}}{g\ TN_{in}}$	81.34	78.6	78.54
Average NO_3^-	$g\ N.m^{-3}$	6.1	9	9.13
Average $\eta_{NO3,ANOX}$	$\%\frac{g\ (NO_3^-)_{rem,ANOX}}{g\ (NO_3^-)_{in,ANOX}}$	92.36	94.82	94.9
EQI	[kg poll.units.d^{-1}]	4969.54	4751.55	4727.82

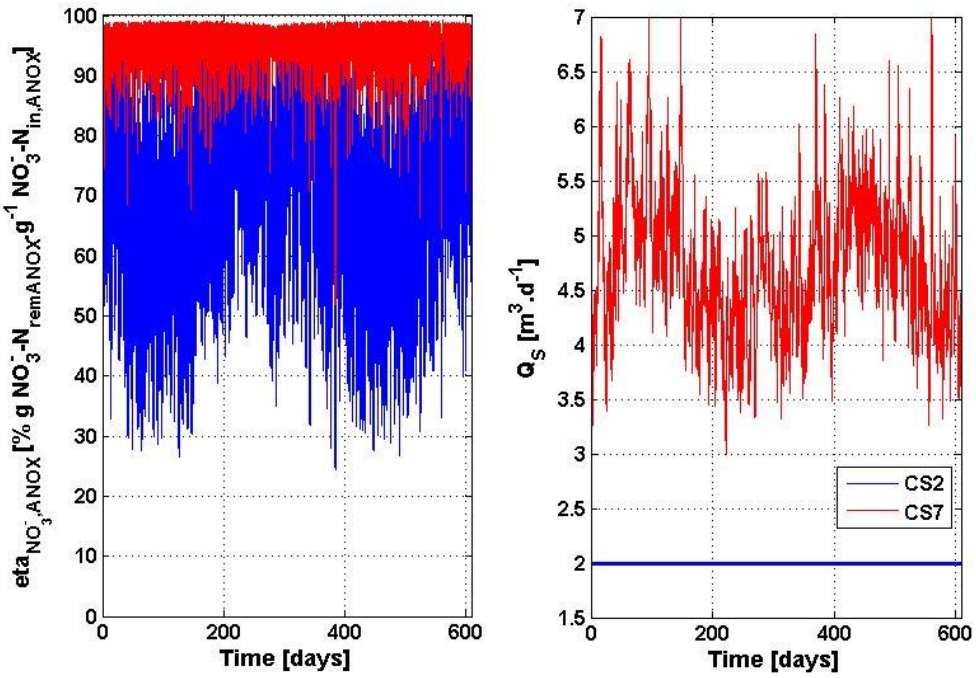

Figure 7.6: **(a)** anoxic removal efficiency of nitrate and **(b)** flow of the external carbon addition according to the BSM2Nc with *CS2* and *CS7*.

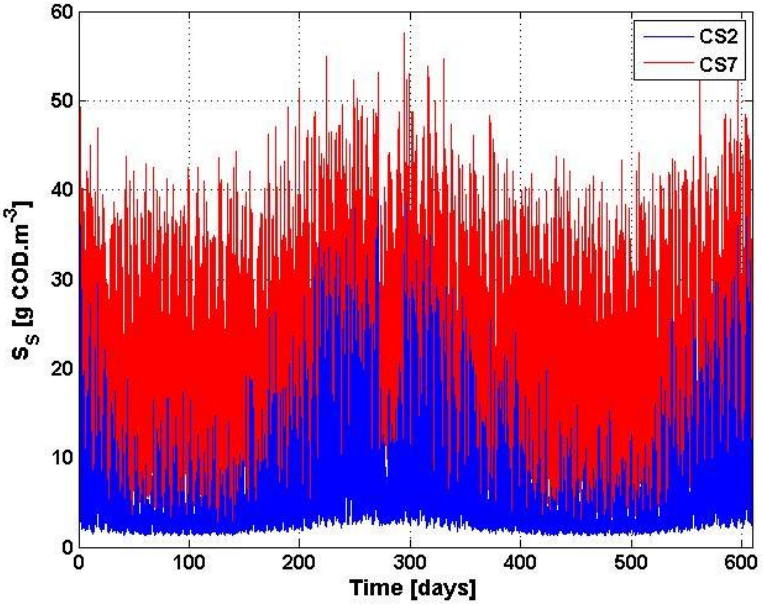

Figure 7.7: Readily-biodegradable organic carbon (S_S) concentration fed to the aerobic zone according to the BSM2Nc with *CS2* and *CS7*.

7.4.2. Impact of the controller on the total N_2O emissions

Tables (7.8-7.10) show the average R_{NatAmm}, $IAE_{RNatAmm}$, $ISE_{RNatAmm}$, TV_{kLa}, N_2O_{ef1}, N_2O_{ef2}, the average N_2O produced according to the different pathways and the average aeration energy consumptions according to the three benchmark simulation models described in Chapter 3.

As can be noted, the controllers developed in Chapter 6 are able to adapt to the different amount of organic carbon entering the aerobic zone by accomplishing average values of R_{NatAmm} with *CS6* and *CS7* similar to the ones accomplished with *CS1* and *CS2*, respectively. However, the higher values of the integral absolute and the integral square errors indicate that the tracking of the set point was worse when organic carbon was externally added. Furthermore, when the oxygen supply is not regulated but constant (*CS5*), the introduction of the carbon-addition controller worsens the ratio R_{NatAmm}. This indicates that the higher amount of organic carbon entering the aerobic zone unbalances the relationship between AOB and NOB activity. Since the average R_{NatAmm} is lower with *CS5* than in open-loop, it can be deduced that NOB activity is more disfavoured by higher organic carbon availability than AOB activity, and this is valid for all the three models. Although a decrease in the amount of nitrous oxide fed to the aerobic zone is achieved through the implementation of the $\eta_{NO3,ANOX}$ controller (see Figure 7.8), without regulation of the oxygen supply, the implementation of the $\eta_{NO3,ANOX}$ controller increases the total amount of N_2O emitted according to all the three benchmark simulation models, which confirms the fact that N_2O emissions are mainly due to imbalance between AOB and NOB, while only marginal contributions come from HB denitrification in the anoxic zone.

When the oxygen supply is regulated in the aerobic zone, much lower N_2O emission factors are achieved according to the three models. More specifically, according to the BSM2Nb and the BSM2Nc the N_2O emissions achieved are lower than the respective cases which do not regulate the addition of external carbon (i.e. CS6 and CS7 compared to CS1 and CS2 respectively). This demonstrates the following: (a) the controllers developed in Chapter 6 are able to arrange the aeration regime to cope with the imbalance between NOB and AOB created by the extra carbon carried to the aerobic zone; and (b) the N_2O net production by HB in the anoxic zone has been drastically reduced, compared to the case when there was not external carbon regulation. Nevertheless, according to the BSM2Na the controllers for low N_2O emissions are not as able as according to the other two models to cope with the increased amount of carbon fed in the aerobic zone. In any case the N_2O emission factors are quite low also according to this model with *CS6* and *CS7*.
As expected, the aeration energy consumptions increase drastically in CS6 and CS7 compared to CS1 and CS2 because more oxygen is needed to keep the desired balance between AOB and NOB.

Table 7.8: Average R_{NatAmm}, IAE and ISE for R_{NatAmm}, TV for k_La, N_2O emission factors, average N_2O produced by HB and AOB, average aeration energy consumptions according to the BSM2Na with *CS5*, *CS6* and *CS7*.

BSM2Na				
	units	**CS5**	**CS6**	**CS7**
Average R_{NatAmm}	$\frac{g\ NO_3^- - N}{g\ NH_4^+ - N}$	0.85	1.314	1.34
$IAE_{RNatAmm}$	[-]	209.12	147.96	146.45
$ISE_{RNatAmm}$	[-]	164.17	96.66	93.3
TV_{kLa}	[d^{-1}]	0	2018.4	2794.3
N_2O_{ef1}	$\%\ \frac{g\ N_2O - N_{gas}}{g\ TKN - N_{in}}$	0.404	0.084	0.056
N_2O_{ef2}	$\%\ \frac{g\ N_2O - N_{gas}}{g\ TKN - N_{rem}}$	0.44	0.09	0.06
Average N_2O produced by HB	$\frac{g\ N_2O - N_{liq}}{d}$	-82.05	-508.75	-681.3
Average N_2O produced from AOB denitrification	$\frac{g\ N_2O - N_{liq}}{d}$	4308.1	1379.6	1259.6
AEC	[$kWh.d^{-1}$]	3126.1	3571.87	3455.14

Table 7.9: Average R_{NatAmm}, IAE and ISE for R_{NatAmm}, TV for k_La, N_2O emission factors, average N_2O produced by HB and AOB, average aeration energy consumptions according to the BSM2Nb with *CS5*, *CS6* and *CS7*.

BSM2Nb				
	units	**CS5**	**CS6**	**CS7**
R_{NatAmm}	$\frac{g\ NO_3^- - N}{g\ NH_4^+ - N}$	1	1.363	1.38
$IAE_{RNatAmm}$	[-]	164.2	161.45	155.83
$ISE_{RNatAmm}$	[-]	106.05	115.3	105.4
TV_{kLa}	[d^{-1}]	0	2225.3	2579.4
N_2O_{ef1}	$\%\ \frac{g\ N_2O - N_{gas}}{g\ TKN - N_{in}}$	0.087	0.021	0.0153
N_2O_{ef2}	$\%\ \frac{g\ N_2O - N_{gas}}{g\ TKN - N_{rem}}$	0.102	0.0224	0.0162
Average N_2O produced by HB	$\frac{g\ N_2O - N_{liq}}{d}$	-2564.3	-848.96	-767.91
Average N_2O produced from AOB denitrification	$\frac{g\ N_2O - N_{liq}}{d}$	127.4	12.54	5.62
Average N_2O produced from inc. NH_2OH oxidation	$\frac{g\ N_2O - N_{liq}}{d}$	3384	1047.6	920.2
AEC	[$kwh.d^{-1}$]	3384	3400.32	3369.2

Table 7.10: Average R_{NatAmm}, IAE and ISE for R_{NatAmm}, TV for k_La, N_2O emission factors, average N_2O produced by HB and AOB, average aeration energy consumptions according to the BSM2Nc with *CS5*, *CS6* and *CS7*.

BSM2Nc				
	units	**CS5**	**CS6**	**CS7**
R_{NatAmm}	$\frac{g\ NO_3^- - N}{g\ NH_4^+ - N}$	0.86	1.22	1.23
$IAE_{RNatAmm}$	[-]	190.54	117.2	116.4
$ISE_{RNatAmm}$	[-]	138.8	56.24	55.24
TV_{kLa}	[d^{-1}]	0	1772.7	2658
AEC	[$kWh.d^{-1}$]	2988.6	3510.84	3427

N_2O_{ef1}	$\% \frac{g\ N_2O - N_{gas}}{g\ TKN - N_{in}}$	0.41	0.052	0.04
N_2O_{ef2}	$\% \frac{g\ N_2O - N_{gas}}{g\ TKN - N_{rem}}$	0.44	0.054	0.0412
Average N_2O produced by HB	$\frac{g\ N_2O - N_{liq}}{d}$	-74947	-13449	-14862
Average N_2O produced by AOB	$\frac{g\ N_2O - N_{liq}}{d}$	73981	14031	13306

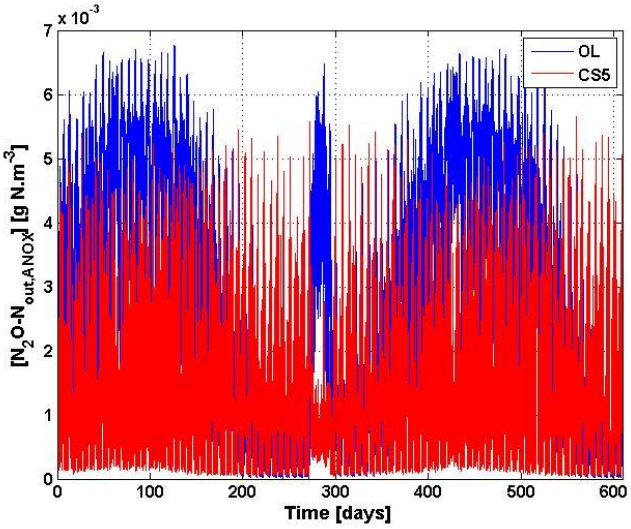

Figure 7.8: Nitrous oxide effluent from the anoxic zone according to the BSM2Nc in open-loop and with *CS5*.

7.5. Discussion

The novel controller for high nitrate removal efficiency in an anoxic zone has showed its capability in reducing drastically the effluent nitrate concentration of WWTPs. However, the strategy of enhancing the removal efficiency by adding an external solution concentrated in carbon has shown to be somewhat controversial in predenitrification configurations linked to oxygen competitions between heterotrophic and autotrophic biomass. More specifically, the higher amount of organic carbon in the anoxic zone, needed to trigger HB denitrification, is carried in the aerobic zone, where it is able to subtract oxygen from AOB and NOB. As a consequence, a higher concentration of ammonium has been found to leave the plant. In addition, the amount of nitrous oxide emitted is triggered because the activity of NOB is more disfavoured on oxygen than the activity of AOB. Regulations of oxygen supply in the aerobic zone are always to be incorporated at the aim of ensuring not only low effluent nitrate concentrations but also low ammonium concentrations and low N_2O emissions. The controllers of Chapter 6 coupled

with this new control strategy have clearly demonstrated their adaptability to different carbon additions, which adds value to the control idea of reducing the N_2O emissions by measuring the ratio R_{NatAmm}. Plants with a ratio between influent biodegradable COD and influent Total Kjeldahl Nitrogen different from the one studied can be deemed to be suitable for N_2O emission mitigation through the control strategy proposed in Chapter 6. However, with regard to the approach of regulating HB denitrification in the anoxic zone by addition of organic carbon, some reservations occur because, to work out the competition among the microbial group for oxygen, much higher aeration costs are due.

7.6. Conclusion

During the present work, a control strategy for high nitrate removal efficiency in an anoxic zone of a wastewater treatment plant was systematically designed and tested. The controller aimed at minimizing the violations of effluent total nitrogen within contained operating costs by adding a concentrated solution of ethanol. Thus a more complete HB denitrification, where all the incoming autotrophically-produced nitrogen oxides are converted into dinitrogen, is accomplished. The controller, benchmarked on three different models, showed its capability in tracking the given set point and thus reducing the effluent nitrate concentration and effluent total nitrogen violations. However, for predenitrification configurations, a distinct disturb of the autotrophic biomass activity is observed. More specifically, the higher amount of organic carbon leaving the anoxic zone, needed to achieve a faster HB denitrification, removes oxygen from AOB and NOB. Higher effluent ammonium concentrations and N_2O emissions are recorded when the nitrate removal controller is implemented. In this case, a regulation of the aeration regime is due. At this purpose, simulation results have shown that the controller developed in Chapter 6 is able to work out the oxygen competition among the different microbial communities. However, this comes at expenses of higher operational costs.

CHAPTER 8
Conclusions and future work

Conclusions

The present work has been carried out with the intent of developing on-line control strategies to minimize N_2O emissions in continuously-aerated wastewater treatment plants. To obtain a virtual simulation platform where the control strategies could be developed and tested, three benchmark simulation models (the BSM2Na, the BSM2Nb and the BSM2Nc) incorporating N_2O dynamics have been developed. These models describe the N_2O dynamics according to different assumptions and parameter choices. Due to this, it has been demonstrated that the amount and the dynamics of N_2O emissions differ quite a lot from one model to another. This finding has been exploited for a better testing of the N_2O-minimizing controllers developed afterwards. As a matter of fact, benchmarking controllers on models which predict differently the N_2O productions gives the chance to test the generic rules of the controller performance in reducing the N_2O emissions. It is important to note that up to now there is no consensus model which is accepted as the model describing comprehensively all possible mechanisms leading to the N_2O emissions from wastewater treatment plants.
Afterwards, at the aim of studying full-scale dynamics of N_2O emissions in a plant-wide context, sensitivity analyses on one of the three different benchmark simulation models (the BSM2Na) were carried out. NOB activity was found to be one of the key processes determining not only the total N_2O emissions but also the TN removal efficiency and the operational costs linked to aeration. More specifically, it was found that enhancing NOB activity by increasing oxygen availability can reduce the total N_2O emissions in all three different models representing different possible WWPTs. However, the same strategy has a side effect, namely it increases the COD demand by facultative heterotrophs for the complete reduction of autotrophically-produced nitrogen oxides into dinitrogen. This in turn leads to a decrease in the overall total nitrogen removal efficiency if organic biodegradable carbon is not sufficiently present. It was also found that a high concentration of oxygen in the mixed liquor carried to the anoxic zone can prevent a complete HB denitrification and increase, in predenitrification configurations, the amount of organic biodegradable carbon influent to the aerobic zone. This enhances the oxygen consumptions by HB and thus slows down NOB activity. A larger amount of oxygen has also been found to increase the operating costs linked to aeration. The sensitivity analysis results are subsequently used to develop a control strategy mitigating the total N_2O emissions from full-scale continuously-aerated wastewater treatment plants. Since the controller is applied and is supposed to deal with the complexity of biological systems, fuzzy-logic approach has been adopted as a reference control technology. However, prior to developing such a control strategy, a systematic methodology for the definition of membership functions of such fuzzy-logic controllers was developed. For this aim, a first-attempt fuzzy-logic controller for high total nitrogen removal in single-stage partial nitritation/Anammox was finely tuned according to a systematic procedure. The finely-tuned control strategy was tested in both lab-scale sequencing-batch and full-scale configuration. The latter came from a fourth benchmark simulation model, built up by including a one-stage partial nitritiation/Anammox (PN/A) treatment reactor in the side-stream of the BSM2Na.

The methodology used to develop systematically the control strategy for the PN/A reactor is later generalized to a plantwide context. The same approach is thus able to be exploited for the design of

control strategy for low N_2O emissions. The control strategy uses the measurements of ammonium and nitrate concentrations in and out of the aerated zone of a wastewater treatment plant to calculate a ratio (R_{NatAmm}) indicating whether nitrification is complete or not. This is because it is the accumulation of nitrification intermediates like nitrites and hydroxylamines to trigger N_2O-producing processes. In case nitrification is not fully completed, the controller acts to increase the oxygen availability by manipulating directly either the oxygen mass transfer coefficient or the oxygen set point in a cascade configuration. The same ratio is also used to detect excessive oxygen availability, which increases unnecessarily the aeration costs without reducing further the N_2O emissions. A control loop avoiding concentrations of oxygen higher than 1 mg (-COD).L^{-1} in the stream carried to the anoxic zone is used to avoid oxygen inhibition on HB-mediated nitrogen oxide reduction. The control strategy incorporates also control actions to ensure a high oxidation rate of influent ammonium, thus respecting effluent ammonium law limits. Such a control strategy has been tested on the three different benchmark simulation models developed (the BSM2Na, the BSM2Nb and the BSM2Nc). More specifically, the capability of the controller in reducing the N_2O emissions compared to a reference scenario is globally evaluated along with effluent quality parameters and operating costs connected to aeration. The control strategy showed its capability in reducing drastically the N_2O emissions while keeping a good ammonium conversion, despite the different modelling assumptions. The robustness of the control strategy against sensor and actuator noises has also been proven, although a higher aggressive behaviour of the control strategy is detected. The performance of the novel control strategy was also tested against a control strategy typically used to keep low effluent ammonium concentrations. It was found that, although this last is able to reduce the N_2O emissions, when AOB denitrification is the main N_2O producing pathway, the novel control strategy using R_{NatAmm} as additional controlled variable enables achieving much more drastic reduction of the total emissions. However, if the incomplete-hydroxylamine-oxidation pathway is the main N_2O producer, using R_{NatAmm} as additional controlled variable has not shown any advantage. In any case, the novel control strategy has shown its ability in drastically reducing the N_2O produced according to AOB denitrification. Comparing oxygen set point manipulation against oxygen mass transfer coefficient manipulation strategies, the former reduces more drastically N_2O emissions since the oxygen supply is changed more in phase with the influent ammonium concentration compared to the case when the latter is used. However, the aggressiveness of the cascade controller configuration is stronger than the regulatory control configuration. As expected, the overall total nitrogen removal efficiency when such a control idea is implemented drops consistently. To cope with this, a fuzzy-logic control strategy regulating the COD supply on the basis of the nitrate removal efficiency in the anoxic zone is proposed. Similar to before, this fuzzy logic strategy for enhancing denitrification in the anoxic zone was tested on the three benchmark simulation models. It was found that the addition of organic biodegradable carbon in predenitrification configurations, although capable of achieving complete HB denitrification and thus the nitrate removal efficiency, it can impact the conversion of ammonium in the aerobic zone and worsen the ratio between NOB and AOB activity, thus enhancing AOB denitrification and consequently N_2O emissions. However, the N_2O control strategy for the aerobic compartment has shown its capability in rejecting this disturbances caused by the anoxic zone control strategy through increase of the amount of oxygen supplied. The combined result of having fuzzy-logic control for anoxic zone and fuzzy-logic control for the aerobic zone, as expected, was a higher aggressiveness of controller actions and higher aeration costs. In postdenitrification systems this combined control strategy may increase the effluent COD and BOD concentrations. Whether or not a fuzzy logic control for complete denitrification is needed, it will be plant specific and, in particular, it will depend a lot on COD/N ratio in the anoxic denitrification zones. The simulation results suggest therefore that the control strategy regulating the carbon addition should

be used only in combination with other control strategies regulating the oxygenation regime in the aerated compartment to overcome the increase amount of influent organic carbon. Other strategies should also be considered for the regulation of the COD demand like the manipulation of the internal recycle flow rate, or anoxic reaction time in periodic/cyclic aerated plants.

Summarizing, the following milestones were achieved:

- Three different benchmark simulation models, incorporating different N_2O dynamics: the BSM2Na, the BSM2Nb and BSM2Nc;
- A benchmark simulation model (the BSM2NaPlusCANR) incorporating a side-stream single-stage partial nitritation/Anammox treatment unit;
- plant-wide insights regarding total N_2O emissions, total nitrogen removal efficiency and operating costs linked to aeration are achieved through sensitivity analyses on the BSM2Na;
- NOB activity has been found as the key process determining N_2O emissions and the total nitrogen removal efficiency and the economical trade-off of the a predenitrification WWTP under oxygen-limited conditions;
- A novel control strategy for low N_2O emissions and low effluent NH_4^+ concentration was developed and tested in multiple simulation environments (patented technology);
- A novel control strategy for high removal efficiency of nitrate in the anoxic zone was developed and tested in multiple simulation environments.

Future work

As future work, sensitivity analyses on the BSM2Nb and the BSM2Nc could be performed at the aim of achieving more insight on the N_2O production and emission dynamics and eventually design control strategies specifically for the minimization of N_2O production according to the incomplete-hydroxylamine-oxidation pathway. This is because the sensitivity analysis performed during the present work could enable building up the control idea to slow down AOB denitrification and it is therefore more effective in reducing N_2O emissions in those plants where AOB denitrification is the main N_2O-production pathway. As demonstrated, the control strategy is not as effective for the minimization of N_2O production from the other AOB-mediated pathway. However, in literature some observations regarding the activation of this pathway have already been given. More specifically, Peng *et al.* [19] found that the pathway starts giving significant contribution to the total N_2O emissions when oxygen is increased up to 3 mg (-COD).L^{-1}. However, even at such a high oxygen concentration AOB denitrification would be the main N_2O production pathway. Similarly, according to Pocquet *et al.* [38] the incomplete NH_2OH oxidation pathway has only a small contributing effect on the total N_2O emissions, effect which increases with oxygen concentration. It is here important to point out that these observations have been performed in lab-scale experiments where no heterotrophic biomass was present. The achieved results suggest that an interaction between this pathway and HB denitrification occurs. More specifically, in integrated systems like the biological mainstream zone of a full-scale wastewater treatment plant where heterotrophic and autotrophic biomass coexist, the nitric oxide produced by heterotrophic denitrifiers can be used by AOB to produce N_2O with the accumulated NH_2OH as electron donor. This kind of interaction is not taken into account in lab experiments where heterotrophic biomass is generally washed out in order to isolate autotrophic biomass. Given the results, it becomes more and more important to calibrate models according to full-scale measurements rather than according to lab-scale experiences, as already pointed out in Snip *et al.* [99].

With regard to the insights achieved regarding the TN removal efficiency and the operating costs linked to aeration, the sensitivity analysis performed on the BSM2Na could be considered enough.

With regard to the BSM2NaPlusCANR, the N_2O-producing processes should be incorporated in the model for single-stage PN/A treatment at the aim of having a global description of the N_2O. This way, control strategies minimizing N_2O emissions both in the mainstream and in the side-stream would be able to be benchmarked. For the mitigation of N_2O emitted from the side-stream, the control strategy by Boiocchi *et al.* [73] could be valid since it designed to avoid accumulation of nitrites by balancing between the AOB and the AnAOB activities. However, it is still unknown whether AOB denitrification will be the main N_2O production pathway in such a system since the high presence of AnAOB, consuming nitrites as electron acceptors, should slow down this process. At the same time, the very low oxygen concentrations typical of single-state PN/A systems should not promote the incomple-NH_2OH-pathway, found to be triggered by very high oxygen concentrations [19].

With regard to the control for N_2O emission minimization, the simulation results achieved should encourage WWTP managers to try out the developed control strategy, because drastic reductions in N_2O emissions have been demonstrated to be achieved only by changing aeration regime which does not require additional capital investments. On the basis of the fact that the cascade controller gives better performance thanks to a better tracking of the influent ammonium dynamics, a feedforward element could be added to the present control actions. More specifically, it could be a valid idea to use the developed feedback controller to update the optimal ratio between oxygen supply and influent ammonium of a feedforward controller which would then infer the oxygen supply to the aerated zone. This way an even better tracking of the influent ammonium dynamics would be achieved, compared to the cascade controller.

As for the control actions to respect the COD demand by heterotrophic denitrifiers at the aim of respecting the effluent limitations of nitrate and total nitrogen concentrations, manipulated variables other than the flow rate for the addition of organic carbon should be considered. As a matter of fact, in Chapter 7 it was clearly shown how the addition of external carbon can somehow compromise and unbalance the autotrophic biomass, increasing thereby the effluent ammonium concentrations and the total N_2O emissions. Higher aeration energy consumptions are due in order to overcome these challenges. Overall, this increases considerably the operating costs.

Improvements of the BSM evaluation criteria could also be considered. More specifically, an overall performance index should be studied and developed to understand which one of the different control configurations simulated is generally the best, namely that it represents the best trade-off among carbon footprint, effluent quality and operating costs.

Finally, besides developing control strategies, improvements of the plant design and/or inclusion of new treatment units for the achievement not only of high effluent quality and low operating costs but also taking into account the minimization of the N_2O emissions and – more generically – the carbon footprint should be considered.

Dissemination activities

Patent

R. Boiocchi, G. Sin, K. V. Gernaey, Control of N_2O-emissions by aeration, 2016.

Publication List

Journal articles:

R. Boiocchi, M. Mauricio-Iglesias, A.K. Vangsgaard, K.V. Gernaey, G. Sin, Aeration control by monitoring the microbiological activity using fuzzy logic diagnosis and control. Application to a complete autotrophic nitrogen removal reactor, J. Process Control. 30 (2015) 22–23.

R. Boiocchi, K. V. Gernaey, G. Sin, Systematic design of membership functions for fuzzy-logic control: A case study on one-stage partial nitritation/anammox treatment systems, Water Res. 102 (2016) 346–361.

R. Boiocchi, K.V. Gernaey, G. Sin, Understanding the N_2O production mechanisms through sensitivity analyses on a benchmark simulation model. *In preparation*

Peer-reviewed conference proceedings:

R. Boiocchi, K.V. Gernaey, G. Sin, Control of wastewater N_2O emissions by balancing the microbial communities communities using a fuzzy-logic approach, IFAC-PapersOnLine. 49 (2016) 1157–1162.

R. Boiocchi, K.V. Gernaey, G. Sin, Extending the benchmark simulation model n°2 with processes for nitrous oxide production and side-stream nitrogen removal, in: Comput. Aided Chem. Eng., 2015: pp. 2477–2482.

Other conference proceedings:

R. Boiocchi, K.V. Gernaey, G. Sin, An extended Benchmark Simulation Model no2 with processes for nitrous oxide emission and side-stream pH-dependent partial nitritation/Anammox treatment, in: 9th IWA Symp. Syst. Anal. Integr. Assess., 2015.

R. Boiocchi, K. V. Gernaey, G. Sin, Investigation of tuning of a fuzzy-logic controller for biological wastewater treatment systems, in: 9th IWA Symp. Syst. Anal. Integr. Assess., 2015.

R. Boiocchi, K. V. Gernaey, G. Sin, Uncertainty And Sensitivity Analysis Of A Model Describing Nitrous Oxide Emissions From Wastewater Treatment Plants, in: 3rd IWA Spec. Int. Conf. Ecotechnologies Wastewater Treat., 2016.

R. Boiocchi, K. V. Gernaey, G. Sin, Performance Evaluation Of A Single-Stage Partial Nitritation-Anammox Within The Context Of A Plant-Wide Watewater treatment plant, in: 3rd IWA Spec. Int. Conf. Ecotechnologies Wastewater Treat., 2016.

Attended conferences

R. Boiocchi, K.V. Gernaey, G. Sin, Investigation of tuning of a fuzzy-logic control for biological wastewater treatment systems, *Oral presentation at the 19th Nordic Process Control workshop (NPCW 2015).*

R. Boiocchi, K.V. Gernaey, G. Sin, Extending the benchmark simulation model n°2 with processes for nitrous oxide production and side-stream nitrogen removal, *Poster presentation at the 12th PSE and the 25th ESCAPE joint conference (PSE2015/ESCAPE25).*

R. Boiocchi, K.V. Gernaey, G. Sin, An extended Benchmark Simulation Model no2 with processes for nitrous oxide emission and side-stream pH-dependent partial nitritation/Anammox treatment, *Oral presentation at the 9th IWA Symposium on Systems Analysis amd Integrated Assessment (WATERMATEX 2015).*

R. Boiocchi, K. V. Gernaey, G. Sin, Investigation of tuning of a fuzzy-logic controller for biological wastewater treatment systems, *Oral presentation at the 9th IWA Symposium on Systems Analysis amd Integrated Assessment (WATERMATEX 2015).*

R. Boiocchi, K.V. Gernaey, G. Sin, Control of wastewater N_2O emissions by balancing the microbial communities communities using a fuzzy-logic approach, *Oral presentation at the 11th IFAC Symposium on Dynamics and Control of Process Systems, Including Biosystems (DYCOPS-CAB 2016).*

R. Boiocchi, K. V. Gernaey, G. Sin, Uncertainty And Sensitivity Analysis Of A Model Describing Nitrous Oxide Emissions From Wastewater Treatment Plants, *Oral presentation at the 3rd IWA Specialized International Conference "Ecotechnologies for Wastewater Treatment" (ECOstp 2016).*

R. Boiocchi, K. V. Gernaey, G. Sin, Performance Evaluation Of A Single-Stage Partial Nitritation-Anammox Within The Context Of A Plant-Wide Watewater treatment plant, *Oral presentation at the 3rd IWA Specialized International Conference "Ecotechnologies for Wastewater Treatment" (ECOstp 2016).*

R. Boiocchi, M. Johansen, K.V. Gernaey, G. Sin, Benchmarking of Control Strategies for the Prevention of Nitrous Oxide Accumulation in Wastewater Treatment Plants, *Oral presentation at the 20th Nordic Process Control workshop (NPCW 2016).*

References

[1] F. M., J. Roy, A. Abdel-Aziz, A. Acquaye, J.M. Allwood, J.-P. Ceron, et al., Industry. In: Climate Change 2014: Mitigation of Climate Change. Contribution of Working Group III to the Fifth Assessment Report of the Intergovernmental Panel on Climate Change [Edenhofer, O., R. Pichs-Madruga, Y. Sokona, E. Farahani, S. Kadner, K. Seyb, 2014.

[2] Y. Law, B. Ni, P. Lant, Z. Yuan, N2O production rate of an enriched ammonia-oxidising bacteria culture exponentially correlates to its ammonia oxidation rate, Water Res. 46 (2012) 3409–3419.

[3] J.H. Anderson, The Metabolism of Hydroxylamine to Nitrite by Nitrosomonas, Biochem. J. 91 (1964) 8–17.

[4] A.B. Falcone, A.L. Shug, Oxidation of hydroxylamine by particles from nitrosomonas, Biochem. Biophys. Res. Commun. 9 (1962) 126–131.

[5] G.A.F. Ritchie, D.J.D. Nicholas, Identification of the Sources of Nitrous Oxide Produced by Oxidative and Reductive Processes in Nitrosomonas europaea, Biochem. J. 126 (1972) 1181–1191.

[6] B. Ni, L. Peng, Y. Law, J. Guo, Z. Yuan, Modeling of Nitrous Oxide Production by Autotrophic Ammonia- Oxidizing Bacteria with Multiple Production Pathways, Environ. Sci. Technol. 48 (2014) 3916–3924.

[7] A.B. Hooper, K.R. Terry, Hydroxylamine oxidoreductase of Nitrosomonas production of nitric oxide from hydroxylamine, Biochim. Biophys. Acta. 571 (1979) 12–20.

[8] A.B. Hooper, A nitrite-reducing enzyme from Nitrosomonas europaea - preliminary characterization with hydroxylmaine as electron donor, Biochim. Biophys. Acta. 162 (1968) 49–65.

[9] M.J. Kampschreur, H. Temmink, R. Kleerebezem, M.S.M. Jetten, M.C.M. Van Loosdrecht, Nitrous oxide emission during wastewater treatment, Water Res. 43 (2009) 4093–4103.

[10] P. Wunderlin, J. Mohn, A. Joss, L. Emmenegger, H. Siegrist, Mechanisms of N2O production in biological wastewater treatment under nitrifying and denitrifying conditions, Water Res. 46 (2012) 1027–1037.

[11] W.C. Hiatt, C.P.L. Grady, An updated process model for carbon oxidation, nitrification, and denitrification., Water Environ. Res. 80 (2008) 2145–56.

[12] A.G. Mutlu, Management of microbial community composition, architecture and performance in autotrophic nitrogen removing bioreactors through aeration regimes, 2015.

[13] M. Strous, J.J. Heijnen, J.G. Kuenen, M.S.M. Jetten, The sequencing batch reactor as a powerful tool for the study of slowly growing anaerobic ammonium-oxidizing microorganisms, Appl. Microbiol. Biotechnol. 50 (1998) 589–596.

[14] Y. Law, L. Ye, Y. Pan, Z. Yuan, Nitrous oxide emissions from wastewater treatment processes., Philos. Trans. R. Soc. Lond. B. Biol. Sci. 367 (2012) 1265–77.

[15] J. Desloover, S.E. Vlaeminck, P. Clauwaert, W. Verstraete, N. Boon, Strategies to mitigate N2O emissions from biological nitrogen removal systems, Curr. Opin. Biotechnol. 23 (2012) 474–482.

[16] D. Richardson, H. Felgate, N. Watmough, A. Thomson, E. Baggs, Mitigating release of the potent greenhouse gas N2O from the nitrogen cycle – could enzymic regulation hold the key ?, Trends Biotechnol. 27 (2009) 388–397.

[17] V. Rassamee, C. Sattayatewa, K. Pagilla, K. Chandran, Effect of oxic and anoxic conditions on nitrous oxide emissions from nitrification and denitrification processes, Biotechnol. Bioeng. 108 (2011) 2036–2045.

[18] L. Peng, B.-J. Ni, D. Erler, L. Ye, Z. Yuan, The combined effect of dissolved oxygen and nitrite on N2O production by ammonia oxidizing bacteria in an enriched nitrifying sludge, Water Res. 73 (2015) 29–36.

[19] L. Peng, B.-J. Ni, D. Erler, L. Ye, Z. Yuan, The effect of dissolved oxygen on N2O production by ammonia-oxidizing bacteria in an enriched nitrifying sludge, Water Res. 66 (2014) 12–21.

[20] Z. Peng, L., Ni, B.J., Liu, Y. and Yuan, Guideline of Selecting N2O Models to predict N2O Production by Ammonia Oxidizing Bacteria, in: 9th IWA Symp. Syst. Anal. Integr. Assess., 2015.

[21] J. Alex, L. Benedetti, J. Copp, K. V Gernaey, Benchmark Simulation Model no . 1 (BSM1) Contributors, 1 (2008).

[22] U. Jeppsson, M.-N. Pons, I. Nopens, J. Alex, J.B. Copp, K. V Gernaey, et al., Benchmark simulation model no 2: general protocol and exploratory case studies., Water Sci. Technol. 56 (2007) 67–78.

[23] K.I.Y. Park, J.Y. Inamori, M. Mizuochi, K.Y.U.H. Ahn, Emission and Control of Nitrous Oxide from a Biological Wastewater Treatment System with Intermittent Aeration, J. Biosci. Bioeng. 90 (2000) 247–252.

[24] X. Zhu, Y. Chen, H. Chen, X. Li, Y. Peng, S. Wang, Minimizing nitrous oxide in biological nutrient removal from municipal wastewater by controlling copper ion concentrations, Appl. Microbiol. Biotechnol. 97 (2013) 1325–1334.

[25] Z. Hu, J. Zhang, H. Xie, S. Liang, S. Li, Minimization of nitrous oxide emission from anoxic e oxic biological nitrogen removal process : Effect of in fl uent COD / NH 4 þ ratio and feeding strategy, J. Biosci. Bioeng. 115 (2013) 272–278.

[26] S. Sun, Z. Bao, D. Sun, Study on emission characteristics and reduction strategy of nitrous oxide during wastewater treatment by different processes, Environ. Sci. Pollut. Res. 22 (2014) 4222–4229.

[27] C.R. Behera, B. Srinivasan, K. Chandran, V. Venkatasubramanian, Model based predictive control for energy efficient biological nitrification process with minimal nitrous oxide production, Chem. Eng. J. 268 (2015) 300–310.

[28] A. Rodriguez-Caballero, I. Aymerich, R. Marques, M. Poch, M. Pijuan, Minimizing N2O emissions and carbon footprint on a full-scale activated sludge sequencing batch reactor, Water Res. 71 (2015) 1–10.

[29] R. Otterpohl, M. Freund, DYNAMIC MODELS FOR CLARIFIERS OF ACTIV ATED SLUDGE PLANTS WITH DRY AND WET WEATHER FLOWS, Water Sci. Technol. 26 (1992) 1391–1400.

[30] M. Henze, C.P.L.G. Jr, W. Gujer, G.V.R. Marais, T. Matsuo, A general model for single-sludge wastewater treatment systems., Water Res. 21 (1987) 505–515.

[31] I. Takacs, G.G. Patry, D. Nolasco, A dynamic model of the clarification-thickening process, Water Res. 25 (1991) 1263–1271.

[32] D.J. Batstone, J. Keller, I. Angelidaki, S. V Kalyuzhnyi, S.G. Pavlostathis, a Rozzi, et al., The IWA Anaerobic Digestion Model No 1 (ADM1)., Water Sci. Technol. 45 (2002) 65–73.

[33] L.R. Iman, W.J. Conover, A distribution-free approach to including rank correlation among input variables, Commun. Stat. Comput. 11 (1982) 311–334.

[34] G. Sin, K. V Gernaey, M.B. Neumann, M.C.M. van Loosdrecht, W. Gujer, Global sensitivity analysis in wastewater treatment plant model applications: prioritizing sources of uncertainty., Water Res. 45 (2011) 639–651.

[35] M.D. Morris, Factorial Sampling Plans for Preliminary Computational Experiments, Technometrics. 33 (1991) 161–174.

[36] G. Sin, K. V. Gernaey, Improving the Morris method for sensitivity analysis by scaling the elementary effects, in: Comput. Aided Chem. Eng., 2009: pp. 925–930.

[37] L. Guo, P.A. Vanrolleghem, Calibration and validation of an activated sludge model for greenhouse gases no. 1 (ASMG1): prediction of temperature-dependent N2O emission dynamics., Bioprocess Biosyst. Eng. 37 (2014) 151–163.

[38] M. Pocquet, Z. Wu, I. Queinnec, M. Spérandio, A two pathway model for N2O emissions by ammonium oxidizing bacteria supported by the NO/N2O variation., Water Res. 88 (2015) 948–959.

[39] C. Domingo-Felez, B.F. Smets, A consilience model to describe N2O production during biological N-removal, Environ. Sci. Water Res. Technol. (2016).

[40] M.R.J. Daelman, E.M. van Voorthuizen, U.G.J.M. van Dongen, E.I.P. Volcke, M.C.M. van Loosdrecht, Seasonal and diurnal variability of N2O emissions from a full-scale municipal wastewater treatment plant, Sci. Total Environ. 536 (2015) 1–11.

[41] A. Aboobakar, E. Cartmell, T. Stephenson, M. Jones, P. Vale, G. Dotro, Nitrous oxide emissions and dissolved oxygen profiling in a full-scale nitrifying activated sludge treatment plant, Water Res. 47 (2013) 524–534.

[42] M.J. Kampschreur, W.R.L. van der Star, H. a. Wielders, J.W. Mulder, M.S.M. Jetten, M.C.M. van Loosdrecht, Dynamics of nitric oxide and nitrous oxide emission during full-scale reject water treatment, Water Res. 42 (2008) 812–826.

[43] A.K. Vangsgaard, M. Mauricio-Iglesias, K. V Gernaey, B.F. Smets, G. Sin, Sensitivity analysis of autotrophic N removal by a granule based bioreactor: Influence of mass transfer versus microbial kinetics., Bioresour. Technol. 123 (2012) 230–241.

[44] S. Lackner, E.M. Gilbert, S.E. Vlaeminck, A. Joss, H. Horn, M.C.M. van Loosdrecht, Full-scale partial nitritation/anammox experiences - An application survey, Water Res. 55 (2014) 292–303.

[45] R. Boiocchi, K.V. Gernaey, G. Sin, Extending the benchmark simulation model n°2 with processes for nitrous oxide production and side-stream nitrogen removal, in: Comput. Aided Chem. Eng., 2015: pp. 2477–2482.

[46] R. Boiocchi, K. V. Gernaey, G. Sin, Uncertainty And Sensitivity Analysis Of A Model Describing Nitrous Oxide Emissions From Wastewater Treatment Plants, in: 3rd IWA Spec. Int. Conf. Ecotechnologies Wastewater Treat., 2016.

[47] R. Boiocchi, K. V. Gernaey, G. Sin, Performance Evaluation Of A Single-Stage Partial Nitritation-Anammox Within The Context Of A Plant-Wide Watewater treatment plant, in: 3rd IWA Spec. Int. Conf. Ecotechnologies Wastewater Treat., 2016.

[48] K.E. Mampaey, B. Beuckels, M.J. Kampschreur, R. Kleerebezem, M.C.M. van Loosdrecht, E.I.P. Volcke, Modelling nitrous and nitric oxide emissions by autotrophic ammonia-oxidizing bacteria, Environ. Technol. 34 (2013) 1555–1566.

[49] C. Hellinga, M.C.M. van Loosdrecht, J.J. Heijnen, Model Based Design of a Novel Process for Nitrogen Removal from Concentrated Flows, Math. Comput. Model. Dyn. Syst. 5 (1999) 351–371.

[50] A.K. Vangsgaard, a. G. Mutlu, K. V. Gernaey, B.F. Smets, G. Sin, Calibration and validation of a model describing complete autotrophic nitrogen removal in a granular SBR system, J. Chem. Technol. Biotechnol. (2013) 2007–2015.

[51] A.K. Vangsgaard, M. Mauricio-Iglesias, K. V. Gernaey, G. Sin, Development of novel control strategies for single-stage autotrophic nitrogen removal: A process oriented approach, Comput. Chem. Eng. 66 (2014) 71–81.

[52] E.I.P. Volcke, M.C.M. van Loosdrecht, P. a Vanrolleghem, Continuity-based model interfacing for plant-wide simulation: a general approach., Water Res. 40 (2006) 2817–2828.

[53] Vanrolleghem, Peter A., S. H., P. B., G. P., Takacs I., Estimating (combinations of) Activated Sludge Model no. 1 parameters and components by respirometry, Water Sci. Technol. 39 (1999) 195–214.

[54] U. Jeppsson, Modeling aspects of wastewater treatment processes, 1996.

[55] Zhang TT., Z. J., Y. F., X. HJ., H. X., L. YR, Effect of temperature on pollutant removal and nitrous oxide emission of wastewater nitrogen removal system, Huan Jing Ke Xue. 33 (2012) 1283–1287.

[56] J.H. Ahn, T. Kwan, K. Chandran, Comparison of partial and full nitrification processes applied for treating high-strength nitrogen wastewaters: Microbial ecology through nitrous oxide production, Environ. Sci. Technol. 45 (2011) 2734–2740.

[57] J. Foley, D. de Haas, Z. Yuan, P. Lant, Nitrous oxide generation in full-scale biological nutrient removal wastewater treatment plants., Water Res. 44 (2010) 831–44.

[58] J.H. Ahn, S. Kim, H. Park, B. Rahm, K. Pagilla, K. Chandran, N2O emissions from activated sludge processes, 2008-2009: results of a national monitoring survey in the United States., Environ. Sci. Technol. 44 (2010) 4505–4511.

[59] B.-J. Ni, Z. Yuan, K. Chandran, P. a Vanrolleghem, S. Murthy, Evaluating four mathematical models for nitrous oxide production by autotrophic ammonia-oxidizing bacteria., Biotechnol. Bioeng. 110 (2013) 153–163.

[60] D.J. Kim, D.I. Lee, J. Keller, Effect of temperature and free ammonia on nitrification and nitrite accumulation in landfill leachate and analysis of its nitrifying bacterial community by FISH, Bioresour. Technol. 97 (2006) 459–468.

[61] G. Tallec, J. Garnier, G. Billen, M. Gousailles, Nitrous oxide emissions from secondary activated sludge in nitrifying conditions of urban wastewater treatment plants: Effect of oxygenation level, Water Res. 40 (2006) 2972–2980.

[62] M.J. Kampschreur, N.C.G. Tan, R. Kleerebezem, C. Picioreanu, M.S.M. Jetten, M.C.M. Van Loosdrecht, Effect of dynamic process conditions on nitrogen oxides emission from a nitrifying culture, Environ. Sci. Technol. 42 (2008) 429–435.

[63] E.I.P. Volcke, M.C.M. van Loosdrecht, P.A. Vanrolleghem, Controlling the nitrite:ammonium ratio in a SHARON reactor in view of its coupling with an Anammox process, Water Sci. Technol. 53 (2006) 45–54.

[64] C. Lindberg, B. Carlsson, Nonlinear and set-point control of the dissolved oxygen concentration in an activated sludge process, Water Sci. Technol. 34 (1996) 135–142.

[65] N. a. Wahab, R. Katebi, J. Balderud, Multivariable PID control design for activated sludge process with nitrification and denitrification, Biochem. Eng. J. 45 (2009) 239–248.

[66] J. Serralta, J. Ribes, a Seco, J. Ferrer, A supervisory control system for optimising nitrogen removal and aeration energy consumption in wastewater treatment plants., Water Sci. Technol. 45 (2002) 309–316.

[67] T. Aoi, Y. Okaniwa, K. Hagiwara, K. Motomura, E. Iwaihara, M. Imai, et al., A direct ammonium control system using fuzzy inference in a high-load biological denitrification process treating collected human excreta, Water Sci. Technol. 26 (1992) 1325–1334.

[68] R.M. Tong, M.B. Beck, A. Latten, Fuzzy Control of the Activated Sludge Wastewater Treatment Process, Automatica. 16 (1980) 695–701.

[69] S. Weijers, Modelling, Identification and Control of Activated Sludge Plants for Nitrogen Removal, 2000.

[70] H.M.S. Lababidi, C.G.J. Baker, Fuzzy Modeling, in: Handb. Food Bioprocess Model. Tech., 2006: pp. 451–498.

[71] D.E. Seborg, T.F. Edgar, D.A. Mellichamp, Process dynamics and control, 2004.

[72] R. Boiocchi, M. Mauricio-Iglesias, A.K. Vangsgaard, K.V. Gernaey, G. Sin, Aeration control by monitoring the microbiological activity using fuzzy logic diagnosis and control. Application to a complete autotrophic nitrogen removal reactor, J. Process Control. 30 (2015) 22–23.

[73] R. Boiocchi, K. V. Gernaey, G. Sin, Systematic design of membership functions for fuzzy-logic control: A case study on one-stage partial nitritation/anammox treatment systems, Water Res. 102 (2016) 346–361.

[74] A.M. Saunders, P. Larsen, P.H. Nielsen, Comparison of nutrient-removing microbial communities in activated sludge from full-scale MBRs and conventional plants., Water Sci. Technol. 68 (2013) 366–371.

[75] Y. Bai, D. Wang, Fundamentals of Fuzzy Logic Control – Fuzzy Sets , Fuzzy Rules and Defuzzifications, in: Adv. Fuzzy Log. Technol. Ind. Appl., 1982: pp. 17–36.

[76] E.I.P. Volcke, Modelling , analysis and control of partial nitritation in a SHARON reactor, Ghent University, 2006.

[77] U. Van Dongen, M.S.M. Jetten, M.C.M. Van Loosdrecht, The SHARON(R)-Anammox(R) process for treatment of ammonium rich wastewater, Water Sci. Technol. 44 (2001) 153–160.

[78] E.I.P. Volcke, S.W.H. Van Hulle, M.C.M. Van Loosdrecht, A. Peter, Generation of Anammox-optimal nitrite : ammonium ratio with SHARON process : usefulness of process control ?, in: 9th Spec. Conf. Des. Oper. Econ. Large Wastewater Treat., 2003: pp. 1–4.

[79] H. De Clippeleir, X. Yan, W. Verstraete, S.E. Vlaeminck, OLAND is feasible to treat sewage-like nitrogen concentrations at low hydraulic residence times., Appl. Microbiol. Biotechnol. 90 (2011) 1537–1545.

[80] X. Hao, J.J. Heijnen, M.C.M. Van Loosdrecht, Model-based evaluation of temperature and inflow variations on a partial nitrification-ANAMMOX biofilm process., Water Res. 36 (2002) 4839–4849.

[81] S. Lackner, C. Lindenblatt, H. Horn, "Swinging ORP" as operation strategy for stable reject water treatment by nitritation–anammox in sequencing batch reactors, Chem. Eng. J. 180 (2012) 190–196.

[82] A. Joss, N. Derlon, C. Cyprien, S. Burger, I. Szivak, J. Traber, et al., Combined nitritation-anammox: advances in understanding process stability., Environ. Sci. Technol. 45 (2011) 9735–9742.

[83] H. Bürgmann, S. Jenni, F. Vazquez, K.M. Udert, Regime shift and microbial dynamics in a sequencing batch reactor for nitrification and anammox treatment of urine., Appl. Environ. Microbiol. 77 (2011) 5897–5907.

[84] M. Mauricio-Iglesias, A.K. Vangsgaard, K. V Gernaey, G. Sin, A fuzzy-logic based diagnosis and control of a reactor performing complete autotrophic nitrogen removal, in: CAB/DYCOPS, 2013: pp. 1–6.

[85] A.G. Mutlu, A.K. Vangsgaard, G. Sin, B.F. Smets, An operational protocol for facilitating start-up of single-stage autotrophic nitrogen-removing reactors based on process stoichiometry, Water Sci. Technol. 68 (2013) 514–521.

[86] J. Comas, I. Rodríguez-Roda, K.V. Gernaey, C. Rosen, U. Jeppsson, M. Poch, Risk assessment modelling of microbiology-related solids separation problems in activated sludge systems, Environ. Model. Softw. 23 (2008) 1250–1261.

[87] C. Garcia, F. Molina, E. Roca, J.M. Lema, Fuzzy-Based Control of an Anaerobic Reactor Treating Wastewaters Containing Ethanol and Carbohydrates, Ind. Eng. Chem. Res. 46 (2007) 6707–6715.

[88] M. Yong, P. Yong-zhen, W. Xiao-lian, W. Shu-ying, Intelligent control aeration and external carbon addition for improving nitrogen removal, Environ. Model. Softw. 21 (2006) 821–828.

[89] H. Hellendoorn, C. Thomas, Defuzzification in Fuzzy Controllers, J. Intell. Fuzzy Syst. 1 (1993) 109–123.

[90] T. Larsson, S. Skogestad, Plantwide control — A review and a new design procedure, Model. Indentification Control. 21 (2000) 209–240.

[91] I. Nopens, L. Benedetti, U. Jeppsson, M.-N. Pons, J. Alex, J.B. Copp, et al., Benchmark Simulation Model No 2 : finalisation of plant layout and default control strategy, Water Sci. Technol. 62 (2010) 1967–1974.

[92] M. Mauricio-Iglesias, A.K. Vangsgaard, K. V. Gernaey, B.F. Smets, G. Sin, A novel control strategy for single-stage autotrophic nitrogen removal in SBR, Chem. Eng. J. 260 (2015) 64–73.

[93] R. Boiocchi, M. Mauricio-Iglesias, A.K. Vangsgaard, K.V. Gernaey, G. Sin, Aeration control by monitoring the microbiological activity using fuzzy logic diagnosis and control. Application to a complete autotrophic nitrogen removal reactor, J. Process Control. 30 (2015) 22–33.

[94] C. Fu, M. Poch, Fuzzy model and decision of COD control for anactivated sludge process, Fuzzy Sets Syst. 93 (1998) 281–292.

[95] J. Ferrer, M.A. Rodrigo, A. Seco, J.M. Penya-roja, ENERGY SAVING IN THE AERATION PROCESS BY FUZZY LOGIC CONTROL, Water Sci. Technol. 38 (1998) 209–217.

[96] R. Jager, Fuzzy logic in control, 1995.

[97] J.-I. Horiuchi, K. Hiraga, Industrial application of fuzzy control to large-scale recombinant vitamin B2 production, J. Biosci. Bioeng. 87 (1999) 365–371.

[98] M. a. Hussain, K.B. Ramachandran, Design of a Fuzzy Logic Controller for Regulating Substrate Feed to Fed-Batch Fermentation, Food Bioprod. Process. 81 (2003) 138–146.

[99] L.J.P. Snip, R. Boiocchi, X. Flores-Alsina, U. Jeppsson, K.V. Gernaey, Challenges encountered when expanding activated sludge models: A case study based on N2O production, Water Sci. Technol. 70 (2014) 1251–1260.

APPENDIX 1
MONTE CARLO SENSITIVITY ANALYSIS RESULTS

In this appendix, the standard regression coefficients are presented. The last row shows the coefficients of determination (R^2).

TEMPERATURE = 10 ºC, DO =0.3 mg (-COD).L^{-1}

	N_2O total	η_{TN}	O_2consSpec	O_2 cons by HB	O_2 cons by AOB	O_2 cons by NOB
'b_A_1'	-0,059	-0,082	-0,014	0,035	-0,115	-0,019
'b_A2'	0,083	-0,015	-0,054	0,058	-0,082	-0,130
'b_H'	0,004	0,085	0,010	0,004	0,107	0,148
'f_P'	-0,064	-0,016	-0,084	-0,033	-0,001	-0,093
'i_X_B'	-0,050	-0,084	0,026	0,003	-0,066	-0,078
'i_X_P'	0,043	0,111	-0,083	-0,090	0,082	-0,038
'k_a'	-0,022	0,057	-0,032	-0,037	0,084	0,001
'K_F_A'	-0,022	-0,031	0,112	-0,009	0,082	-0,025
'K_F_N_A'	0,134	0,002	0,011	0,045	-0,068	-0,025
'k_h'	0,064	0,008	0,090	0,012	0,044	0,041
'K_I_1_0_F_A'	0,012	0,031	-0,060	-0,097	-0,012	0,005
'F_I_1_0_F_N_A'	-0,063	0,049	0,088	-0,057	0,100	-0,014
'K_{I3NO}'	0,047	-0,031	0,090	0,024	-0,092	-0,109
'K_{I4NO}'	-0,030	-0,005	0,122	-0,047	0,016	0,059
'K_{I5NO}'	-0,134	-0,058	-0,025	0,013	-0,041	0,134
'K_{I9FA}'	-0,005	0,084	-0,073	-0,062	0,129	0,114
'K_{I9FNA}'	-0,003	-0,027	0,031	0,038	-0,083	-0,077
'K_{N2O}'	0,059	-0,015	0,026	-0,042	-0,037	-0,006
'K_{NO}'	0,019	0,069	0,016	-0,017	0,053	-0,015
'K_N_O_2'	-0,023	-0,005	-0,040	-0,009	0,037	0,048
'K_N_O_3'	0,016	-0,048	0,025	-0,023	0,019	-0,011
'K_{OA1}'	-0,105	-0,567	0,005	0,226	-0,271	-0,311
'K_{OA2}'	0,261	0,237	-0,083	0,062	-0,107	-0,370
'K_O_H'	-0,042	-0,042	0,029	0,070	0,046	0,011
'K_{OH1}'	-0,023	0,067	-0,045	0,195	0,058	-0,003
'K_{OH2}'	0,109	0,017	0,080	-0,029	0,011	0,053
'K_{OH3}'	-0,015	0,028	0,051	-0,080	0,055	0,023
'K_{OH4}'	-0,063	-0,034	0,006	0,030	-0,051	0,011
'K_{OH5}'	-0,094	-0,041	0,082	0,007	-0,024	-0,011

'K_{S1}'	-0,070	-0,011	0,023	0,441	-0,061	0,015
	N_2O total	**η_{TN}**	**O_2consSpec**	**O_2 cons by HB**	**O_2 cons by AOB**	**O_2 cons by NOB**
'K_{S2}'	0,084	-0,027	0,049	0,067	-0,014	-0,048
'K_{S3}'	-0,099	-0,058	0,046	0,024	-0,050	-0,012
'K_{S4}'	0,148	-0,022	0,058	-0,015	-0,038	-0,027
'K_{S5}'	0,211	-0,095	-0,012	0,110	-0,122	-0,019
'K_{X}'	-0,027	0,000	-0,075	-0,059	0,040	0,059
'mu_{A1}'	0,187	0,457	-0,117	-0,164	0,310	0,201
'mu_{A2}'	-0,093	-0,048	0,002	-0,138	0,069	0,284
'mu_{H}'	-0,028	0,011	-0,095	-0,222	0,006	0,117
'n_{g2}'	0,064	0,005	-0,011	0,037	-0,084	-0,018
'n_{g3}'	-0,008	-0,002	0,066	-0,062	-0,025	0,074
'n_{g4}'	-0,126	-0,011	0,036	0,013	-0,025	-0,086
'n_{g5}'	-0,136	0,018	0,085	-0,018	-0,016	0,013
'n_{h}'	0,087	-0,006	0,072	0,028	-0,066	-0,032
'n_{Y}'	-0,013	-0,018	0,030	0,052	-0,017	-0,044
'Y_{A1}'	0,077	0,132	0,010	-0,004	0,120	0,012
'Y_{A2}'	-0,059	0,065	-0,001	-0,038	0,049	0,010
'Y_{H}'	-0,065	-0,126	0,108	0,132	-0,223	-0,098
'K_{SNO_a_o_b}'	-0,004	-0,059	0,043	0,051	-0,055	-0,017
'K_{SO_aobDen1}'	-0,136	-0,027	0,007	-0,058	0,011	0,029
'K_{IO_aobDen1}'	0,061	-0,011	0,025	0,042	-0,047	0,055
'K_{SO_aobDen2}'	-0,016	0,020	-0,127	-0,009	0,052	0,005
'K_{IO_aobDen2}'	0,057	0,013	-0,076	0,071	-0,061	-0,030
'n_{AOB}'	0,029	0,063	-0,018	0,016	0,098	0,051
'K_{FNA_a_o_b}'	-0,018	-0,039	-0,006	0,036	-0,039	-0,024
'K_{FA_a_o_b}'	-0,062	-0,022	0,089	-0,081	0,019	0,038
'Y_{AnAOB}'	-0,044	-0,061	0,070	-0,046	-0,094	-0,015
'mu_{maxAnAOB}'	0,042	0,091	0,109	-0,016	0,117	0,008
'K_{NH3_AnAOB}'	0,111	-0,037	-0,078	0,140	-0,061	-0,123
'K_{HNO2_AnAOB}'	0,043	-0,029	0,001	0,056	-0,062	-0,073
'K_{O2_AnAOB}'	-0,043	-0,053	-0,035	0,042	-0,015	0,008
'b_{AnAOB}'	0,046	-0,027	-0,077	0,013	-0,082	-0,073
R^2	**0,423**	**0,734**	**0,233**	**0,703**	**0,716**	**0,692**

TEMPERATURE = 10 ºC, DO =0.65 mg (-COD).L^{-1}

	N_2O total	η_{TN}	O2consSpec	O_2 cons by HB	O_2 cons by AOB	O_2 cons by NOB
'b_A_1'	-0,064	-0,054	0,042	-0,004	0,034	0,026
'b_A2'	0,089	0,063	-0,075	0,025	-0,102	-0,055
'b_H'	-0,056	0,016	0,169	0,519	0,078	0,136
'f_P'	0,030	0,055	-0,220	-0,346	-0,163	-0,122
'i_X_B'	0,045	-0,044	0,054	0,003	0,038	-0,019
'i_X_P'	-0,014	0,086	-0,105	-0,022	-0,046	-0,004
'k_a'	0,043	0,011	0,009	0,007	0,034	0,016
'K_F_A'	-0,058	-0,050	0,000	0,029	-0,058	-0,058
'K_F_N_A'	0,052	0,071	-0,064	0,014	-0,092	-0,039
'k_h'	0,029	0,086	-0,089	-0,048	0,012	0,044
'K_I_1_0_F_A'	0,024	-0,005	0,002	0,018	-0,030	-0,027
'F_I_1_0_F_N_A'	-0,118	-0,012	0,006	-0,024	0,078	-0,013
'K_{I3NO}'	0,110	0,018	-0,018	0,016	-0,066	-0,009
'K_{I4NO}'	-0,098	-0,017	0,012	-0,008	0,071	-0,034
'K_{I5NO}'	-0,026	-0,007	-0,007	-0,033	-0,001	0,032
'K_{I9FA}'	-0,124	-0,037	0,044	-0,036	0,104	0,033
'K_{I9FNA}'	0,077	0,098	-0,085	0,042	-0,109	-0,097
'K_{N2O}'	-0,053	-0,083	0,080	-0,005	0,030	0,043
'K_{NO}'	0,014	-0,021	0,033	-0,007	0,035	0,030
'K_N_O_2'	-0,103	-0,113	0,117	-0,002	0,070	0,106
'K_N_O_3'	0,000	-0,101	0,100	0,108	-0,028	-0,030
'K_{OA1}'	-0,099	-0,154	0,110	0,015	0,005	0,015
'K_{OA2}'	0,152	0,334	-0,328	0,018	-0,192	-0,257
'K_O_H'	-0,035	-0,013	0,010	-0,026	0,039	0,009
'K_{OH1}'	0,009	0,013	-0,003	-0,069	0,008	0,079
'K_{OH2}'	0,037	-0,044	0,047	-0,151	-0,010	0,285
'K_{OH3}'	-0,051	0,004	-0,005	-0,047	0,049	0,029
'K_{OH4}'	0,036	0,032	-0,034	0,004	-0,047	-0,036
'K_{OH5}'	-0,039	-0,090	0,081	-0,014	0,046	0,092
'K_{S1}'	-0,042	0,094	-0,090	-0,279	0,042	0,265
'K_{S2}'	-0,030	-0,014	-0,003	0,308	0,015	-0,475
'K_{S3}'	0,025	-0,077	0,070	0,014	-0,078	0,045
'K_{S4}'	0,100	-0,005	-0,011	0,046	-0,103	0,011
'K_{S5}'	0,123	0,056	-0,050	0,056	-0,082	-0,078
'K_{X}'	-0,047	-0,055	0,047	-0,021	0,049	0,052
'mu_{A1}'	0,062	0,163	-0,122	-0,024	-0,011	-0,028
'mu_{A2}'	-0,095	-0,250	0,250	0,017	0,107	0,145
	N_2O total	**η_{TN}**	**O_2consSpec**	**O_2 cons by HB**	**O_2 cons by AOB**	**O_2 cons by NOB**
'mu_{H}'	0,093	0,099	-0,099	0,012	-0,085	-0,055

	N_2O total	η_{TN}	O_2consSpec	O_2 cons by HB	O_2 cons by AOB	O_2 cons by NOB
'n_{g2}'	0,052	0,074	-0,066	-0,143	-0,069	0,174
'n_{g3}'	0,038	0,092	-0,112	0,004	-0,035	-0,073
'n_{g4}'	-0,027	0,011	-0,014	-0,025	0,020	-0,035
'n_{g5}'	0,000	0,001	0,001	-0,022	-0,021	0,021
'n_{h}'	0,078	0,344	-0,349	-0,190	-0,057	-0,008
'n_{Y}'	-0,093	-0,313	0,262	0,034	0,019	-0,052
'Y_{A1}'	-0,069	-0,053	0,053	0,005	0,027	0,028
'Y_{A2}'	-0,028	0,031	-0,034	0,006	-0,013	-0,068
'Y_{H}'	-0,025	-0,210	0,032	-0,423	-0,042	-0,075
'K_{SNO_a_o_b}'	0,074	0,027	-0,022	0,012	-0,058	-0,032
'K_{SO_aobDen1}'	-0,083	-0,002	0,000	-0,039	0,089	-0,010
'K_{IO_aobDen1}'	0,126	0,092	-0,093	0,044	-0,163	-0,082
'K_{SO_aobDen2}'	0,064	0,058	-0,046	0,014	-0,072	-0,025
'K_{IO_aobDen2}'	0,044	-0,012	0,001	0,030	-0,041	-0,016
'n_{AOB}'	0,170	0,112	-0,134	0,027	-0,184	-0,081
'K_{FNA_a_o_b}'	-0,152	-0,143	0,158	-0,047	0,244	0,126
'K_{FA_a_o_b}'	-0,004	-0,076	0,084	-0,009	0,055	0,063
'Y_{AnAOB}'	-0,046	0,000	0,003	-0,008	0,011	0,021
'mu_{maxAnAOB}'	-0,027	-0,069	0,061	0,019	0,042	0,032
'K_{NH3_AnAOB}'	0,140	0,030	-0,026	0,041	-0,090	-0,017
'K_{HNO2_AnAOB}'	0,034	-0,030	0,033	0,005	-0,032	0,028
'K_{O2_AnAOB}'	-0,015	0,001	0,007	0,015	0,002	-0,024
'b_{AnAOB}'	-0,043	0,011	-0,007	-0,022	0,034	-0,013
R^2	**0,327**	**0,675**	**0,669**	**0,880**	**0,366**	**0,639**

TEMPERATURE = 10 ºC, DO =1 mg (-COD).L^{-1}

	N_2O total	η_{TN}	O2consSpec	O_2 cons by HB	O_2 cons by AOB	O_2 cons by NOB
'b_A_1'	-0,029	-0,041	-0,004	-0,011	-0,017	-0,011
'b_A2'	0,007	0,059	0,003	0,022	0,051	-0,095
'b_H'	-0,093	0,119	0,073	0,116	0,036	0,031
'f_P'	0,091	0,013	-0,110	-0,038	-0,100	-0,085
'i_X_B'	0,055	-0,100	0,015	-0,059	0,023	0,033
'i_X_P'	0,067	0,102	-0,116	-0,072	-0,007	-0,092
'k_a'	0,028	0,070	-0,004	-0,049	0,097	-0,032
'K_F_A'	-0,055	-0,014	0,199	-0,014	0,362	0,004
'K_F_N_A'	0,003	0,039	0,094	-0,013	-0,014	0,411
'k_h'	0,044	0,184	-0,047	-0,017	0,036	-0,003

	N_2O total	η_{TN}	O_2consSpec	O_2 cons by HB	O_2 cons by AOB	O_2 cons by NOB
'K_I_1_0_F_A'	0,020	0,021	-0,104	-0,111	-0,047	-0,042
'F_I_1_0_F_N_A'	-0,040	0,007	-0,062	-0,057	0,023	-0,117
'K_{I3NO}'	0,139	0,010	-0,044	-0,028	-0,063	0,014
'K_{I4NO}'	-0,206	0,012	-0,053	-0,053	-0,005	-0,030
'K_{I5NO}'	-0,017	-0,013	0,056	0,013	0,027	0,060
'K_{I9FA}'	-0,045	0,016	0,010	0,030	-0,029	0,058
'K_{I9FNA}'	0,023	0,084	-0,057	-0,002	-0,032	-0,030
'K_{N2O}'	-0,066	-0,059	-0,002	-0,038	0,047	-0,066
'K_{NO}'	0,118	0,009	-0,005	-0,022	-0,005	0,039
'K_N_O_2'	-0,116	-0,136	0,069	-0,024	0,075	0,017
'K_N_O_3'	-0,017	-0,140	0,018	-0,040	0,022	-0,029
'K_{OA1}'	-0,038	-0,106	0,206	-0,080	0,396	-0,013
'K_{OA2}'	0,087	0,156	0,019	-0,017	-0,049	0,386
'K_O_H'	-0,031	-0,002	0,061	0,038	0,083	-0,016
'K_{OH1}'	-0,074	0,048	0,079	0,115	0,024	0,002
'K_{OH2}'	0,009	-0,027	0,000	-0,036	0,004	0,040
'K_{OH3}'	-0,107	-0,021	-0,015	-0,056	0,042	-0,011
'K_{OH4}'	-0,003	0,033	-0,003	0,018	-0,035	0,006
'K_{OH5}'	-0,003	-0,070	0,000	-0,028	-0,014	0,074
'K_{S1}'	0,056	0,137	0,315	0,496	-0,029	0,187
'K_{S2}'	-0,064	0,047	-0,033	0,078	-0,029	-0,163
'K_{S3}'	-0,084	-0,121	0,082	-0,013	0,085	0,042
'K_{S4}'	0,146	-0,057	0,031	-0,026	0,004	0,062
'K_{S5}'	0,058	0,069	-0,012	0,090	-0,089	-0,028
'K_{X}'	-0,049	-0,044	-0,070	-0,060	-0,031	-0,052
'mu_{A1}'	0,055	0,120	-0,264	-0,031	-0,360	0,009
'mu_{A2}'	-0,089	-0,138	-0,089	-0,071	-0,007	-0,332
'mu_{H}'	0,141	0,094	-0,222	-0,299	-0,034	0,062
'n_{g2}'	-0,010	0,041	-0,021	-0,016	-0,042	0,080
'n_{g3}'	0,150	0,103	-0,079	-0,048	-0,031	0,029
'n_{g4}'	-0,007	0,060	-0,013	-0,006	0,026	-0,032
'n_{g5}'	0,040	-0,015	-0,031	-0,011	-0,052	0,001
'n_{h}'	0,023	0,443	-0,123	-0,036	0,043	0,062
'n_{Y}'	-0,074	-0,424	0,178	0,072	0,006	-0,035
'Y_{A1}'	-0,046	-0,025	0,059	0,017	0,089	-0,022
'Y_{A2}'	-0,047	-0,015	-0,024	-0,039	-0,051	0,071
'Y_{H}'	0,052	-0,306	0,077	0,097	-0,144	-0,025
'K_{SNO_a_o_b}'	-0,031	-0,014	0,033	0,052	-0,013	0,027
'K_{SO_aobDen1}'	-0,128	-0,005	-0,065	-0,054	-0,035	0,024
'K_{IO_aobDen1}'	0,017	0,088	-0,031	0,067	-0,046	-0,089

	N_2O total	η_{TN}	O_2consSpec	O_2 cons by HB	O_2 cons by AOB	O_2 cons by NOB
'K_{SO_aobDen2}'	0,102	-0,017	0,040	-0,005	0,070	0,005
'K_{IO_aobDen2}'	0,037	0,034	-0,001	0,060	-0,058	-0,002
'n_{AOB}'	0,136	0,057	0,046	0,041	0,056	-0,006
'K_{FNA_a_o_b}'	-0,086	-0,067	0,024	-0,004	-0,012	0,060
'K_{FA_a_o_b}'	-0,008	-0,063	0,006	-0,059	0,033	0,007
'Y_{AnAOB}'	-0,031	0,007	-0,070	-0,054	-0,063	0,009
'mu_{maxAnAOB}'	0,012	-0,034	0,035	0,003	0,061	-0,039
'K_{NH3_AnAOB}'	0,133	0,022	0,099	0,127	0,037	-0,051
'K_{HNO2_AnAOB}'	-0,015	-0,006	0,078	0,063	0,059	-0,003
'K_{O2_AnAOB}'	0,035	0,008	0,034	0,054	0,021	-0,057
'b_{AnAOB}'	-0,032	-0,012	-0,012	-0,004	0,021	-0,082
R^2	**0,340**	**0,778**	**0,735**	**0,982**	**0,491**	**0,672**

TEMPERATURE = 10 ºC, DO =2 mg (-COD).L^{-1}

	N_2O total	η_{TN}	O_2consSpec	O_2 cons by HB	O_2 cons by AOB	O_2 cons by NOB
'b_A_1'	-0,035	-0,001	-0,018	-0,014	-0,015	-0,011
'b_A2'	-0,064	0,031	0,008	0,023	0,044	-0,085
'b_H'	-0,062	0,174	0,055	0,118	0,030	0,016
'f_P'	0,124	0,001	-0,101	-0,034	-0,109	-0,086
'i_X_B'	0,030	-0,135	0,024	-0,060	0,029	0,044
'i_X_P'	0,103	0,113	-0,125	-0,071	-0,015	-0,096
'k_a'	-0,025	0,044	0,000	-0,048	0,095	-0,010
'K_F_A'	-0,030	0,027	0,216	-0,012	0,429	0,003
'K_F_N_A'	-0,047	0,025	0,108	-0,012	0,000	0,473
'k_h'	0,056	0,190	-0,037	-0,019	0,059	0,002
'K_I_1_0_F_A'	-0,047	0,037	-0,120	-0,119	-0,026	-0,077
'F_I_1_0_F_N_A'	0,022	0,027	-0,074	-0,058	0,007	-0,128
'K_{I3NO}'	0,144	-0,040	-0,036	-0,034	-0,058	0,015
'K_{I4NO}'	-0,233	0,091	-0,082	-0,055	-0,011	-0,031
'K_{I5NO}'	-0,056	-0,015	0,055	0,011	0,033	0,069
'K_{I9FA}'	-0,034	0,036	0,006	0,033	-0,027	0,047
'K_{I9FNA}'	-0,082	0,018	-0,034	-0,005	-0,019	-0,020
'K_{N2O}'	-0,052	-0,037	-0,005	-0,036	0,056	-0,080
'K_{NO}'	0,139	-0,036	0,001	-0,024	-0,011	0,050
'K_N_O_2'	-0,065	-0,093	0,053	-0,024	0,071	0,012
'K_N_O_3'	-0,009	-0,139	0,006	-0,045	0,009	-0,015
'K_{OA1}'	-0,045	-0,119	0,136	-0,084	0,284	-0,019

	N_2O total	η_{TN}	O_2consSpec	O_2 cons by HB	O_2 cons by AOB	O_2 cons by NOB
'K_{OA2}'	0,012	0,007	0,039	-0,008	-0,043	0,309
'K_O_H'	0,001	-0,028	0,079	0,040	0,090	-0,006
'K_{OH1}'	-0,066	0,107	0,035	0,080	0,016	0,002
'K_{OH2}'	0,009	-0,034	0,002	-0,028	0,005	0,036
'K_{OH3}'	-0,080	-0,011	-0,008	-0,054	0,056	-0,011
'K_{OH4}'	-0,068	0,016	0,002	0,015	-0,042	0,014
'K_{OH5}'	0,051	-0,020	-0,017	-0,028	-0,018	0,067
'K_{S1}'	0,073	0,166	0,325	0,503	-0,017	0,169
'K_{S2}'	-0,109	0,040	-0,015	0,064	-0,009	-0,129
'K_{S3}'	-0,150	-0,134	0,075	-0,015	0,076	0,045
'K_{S4}'	0,210	-0,088	0,045	-0,028	0,016	0,068
'K_{S5}'	-0,041	0,062	-0,007	0,085	-0,074	-0,040
'K_{X}'	-0,048	-0,026	-0,068	-0,055	-0,038	-0,043
'mu_{A1}'	-0,017	0,082	-0,264	-0,033	-0,389	0,007
'mu_{A2}'	-0,024	-0,040	-0,126	-0,075	-0,023	-0,351
'mu_{H}'	0,078	0,038	-0,214	-0,302	-0,021	0,069
'n_{g2}'	-0,030	0,050	-0,018	-0,008	-0,037	0,068
'n_{g3}'	0,203	0,081	-0,062	-0,048	-0,017	0,047
'n_{g4}'	-0,086	0,051	-0,020	-0,007	0,016	-0,031
'n_{g5}'	-0,010	-0,015	-0,034	-0,009	-0,048	-0,022
'n_{h}'	0,046	0,505	-0,141	-0,037	0,051	0,062
'n_{Y}'	-0,064	-0,427	0,182	0,073	-0,001	-0,021
'Y_{A1}'	0,004	0,010	0,047	0,012	0,092	-0,014
'Y_{A2}'	-0,064	0,007	-0,040	-0,036	-0,068	0,062
'Y_{H}'	0,017	-0,367	0,112	0,099	-0,133	-0,013
'K_{SNO_a_o_b}'	-0,086	-0,040	0,044	0,053	-0,012	0,044
'K_{SO_aobDen1}'	-0,090	-0,016	-0,062	-0,054	-0,040	0,013
'K_{IO_aobDen1}'	-0,050	0,000	0,009	0,062	-0,034	-0,057
'K_{SO_aobDen2}'	0,063	-0,066	0,052	-0,003	0,071	-0,012
'K_{IO_aobDen2}'	0,005	0,042	-0,005	0,057	-0,055	-0,004
'n_{AOB}'	0,052	-0,032	0,082	0,042	0,069	0,014
'K_{FNA_a_o_b}'	0,013	0,026	-0,007	-0,005	-0,014	0,043
'K_{FA_a_o_b}'	-0,039	-0,052	-0,006	-0,061	0,027	0,001
'Y_{AnAOB}'	-0,006	0,007	-0,068	-0,051	-0,069	0,021
'mu_{maxAnAOB}'	0,019	-0,002	0,017	-0,003	0,060	-0,042
'K_{NH3_AnAOB}'	0,100	-0,026	0,116	0,124	0,044	-0,036
'K_{HNO2_AnAOB}'	-0,067	-0,010	0,079	0,066	0,052	0,001
'K_{O2_AnAOB}'	0,014	-0,019	0,039	0,055	0,020	-0,070
'b_{AnAOB}'	0,006	-0,004	-0,010	-0,005	0,029	-0,088
R^2	**0,374**	**0,846**	**0,525**	**0,504**	**0,581**	**0,605**

TEMPERATURE = 15 ºC, DO =0.3 mg (-COD).L^{-1}

	N_2O total	η_{TN}	O_2consSpec	O_2 cons by HB	O_2 cons by AOB	O_2 cons by NOB
'b_A_1'	-0,051	-0,085	0,072	-0,002	-0,045	0,020
'b_A2'	0,140	0,191	-0,072	0,045	0,034	-0,224
'b_H'	-0,025	-0,014	-0,046	0,041	0,072	0,104
'f_P'	-0,030	0,010	0,002	-0,065	-0,081	-0,115
'i_X_B'	-0,044	0,040	-0,083	-0,049	-0,010	-0,072
'i_X_P'	-0,020	0,087	-0,083	-0,069	0,045	-0,077
'k_a'	0,037	0,029	-0,006	-0,044	0,080	-0,066
'K_F_A'	-0,010	-0,095	0,064	-0,043	0,236	0,099
'K_F_N_A'	0,143	0,083	-0,103	0,007	-0,001	0,158
'k_h'	0,060	0,039	0,006	-0,001	0,016	0,050
'K_I_1_0_F_A'	-0,007	0,016	0,021	-0,074	-0,122	-0,043
'F_I_1_0_F_N_A'	-0,099	-0,003	0,076	-0,024	0,002	-0,109
'K_{I3NO}'	0,044	0,017	-0,024	-0,022	-0,018	0,000
'K_{I4NO}'	-0,026	-0,012	0,007	-0,058	-0,013	0,018
'K_{I5NO}'	-0,074	-0,034	0,049	0,017	-0,012	0,008
'K_{I9FA}'	-0,072	0,015	-0,110	-0,018	0,010	0,114
'K_{I9FNA}'	0,023	0,046	-0,023	0,023	-0,069	-0,087
'K_{N2O}'	0,030	-0,103	0,109	-0,042	0,004	0,077
'K_{NO}'	-0,031	-0,004	-0,084	-0,036	0,041	0,084
'K_N_O_2'	-0,017	-0,020	-0,070	-0,045	0,058	0,047
'K_N_O_3'	0,023	0,003	-0,117	-0,039	0,056	-0,042
'K_{OA1}'	-0,082	-0,164	0,162	-0,041	0,485	0,016
'K_{OA2}'	0,272	0,626	-0,067	0,096	-0,133	-0,201
'K_O_H'	-0,017	0,017	-0,030	0,031	0,075	0,009
'K_{OH1}'	-0,058	0,020	-0,008	0,191	0,048	0,097
'K_{OH2}'	0,078	-0,043	0,050	-0,041	-0,006	0,068
'K_{OH3}'	-0,009	0,051	0,001	-0,062	0,024	0,011
'K_{OH4}'	-0,013	0,013	0,089	0,038	-0,052	-0,044
'K_{OH5}'	-0,026	-0,027	0,057	-0,032	-0,025	0,110
'K_{S1}'	-0,087	0,048	0,061	0,449	-0,028	0,110
'K_{S2}'	0,063	-0,037	0,065	0,113	-0,084	-0,170
'K_{S3}'	-0,062	-0,104	0,079	-0,017	0,050	0,086
'K_{S4}'	0,133	-0,043	0,053	-0,022	-0,018	0,082
'K_{S5}'	0,253	0,025	-0,039	0,094	-0,103	-0,021
'K_{X}'	-0,035	0,061	-0,131	-0,099	0,008	-0,002
'mu_{A1}'	0,117	0,171	-0,127	-0,036	-0,236	0,052
'mu_{A2}'	-0,145	-0,418	0,065	-0,163	0,044	0,257
'mu_{H}'	0,022	0,015	-0,107	-0,271	-0,015	0,095
'n_{g2}'	0,024	0,041	-0,101	-0,037	-0,044	0,127

	N_2O total	η_{TN}	O_2consSpec	O_2 cons by HB	O_2 cons by AOB	O_2 cons by NOB
'n_{g3}'	0,039	-0,029	0,073	-0,045	-0,010	0,025
'n_{g4}'	-0,134	-0,014	0,041	0,013	0,035	-0,069
'n_{g5}'	-0,116	-0,039	0,101	0,005	-0,066	0,004
'n_{h}'	0,089	0,113	-0,020	0,009	0,017	0,005
'n_{Y}'	-0,028	-0,069	-0,061	0,037	0,040	-0,010
'Y_{A1}'	-0,002	-0,062	0,092	0,029	0,075	0,019
'Y_{A2}'	-0,047	-0,041	0,030	-0,064	0,008	0,109
'Y_{H}'	0,024	-0,037	0,016	0,110	-0,176	-0,080
'K_{SNO_a_o_b}'	-0,005	-0,016	0,035	0,056	-0,045	-0,002
'K_{SO_aobDen1}'	-0,128	-0,048	-0,059	-0,060	-0,003	0,081
'K_{IO_aobDen1}'	0,072	-0,003	-0,044	0,067	-0,016	-0,002
'K_{SO_aobDen2}'	-0,070	-0,030	-0,009	-0,001	0,077	0,001
'K_{IO_aobDen2}'	0,066	0,027	0,065	0,082	-0,087	-0,024
'n_{AOB}'	0,062	0,017	0,099	0,054	0,004	-0,032
'K_{FNA_a_o_b}'	-0,115	-0,029	-0,021	-0,009	0,000	0,032
'K_{FA_a_o_b}'	-0,023	-0,009	-0,045	-0,056	0,030	-0,005
'Y_{AnAOB}'	0,018	-0,038	0,032	-0,052	-0,040	-0,063
'mu_{maxAnAOB}'	-0,005	0,021	0,059	-0,002	0,041	-0,027
'K_{NH3_AnAOB}'	0,086	0,068	-0,053	0,131	0,041	-0,139
'K_{HNO2_AnAOB}'	0,058	0,012	-0,100	0,005	0,074	0,086
'K_{O2_AnAOB}'	0,000	0,037	-0,050	0,038	0,023	-0,007
'b_{AnAOB}'	0,055	0,006	0,058	0,015	0,004	-0,086
R^2	**0,340**	**0,778**	**0,514**	**0,502**	**0,580**	**0,615**

TEMPERATURE = 15 ºC, DO =0.65 mg (-COD).L^{-1}

	N_2O total	η_{TN}	O_2consSpec	O_2 cons by HB	O_2 cons by AOB	O_2 cons by NOB
'b_A_1'	-0,074	-0,052	0,047	-0,007	0,049	0,028
'b_A2'	0,089	0,095	-0,097	0,032	-0,109	-0,065
'b_H'	-0,063	-0,054	0,207	0,431	0,053	0,097
'f_P'	0,082	0,046	-0,281	-0,480	-0,218	-0,143
'i_X_B'	0,066	-0,077	0,078	-0,003	0,048	0,018
'i_X_P'	0,022	0,107	-0,118	-0,009	-0,090	-0,003
'k_a'	0,021	0,011	0,012	-0,005	0,053	0,016
'K_F_A'	-0,048	-0,038	0,020	0,021	0,002	-0,022
'K_F_N_A'	0,029	0,063	-0,059	0,024	-0,075	-0,066
'k_h'	0,016	0,147	-0,135	-0,090	0,010	0,036
'K_I_1_0_F_A'	0,005	0,007	-0,014	0,009	-0,013	-0,041
'F_I_1_0_F_N_A'	-0,080	0,001	-0,002	-0,024	0,053	0,010

	N_2O total	η_{TN}	O_2consSpec	O_2 cons by HB	O_2 cons by AOB	O_2 cons by NOB
'K_{I3NO}'	0,131	0,020	-0,026	0,015	-0,072	-0,008
'K_{I4NO}'	-0,116	-0,013	0,018	0,000	0,079	-0,040
'K_{I5NO}'	-0,046	0,000	-0,012	-0,029	0,013	0,013
'K_{I9FA}'	-0,095	-0,021	0,016	-0,027	0,059	0,016
'K_{I9FNA}'	0,056	0,089	-0,083	0,045	-0,098	-0,097
'K_{N2O}'	-0,045	-0,100	0,097	-0,017	0,055	0,076
'K_{NO}'	0,040	-0,032	0,036	-0,015	0,023	0,058
'K_N_O_2'	-0,129	-0,114	0,108	-0,019	0,065	0,098
'K_N_O_3'	0,004	-0,158	0,139	0,134	-0,032	-0,037
'K_{OA1}'	-0,087	-0,124	0,106	-0,015	0,060	0,073
'K_{OA2}'	0,156	0,357	-0,334	0,042	-0,202	-0,267
'K_O_H'	-0,010	-0,023	0,022	-0,017	0,025	0,034
'K_{OH1}'	-0,019	0,000	0,003	-0,062	0,009	0,065
'K_{OH2}'	-0,008	-0,068	0,071	-0,174	0,031	0,312
'K_{OH3}'	-0,064	0,003	0,000	-0,038	0,060	0,018
'K_{OH4}'	0,028	0,047	-0,045	0,009	-0,026	-0,054
'K_{OH5}'	-0,030	-0,048	0,040	-0,027	0,034	0,067
'K_{S1}'	-0,042	0,094	-0,080	-0,284	0,036	0,291
'K_{S2}'	-0,040	-0,023	0,010	0,320	0,010	-0,485
'K_{S3}'	-0,001	-0,095	0,080	0,011	-0,041	0,055
'K_{S4}'	0,127	-0,007	-0,007	0,031	-0,109	0,033
'K_{S5}'	0,102	0,046	-0,039	0,045	-0,054	-0,080
'K_{X}'	-0,066	-0,039	0,020	-0,017	0,035	0,012
'mu_{A1}'	0,048	0,143	-0,135	-0,002	-0,075	-0,085
'mu_{A2}'	-0,072	-0,270	0,251	-0,004	0,096	0,178
'mu_{H}'	0,115	0,108	-0,108	0,007	-0,099	-0,043
'n_{g2}'	0,033	0,071	-0,062	-0,136	-0,067	0,171
'n_{g3}'	0,058	0,074	-0,083	0,000	-0,037	-0,034
'n_{g4}'	-0,036	-0,002	0,004	-0,029	0,043	-0,004
'n_{g5}'	0,010	0,015	-0,013	-0,028	-0,024	0,040
'n_{h}'	0,062	0,381	-0,343	-0,174	-0,041	-0,012
'n_{Y}'	-0,094	-0,308	0,225	0,044	0,010	-0,065
'Y_{A1}'	-0,067	-0,055	0,053	0,000	0,029	0,033
'Y_{A2}'	-0,010	0,027	-0,027	0,017	-0,024	-0,057
'Y_{H}'	-0,020	-0,162	-0,014	-0,366	-0,032	-0,048
'K_{SNO_a_o_b}'	0,038	0,000	0,007	0,021	-0,012	-0,037
'K_{SO_aobDen1}'	-0,085	-0,011	0,020	-0,028	0,085	0,004
'K_{IO_aobDen1}'	0,107	0,070	-0,073	0,051	-0,155	-0,060
'K_{SO_aobDen2}'	0,070	0,028	-0,026	0,019	-0,069	-0,002
'K_{IO_aobDen2}'	0,027	0,007	-0,019	0,014	-0,037	-0,024

	N_2O total	η_{TN}	O_2consSpec	O_2 cons by HB	O_2 cons by AOB	O_2 cons by NOB
'n_{AOB}'	0,163	0,104	-0,127	0,030	-0,178	-0,070
'K_{FNA_a_o_b}'	-0,170	-0,142	0,162	-0,063	0,259	0,111
'K_{FA_a_o_b}'	-0,042	-0,072	0,078	-0,021	0,095	0,043
'Y_{AnAOB}'	-0,041	0,006	-0,001	-0,006	-0,001	0,014
'mu_{maxAnAOB}'	-0,006	-0,043	0,035	0,005	0,040	0,026
'K_{NH3_AnAOB}'	0,146	0,018	-0,022	0,034	-0,089	-0,004
'K_{HNO2_AnAOB}'	0,024	-0,041	0,038	-0,001	-0,019	0,034
'K_{O2_AnAOB}'	0,025	0,000	0,002	0,011	-0,021	0,006
'b_{AnAOB}'	-0,028	0,007	0,002	-0,018	0,036	-0,007
R^2	**0,328**	**0,721**	**0,717**	**0,883**	**0,388**	**0,686**

TEMPERATURE = 15 ºC, DO =1 mg (-COD).L^{-1}

	N_2O total	η_{TN}	O_2consSpec	O_2 cons by HB	O_2 cons by AOB	O_2 cons by NOB
'b_A_1'	-0,045	-0,057	0,054	0,002	0,042	0,031
'b_A2'	-0,005	0,082	-0,094	-0,002	-0,059	-0,077
'b_H'	-0,079	-0,014	0,211	0,493	0,037	0,062
'f_P'	0,131	0,020	-0,320	-0,550	-0,414	-0,146
'i_X_B'	0,056	-0,116	0,114	-0,015	0,165	0,025
'i_X_P'	0,075	0,128	-0,151	-0,004	-0,214	-0,019
'k_a'	0,009	0,057	-0,032	-0,002	0,079	-0,023
'K_F_A'	-0,031	-0,025	0,018	0,018	-0,005	-0,033
'K_F_N_A'	-0,009	0,018	-0,021	0,005	-0,046	-0,038
'k_h'	0,048	0,256	-0,238	-0,101	-0,051	0,022
'K_I_1_0_F_A'	-0,011	-0,017	0,026	0,002	0,016	-0,008
'F_I_1_0_F_N_A'	-0,023	0,010	-0,017	0,000	0,051	-0,025
'K_{I3NO}'	0,149	-0,004	0,008	0,004	-0,120	0,050
'K_{I4NO}'	-0,212	0,041	-0,041	0,004	0,143	-0,126
'K_{I5NO}'	-0,038	-0,020	0,004	-0,028	-0,015	0,029
'K_{I9FA}'	-0,039	0,000	-0,003	-0,014	0,024	-0,012
'K_{I9FNA}'	-0,015	0,065	-0,065	0,003	-0,048	-0,071
'K_{N2O}'	-0,057	-0,103	0,100	-0,024	0,063	0,085
'K_{NO}'	0,118	0,005	-0,004	0,002	-0,046	0,042
'K_N_O_2'	-0,114	-0,102	0,094	0,005	0,079	0,075
'K_N_O_3'	-0,009	-0,200	0,170	0,124	-0,014	-0,047
'K_{OA1}'	-0,042	-0,098	0,077	0,004	0,022	0,028
'K_{OA2}'	0,068	0,135	-0,115	0,011	-0,088	-0,090
'K_O_H'	-0,019	-0,001	-0,007	-0,010	0,018	0,006
'K_{OH1}'	-0,069	0,035	-0,024	-0,061	0,034	0,049

	N_2O total	η_{TN}	O_2consSpec	O_2 cons by HB	O_2 cons by AOB	O_2 cons by NOB
'K_{OH2}'	0,001	-0,037	0,040	-0,135	-0,008	0,304
'K_{OH3}'	-0,098	-0,002	0,001	-0,019	0,072	-0,003
'K_{OH4}'	-0,013	0,003	0,002	-0,007	0,005	-0,017
'K_{OH5}'	0,024	-0,049	0,047	-0,006	-0,004	0,078
'K_{S1}'	0,045	0,125	-0,114	-0,213	0,010	0,264
'K_{S2}'	-0,080	0,017	-0,040	0,289	0,030	-0,569
'K_{S3}'	-0,092	-0,117	0,095	-0,020	0,013	0,061
'K_{S4}'	0,177	-0,059	0,055	0,020	-0,127	0,112
'K_{S5}'	0,024	0,060	-0,059	0,018	-0,002	-0,098
'K_{X}'	-0,059	-0,039	0,021	-0,002	0,020	-0,001
'mu_{A1}'	0,026	0,087	-0,089	-0,023	-0,059	-0,037
'mu_{A2}'	-0,070	-0,134	0,130	-0,007	0,095	0,090
'mu_{H}'	0,127	0,095	-0,095	-0,023	-0,119	-0,001
'n_{g2}'	-0,020	0,080	-0,073	-0,150	-0,022	0,192
'n_{g3}'	0,156	0,105	-0,119	0,015	-0,095	-0,047
'n_{g4}'	-0,047	0,063	-0,080	-0,022	0,021	-0,085
'n_{g5}'	0,016	-0,011	0,002	-0,039	-0,005	0,064
'n_{h}'	0,021	0,515	-0,471	-0,225	0,015	0,005
'n_{Y}'	-0,070	-0,392	0,285	0,059	0,002	-0,096
'Y_{A1}'	-0,035	-0,040	0,038	0,012	0,013	0,020
'Y_{A2}'	-0,049	-0,005	-0,004	0,000	0,030	-0,059
'Y_{H}'	0,032	-0,218	-0,017	-0,381	-0,129	-0,075
'K_{SNO_a_o_b}'	-0,039	-0,015	0,018	-0,009	0,011	-0,010
'K_{SO_aobDen1}'	-0,116	0,015	-0,010	-0,011	0,090	-0,029
'K_{IO_aobDen1}'	-0,003	0,087	-0,088	-0,005	-0,113	-0,051
'K_{SO_aobDen2}'	0,092	0,006	-0,019	-0,003	-0,090	0,035
'K_{IO_aobDen2}'	0,024	0,052	-0,059	0,015	-0,062	-0,056
'n_{AOB}'	0,117	0,061	-0,087	-0,015	-0,182	-0,014
'K_{FNA_a_o_b}'	-0,069	-0,061	0,072	0,019	0,172	0,007
'K_{FA_a_o_b}'	-0,034	-0,059	0,076	0,001	0,068	0,051
'Y_{AnAOB}'	-0,028	0,006	-0,003	-0,004	0,014	0,010
'mu_{maxAnAOB}'	0,017	-0,029	0,028	0,017	0,011	0,016
'K_{NH3_AnAOB}'	0,121	0,034	-0,030	0,014	-0,088	0,018
'K_{HNO2_AnAOB}'	-0,019	-0,026	0,027	-0,019	-0,021	0,028
'K_{O2_AnAOB}'	0,031	-0,007	0,004	-0,003	-0,018	0,014
'b_{AnAOB}'	-0,011	-0,010	0,011	-0,014	0,040	0,008
R^2	**0,331**	**0,800**	**0,779**	**0,966**	**0,513**	**0,675**

TEMPERATURE = 15 ºC, DO =2 mg (-COD).L^{-1}

	N_2O total	η_{TN}	O_2consSpec	O_2 cons by HB	O_2 cons by AOB	O_2 cons by NOB
'b_A_1'	-0,037	-0,024	-0,010	-0,016	-0,012	-0,002
'b_A2'	-0,075	0,039	0,004	0,020	0,048	-0,088
'b_H'	-0,049	0,046	0,083	0,094	0,027	0,017
'f_P'	0,126	-0,045	-0,108	-0,064	-0,110	-0,089
'i_X_B'	0,032	-0,141	0,018	-0,063	0,034	0,052
'i_X_P'	0,097	0,131	-0,126	-0,071	-0,017	-0,101
'k_a'	-0,028	0,050	-0,003	-0,047	0,092	-0,010
'K_F_A'	-0,019	0,019	0,229	-0,014	0,455	0,015
'K_F_N_A'	-0,039	0,011	0,107	-0,010	0,006	0,472
'k_h'	0,043	0,271	-0,062	-0,025	0,059	-0,008
'K_I_1_0_F_A'	-0,041	0,014	-0,112	-0,118	-0,026	-0,071
'F_I_1_0_F_N_A'	0,016	0,030	-0,077	-0,059	0,007	-0,131
'K_{I3NO}'	0,154	-0,046	-0,035	-0,033	-0,059	0,017
'K_{I4NO}'	-0,242	0,102	-0,086	-0,058	-0,010	-0,033
'K_{I5NO}'	-0,055	-0,025	0,053	0,008	0,030	0,075
'K_{I9FA}'	-0,027	0,014	0,019	0,032	-0,025	0,057
'K_{I9FNA}'	-0,086	0,012	-0,031	-0,006	-0,019	-0,020
'K_{N2O}'	-0,045	-0,053	-0,001	-0,036	0,056	-0,072
'K_{NO}'	0,130	-0,025	-0,009	-0,023	-0,016	0,042
'K_N_O_2'	-0,074	-0,062	0,032	-0,024	0,065	0,001
'K_N_O_3'	-0,002	-0,193	0,017	-0,043	0,006	-0,014
'K_{OA1}'	-0,047	-0,119	0,117	-0,085	0,272	-0,012
'K_{OA2}'	0,021	0,004	0,036	-0,008	-0,045	0,305
'K_O_H'	-0,008	-0,010	0,071	0,040	0,093	-0,011
'K_{OH1}'	-0,059	0,104	0,039	0,080	0,011	0,000
'K_{OH2}'	0,005	-0,032	-0,002	-0,027	0,004	0,036
'K_{OH3}'	-0,083	-0,007	-0,015	-0,054	0,053	-0,014
'K_{OH4}'	-0,056	-0,001	0,011	0,014	-0,043	0,023
'K_{OH5}'	0,065	-0,019	-0,016	-0,031	-0,018	0,074
'K_{S1}'	0,066	0,162	0,346	0,503	-0,015	0,165
'K_{S2}'	-0,122	0,015	0,000	0,063	-0,004	-0,139
'K_{S3}'	-0,146	-0,110	0,058	-0,020	0,075	0,046
'K_{S4}'	0,210	-0,086	0,038	-0,028	0,015	0,069
'K_{S5}'	-0,058	0,066	-0,005	0,085	-0,074	-0,050
'K_{X}'	-0,044	-0,041	-0,061	-0,054	-0,037	-0,041
'mu_{A1}'	-0,023	0,067	-0,241	-0,034	-0,371	0,004
'mu_{A2}'	-0,032	-0,033	-0,128	-0,077	-0,023	-0,353
'mu_{H}'	0,074	0,041	-0,227	-0,304	-0,023	0,070
'n_{g2}'	-0,045	0,080	-0,030	-0,008	-0,037	0,065

	N_2O total	η_{TN}	O_2consSpec	O_2 cons by HB	O_2 cons by AOB	O_2 cons by NOB
'n_{g3}'	0,185	0,082	-0,062	-0,049	-0,016	0,041
'n_{g4}'	-0,106	0,061	-0,024	-0,008	0,018	-0,034
'n_{g5}'	-0,025	-0,004	-0,037	-0,007	-0,045	-0,024
'n_{h}'	0,035	0,561	-0,143	-0,033	0,053	0,043
'n_{Y}'	-0,067	-0,396	0,160	0,072	-0,003	-0,020
'Y_{A1}'	0,002	0,010	0,045	0,014	0,089	-0,016
'Y_{A2}'	-0,074	0,008	-0,045	-0,038	-0,066	0,061
'Y_{H}'	0,002	-0,278	0,094	0,119	-0,131	-0,014
'K_{SNO_a_o_b}'	-0,072	-0,041	0,045	0,051	-0,011	0,052
'K_{SO_aobDen1}'	-0,088	-0,004	-0,066	-0,056	-0,036	0,011
'K_{IO_aobDen1}'	-0,053	0,010	0,010	0,064	-0,033	-0,060
'K_{SO_aobDen2}'	0,053	-0,055	0,041	-0,003	0,067	-0,013
'K_{IO_aobDen2}'	-0,002	0,057	-0,008	0,058	-0,057	-0,013
'n_{AOB}'	0,043	-0,029	0,078	0,043	0,070	0,014
'K_{FNA_a_o_b}'	0,009	0,036	-0,011	-0,003	-0,015	0,034
'K_{FA_a_o_b}'	-0,025	-0,053	-0,011	-0,062	0,024	0,004
'Y_{AnAOB}'	-0,015	0,001	-0,066	-0,051	-0,068	0,021
'mu_{maxAnAOB}'	0,025	0,000	0,015	-0,004	0,058	-0,042
'K_{NH3_AnAOB}'	0,093	-0,011	0,111	0,125	0,044	-0,041
'K_{HNO2_AnAOB}'	-0,060	-0,021	0,085	0,064	0,052	0,009
'K_{O2_AnAOB}'	0,006	-0,022	0,040	0,054	0,019	-0,068
'b_{AnAOB}'	0,001	-0,001	-0,011	-0,007	0,035	-0,094
R^2	**0,371**	**0,846**	**0,788**	**0,981**	**0,881**	**0,571**

TEMPERATURE = 20ºC, DO =0.3 mg (-COD).L^{-1}

	N_2O total	η_{TN}	O_2consSpec	O_2 cons by HB	O_2 cons by AOB	O_2 cons by NOB
'b_A_1'	0,007	-0,041	-0,073	-0,026	-0,080	-0,067
'b_A2'	0,105	0,200	-0,023	0,162	0,013	-0,280
'b_H'	-0,027	-0,056	0,053	0,033	0,007	0,025
'f_P'	0,085	0,046	-0,184	-0,113	-0,052	-0,213
'i_X_B'	0,074	-0,076	-0,072	-0,131	-0,066	0,107
'i_X_P'	-0,046	0,002	-0,058	-0,011	-0,081	-0,014
'k_a'	-0,083	-0,013	0,080	0,031	0,088	0,027
'K_F_A'	-0,047	-0,053	0,192	-0,011	0,310	0,017
'K_F_N_A'	-0,018	0,016	-0,018	-0,071	0,011	0,106
'k_h'	-0,027	0,120	-0,062	0,005	-0,038	0,011
'K_I_1_0_F_A'	-0,008	-0,022	0,044	-0,054	0,111	0,035
'F_I_1_0_F_N_A'	0,029	-0,003	-0,051	0,006	-0,090	0,005

	N_2O total	η_{TN}	O_2consSpec	O_2 cons by HB	O_2 cons by AOB	O_2 cons by NOB
'K_{I3NO}'	-0,045	-0,005	0,018	0,076	-0,002	-0,053
'K_{I4NO}'	-0,025	0,021	0,099	0,069	0,094	-0,013
'K_{I5NO}'	-0,011	0,000	-0,003	-0,005	-0,014	-0,001
'K_{I9FA}'	-0,046	0,018	0,019	0,022	0,025	-0,015
'K_{I9FNA}'	-0,005	0,003	0,057	0,075	-0,008	-0,006
'K_{N2O}'	0,131	0,009	0,005	-0,001	0,012	-0,032
'K_{NO}'	0,048	0,053	-0,066	-0,084	0,025	-0,028
'K_N_O_2'	-0,011	-0,065	0,079	0,001	0,033	0,109
'K_N_O_3'	0,051	-0,016	0,025	0,066	0,035	-0,156
'K_{OA1}'	-0,107	-0,189	0,389	-0,011	0,467	0,207
'K_{OA2}'	0,295	0,701	-0,252	0,174	-0,143	-0,210
'K_O_H'	0,009	-0,023	0,014	0,017	-0,057	0,042
'K_{OH1}'	-0,082	0,025	0,165	0,233	0,025	0,022
'K_{OH2}'	0,089	-0,025	-0,013	-0,071	-0,004	0,055
'K_{OH3}'	0,071	0,002	0,038	0,010	0,036	0,057
'K_{OH4}'	-0,094	0,025	0,057	0,033	0,076	0,002
'K_{OH5}'	-0,104	0,008	-0,037	-0,014	-0,019	-0,017
'K_{S1}'	-0,191	0,099	0,231	0,400	-0,038	0,053
'K_{S2}'	0,033	-0,031	0,001	0,055	-0,018	-0,180
'K_{S3}'	-0,132	-0,099	-0,061	-0,095	-0,050	-0,030
'K_{S4}'	0,103	-0,057	-0,018	-0,082	0,031	0,013
'K_{S5}'	0,205	0,008	0,009	0,015	0,000	-0,035
'K_{X}'	-0,023	-0,031	0,067	-0,002	0,072	0,052
'mu_{A1}'	0,056	0,125	-0,218	0,048	-0,321	-0,036
'mu_{A2}'	-0,162	-0,417	0,084	-0,209	0,035	0,254
'mu_{H}'	0,054	0,000	-0,244	-0,303	-0,084	0,045
'n_{g2}'	-0,037	0,025	-0,066	-0,063	-0,054	0,041
'n_{g3}'	0,047	0,050	-0,104	-0,019	-0,097	-0,025
'n_{g4}'	-0,028	0,018	0,015	0,033	-0,011	0,021
'n_{g5}'	-0,136	-0,023	-0,015	0,003	-0,050	0,010
'n_{h}'	-0,109	0,116	-0,025	0,045	0,033	-0,064
'n_{Y}'	0,066	-0,046	-0,047	0,004	-0,073	-0,079
'Y_{A1}'	-0,045	0,005	0,035	-0,040	0,088	0,053
'Y_{A2}'	-0,044	0,057	0,032	0,051	-0,001	0,075
'Y_{H}'	-0,069	0,012	0,024	-0,007	0,121	-0,126
'K_{SNO_a_o_b}'	0,044	0,010	0,029	0,022	0,032	-0,001
'K_{SO_aobDen1}'	-0,021	-0,080	0,060	-0,059	0,111	0,030
'K_{IO_aobDen1}'	-0,033	-0,024	-0,041	-0,077	-0,008	0,017
'K_{SO_aobDen2}'	0,001	-0,032	0,056	-0,004	0,067	0,052
'K_{IO_aobDen2}'	0,091	-0,031	0,030	-0,028	0,066	-0,004

	N_2O total	η_{TN}	O_2consSpec	O_2 cons by HB	O_2 cons by AOB	O_2 cons by NOB
'n_{AOB}'	0,001	0,060	-0,029	-0,007	-0,005	0,029
'K_{FNA_a_o_b}'	-0,087	-0,044	-0,017	-0,065	0,008	0,039
'K_{FA_a_o_b}'	-0,029	-0,013	0,037	-0,046	0,073	0,084
'Y_{AnAOB}'	0,075	-0,007	-0,061	-0,020	-0,045	-0,061
'mu_{maxAnAOB}'	0,080	0,005	-0,056	-0,043	-0,044	0,021
'K_{NH3_AnAOB}'	-0,051	-0,066	-0,027	-0,074	-0,055	0,107
'K_{HNO2_AnAOB}'	0,035	-0,019	-0,034	-0,107	0,068	-0,038
'K_{O2_AnAOB}'	0,118	-0,003	0,025	0,034	-0,007	-0,014
'b_{AnAOB}'	0,056	0,021	0,045	0,049	0,022	0,021
R^2	**0,450**	**0,889**	**0,597**	**0,556**	**0,592**	**0,469**

TEMPERATURE = 20ºC, DO =0.65 mg (-COD).L^{-1}

	N_2O total	η_{TN}	O_2consSpec	O_2 cons by HB	O_2 cons by AOB	O_2 cons by NOB
'b_A_1'	-0,005	-0,020	0,020	0,022	-0,018	0,014
'b_A2'	0,135	0,180	-0,156	0,051	-0,142	-0,152
'b_H'	-0,014	-0,087	0,167	0,326	0,008	0,029
'f_P'	0,030	0,027	-0,321	-0,644	-0,162	-0,171
'i_X_B'	0,012	-0,161	0,143	-0,059	0,127	0,091
'i_X_P'	-0,059	0,040	-0,046	0,033	-0,083	-0,035
'k_a'	-0,028	-0,027	0,047	-0,035	0,086	0,062
'K_F_A'	-0,055	-0,064	0,042	-0,009	0,038	0,041
'K_F_N_A'	0,093	0,050	-0,041	0,020	-0,061	-0,035
'k_h'	0,018	0,272	-0,238	-0,059	-0,070	-0,077
'K_I_1_0_F_A'	-0,003	-0,002	-0,004	0,014	-0,054	-0,009
'F_I_1_0_F_N_A'	-0,056	-0,020	0,012	-0,030	0,095	0,020
'K_{I3NO}'	-0,016	-0,052	0,059	-0,007	0,065	0,031
'K_{I4NO}'	0,011	0,041	-0,058	0,022	-0,066	-0,062
'K_{I5NO}'	0,034	0,005	-0,017	0,006	-0,041	-0,016
'K_{I9FA}'	0,041	0,062	-0,057	0,022	-0,042	-0,053
'K_{I9FNA}'	-0,023	-0,012	0,026	-0,013	0,033	0,019
'K_{N2O}'	0,002	0,002	0,001	-0,008	0,066	-0,005
'K_{NO}'	-0,054	-0,017	0,012	-0,020	0,009	0,027
'K_N_O_2'	-0,019	-0,071	0,049	0,008	-0,061	0,035
'K_N_O_3'	-0,005	-0,198	0,145	0,130	-0,005	-0,071

	N_2O total	η_{TN}	O_2consSpec	O_2 cons by HB	O_2 cons by AOB	O_2 cons by NOB
'K_{OA1}'	-0,126	-0,153	0,141	-0,033	0,101	0,129
'K_{OA2}'	0,281	0,398	-0,367	0,073	-0,305	-0,302
'K_O_H'	0,016	0,038	-0,036	0,011	-0,028	-0,019
'K_{OH1}'	-0,086	0,007	0,000	-0,089	0,046	0,084
'K_{OH2}'	0,034	-0,042	0,051	-0,194	0,018	0,329
'K_{OH3}'	-0,008	0,058	-0,058	-0,002	-0,004	-0,042
'K_{OH4}'	-0,143	-0,052	0,057	-0,016	0,087	0,015
'K_{OH5}'	-0,075	-0,034	0,033	-0,015	0,011	0,037
'K_{S1}'	-0,050	0,084	-0,059	-0,263	0,035	0,285
'K_{S2}'	0,114	-0,024	0,000	0,349	-0,079	-0,472
'K_{S3}'	-0,038	-0,095	0,088	-0,017	0,011	0,093
'K_{S4}'	-0,009	-0,026	0,026	0,000	0,009	0,035
'K_{S5}'	0,061	-0,016	0,016	0,010	0,004	0,003
'K_{X}'	0,055	-0,035	0,026	0,029	-0,010	0,002
'mu_{A1}'	0,068	0,098	-0,084	-0,013	-0,093	-0,039
'mu_{A2}'	-0,178	-0,298	0,257	-0,044	0,191	0,228
'mu_{H}'	0,029	0,041	-0,033	-0,032	0,058	0,022
'n_{g2}'	-0,026	0,054	-0,038	-0,172	0,023	0,217
'n_{g3}'	-0,028	0,009	0,017	-0,006	0,032	0,001
'n_{g4}'	-0,033	0,031	-0,037	0,005	-0,009	-0,042
'n_{g5}'	-0,013	-0,033	0,045	0,009	0,007	0,036
'n_{h}'	0,046	0,374	-0,310	-0,106	-0,058	-0,093
'n_{Y}'	0,033	-0,256	0,180	0,046	-0,024	-0,027
'Y_{A1}'	0,060	-0,011	0,018	0,010	-0,041	0,020
'Y_{A2}'	0,066	0,092	-0,097	0,009	-0,088	-0,049
'Y_{H}'	0,175	-0,005	-0,158	-0,282	-0,198	-0,117
'K_{SNO_a_o_b}'	-0,059	-0,047	0,068	-0,016	0,124	0,031
'K_{SO_aobDen1}'	0,049	-0,002	0,000	-0,007	-0,032	0,022
'K_{IO_aobDen1}'	0,053	0,013	-0,029	-0,004	-0,085	0,012
'K_{SO_aobDen2}'	0,016	-0,009	0,013	-0,001	-0,022	0,018
'K_{IO_aobDen2}'	0,051	-0,013	0,002	0,010	-0,040	0,005
'n_{AOB}'	0,157	0,123	-0,143	0,049	-0,214	-0,081
'K_{FNA_a_o_b}'	-0,177	-0,184	0,204	-0,083	0,273	0,163
'K_{FA_a_o_b}'	-0,006	-0,048	0,055	-0,002	0,045	0,043
'Y_{AnAOB}'	0,059	-0,008	0,006	0,001	-0,043	0,012
'mu_{maxAnAOB}'	0,051	0,032	-0,045	0,000	-0,014	-0,034
'K_{NH3_AnAOB}'	0,035	0,000	-0,016	0,034	-0,034	-0,033
'K_{HNO2_AnAOB}'	-0,017	-0,053	0,057	-0,004	0,030	0,025
'K_{O2_AnAOB}'	0,086	0,039	-0,045	0,033	-0,040	-0,068
'b_{AnAOB}'	0,105	0,070	-0,060	0,029	-0,054	-0,053

	N_2O total	η_{TN}	O_2consSpec	O_2 cons by HB	O_2 cons by AOB	O_2 cons by NOB
R^2	0,374	0,794	0,773	0,919	0,489	0,793

TEMPERATURE = 20ºC, DO =1 mg (-COD).L^{-1}

	N_2O total	η_{TN}	O_2consSpec	O_2 cons by HB	O_2 cons by AOB	O_2 cons by NOB
'b_A_1'	0,001	0,000	0,004	0,015	-0,014	0,000
'b_A2'	0,120	0,086	-0,074	0,032	-0,131	-0,078
'b_H'	-0,046	-0,104	0,196	0,348	0,034	0,027
'f_P'	0,019	0,015	-0,370	-0,693	-0,286	-0,207
'i_X_B'	-0,002	-0,177	0,161	-0,055	0,201	0,096
'i_X_P'	0,002	0,091	-0,094	0,029	-0,174	-0,061
'k_a'	0,039	0,025	-0,001	-0,019	0,038	0,025
'K_F_A'	-0,081	-0,034	0,019	0,004	0,020	0,011
'K_F_N_A'	0,129	0,039	-0,026	0,018	-0,075	-0,024
'k_h'	0,048	0,352	-0,306	-0,095	-0,086	-0,069
'K_I_1_0_F_A'	-0,010	-0,009	0,006	0,004	-0,038	0,004
'F_I_1_0_F_N_A'	-0,029	0,015	-0,030	-0,005	0,029	-0,018
'K_{I3NO}'	0,023	-0,007	0,014	0,006	-0,005	0,008
'K_{I4NO}'	0,035	0,040	-0,056	0,026	-0,083	-0,093
'K_{I5NO}'	0,058	-0,001	-0,013	0,007	-0,074	-0,004
'K_{I9FA}'	-0,005	0,035	-0,033	0,003	0,003	-0,033
'K_{I9FNA}'	-0,020	-0,039	0,046	-0,014	0,047	0,053
'K_{N2O}'	-0,045	-0,010	0,005	-0,005	0,067	0,005
'K_{NO}'	-0,035	-0,015	0,012	-0,012	-0,010	0,023
'K_N_O_2'	-0,039	-0,069	0,058	-0,013	0,003	0,042
'K_N_O_3'	-0,014	-0,263	0,198	0,139	-0,001	-0,088
'K_{OA1}'	-0,099	-0,122	0,109	0,001	0,046	0,100
'K_{OA2}'	0,215	0,210	-0,202	0,018	-0,208	-0,166
'K_O_H'	0,034	0,014	-0,010	0,014	-0,005	-0,012
'K_{OH1}'	-0,077	0,048	-0,038	-0,067	0,055	0,035
'K_{OH2}'	0,067	0,009	0,000	-0,159	-0,022	0,324
'K_{OH3}'	0,050	0,066	-0,066	-0,001	-0,033	-0,060
'K_{OH4}'	-0,131	-0,078	0,076	-0,005	0,105	0,031
'K_{OH5}'	-0,014	-0,005	0,005	-0,002	-0,042	0,024
'K_{S1}'	-0,045	0,070	-0,053	-0,221	0,055	0,328
'K_{S2}'	0,146	-0,059	0,025	0,306	-0,106	-0,520
'K_{S3}'	0,020	-0,076	0,069	-0,010	-0,027	0,098
'K_{S4}'	0,004	-0,032	0,038	0,011	-0,012	0,048
'K_{S5}'	0,048	-0,021	0,025	0,016	0,009	-0,004
'K_{X}'	0,053	-0,037	0,029	0,041	-0,040	-0,005

	N_2O total	η_{TN}	O_2consSpec	O_2 cons by HB	O_2 cons by AOB	O_2 cons by NOB
'mu_{A1}'	0,069	0,065	-0,055	-0,024	-0,084	-0,015
'mu_{A2}'	-0,139	-0,146	0,125	-0,012	0,119	0,125
'mu_{H}'	0,052	0,103	-0,093	-0,025	0,013	-0,023
'n_{g2}'	-0,008	0,091	-0,073	-0,148	-0,014	0,241
'n_{g3}'	-0,024	0,007	0,020	0,007	0,014	0,000
'n_{g4}'	-0,069	0,026	-0,033	-0,004	0,015	-0,049
'n_{g5}'	0,021	-0,011	0,027	0,004	0,002	0,031
'n_{h}'	0,014	0,511	-0,423	-0,175	-0,021	-0,096
'n_{Y}'	0,034	-0,350	0,255	0,068	-0,064	-0,028
'Y_{A1}'	0,027	-0,038	0,045	-0,003	-0,007	0,058
'Y_{A2}'	0,038	0,041	-0,051	-0,008	-0,037	-0,003
'Y_{H}'	0,141	-0,073	-0,129	-0,330	-0,200	-0,101
'K_{SNO_a_o_b}'	-0,050	-0,030	0,042	-0,007	0,085	0,016
'K_{SO_aobDen1}'	0,077	0,031	-0,033	-0,001	-0,105	0,006
'K_{IO_aobDen1}'	0,057	0,017	-0,024	-0,012	-0,074	0,010
'K_{SO_aobDen2}'	0,015	-0,006	0,012	0,001	-0,037	0,015
'K_{IO_aobDen2}'	0,060	0,021	-0,024	0,009	-0,071	-0,021
'n_{AOB}'	0,166	0,106	-0,117	0,018	-0,188	-0,059
'K_{FNA_a_o_b}'	-0,127	-0,143	0,156	-0,022	0,175	0,127
'K_{FA_a_o_b}'	-0,043	-0,057	0,064	-0,010	0,107	0,062
'Y_{AnAOB}'	0,053	-0,022	0,023	0,005	-0,050	0,022
'mu_{maxAnAOB}'	0,069	0,045	-0,060	0,007	-0,053	-0,065
'K_{NH3_AnAOB}'	0,073	0,035	-0,044	0,035	-0,078	-0,059
'K_{HNO2_AnAOB}'	-0,020	-0,032	0,038	-0,007	0,042	0,004
'K_{O2_AnAOB}'	0,073	0,055	-0,063	0,029	-0,082	-0,090
'b_{AnAOB}'	0,029	0,003	0,000	-0,004	0,026	0,021
R^2	**0,311**	**0,818**	**0,778**	**0,973**	**0,474**	**0,757**

TEMPERATURE = 20ºC, DO =2 mg (-COD).L^{-1}

	N_2O total	η_{TN}	O_2consSpec	O_2 cons by HB	O_2 cons by AOB	O_2 cons by NOB
'b_A_1'	0,070	-0,019	0,019	0,024	-0,020	0,014
'b_A2'	0,072	-0,014	0,023	0,017	-0,025	0,017
'b_H'	-0,093	-0,066	0,163	0,369	-0,025	-0,039
'f_P'	0,008	-0,008	-0,369	-0,719	-0,644	-0,230
'i_X_B'	0,001	-0,180	0,172	-0,045	0,427	0,111
'i_X_P'	0,100	0,118	-0,124	0,032	-0,460	-0,088
'k_a'	0,021	0,023	0,005	-0,014	0,181	0,012
'K_F_A'	-0,047	-0,012	0,005	0,008	-0,019	-0,014
'K_F_N_A'	0,135	-0,003	0,019	0,014	-0,040	0,024

	N_2O total	η_{TN}	O_2consSpec	O_2 cons by HB	O_2 cons by AOB	O_2 cons by NOB
'k_h'	0,065	0,361	-0,318	-0,133	-0,032	-0,022
'K_I_1_0_F_A'	0,057	0,002	0,005	0,004	-0,016	-0,004
'F_I_1_0_F_N_A'	0,045	0,024	-0,042	0,000	0,004	-0,031
'K_{I3NO}'	0,087	-0,011	0,021	0,009	-0,012	0,026
'K_{I4NO}'	-0,102	0,025	-0,038	0,012	-0,003	-0,118
'K_{I5NO}'	0,064	-0,012	0,007	0,000	-0,024	0,016
'K_{I9FA}'	-0,008	0,027	-0,025	0,007	-0,002	-0,043
'K_{I9FNA}'	0,090	-0,017	0,023	-0,002	-0,021	0,050
'K_{N2O}'	0,118	0,020	-0,024	0,006	-0,037	-0,006
'K_{NO}'	0,034	-0,010	0,011	-0,006	-0,027	0,016
'K_N_O_2'	-0,121	-0,053	0,042	-0,022	0,026	0,039
'K_N_O_3'	-0,089	-0,283	0,223	0,142	-0,015	-0,112
'K_{OA1}'	-0,036	-0,124	0,114	0,019	0,007	0,111
'K_{OA2}'	0,086	0,062	-0,069	0,006	-0,035	-0,077
'K_O_H'	0,033	-0,008	0,009	0,016	0,008	0,006
'K_{OH1}'	-0,106	0,110	-0,104	-0,060	0,026	-0,041
'K_{OH2}'	0,033	0,006	0,002	-0,099	-0,005	0,268
'K_{OH3}'	0,076	0,039	-0,044	-0,001	-0,011	-0,050
'K_{OH4}'	-0,048	-0,020	0,017	0,008	0,017	-0,023
'K_{OH5}'	-0,003	-0,004	0,006	-0,008	-0,005	0,038
'K_{S1}'	-0,043	0,107	-0,094	-0,164	0,030	0,249
'K_{S2}'	0,048	-0,153	0,116	0,243	-0,013	-0,440
'K_{S3}'	-0,085	-0,105	0,098	-0,015	0,013	0,150
'K_{S4}'	0,118	-0,027	0,042	0,009	-0,047	0,084
'K_{S5}'	-0,048	-0,031	0,037	0,008	0,048	0,005
'K_{X}'	-0,056	-0,065	0,056	0,030	-0,005	0,028
'mu_{A1}'	-0,019	0,056	-0,047	-0,031	-0,036	-0,022
'mu_{A2}'	0,067	-0,013	0,008	0,000	-0,028	0,047
'mu_{H}'	0,034	0,132	-0,126	-0,024	-0,009	-0,062
'n_{g2}'	0,022	0,111	-0,093	-0,130	-0,031	0,248
'n_{g3}'	-0,026	0,005	0,022	0,006	0,027	0,005
'n_{g4}'	-0,137	0,032	-0,044	-0,010	0,038	-0,076
'n_{g5}'	-0,065	-0,024	0,036	0,003	0,007	0,050
'n_{h}'	-0,097	0,553	-0,483	-0,226	0,036	-0,083
'n_{Y}'	-0,090	-0,416	0,334	0,072	-0,023	0,009
'Y_{A1}'	-0,018	-0,034	0,041	-0,004	-0,053	0,074
'Y_{A2}'	0,120	0,016	-0,027	-0,003	-0,054	0,024
'Y_{H}'	-0,041	-0,171	-0,044	-0,349	-0,192	-0,057
'K_{SNO_a_o_b}'	-0,004	-0,014	0,023	0,005	0,023	0,000
'K_{SO_aobDen1}'	0,120	-0,021	0,029	-0,008	0,013	0,066

	N_2O total	η_{TN}	O_2consSpec	O_2 cons by HB	O_2 cons by AOB	O_2 cons by NOB
'K_{IO_aobDen1}'	0,042	-0,005	0,005	-0,015	0,005	0,026
'K_{SO_aobDen2}'	0,000	-0,018	0,027	0,001	0,035	0,021
'K_{IO_aobDen2}'	0,053	0,015	-0,012	0,006	-0,021	-0,022
'n_{AOB}'	0,100	0,036	-0,043	0,000	-0,061	0,003
'K_{FNA_a_o_b}'	-0,050	-0,062	0,078	-0,004	0,062	0,074
'K_{FA_a_o_b}'	-0,047	-0,025	0,029	-0,002	0,040	0,044
'Y_{AnAOB}'	0,042	-0,031	0,040	0,001	-0,016	0,042
'mu_{maxAnAOB}'	-0,030	0,036	-0,051	-0,003	-0,009	-0,077
'K_{NH3_AnAOB}'	0,038	0,013	-0,020	0,017	-0,007	-0,032
'K_{HNO2_AnAOB}'	-0,048	-0,019	0,021	0,000	0,028	-0,027
'K_{O2_AnAOB}'	0,038	0,012	-0,019	0,016	-0,010	-0,057
'b_{AnAOB}'	0,068	-0,018	0,015	-0,001	-0,018	0,063
R^2	**0,307**	**0,873**	**0,804**	**0,989**	**0,905**	**0,590**

APPENDIX 2
MORRIS SCREENING SENSITIVITY ANALYSIS RESULTS

The histograms resulting from sensitivity analysis according the Morris screening procedure can be found in the following link:

https://www.dropbox.com/s/srh1sonrer9deuu/appendix_2.pdf?dl=0

or can be directly opened pressing Ctrl while clicking on the following link: Morris screening histograms

Department of Chemical and Biochemical Engineering
Technical University of Denmark
Søltofts Plads, Building 229
2800 Kgs. Lyngby
Denmark

Phone: +45 45 25 28 00
Web: www.kt.dtu.dk/